Environmental Impact Assessment Report

Volume 4

Appendix 6.3 Modelling Report

PARTRAC

Codling Wind Park Environmental Statement

Numerical Modelling Technical Appendix

January 2024

PARTRAC

DOCUMENT CONTROL

Version History					
Version	Date	Prepared by	Reviewed by	Approved by	Approved as
V01	31/08/2022	MG/LH/JP	JP	MRW	Draft
V02	14/10/2022	JP	JP/MRW	MRW	Draft
V03	29/11/2022	JP	JP/MRW	MRW	Draft
V04	31/03/2023	MG/LH/JP	JP/MRW	MRW	Draft
V05	14/04/2023	MG/LH/JP	JP/MRW	MRW	Draft
V06	27/10/2023	MG/LH	JP/MRW	MRW	Draft
V07	19/01/2024	MG/JP	JP	MRW	Final

Changes from the Previous Version	
n/a	Original version.
V02	Updated in line with comments received from Natural Power Consultants and Codling Wind Park
V03	Updated in response to comments received from Codling Wind Park
V04	Updated to include validation of the model against the new measurement data received from Codling Wind Park and to include the sediment transport modelling performed
V05	Updated to include the post construction modelling assessment
V06	Updated following amendments to project design parameters
V07	Updated following client and legal review

Recipient	Distribution Method		
	Paper (copies)	PDF	Online
Stuart McCallum (Natural Power) Ciara Gilligan (Natural Power) Sean Leake (Codling Wind Park)		x	
Holders of controlled copies will automatically be provided with subsequent approved versions of this document when they become available.			

Glossary

EIA	Environmental Impact Assessment
COWRIE	Collaborative Offshore Windfarm Research into the Environment
DNV GL	Det Norske Veritas
DHI	Danish Hydraulic Institute
GEBCO	General Bathymetric Chart of the Oceans
DTM	Digital Terrain Model
MBES	Multibeam Echosounder
MSL	Mean Sea Level
LAT	Lowest Astronomical Tide
ECMWF	European Centre for Medium-Range Weather Forecasts
WAM	Wave Analysis Model
CFL	Courant–Friedrichs–Lewy
ADCP	Acoustic Doppler Current Profiler
IMarEST	Institute of Marine Engineering, Science & Technology
ITGN	Irish Tide Gauge Network
SSC	Suspended Sediment Concentration

Units and Conventions

The following list describes the units and conventions used in this report. Unless stated otherwise, units have been expressed using the SI convention.

- Wave direction is expressed in compass points or degrees, relative to true North (°T), and describes the direction from which the waves are propagating.
- • Wave heights are expressed in metres (m).
- • Wave periods are expressed in seconds (s).
- Current direction is expressed in compass points or degrees, relative to true North (°T), and describes the direction towards which the currents are flowing.
- Current speeds are expressed in metres per second (m/s).
- Water levels are expressed in metres [m] relative to Mean Sea Level (MSL).
- Positions are quoted relative to WGS 84 except where stated.
- All times are quoted in Coordinated Universal Time [UTC]

Contents

Figures

Tables

Executive Summary

A marine area coupled hydrodynamic wave model has been constructed to support determination of the baseline hydrodynamic and wave regimes prevailing within the MAC application boundary and wider region. These models, form the driving models for post construction and sediment transport simulations performed to support the assessment of potential impacts of the CWP project upon relevant receptors. This report describes the approach adopted to set-up, calibrate, and validate the marine area model. The primary purpose of the calibration and validation exercise is to demonstrate robust model skill, to provide quantitative evidence to prove that the constructed marine area models are considered to be acceptable. Comparing model performance against criteria set out in established industry guidance indicates that the model is of suitable skill to be utilised as part of this assessment.

Following model calibration and validation, an exercise has been performed to assess the potential impacts of the CWP project upon the prevailing hydrodynamic, wave and sedimentary regime at, and in proximity to, the MAC application boundary.

Significant points to note from the outputs of the model simulations performed are:

- The construction of the windfarm is predicted to have only a small and limited effect on the prevailing hydrodynamic and wave regimes both within the array site and at locations towards the coastline.
- During disposal of dredge arisings and trenching activities, SSC's local to the release locations are predicted to be enhanced to up to circa 150 mg\l for only a limited time.
- Enhanced SSCs are transient, and concentrations are predicted to reduce to baseline levels no more than 25 days after the release activity.
- The suspended sediment plumes were predicted during the simulation testing to be dispersed towards the East quadrant (i.e. offshore), except for disposal of dredge arisings OECC scenario 1 where a dominantly westward (inshore) propagation is observed.
- The predicted thickness of the sediment deposited during the simulations of dredge disposal and cable trenching activities are almost negligible (< 1 cm). The thickness of the deposit is a function of the location and timing of the release, the composition of the material released and the prevailing metocean and hydrodynamic conditions.

1 Preface

In line with key industry guidance (e.g. COWRIE, 2009; DNV-GL, 2018; Brooks *et al.*, 2018; IMarEST, 2018; and Pye *et al.*, 2017) and best practice, a high resolution, 2D marine area model (hydrodynamic and wave model) has been developed and configured to support accurate determination of the oceanographic regime within the MAC application boundary, coastline, and wider region. The model has been calibrated and validated against measured metocean data acquired locally and publicly available measured data from locations proximal to the proposed development area.

This technical appendix describes the setup, calibration, and validation of the marine area model and the results of simulations performed to assess the potential impacts of the CWP project upon the prevailing hydrodynamic, wave and sedimentary regime at, and in proximity to, the Codling OWF site.

2 Development of the Marine Area Model

This section presents details of the set-up of the coupled hydrodynamic wave model and provides information on the associated calibration and validation procedures. Model performance is assessed by comparing the modelled conditions with measured metocean data derived from public data records and an ongoing project specific measurement campaign conducted within the MAC boundary. Section 2.1 to Section 2.4 describe the following:

- The modelling software that is used.
- Boundary forcing and implementation of the bathymetry across the model domain.
- Model setup and parameterisation.
- Model calibration procedures, Quality Control (QC) of data received and performance during validation.

2.1 Software

A bespoke coupled hydrodynamic wave model has been developed for this study utilising the MIKE21 software package (developed and operated by the Danish Hydraulic Institute [DHI]). MIKE21 software is ideally suited for modelling a wide range of hydraulic, oceanographic, and environmental phenomena in aqueous environments.

The MIKE 21 Flow Model (termed the hydrodynamic model) provides a comprehensive modelling system of two-dimensional (2D) free-surface flows using an unstructured flexible mesh grid. The unstructured mesh approach provides an optimal degree of flexibility in the representation of complex geometries and enables smooth representations of boundaries (i.e. small mesh elements are used in the local areas around sites of interest where greater detail is required). The model simulates water level variations and flows in response to a variety of forcing functions, these include:

- Bottom shear stress.
- Wind shear stress.
- Barometric pressure gradient.
- Coriolis force.
- Momentum dispersion.
- Sources and sinks.
- Flooding and drying.
- Wave radiation stresses.

The MIKE21 Flow Model provides the following relevant parameters at 10-minute intervals:

- Current velocity magnitude and direction of flow.
- Water level.

A bespoke MIKE21SW spectral wave model (termed the wave model) has also been developed. MIKE21SW is a third-generation wave model, developed by DHI, which computes random, short-crested wind-generated waves in coastal regions and inland waters. MIKE21SW accounts for the following physics:

- Wave propagation in time and space, shoaling, refraction due to current and depth.
- frequency shifting due to currents and non-stationary depth.
- Wave generation by wind.
- Three- and four-wave interactions.
- Whitecapping, bottom friction and depth-induced breaking.
- Wave-induced set-up.
- Transmission through and reflection (specular and diffuse) against obstacles.
- Diffraction.

The following relevant parameters have been output from the wave model at 1-hour intervals:

- Significant wave height (H_s, m).
- Mean wave direction (M_{dir}, deg).
- Mean zero-crossing wave period (T_z, s).
- Peak wave period (T_p, s).

2.2 Boundary Conditions and Bathymetry

Boundary conditions to the hydrodynamic model originated from DHI's Global Tide Model which is available in 0.125° x 0.125° resolution for the 12 major constituents in the tidal spectra. This global dataset has been produced using numerical modelling which assimilates 17 years of multi-mission satellite observations of water level. The dataset includes tide elevations (amplitude and phase) of the main semidiurnal M2, S2, K2, N2, the diurnal S1, K1, O1, P1, Q1, and the shallow water constituents M4.

Atmospheric data (comprising wind and surface pressure fields) were derived from the ERA5-Reanalysis and Forecast atmospheric model established by the European Centre for Medium-range Weather Forecasts (ECMWF). ERA5 offers a comprehensive reanalysis, from 1979 to near real time, which assimilates observations in the upper air and near surface. The ERA5 atmospheric model is coupled with a global wave model and is available in 0.5° x 0.5° resolution. The wave model incorporates three fully coupled components: the atmosphere, land surface, and ocean waves. The wave model is based on the Wave Analysis Model (WAM) approach (Komen *et al.*, 1984). Data from this model were used to drive surge effects in the hydrodynamic model and provide spectral wave boundary conditions to the European scale model.

The following bathymetry datasets were implemented within the coupled hydrodynamic wave model:

- *GEBCO \ EMODnet dataset*: These data deliver the best available information on water depth within the Irish Sea as it provides a harmonized Digital Terrain Model (DTM) that covers the European shelf Sea at resolutions of up to 1/16 * 1/16 arc minutes (circa 115 * 115 meters, depending on the latitude). At this scale, physical features such as trenches, ridges, sand banks and sand waves are well represented.
- *Osiris Projects, 2014*[1]: This dataset provides high resolution MultiBeam Echo Sounder (MBES) bathymetric data that covers the entirety of the Codling Wind Park at a resolution of 0.5 m * 0.5 m.
- *G-tec, 2021*: This dataset provides high resolution MBES bathymetric data that covers the proposed cable routes P1, P2, P3, and P4 at a resolution of 0.5 m * 0.5 m.

All bathymetry data were reduced to the Mean Sea Level (MSL) datum prior to implementation within the models. The existence of vertical discontinuities in the bathymetry implemented within the model domain may cause the model to collapse, and thus a low pass filtering technique was applied to the composite bathymetry used in the model to smooth the data at the model boundaries. The coastlines of the island of Ireland, and the Isle of Man, were derived from the MSL coastline shapefiles available from EMODnet. These shapefiles were developed using data from OpenStreetMap and calibrated against satellite imagery to provide the most accurate and appropriate coastline description for numerical models. The coastlines of England, Scotland and Wales were discretised using the data available from the Ordnance Survey which describes the position of Mean High-Water Springs For continental Europe. Figure 1 shows the extent of the model domain, mesh design and implementation of the bathymetry.

1 Comparison of MBES data acquired in 2014 and 2021 show only localised changes to seabed elevation associated with the migration through time of isolated bedforms within the central region of the Array site.

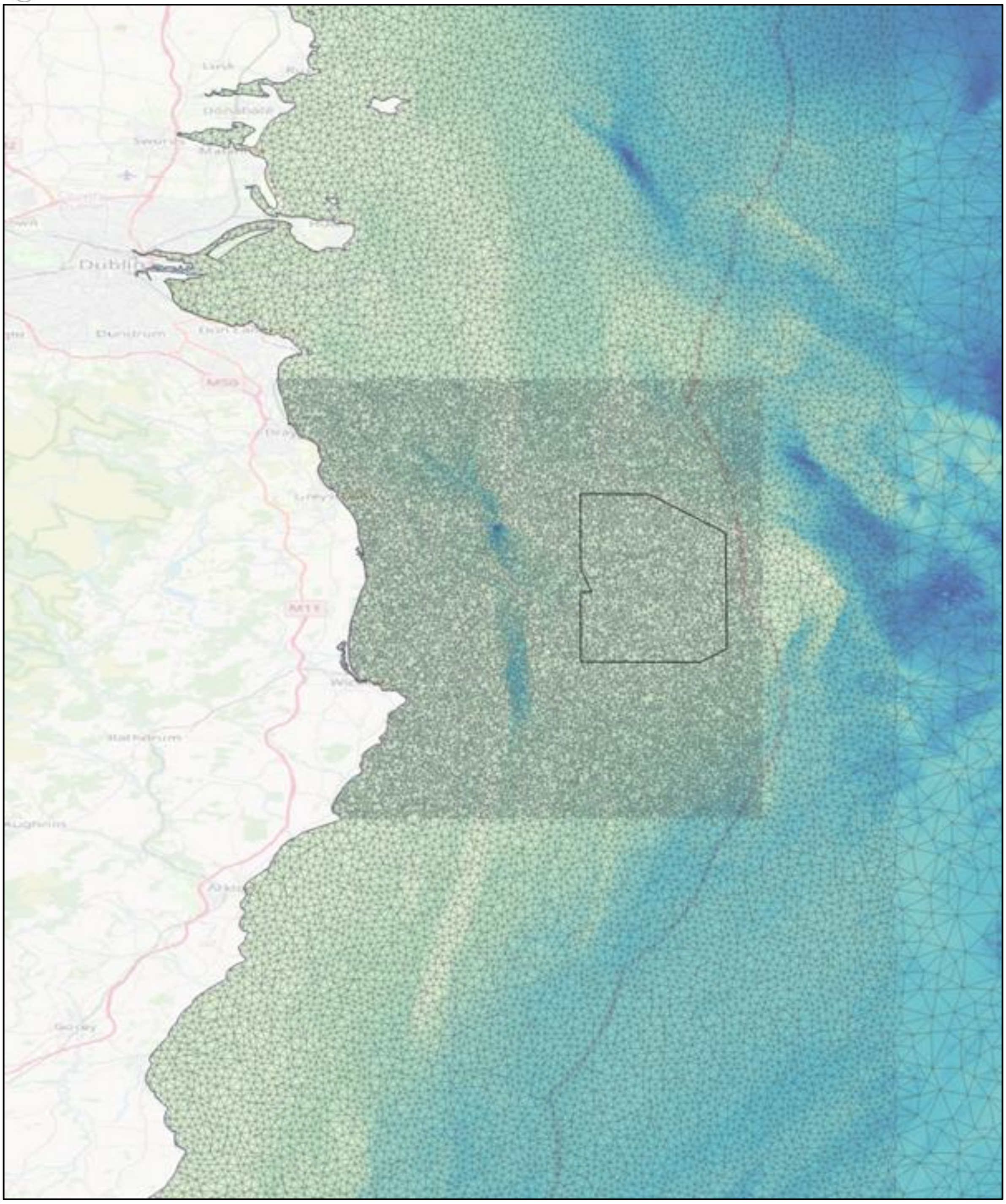

Figure 1. The model domain, flexible model mesh and implemented bathymetry. The higher-resolution model mesh coincident with the proposed development area, cable routes and adjacent coastline of Ireland is shown.

2.3 Model Setup and Parameterisation

Within the wave model, the JONSWAP (Joint North Sea Wave Project) bottom friction formulation was utilised, and depth-limited wave breaking was modelled according to the bore-model of Battjes and Janssen (1978). Wave spectra were discretised using 36 directions and 36 frequencies from 0.0345 to 0.9695Hz and diffraction was included. The wind forcing from ERA5 was nested into the model using a linear interpolation. The model was run in non-stationary mode to allow for proper wave growth within the model domain. Wave and hydrodynamic data were output from the model at the timestep of 1 hour. Table 1 details the main parameters that were used to set-up the model.

Table 1: Parameters used in the setup of the hydrodynamic and wave model.

Parameters	Settings
Critical CFL number	0.8
Drying, flooding and wetting depth	0.01 m, 0.05 m, and 0.1 m
Horizontal eddy viscosity	Smagorinsky, 0.28
Bed resistance	Manning's N varied between 26 and 34

3 Model Calibration Validation – Stage 1

Model calibration is a process whereby model skill is incrementally improved as model predictions are compared with physical observations/measurements of the same parameter. Model validation is the process by which model skill is demonstrated by comparing model predictions against physical observations/measurements.

Model calibration validation was performed using several hydrodynamic and wave datasets acquired from within the MAC application boundary and the region proximal to the development area. To calibrate the model and improve upon the skill of the model in predicting oceanographic phenomena, the bed friction and diffusion/dispersion coefficients were adjusted within the model to obtain the best fit against the observation data.

3.1 Quality Control of Measured Data

Uniquely, a comparable model validated against the same site specific and publicly available measured datasets has been developed during a study for the purposes of engineering design (MetOceanWorks, 2022)[2]. This study identified several relevant issues within the metocean measurement data record that were acquired from within the MAC application boundary, including the provision of erroneous results. Quality control of these data performed by MetOceanWorks (2022), reviewed, and corroborated during the present study, can be briefly summarised as follows:

- The data acquired from the Metocean Buoy, Wave Buoy 1 and Wave Buoy 2 provide reasonable quality wave measurements, however these buoys utilised a cut-off period of 12 s and so fail to capture any longer period swell waves. Periods of greater noise, which have not been resolved in post processing, are observed on individual instruments which is not seen across the measurement array. There is also concern raised regarding ambiguity as to how the wave parameters have been derived (i.e. how the significant wave height has been determined) and no spectra have been made available. In regard to current measurements, issues are also noted including a deterioration of measurement quality with depth generating what appear to be erroneous results.
- The data acquired by the two Floating LiDAR systems appear to provide what is considered to be reliable wave height parameters. However, concerns are raised regarding the determination of wave

2 Comparisons were also made against data extracted from 5 discrete locations across the development area from this model. Comparisons of predictions, though not presented within this report, showed generally good agreement.

periods given the size of the measurement platforms and nature of the mooring used. This can lead to an underestimation of wave heights and/or missing data during periods of higher frequency waves and a general bias towards longer wave periods. In addition, the current measurements acquired from instruments deployed on the two Floating LiDAR systems appear unreliable during periods when significant wave heights exceed circa 1 m.

- It is noted that the data acquired from the instrument deployed on the seabed frame provides the highest quality measurements which span the entire water column and provide good quality information.

Considering the outcome of the data review, and in accordance with recommendations from MetOceanWorks (2022), the current measurements acquired from the downward looking ADCP deployed on each of the two floating LiDAR systems has not been considered as part of the calibration and validation process. The measurement datasets utilised to support the calibration and validation of the hydrodynamic wave model are detailed in Table 2; the locations of these instruments are shown on a map of the region in Figure 2.

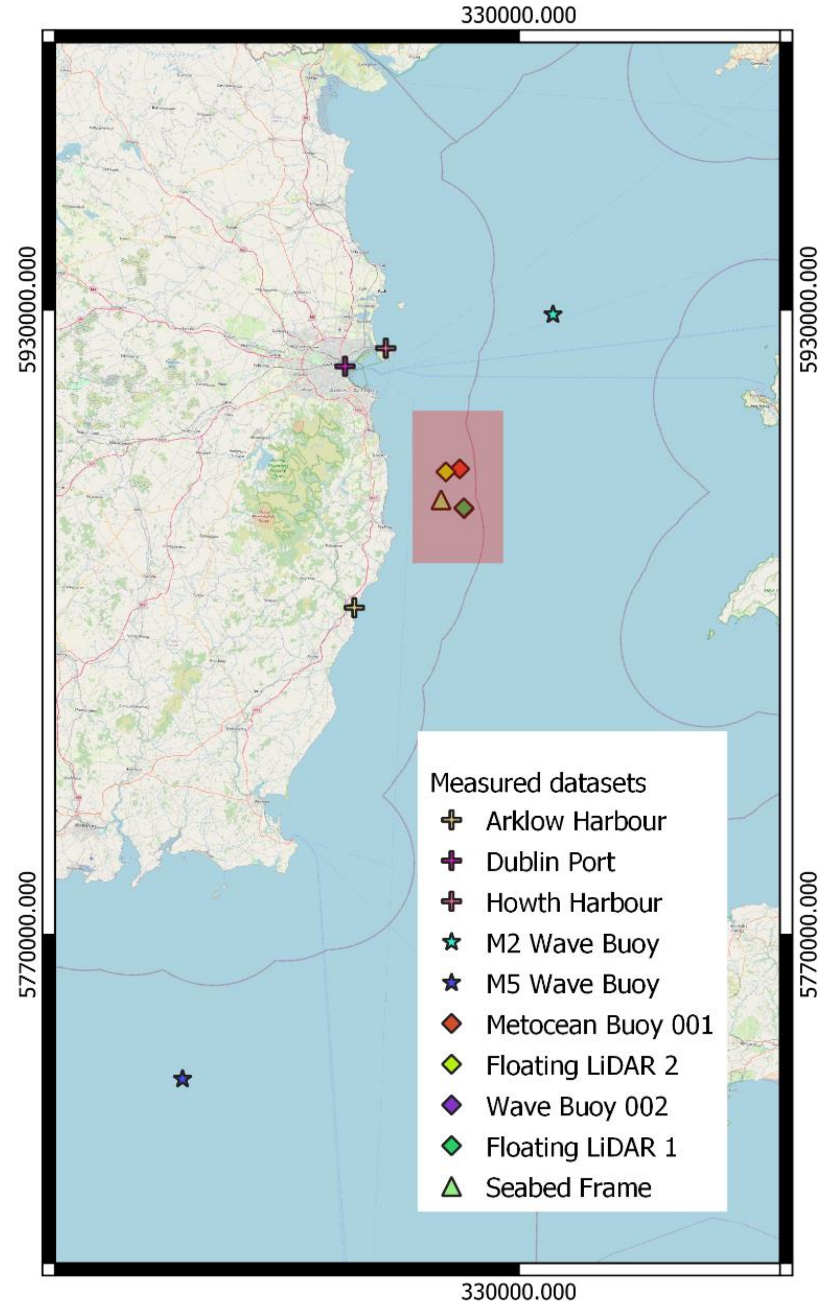

Figure 2. Locations of the measured data used as part of the calibration validation exercise.

Table 2: Data utilised in the calibration and validation of the model.

Data ID	Data Type and utilisation	Coverage Period		Location	
		Begin	End	Latitude	Longitude
Dublin Port	Water level data, hydrodynamic model validation	26/7/2000	To Present	53.345	-6.221
Howth Harbour	Water level data, hydrodynamic model validation	18/11/2020	To Present	53.391	-6.068

Data ID	Data Type and utilisation	Coverage Period		Location	
		Begin	End	Latitude	Longitude
Arklow Harbour	Water level data, hydrodynamic model validation	04/01/2018	26/02/2019	52.792	-6.1452
M2 Wave Buoy	Wave data, wave model validation	03/05/2001	To Present	53.483	-5.430
M5 Wave Buoy	Wave data, wave model validation	18/10/2004	To Present	51.690	-6.704
Metocean Buoy 001	Wave data and ADCP (wave and currents), hydrodynamic and wave model validation	01/07/2021	30/11/2021	53.120	-5.766
Wave Buoy 001	Wave data, wave model validation	02/07/2021	30/11/2021	53.0432	- 5.6882
Wave Buoy 002	Wave data and ADCP (wave and currents), hydrodynamic and wave model validation	01/07/2021	30/11/2021	53.030	-5.743
Seabed Frame	ADCP Data (waves and currents), hydrodynamic and wave model validation	01/07/2021	30/11/2021	53.048	-5.832
Floating LiDAR 1	Wave Data and ADCP (ADCP data not used due to erroneous results), wave model validation	01/05/2021	01/11/2021	53.031	-5.744
Floating LiDAR 2	Wave Data and ADCP (ADCP data not used due to erroneous results), wave model validation	02/05/2021	03/11/2021	53.112	-5.818

3.2 Validation of the Wave Model Against Publicly Available Data

Wave predictions obtained from the model were validated against measurement data from the M2 and M5 monitoring buoys positioned along the east and southeast coast of Ireland (Figure 2). These two buoys form part of the Irish Marine Data Buoy Observation Network, which is managed by the Marine Institute Ireland in collaboration with Met Éireann and the UK Met Office. As part of the model validation process, comparisons were made against one-year (2018) of data retrieved from the public records. Model predictions over this period were compared with measured observations of T_p, T_z and H_s. Quantile / Quantile and scatter plot comparisons of modelled predictions vs measured observations are presented for the data acquired from the M2 and M5 buoy in Figure 3 and Figure 4, respectively. These comparisons are also presented in the form of time series for the data acquired from the M2 and M5 buoy in Figure 5 and Figure 6, respectively. The Root Mean Square Error (RMSE) between predictions and observations for each parameter are presented in Table 3.

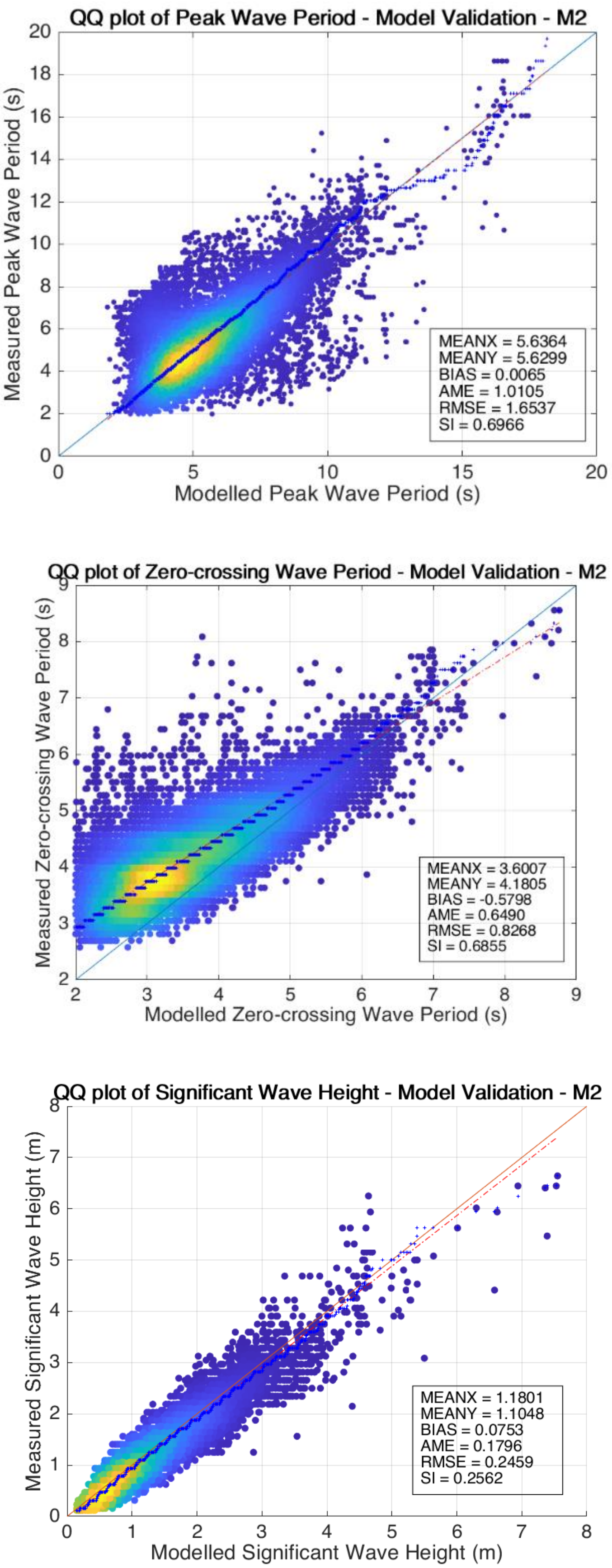

Figure 3. Quantile-Quantile and scatter comparisons of model predictions and measured data acquired by the M2 buoy for T_p, (top panel) T_z (middle panel) and H_s (bottom panel).

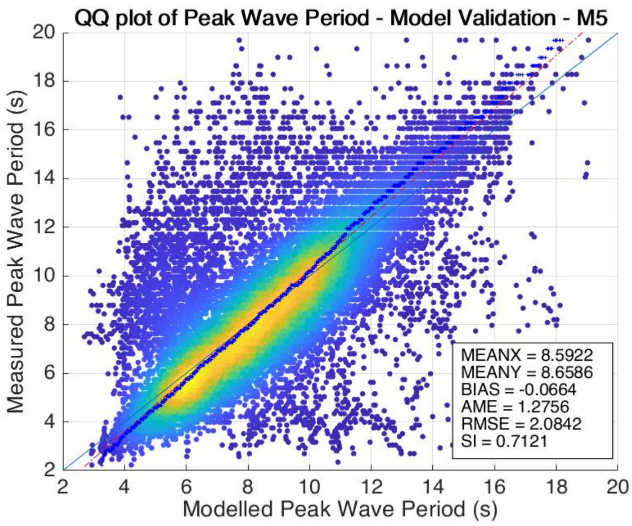

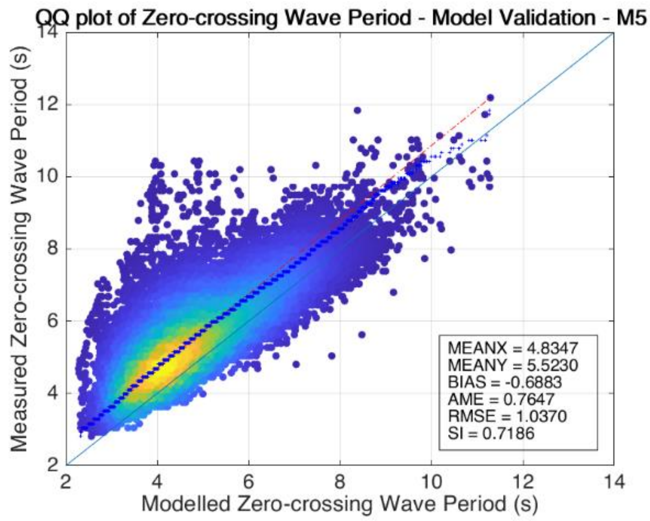

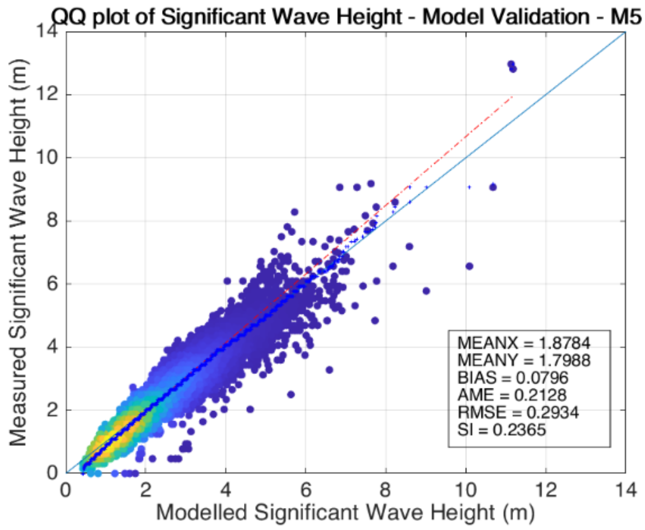

Figure 4. Quantile-Quantile and scatter comparisons of model predictions and measured data acquired by the M5 buoy for T_p, (top panel) T_z (middle panel) and H_s (bottom panel).

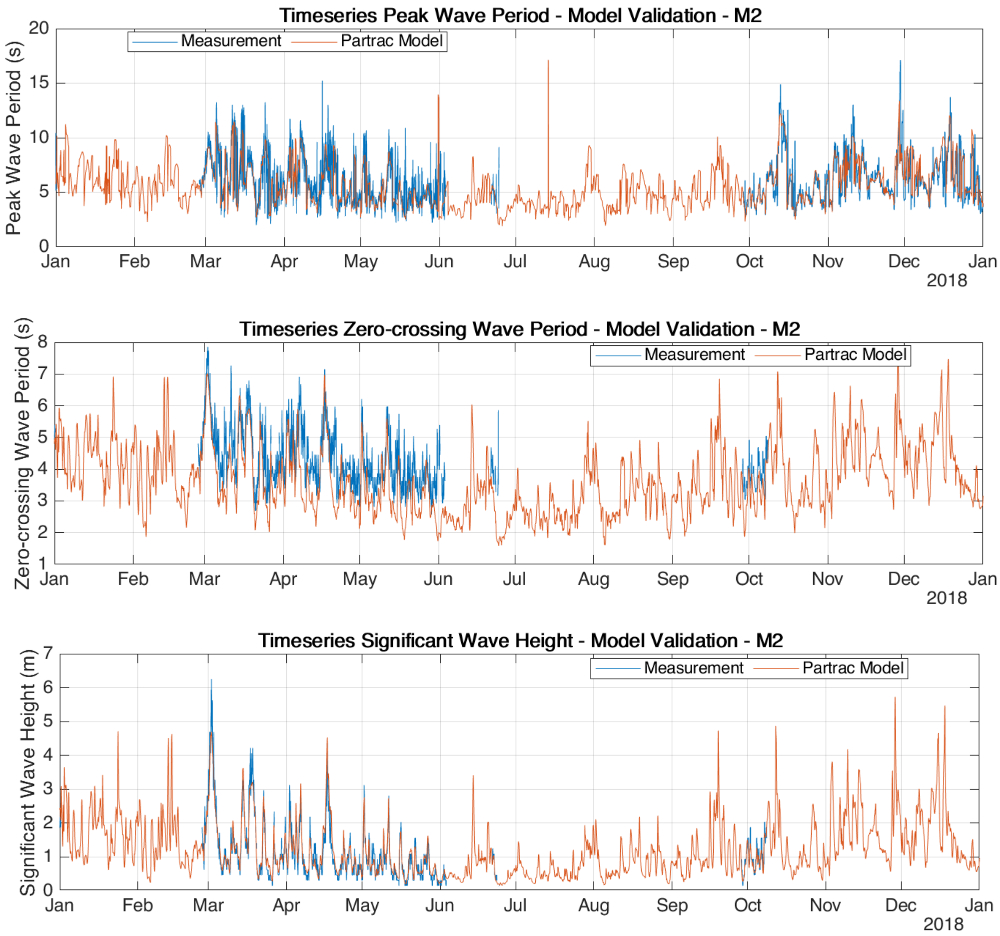

Figure 5: Time series showing coincident model predictions and measured data acquired by the M2 buoy data for T_p, (top panel) T_z (middle panel) and H_s (bottom panel).

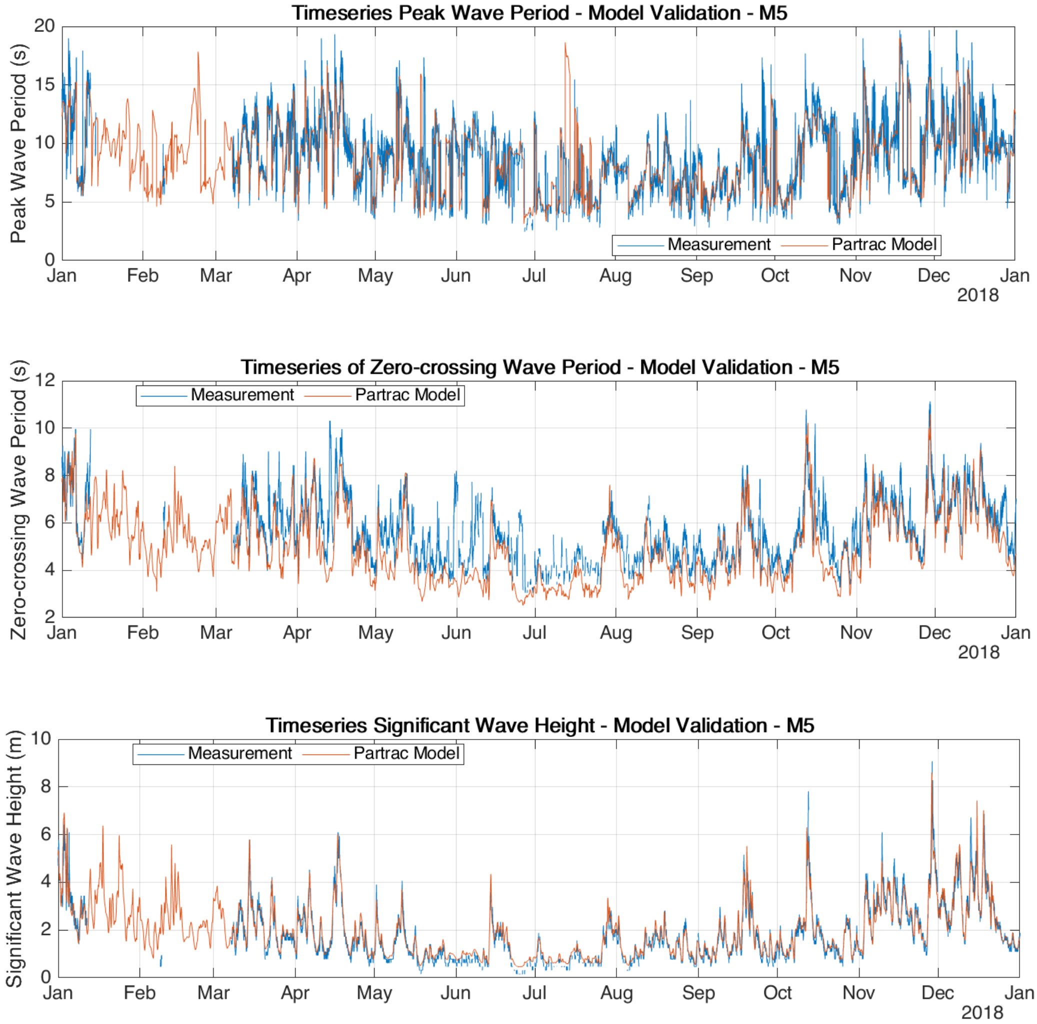

Figure 6. Time series showing coincident model predictions and measured data acquired by the M5 buoy data for T_p, (top panel) T_z (middle panel) and H_s (bottom panel).

Table 3. Root Mean Square Error (RMSE) values obtained from the validation of the wave model against data acquired from the public data records.

Location	Variable	RMSE
M2 Wave buoy	T_p	1.65
	T_z	0.83
	H_s	0.25
M5 Wave buoy	T_p	2.08
	T_z	1.03
	H_s	0.29

3.1 Validation of the Wave Model Against Site Measurement Data

Wave predictions obtained from the model were also validated against measurement data acquired from several locations within the MAC application boundary (Figure 2). Oceanographic instrumentation was deployed including a seabed frame mounted ADCP, three surface riding wave buoys (termed Wave Buoy 001 and 002 and Metocean Buoy 001) and two larger floating LiDAR system's which included wave sensors (termed FLiDAR Buoy 001 and 002). Following quality control of the data received, comparisons were made against all coincident data received to date that were deemed acceptable for model validation (see Section 3.1). Model predictions over this period were compared with measured observations for T_p, T_z and H_s. Quantile / Quantile and scatter plot comparisons of modelled predictions vs measured observations are presented for each monitoring location in Figure 7 to Figure 12 . These comparisons are also presented in the form of time series in Figure 13 to Figure 18. The RMSE between predictions and observations for each parameter, and each monitoring platform, are presented in Table 4.

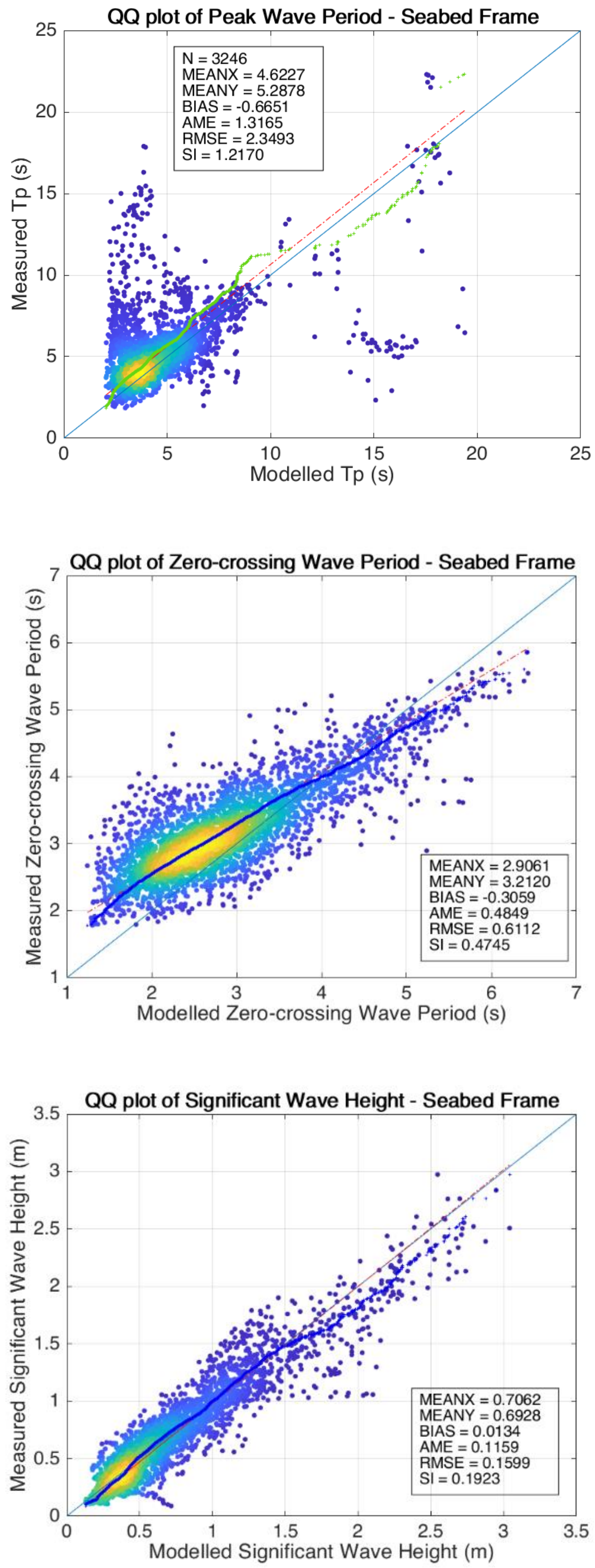

Figure 7. Quantile-Quantile and scatter comparisons of model predictions and measured data acquired by the seabed frame mounted ADCP for T_p, (top panel) T_z (middle panel) and H_s (bottom panel).

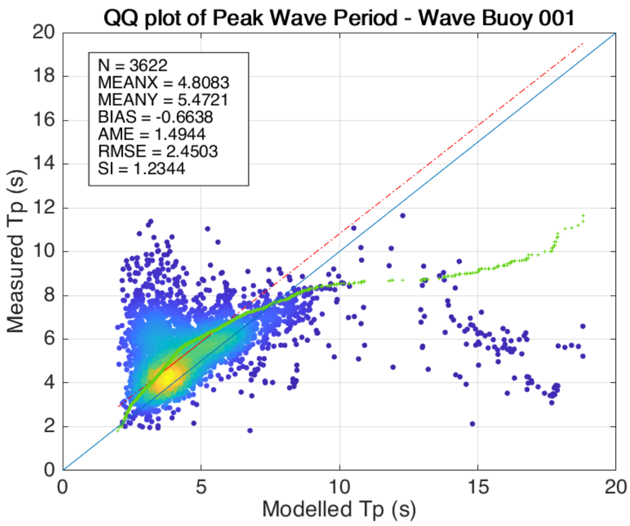

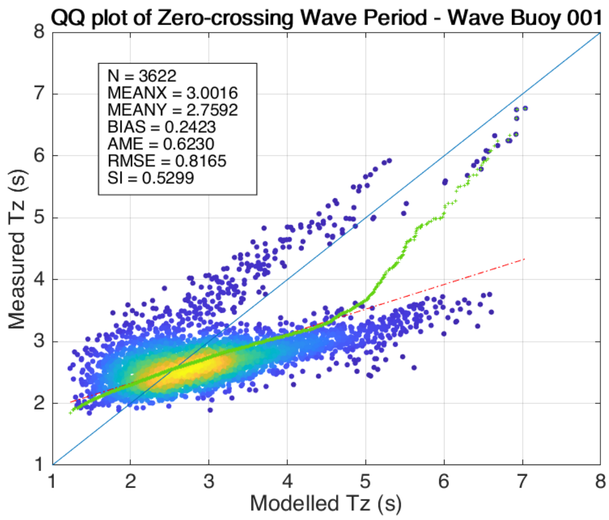

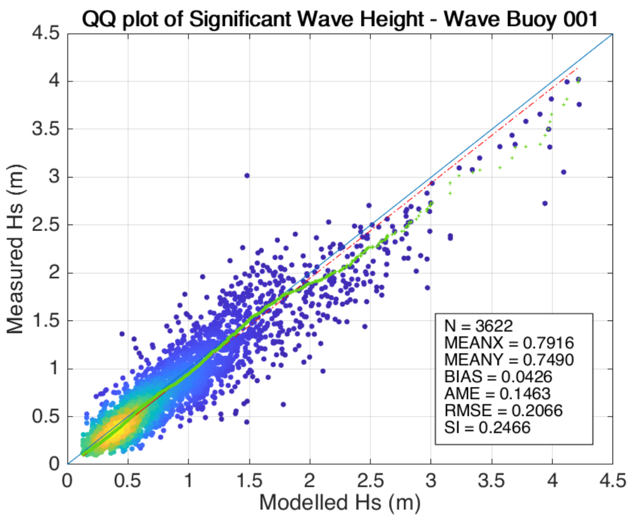

Figure 8. Quantile-Quantile and scatter comparisons of model predictions and measured data acquired by Wave Buoy 001 for T_p, (top panel) T_z (middle panel) and H_s (bottom panel).

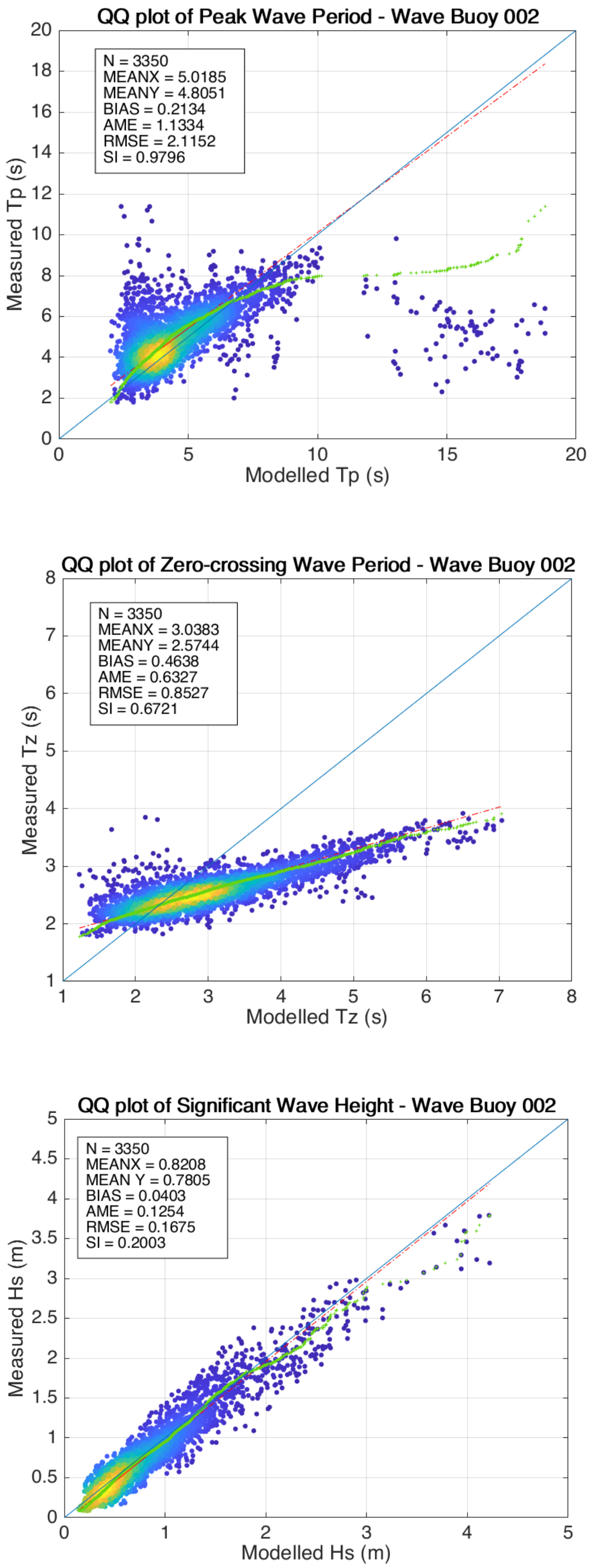

Figure 9. Quantile-Quantile and scatter comparisons of model predictions and measured data acquired by Wave Buoy 002 for T_p, (top panel) T_z (middle panel) and H_s (bottom panel).

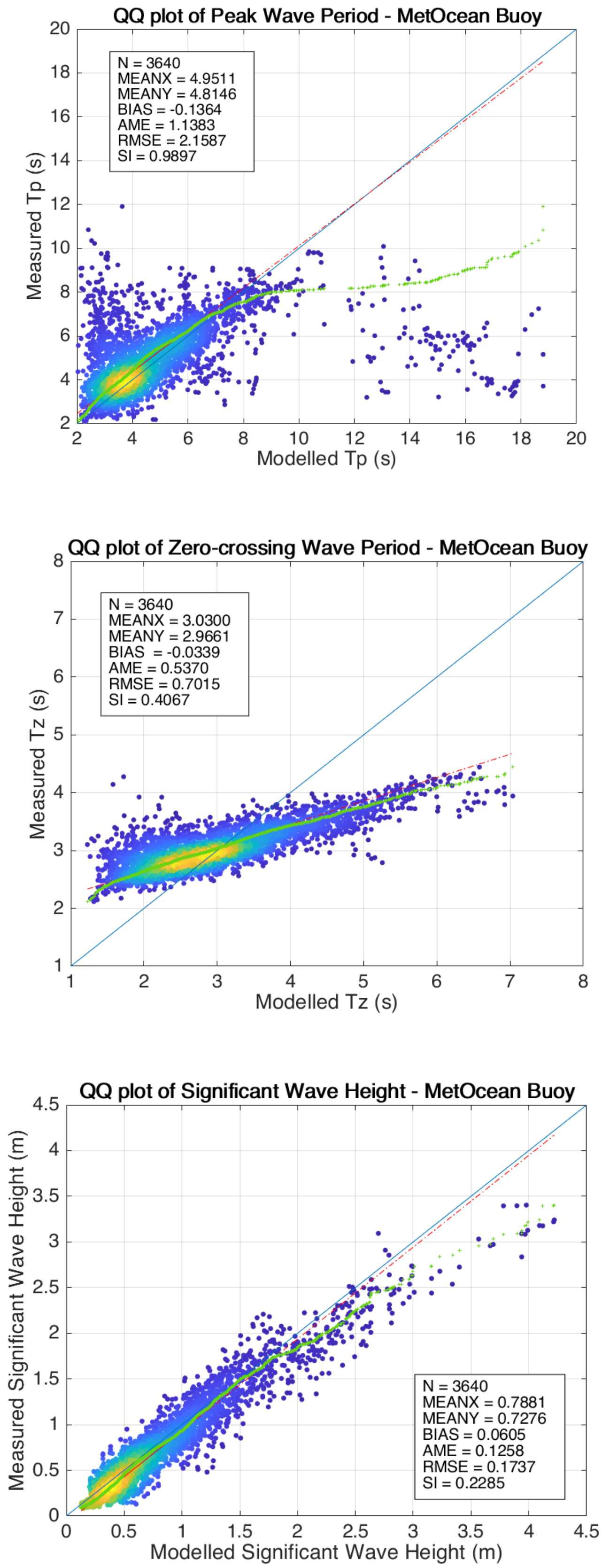

Figure 10. Quantile-Quantile and scatter comparisons of model predictions and measured data acquired by the Metocean buoy 001 for T_p, (top panel) T_z (middle panel) and H_s (bottom panel).

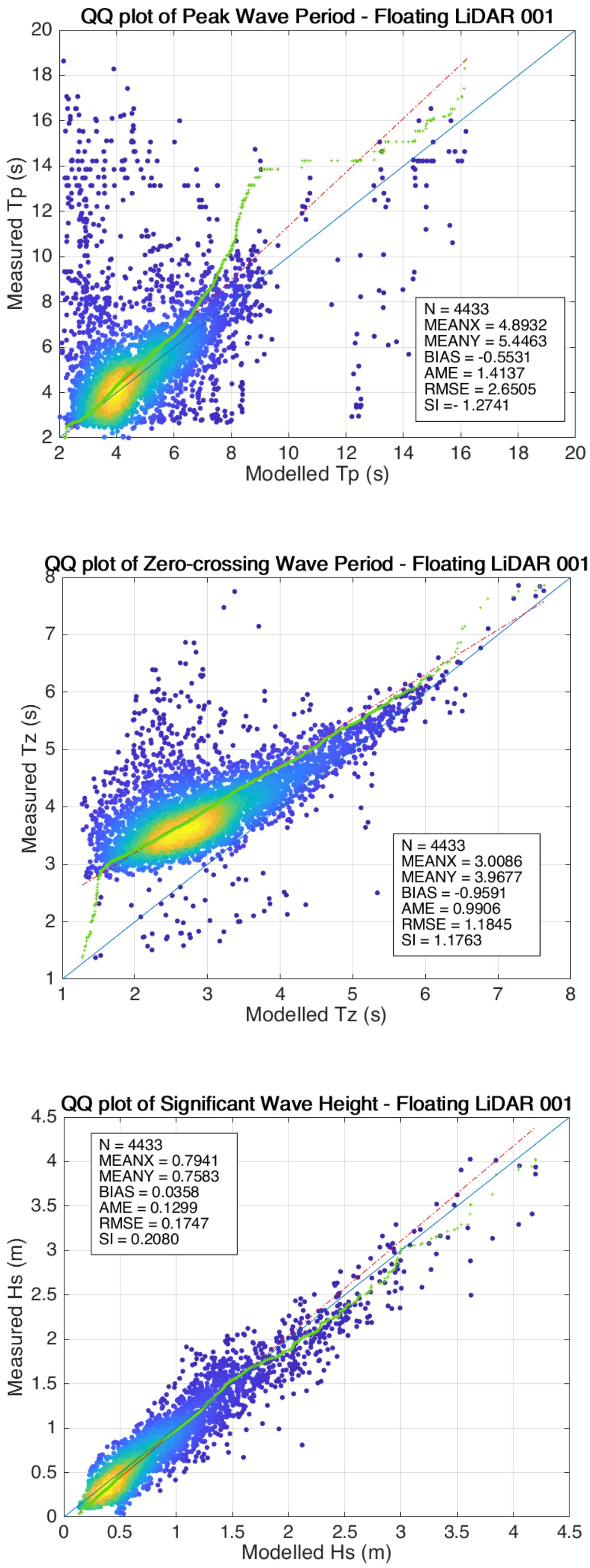

Figure 11. Quantile-Quantile and scatter comparisons of model predictions and measured data acquired by the Floating LiDAR buoy 001 for T_p, (top panel) T_z (middle panel) and H_s (bottom panel).

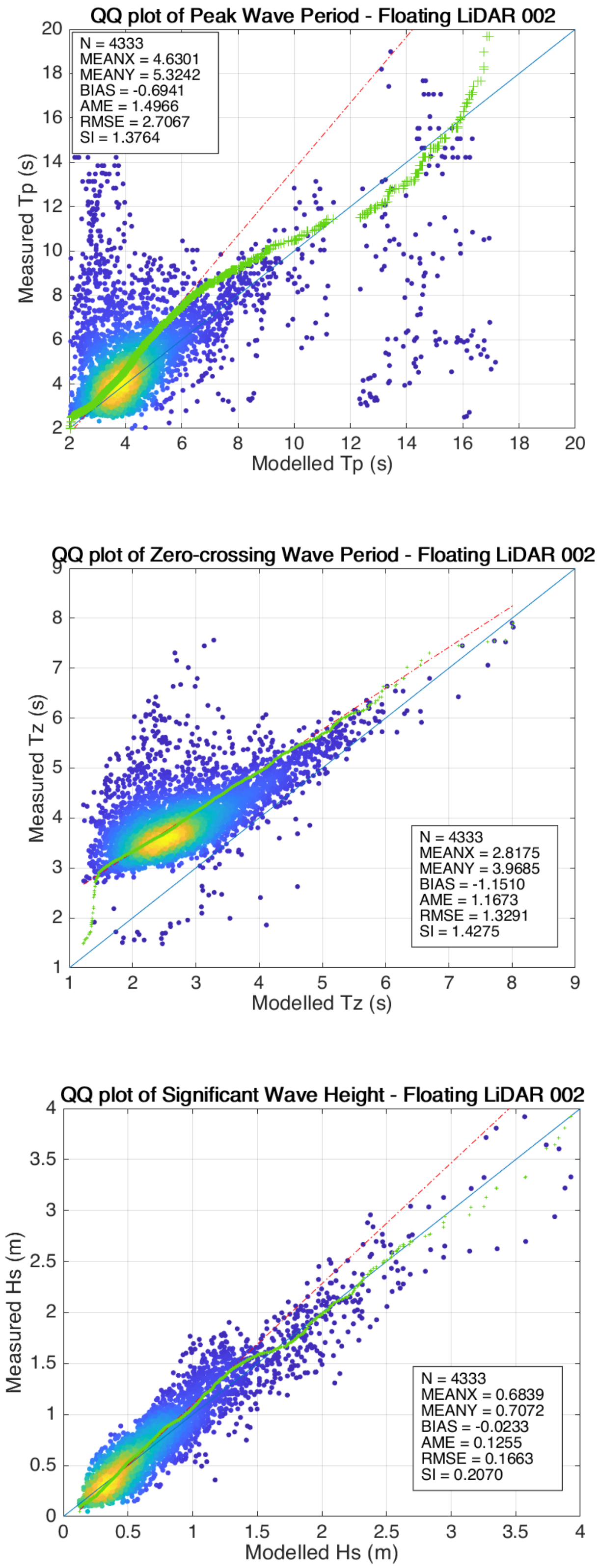

Figure 12. Quantile-Quantile and scatter comparisons of model predictions and measured data acquired by the Floating LiDAR buoy 0021 for T_p, (top panel) T_z (middle panel) and H_s (bottom panel).

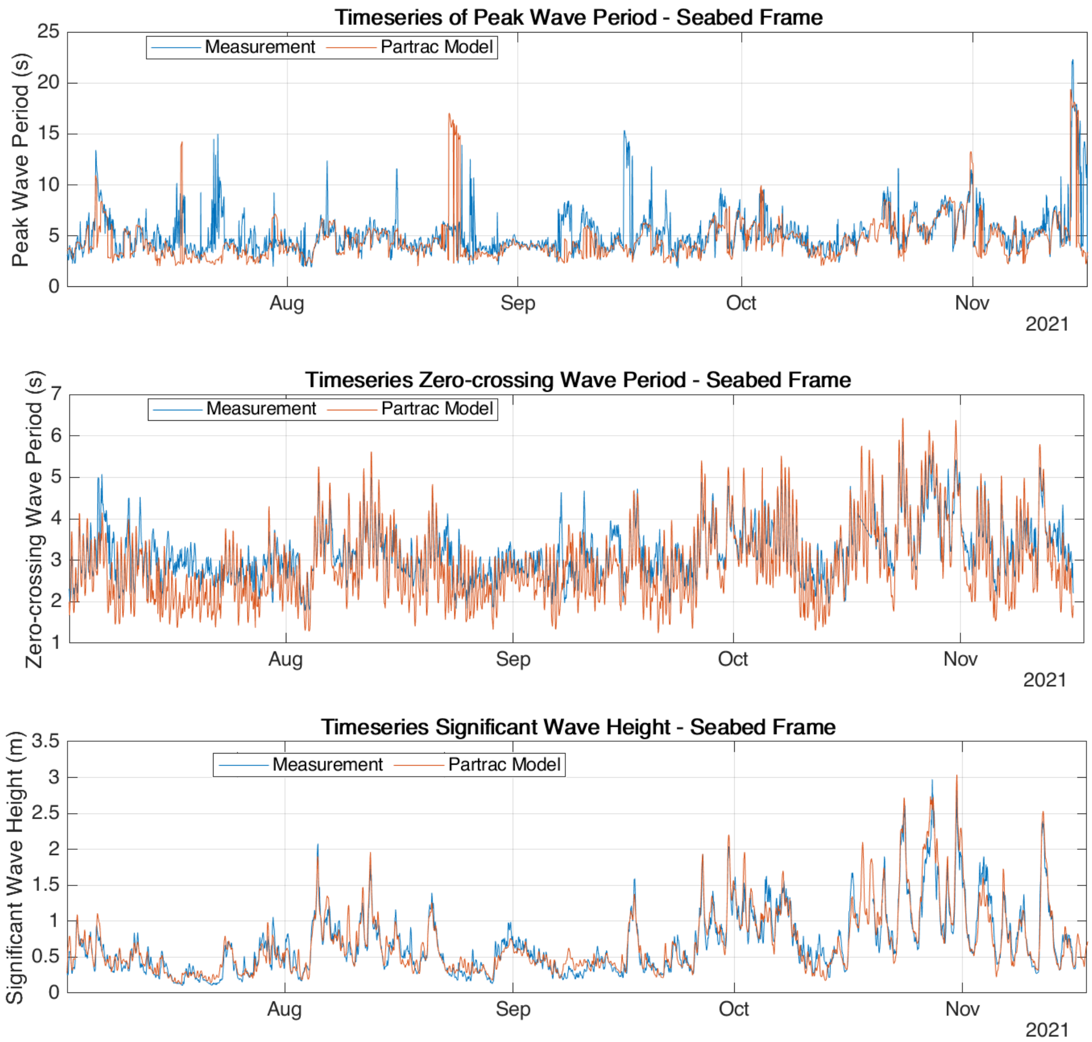

Figure 13: Time series showing coincident model predictions and measured data acquired by the *seabed frame mounted ADCP for T_p, (top panel) T_z (middle panel) and H_s (bottom panel).*

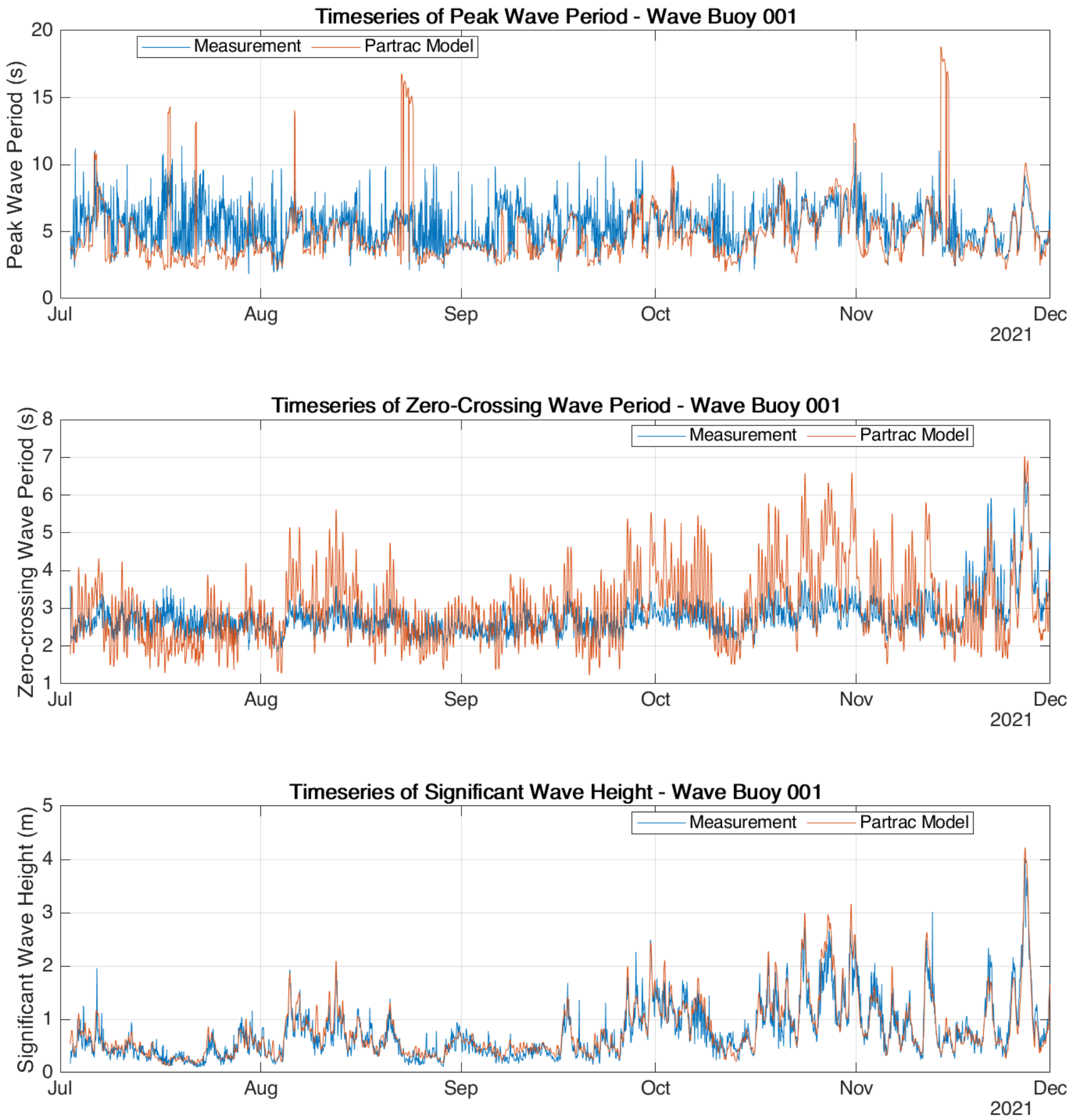

Figure 14. Time series showing coincident model predictions and measured data acquired by the *Wave Buoy 001 for T_p, (top panel) T_z (middle panel) and H_s (bottom panel).*

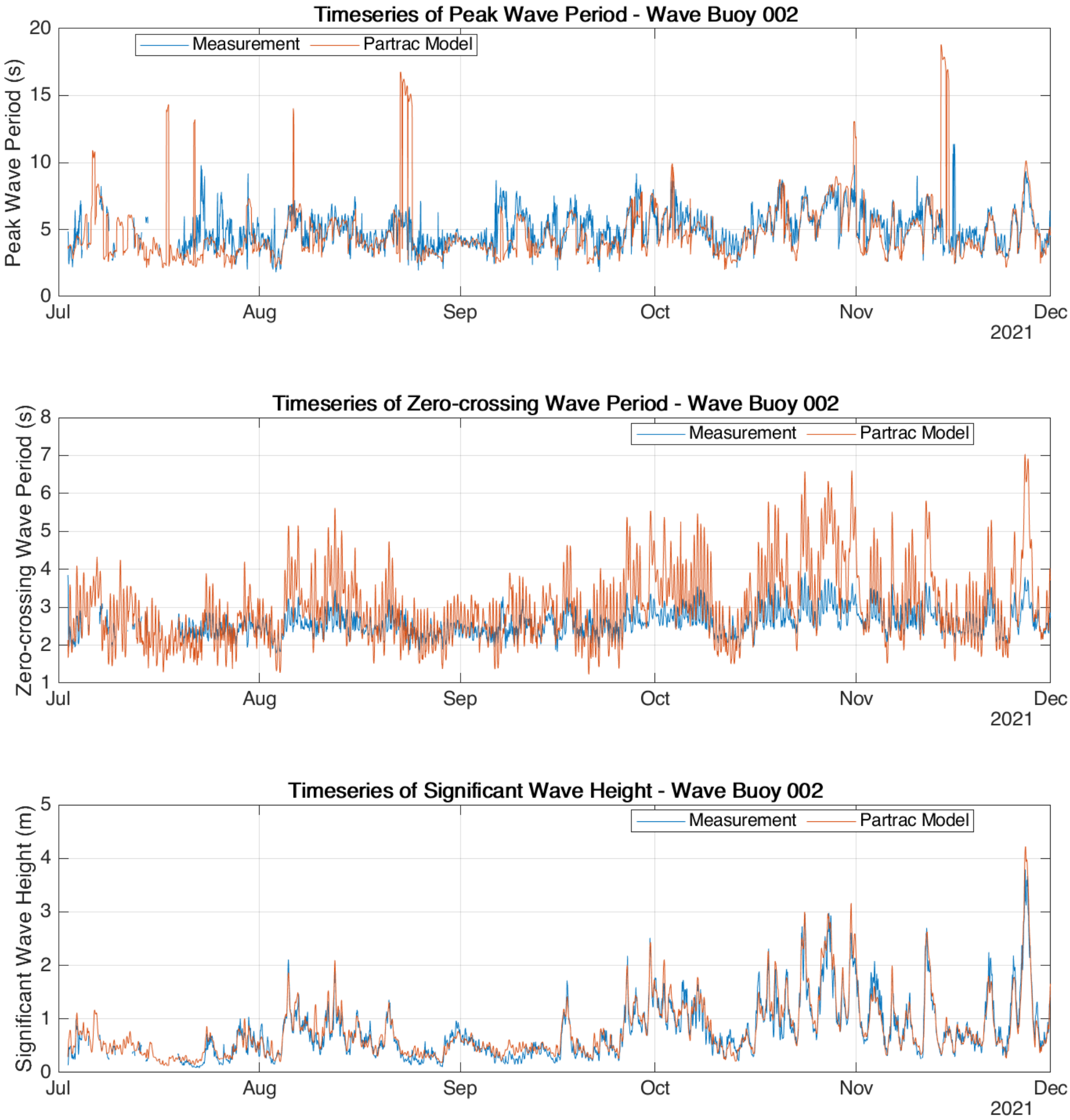

Figure 15. Time series showing coincident model predictions and measured data acquired by the Wave Buoy 002 for T_p, (top panel) T_z (middle panel) and H_s (bottom panel).

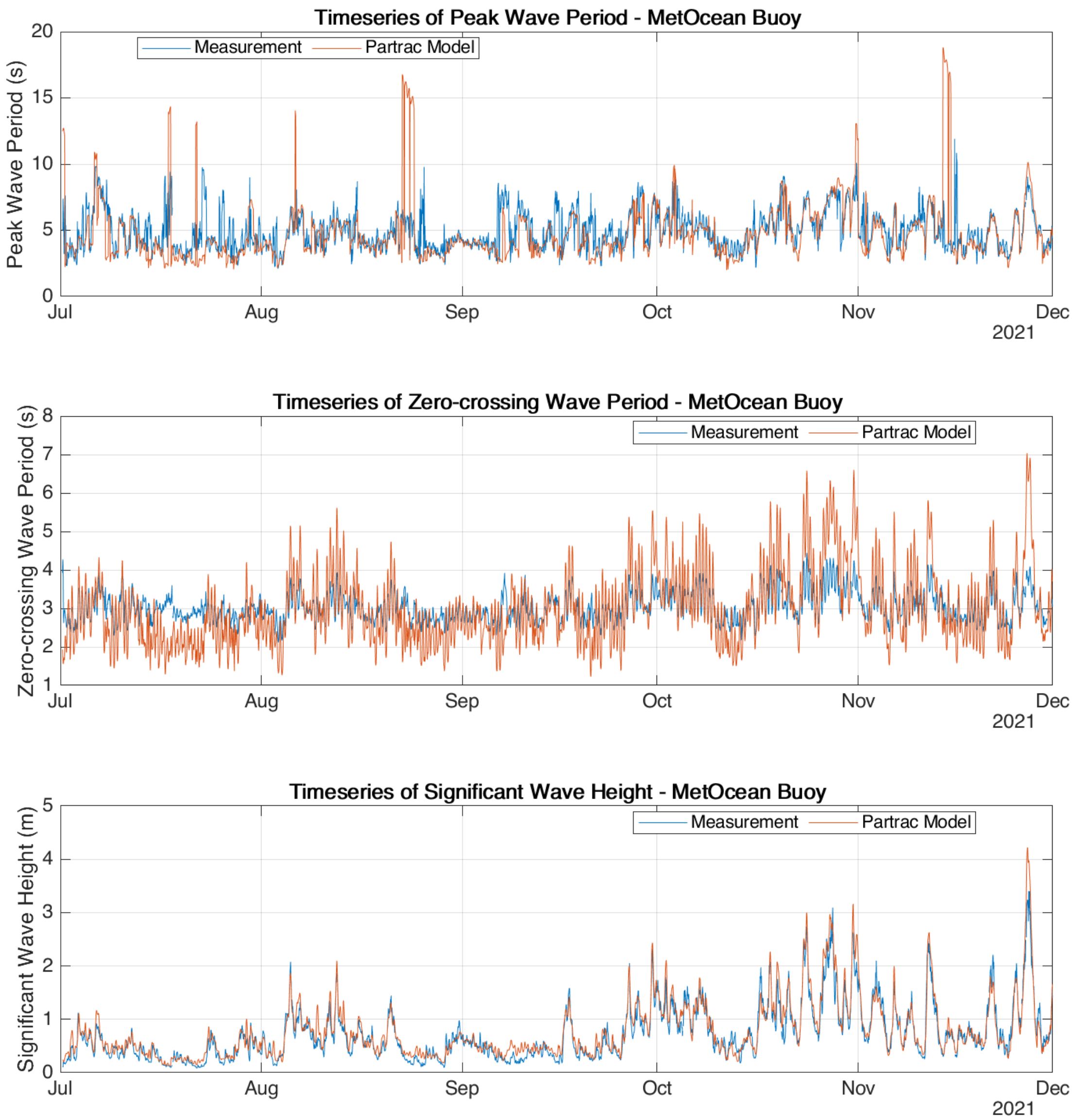

Figure 16. Time series showing coincident model predictions and measured data acquired by the Metocean buoy001 for T_p, (top panel) T_z (middle panel) and H_s (bottom panel).

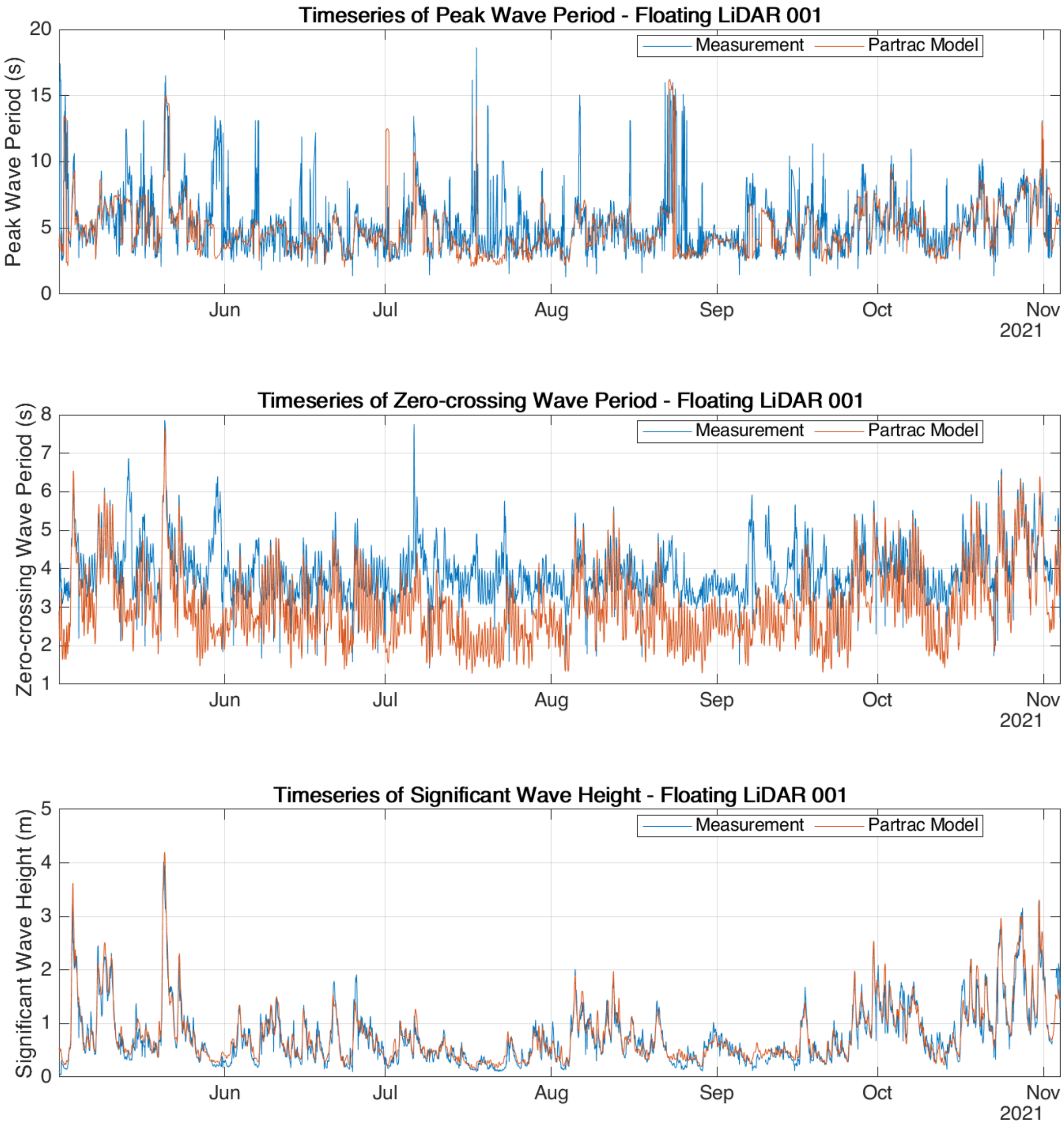

Figure 17. Time series showing coincident model predictions and measured data acquired by the *Floating LiDAR buoy 001 for T_p, (top panel) T_z (middle panel) and H_s (bottom panel).*

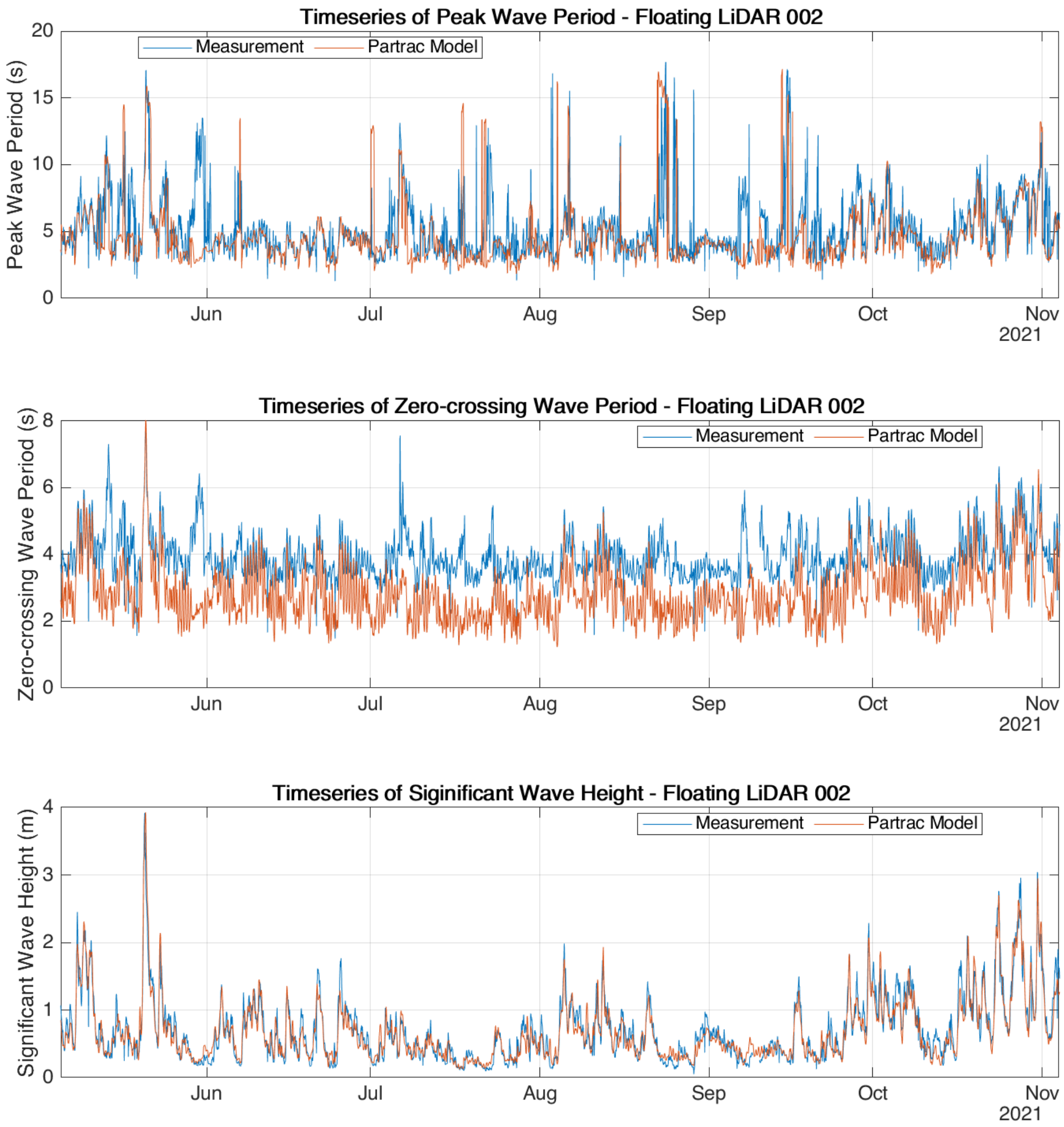

Figure 18. Time series showing coincident model predictions and measured data acquired by the *Floating LiDAR buoy 002 for T_p, (top panel) T_z (middle panel) and H_s (bottom panel).*

Table 4: Root Mean Square Error (RMSE) values obtained from the validation of the wave model against data acquired from the site.

Location	Variable	RMSE
Wave buoy 001	T_p	2.45
	T_z	0.82
	H_s	0.21
Wave buoy 002	T_p	2.12
	T_z	0.85
	H_s	0.17
Metocean buoy 001	T_p	2.16

Location	Variable	RMSE
	T_z	0.70
	H_s	0.12
FLlidar 001	T_p	2.65
	T_z	1.18
	H_s	0.17
FLidar 002	T_p	2.71
	T_z	1.33
	H_s	0.17
Seabed Frame mounted ADCP	T_p	2.35
	T_z	0.61
	H_s	0.16

3.2 Validation of the Hydrodynamic Model Against Publicly Available Data

Predictions of water level obtained from the model were validated against measurements from three tide gauges along the Irish Coast located at Arklow Harbour, Dublin Port and Howth Harbour (Figure 2). These tide gauges form part of the Irish National Tide Gauge Network (ITGN) which is managed by the Marine Institute Ireland. As part of the model validation process, comparisons were made against one-year (2018) of data retrieved from the public records. Model predictions over this period were compared with measured observations of water level relative to MSL. Quantile / Quantile and scatter plot comparisons of modelled predictions vs measured observations are presented for the data acquired from the three tide gauges in Figure 19. These comparisons are presented in the form of time series in Figure 20. The RMSE between predictions and observations for each parameter are presented in Table 5.

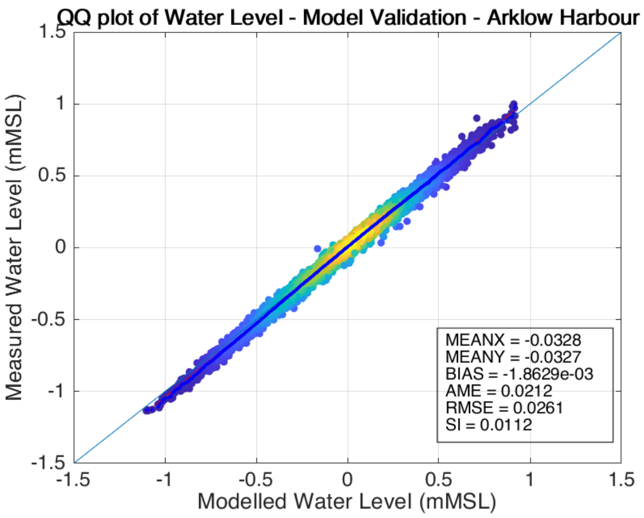

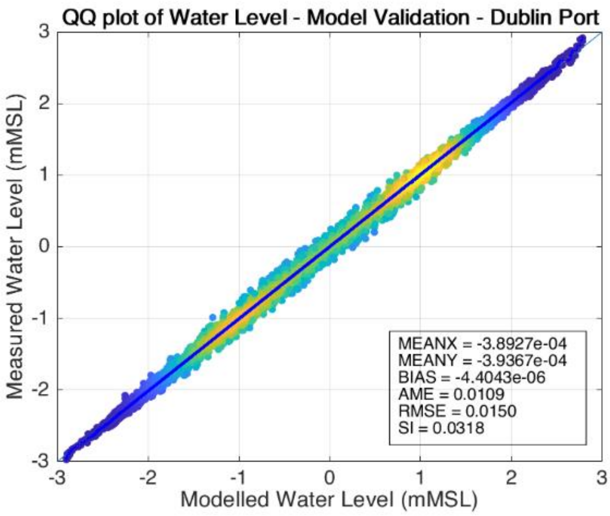

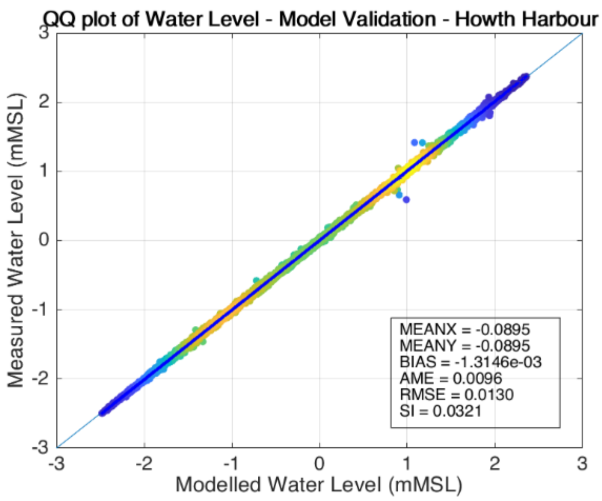

Figure 19. Quantile-Quantile and scatter comparisons of model predictions and measured data acquired by the tide gauges installed at Arklow Harbour (top panel), Dublin Port (middle panel) and Howth Harbour (bottom panel).

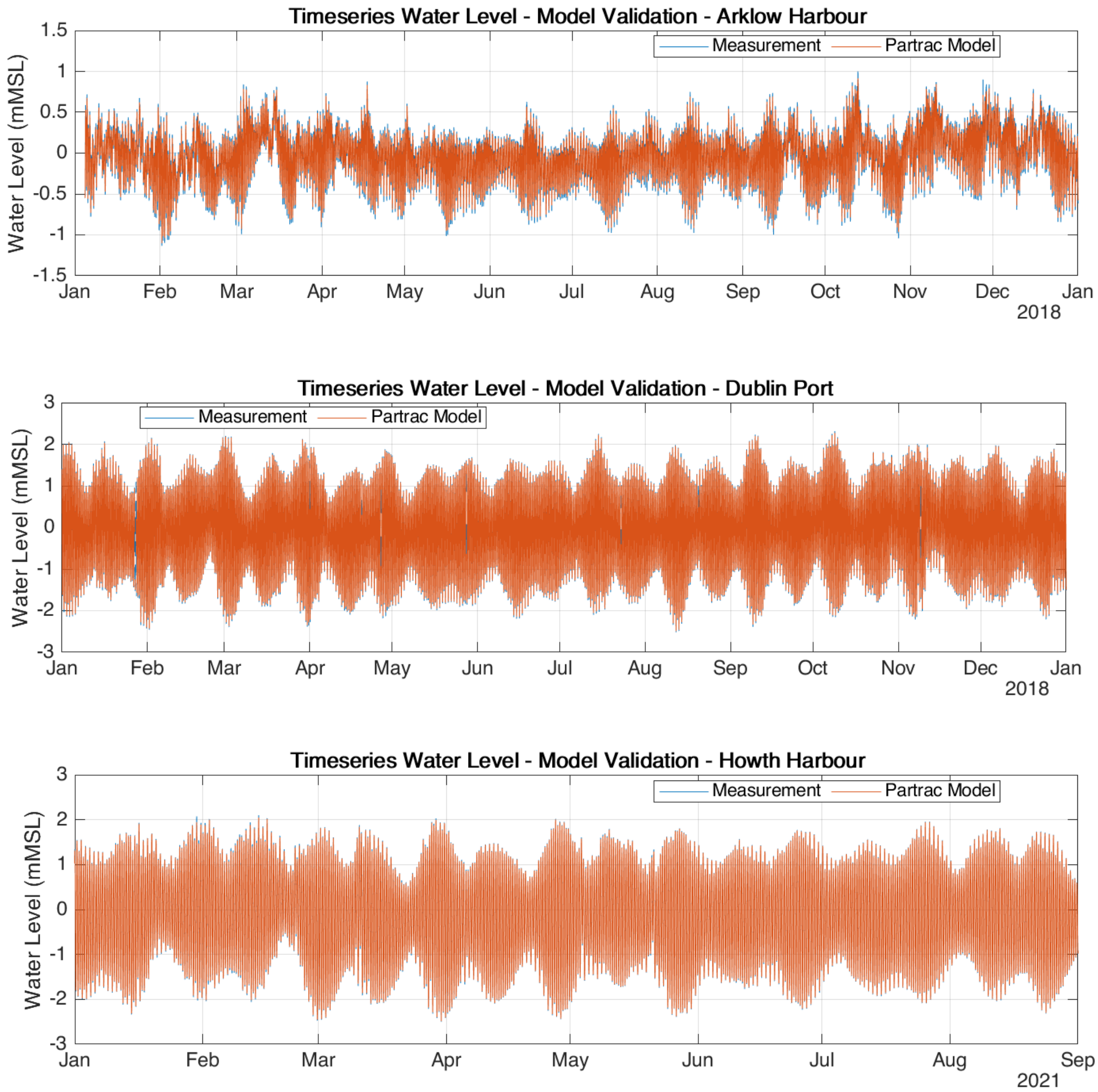

Figure 20: Time series showing coincident model predictions and measured data acquired by the by the tide gauges installed at Arklow Harbour (top panel), Dublin Port (middle panel) and Howth Harbour (bottom panel).

Table 5. Root Mean Square Error (RMSE) values obtained from the validation of the hydrodynamic model against water level data acquired from the public data records.

Location	Variable	RMSE
Arklow Harbour	Water level (mMSL)	0.03
Dublin Port	Water level (mMSL)	0.02
Howth Harbour	Water level (mMSL)	0.01

3.3 Validation of the Hydrodynamic Model Against Site Measurement Data

Hydrodynamic predictions obtained from the model were also validated against data acquired from across the proposed development area (Figure 2). Hydrodynamic measurements were acquired from instrumentation deployed on the seabed frame, one of the surface riding buoys (i.e. Wave Buoy 002) and the Metocean Buoy. Comparisons were made against all coincident data received to date deemed acceptable for model validation (see Section 3.1). Model predictions over this period were compared with measured observations of current speed. Quantile / Quantile and scatter plot comparisons of modelled predictions vs measured observations are presented for each monitoring platform in Figure 21. These comparisons are also presented in the form of time series in Figure 22. The RMSE between predictions and observations for each parameter, and each monitoring platform, are presented in Table 6.

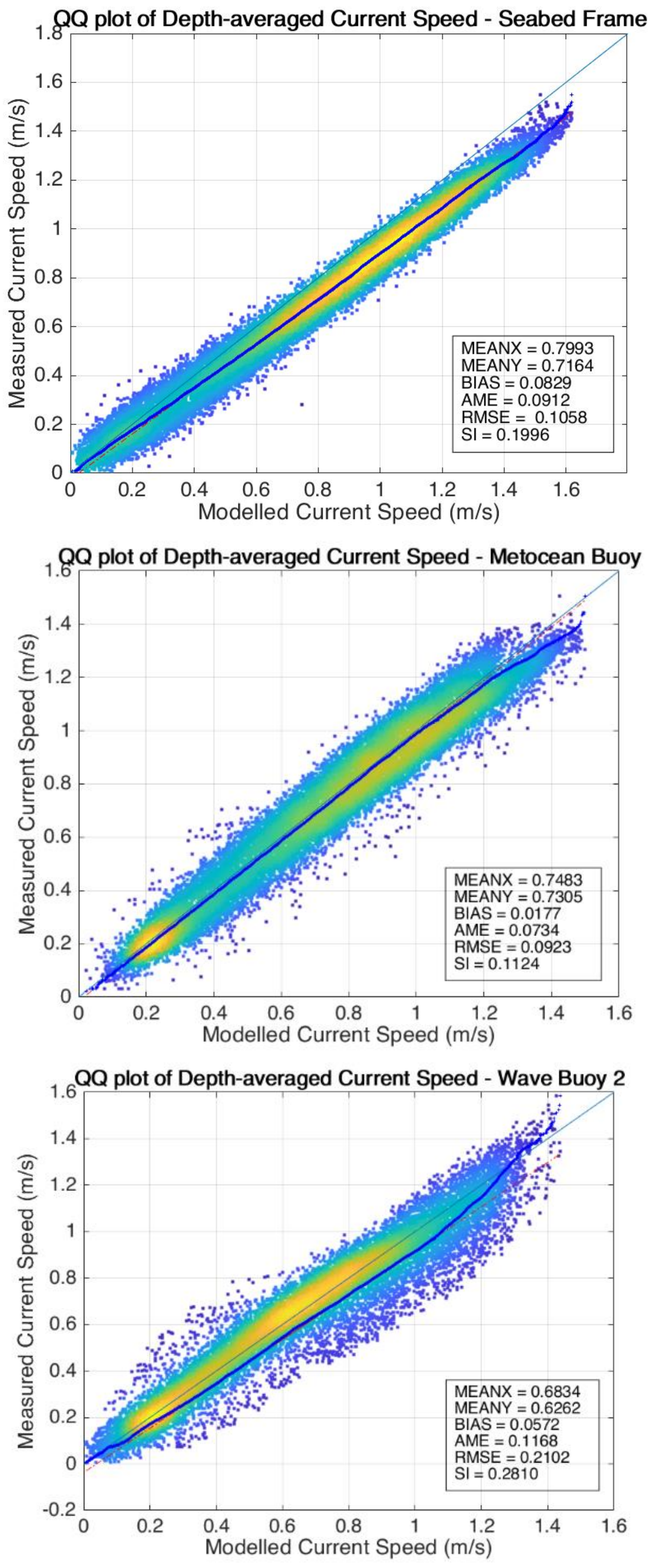

Figure 21. Quantile-Quantile and scatter comparisons of model predictions and measured data acquired by instruments deployed on the seabed frame (top panel), metocean buoy (middle panel) and wave buoy 2 (bottom panel).

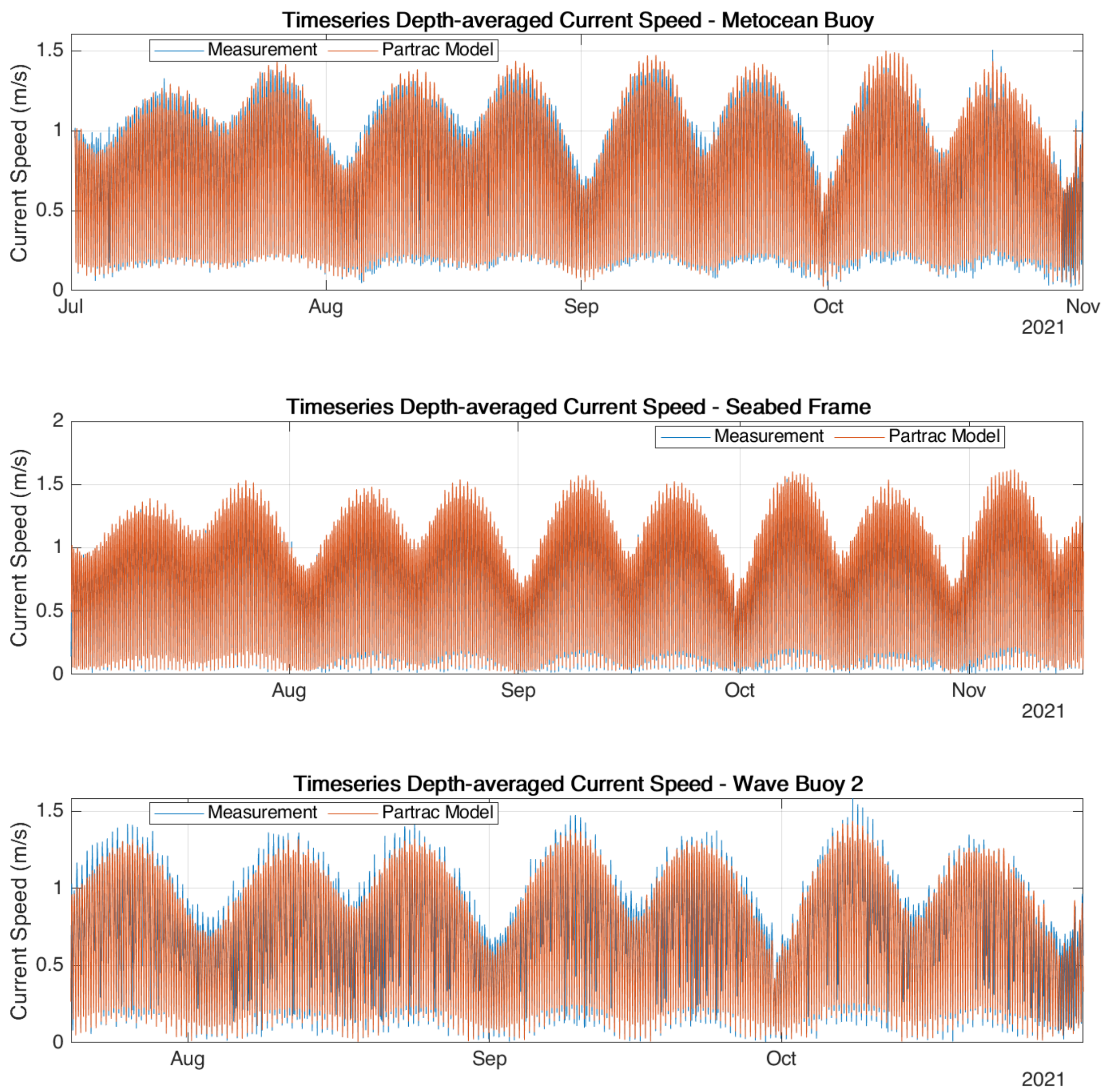

Figure 22: Time series showing coincident model predictions and measured data acquired by instruments deployed on the seabed frame (top panel), Metocean buoy 001 (middle panel) and Wave Buoy 2 (bottom panel).

Table 6. Root Mean Square Error (RMSE) values obtained from the validation of the hydrodynamic model against data acquired from the site.

Location	Variable	RMSE
Seabed frame	Current speed (m/s)	0.12
Metocean buoy 001	Current speed (m/s)	0.09
Wave buoy 2	Current speed (m/s)	0.21

4 Model Calibration Validation – Stage 2

In stage 2 of the model calibration validation exercise, measurements obtained between the 30th of November 2021 and the 8th of November 2022 at the locations shown in Figure 2 were utilised to further assess the performance of the model against site-specific measurements. Only parameters that were deemed appropriate for the purposes of model calibration validation were used to assess the model performance in this stage (see section 3.1). Table 7 details the data used in stage 2 of the calibration validation exercise.

Table 7: Data utilised in the calibration and validation of the model in Stage 2.

Data ID	Data Type and utilisation	Coverage Period		Location	
		Begin	End	Latitude	Longitude
Metocean Buoy 001	Wave data and ADCP (wave and currents), hydrodynamic and wave model validation	30/11/2021	04/07/2022	53.120	-5.766
Wave Buoy 002	Wave data and ADCP (wave and currents), hydrodynamic and wave model validation	30/11/2021	25/06/2022	53.030	-5.743
Seabed Frame	ADCP Data (waves and currents), hydrodynamic and wave model validation	30/11/2021	29/04/2022	53.048	-5.832
Floating LiDAR 1	Wave Data and ADCP (ADCP data not used due to erroneous results), wave model validation	24/06/2022	09/11/2022	53.031	-5.744
Floating LiDAR 2	Wave Data and ADCP (ADCP data not used due to erroneous results), wave model validation	24/06/2022	08/11/2022	53.112	-5.818

4.1 Validation of the Wave Model Against Site Data

Wave predictions obtained from the model were validated against the data received at the locations shown in Figure 2. Model predictions over this period were compared with measured observations for T_p, T_z, and H_s. Quantile / Quantile and scatter plot comparisons of modelled predictions vs measured observations are presented for each monitoring location in Figure 23 to Figure 27. These comparisons are also presented in the form of time series in Figure 28 to Figure 32. The RMSE between predictions and observations for each parameter, and each monitoring platform, are presented in

Table 8.

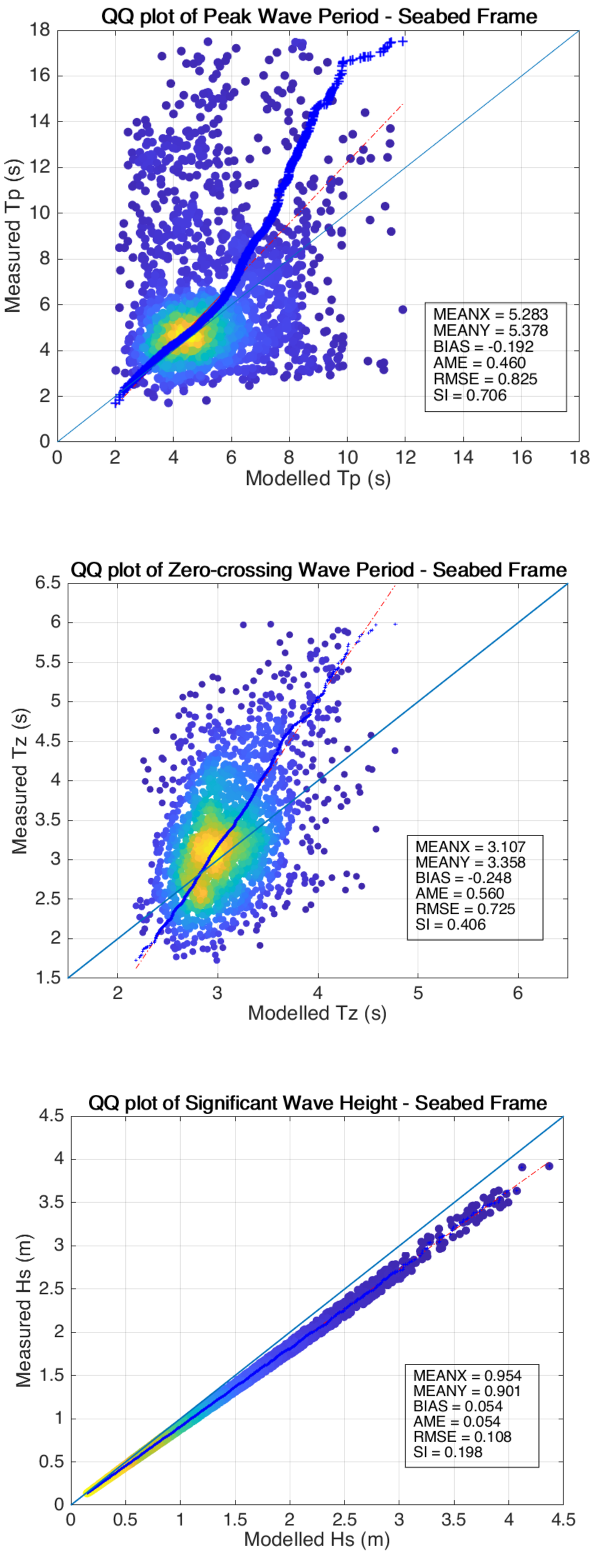

Figure 23. Quantile-Quantile and scatter comparisons of model predictions and measured data newly acquired by the seabed frame mounted ADCP for T_p, (top panel) T_z (middle panel) and H_s (bottom panel).

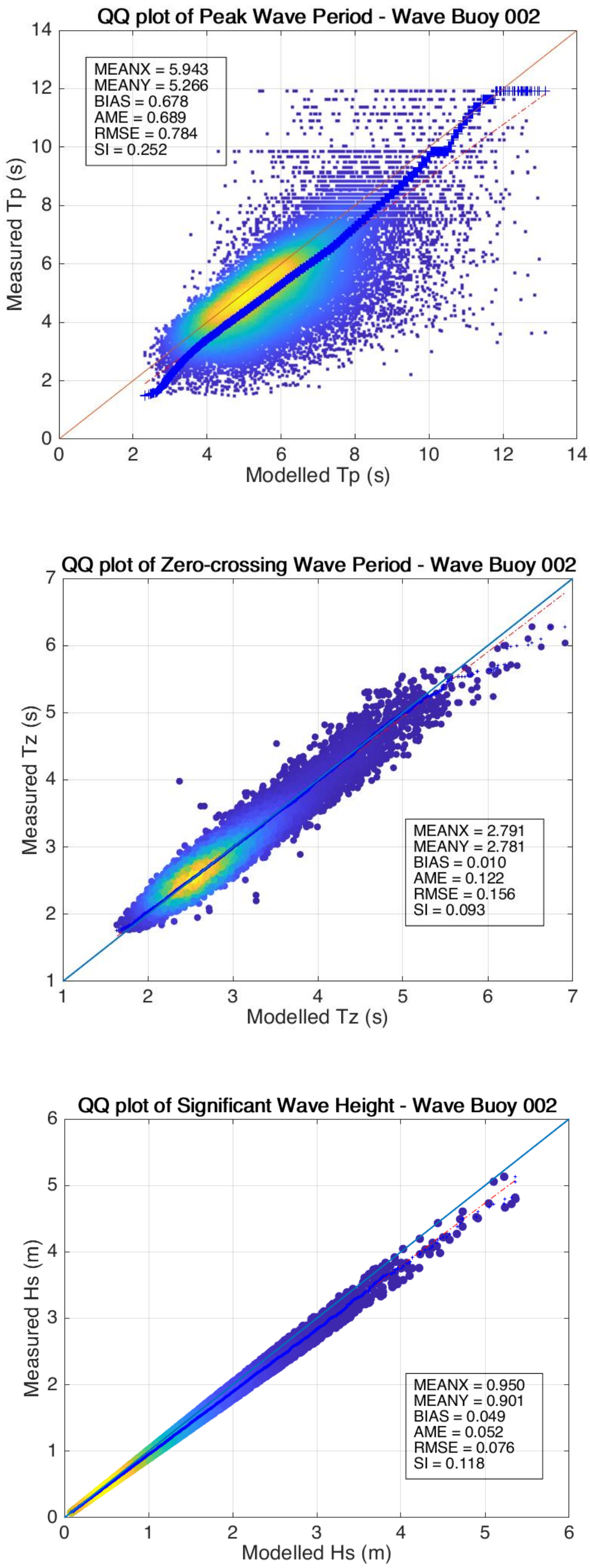

Figure 24. Quantile-Quantile and scatter comparisons of model predictions and measured data newly acquired by Wave Buoy 002 for T_p, (top panel) T_z (middle panel) and H_s (bottom panel).

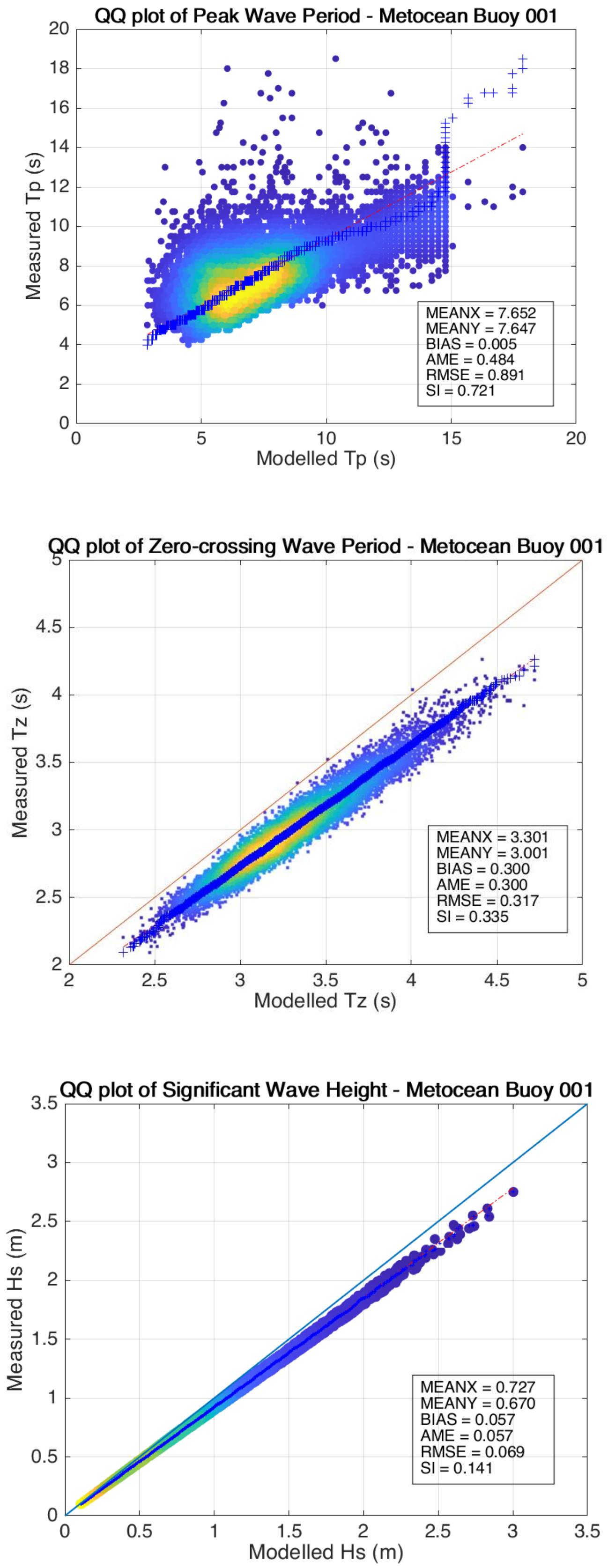

Figure 25. Quantile-Quantile and scatter comparisons of model predictions and measured data newly acquired by the Metocean buoy 001 for T_p, (top panel) T_z (middle panel) and H_s (bottom panel).

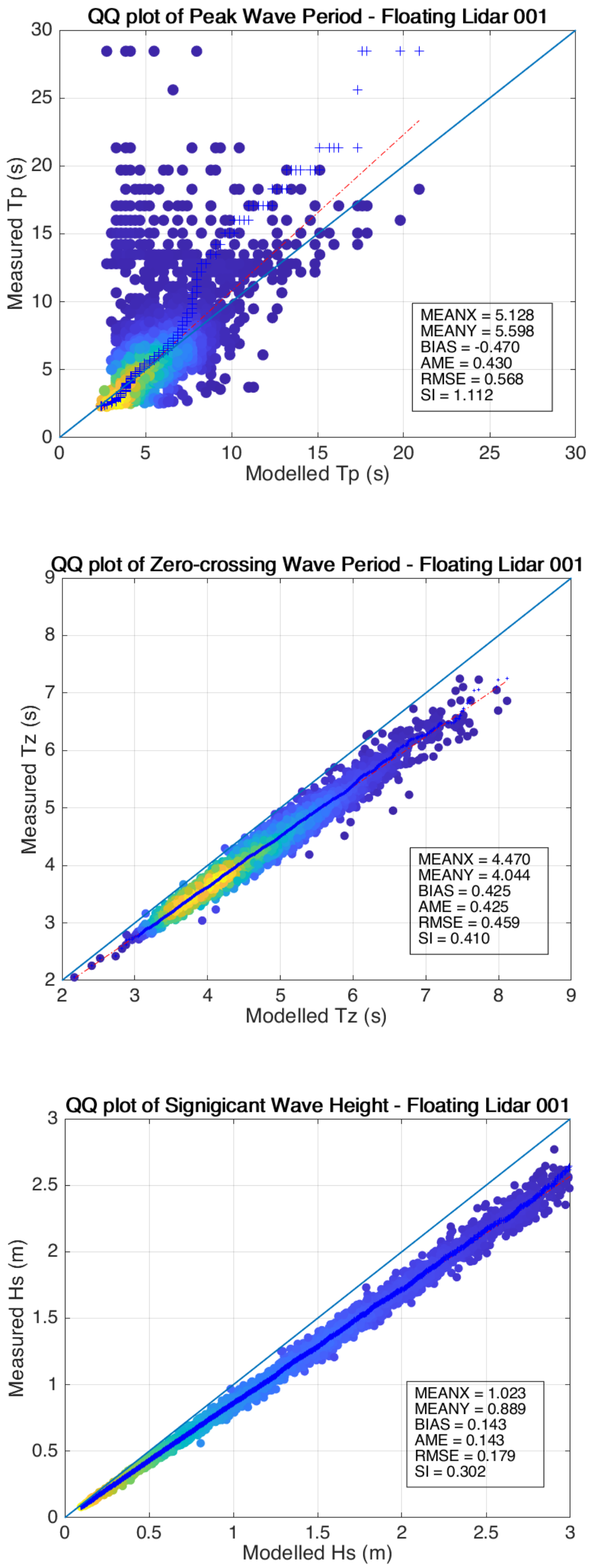

Figure 26. Quantile-Quantile and scatter comparisons of model predictions and measured data newly acquired by the Floating LiDAR buoy 001 for T_p, (top panel) T_z (middle panel) and H_s (bottom panel).

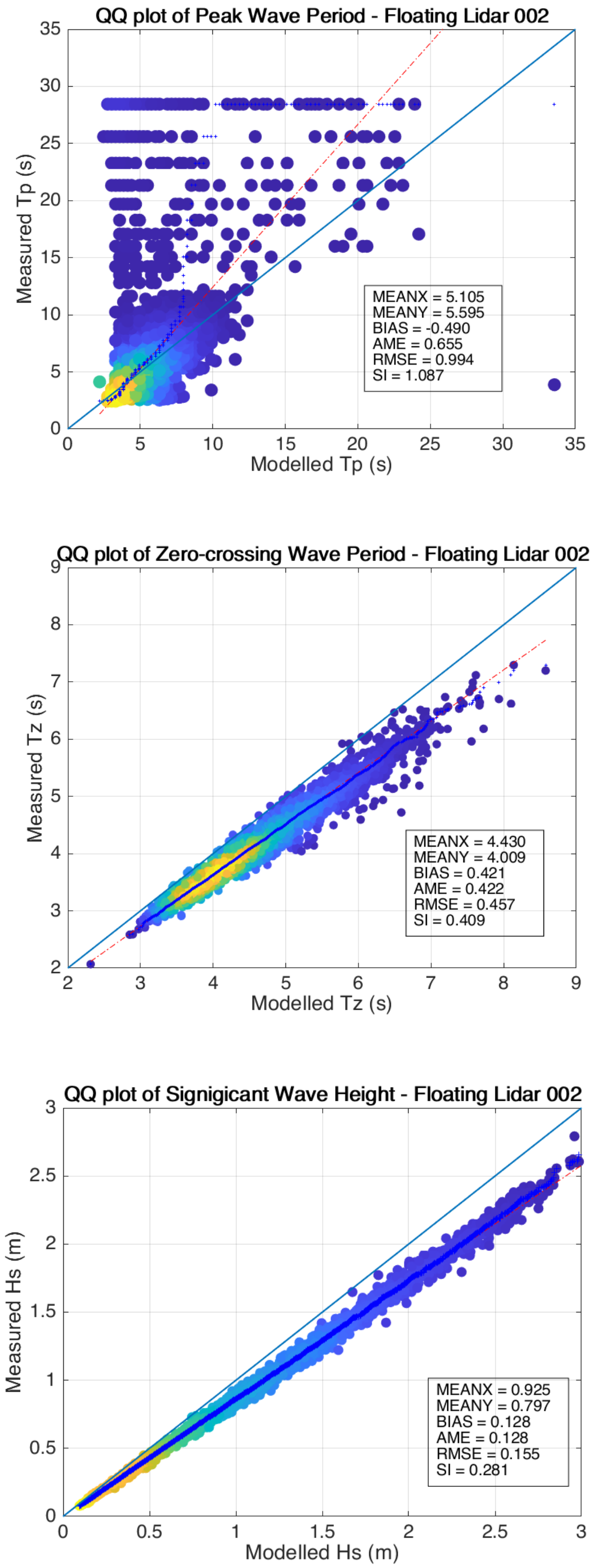

Figure 27. Quantile-Quantile and scatter comparisons of model predictions and measured data newly acquired by the Floating LiDAR buoy 0021 for T_p, (top panel) T_z (middle panel) and H_s (bottom panel).

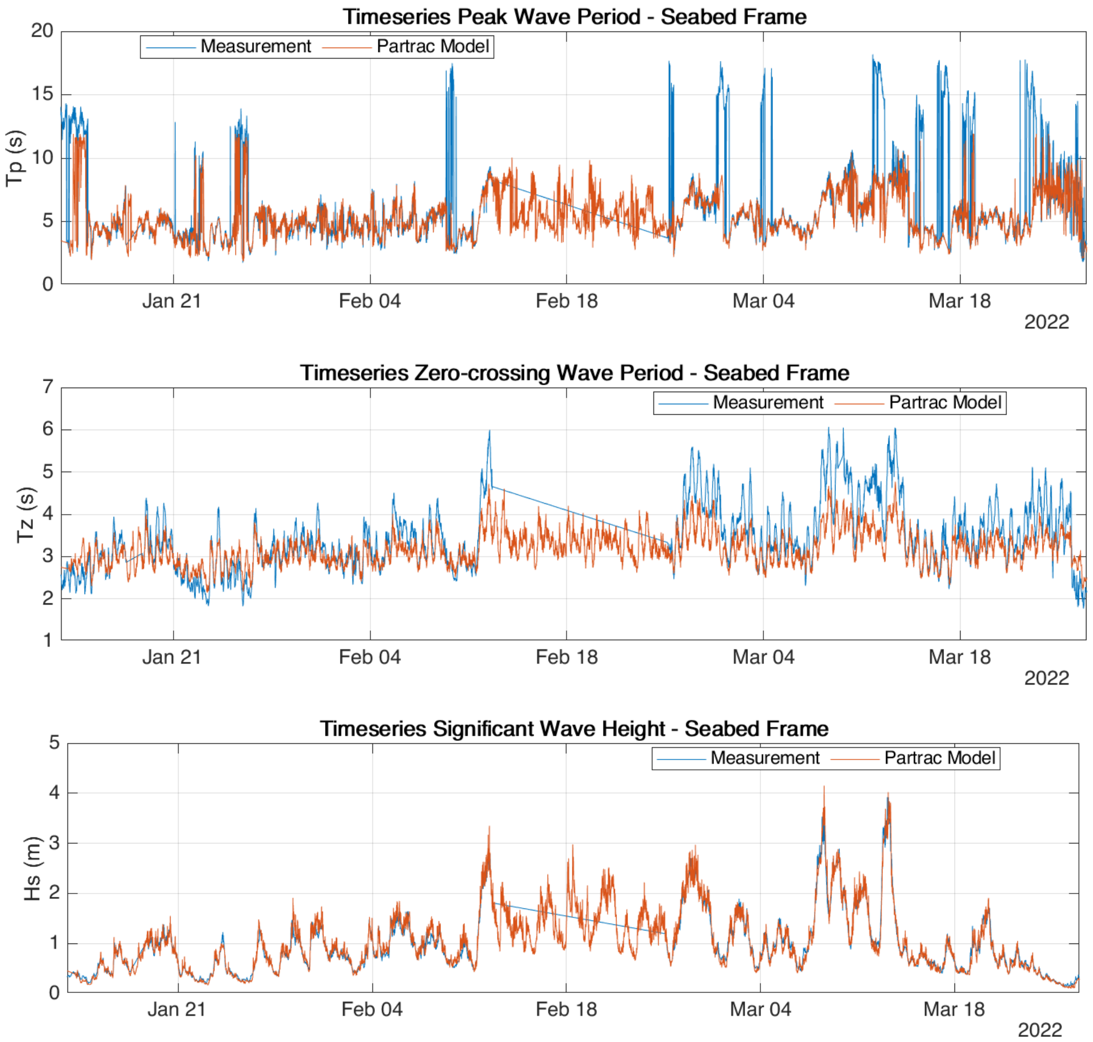

Figure 28: Time series showing coincident model predictions and *newly* measured data acquired by the *seabed frame mounted ADCP for T_p, (top panel) T_z (middle panel) and H_s (bottom panel).*

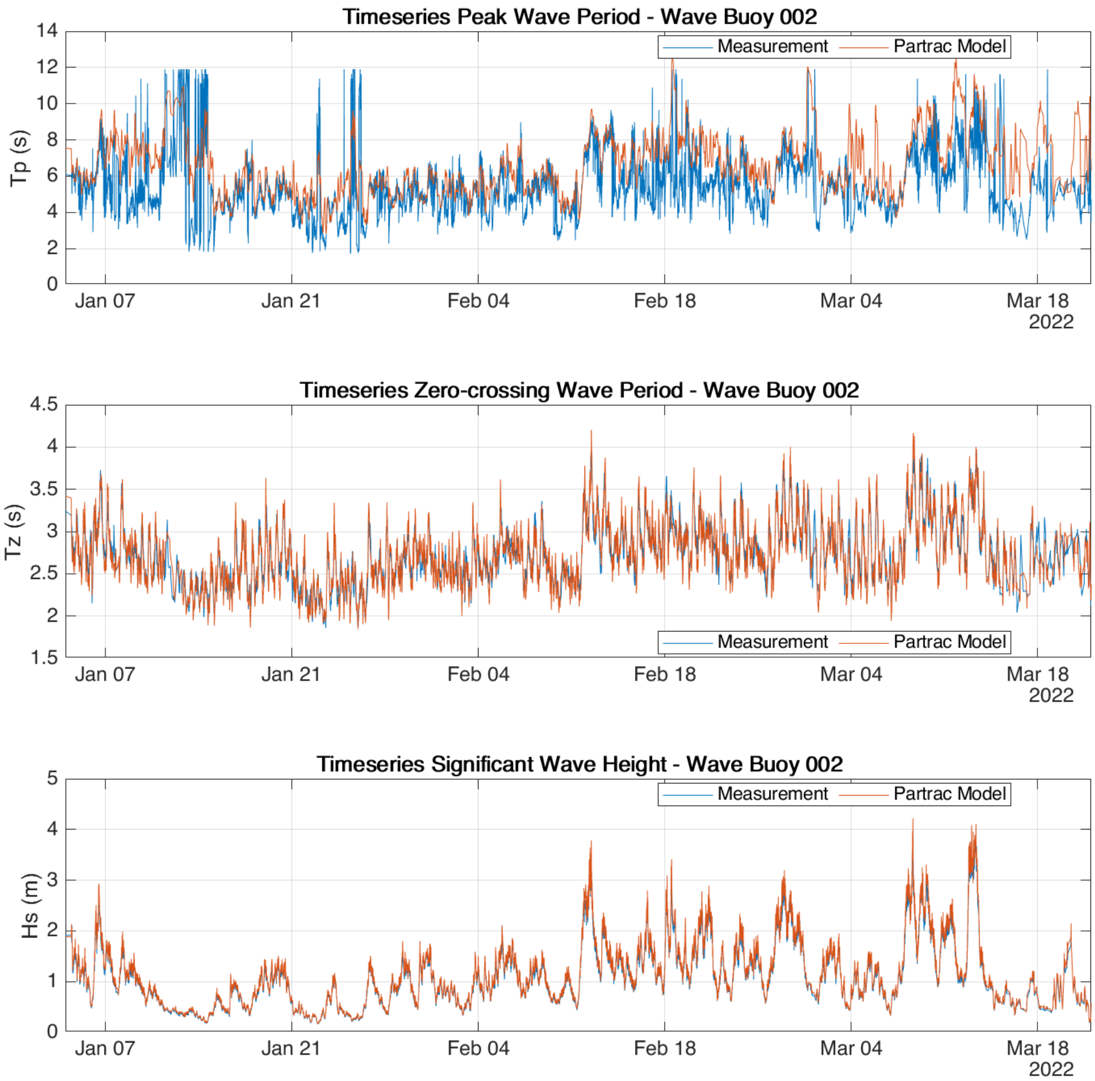

Figure 29. Time series showing coincident model predictions and newly measured data acquired by the Wave Buoy 002 for T_p, (top panel) T_z (middle panel) and H_s (bottom panel).

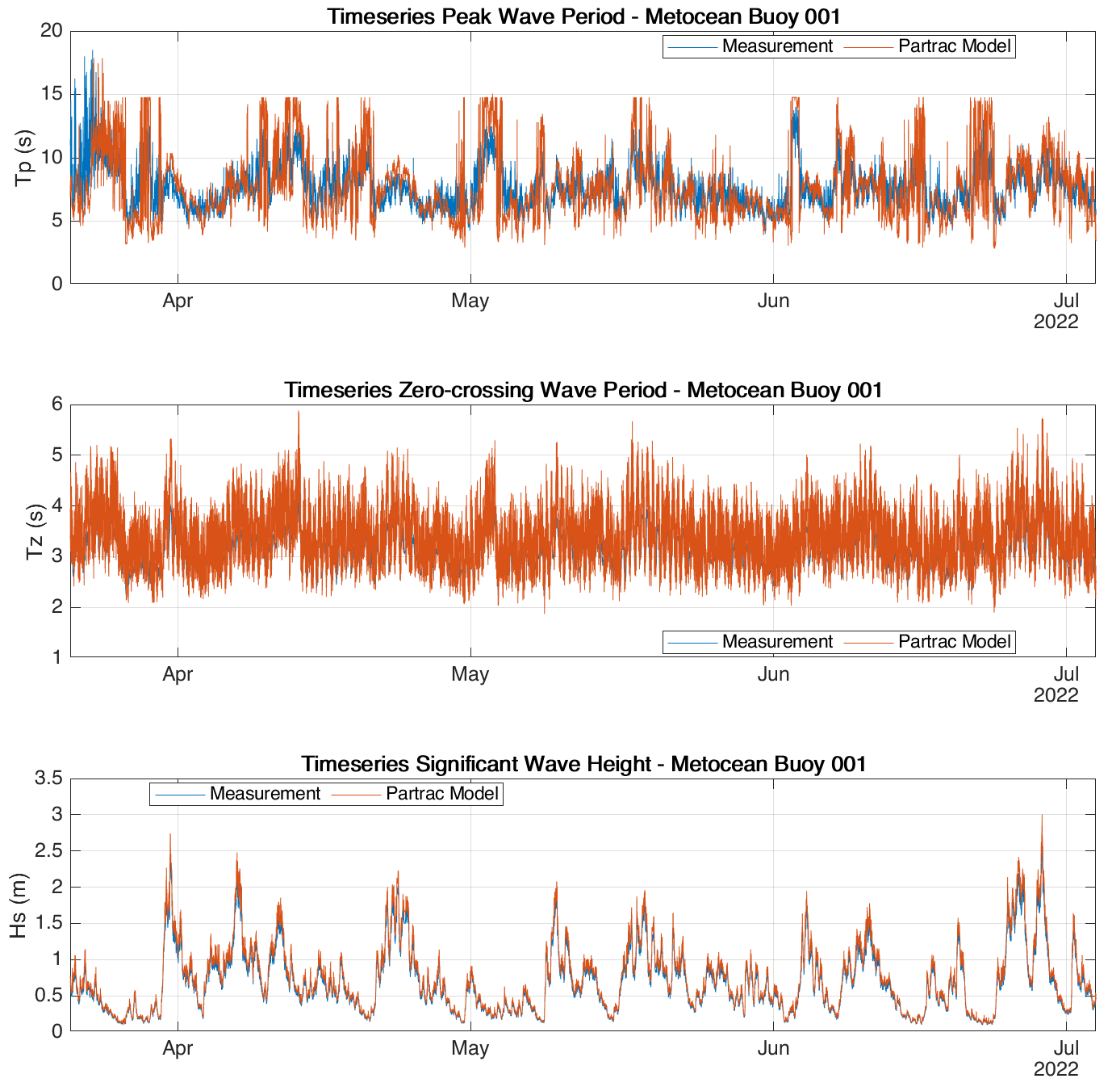

Figure 30. Time series showing coincident model predictions and newly measured data acquired by the Metocean buoy 001 for T_p, (top panel) T_z (middle panel) and H_s (bottom panel).

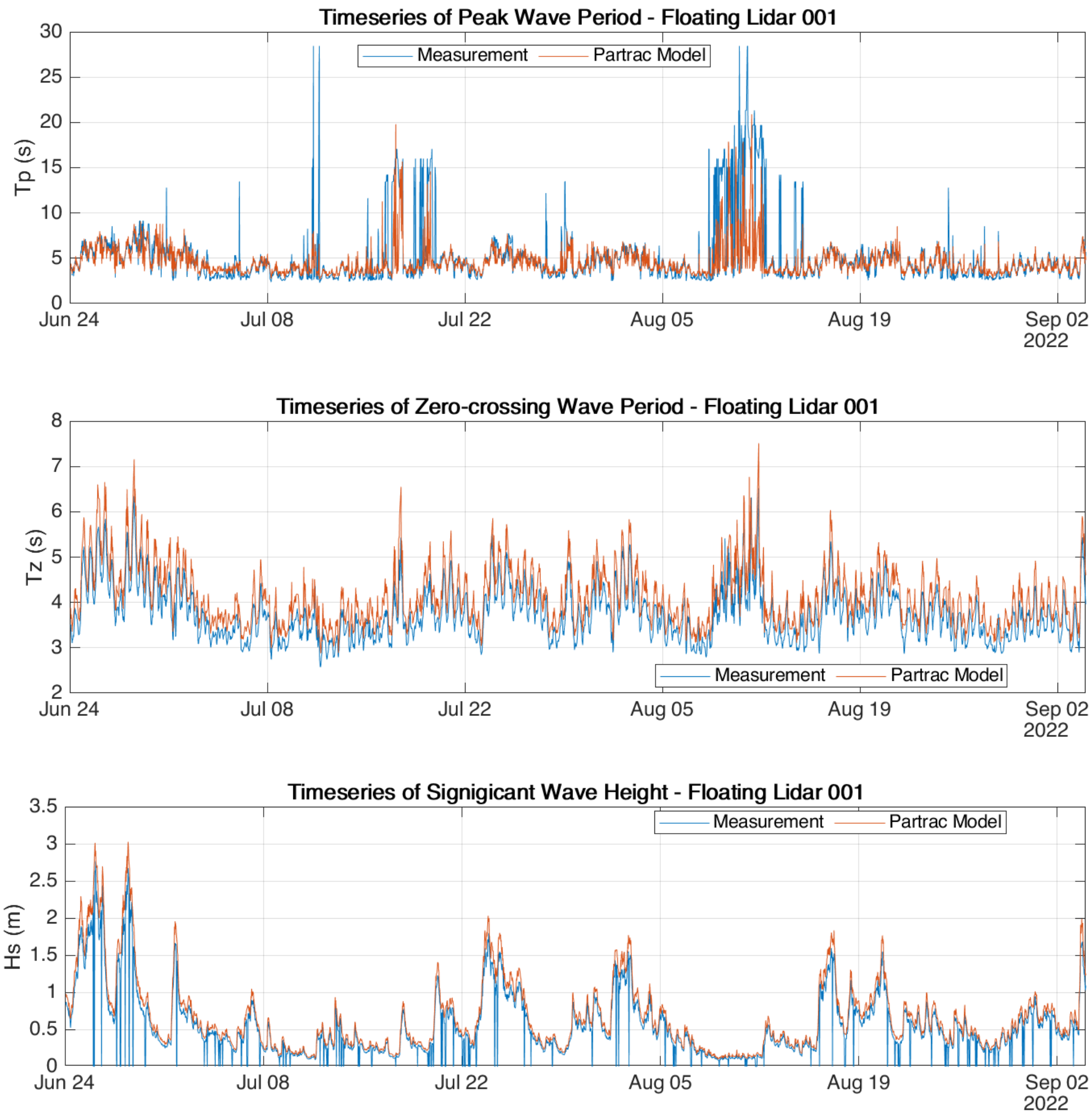

Figure 31. Time series showing coincident model predictions and *newly* measured data acquired by the *Floating LiDAR buoy 001 for* T_p*, (top panel)* T_z *(middle panel) and* H_s *(bottom panel).*

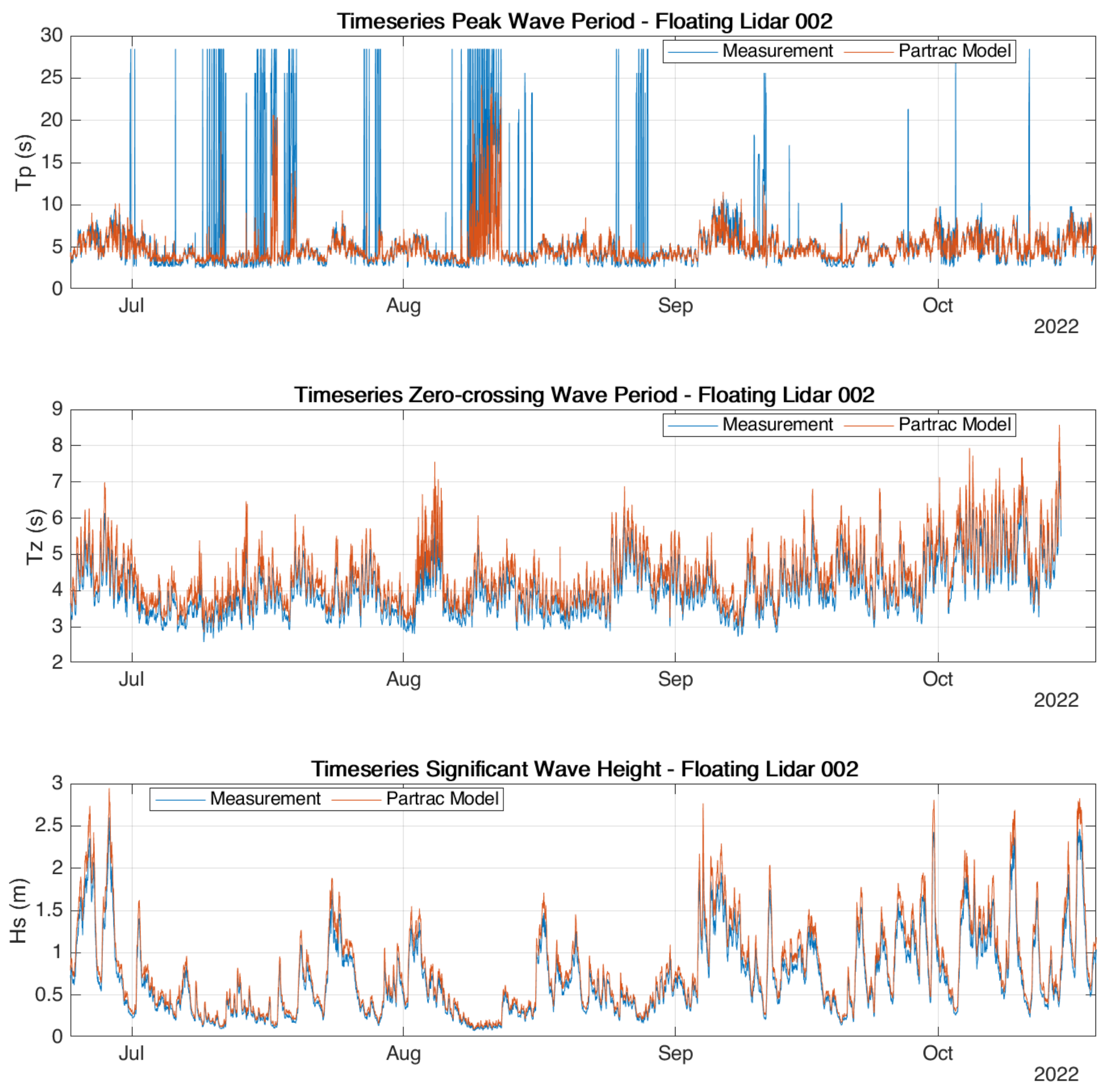

Figure 32. Time series showing coincident model predictions and *newly* measured data acquired by the *Floating LiDAR buoy 002 for T_p, (top panel) T_z (middle panel) and H_s (bottom panel).*

Table 8: Root Mean Square Error (RMSE) values obtained from the validation of the wave model against data acquired from the site in Stage 2.

Location	Variable	RMSE
Wave buoy 002	T_p	0.784
	T_z	0.156
	H_s	0.076
Metocean buoy 001	T_p	0.891
	T_z	0.317
	H_s	0.069
FLlidar 001	T_p	0.568
	T_z	0.459

Location	Variable	RMSE
	H_s	0.179
FLidar 002	T_p	0.994
	T_z	0.457
	H_s	0.155
Seabed Frame mounted ADCP	T_p	0.825
	T_z	0.725
	H_s	0.108

4.2 Validation of the Hydrodynamic Model Against Site Data

Hydrodynamic predictions obtained from the model were validated against the data acquired from within the MAC application boundary (Figure 2). Model predictions over this period were compared with measured observations of current speed. Quantile / Quantile and scatter plot comparisons of modelled predictions vs measured observations are presented for each monitoring platform in Figure 33. These comparisons are also presented in the form of time series in Figure 34. The RMSE between predictions and observations for each monitoring platform, are presented in Table 9.

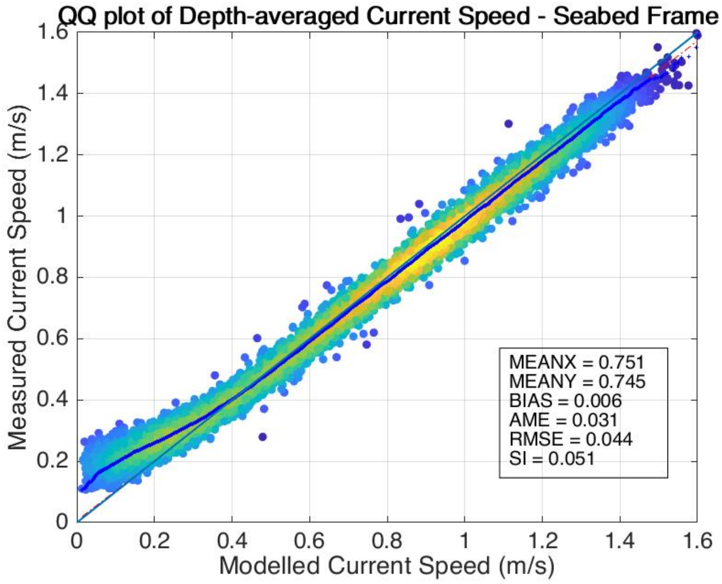

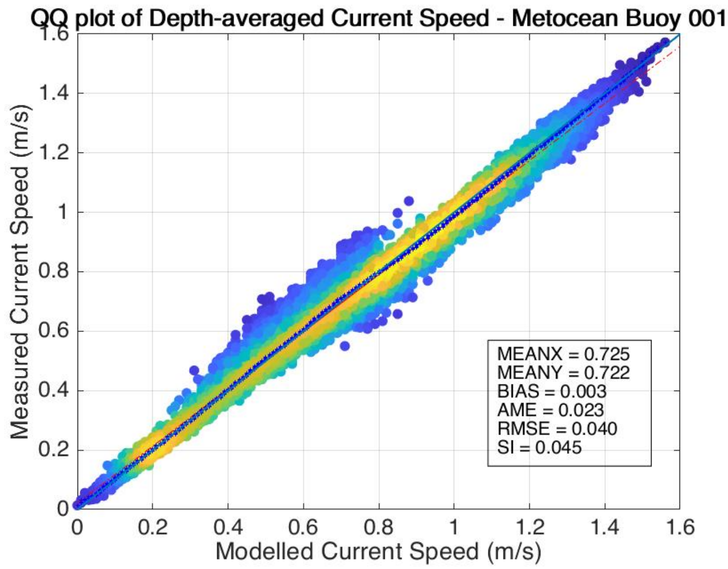

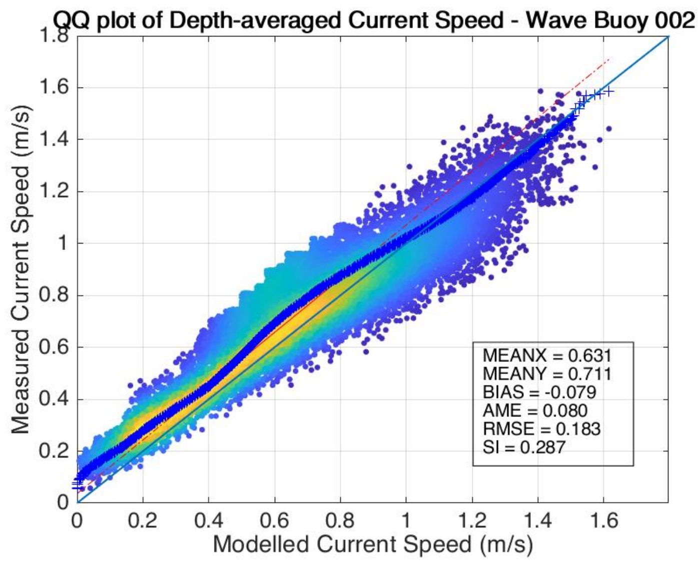

Figure 33. Quantile-Quantile and scatter comparisons of model predictions and measured data newly acquired by instruments deployed on the seabed frame (top panel), metocean buoy (middle panel) and wave buoy 2 (bottom panel).

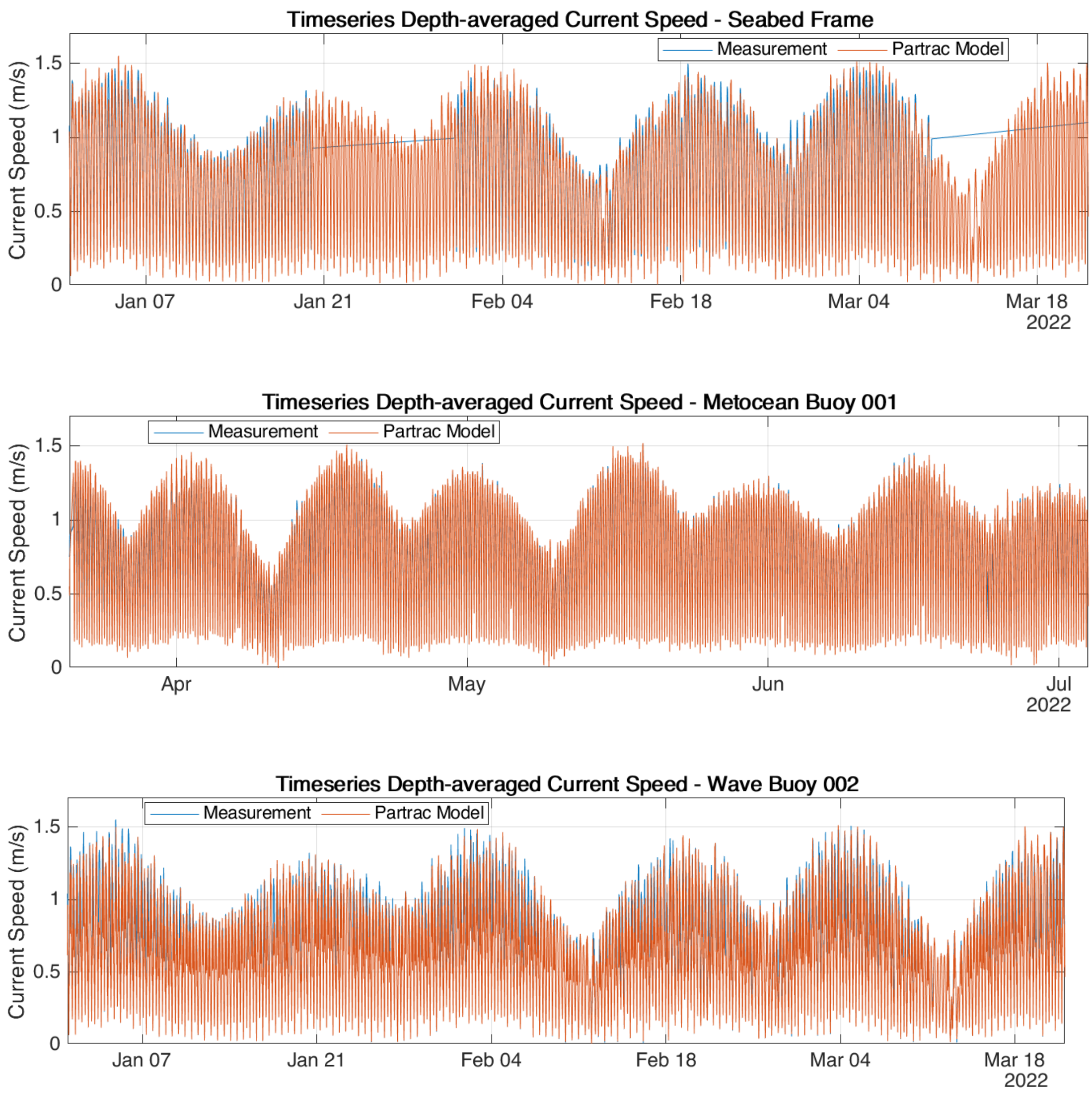

Figure 34: Time series showing coincident model predictions and measured data newly acquired by instruments deployed on the seabed frame (top panel), Metocean buoy 001 (middle panel) and wave buoy 2 (bottom panel).

Table 9. Root Mean Square Error (RMSE) values obtained from the validation of the hydrodynamic model against data acquired from the site in Stage 2.

Location	Variable	RMSE
Seabed frame	Current speed (m/s)	0.044
Metocean buoy 001	Current speed (m/s)	0.040
Wave buoy 2	Current speed (m/s)	0.183

4.3 Model Skill

Consideration of the RMSE which occurs between modelled predictions and measured observations provides a quantitative measure of the accuracy of the model prediction. Consequently, this is commonly used as a direct measure of model skill with lower RMSE values indicative of improved model skill.

The following provides a summary discussion of the performance of the wave and hydrodynamic models during the validation exercise:

- Within the nested higher resolution mesh implemented across the proposed development area, the model shows generally good skill. When comparing predictions of wave parameters to the measured data acquired by instruments deployed on the seabed frame in both Stage 1 and Stage 2 (considered to have provided the most robust wave data record to date, see Section 3.1), good model skill is found.
- Good agreement between the model and the wave parameters measured by instruments deployed on the Floating LiDAR 001 and the Floating LiDAR 002. In Stage 2 of this work, measurements by the FLS001 and the FLS002 showed numerous spikes that are considered to be most likely the result of issues with the instruments, rather than observations.
- The wave model better predicts wave parameters measured by instrumentation deployed within the MAC application boundary when compared to the M2 and M5 locations positioned further offshore. Improved model skill in areas coincident with the proposed development area is a consequence of the higher resolution mesh implemented in this area, as opposed to the coarser grid mesh implemented regionally, coincident with the locations of the M2 and M5 buoy.
- Though predictions of significant wave height values remain generally within 0.5 m of the measured observations, even in the more extreme cases, the wave model generally underpredicts higher values of wave period (both T_z and T_p) at the M2 and M5 wave buoy locations. These discrepancies are considered to be primarily a function of re-sampling and interpolation of the data to produce comparative timesteps for model validation.
- Production of the time series plots demonstrated the ability of the constructed wave model to accurately reproduce events within a similar timestep which is important to consider effects associated with different tidal phases. Outside of the nested higher resolution grid mesh significant fluctuation within the model is observed, however within the MAC application boundary good model skill in terms of event timing is observed for the parameters of wave height and wave period.
- The hydrodynamic model showed good model skill. Water levels obtained from the model show strong agreement with the measured datasets at the three tide gauges located at Arklow Harbour, Dublin Port, and Howth Harbour (RMSE of < 0.05 m). Comparisons of locally acquired depth

averaged current speed data also showed generally good agreement between the modelled and measured data (< 0.2 m\s for current speed with the model generally slightly overpredicting circa by 3 – 5%).

Pye *et al.* (2017) provide useful recommendations for numerical modelling when employed to support EIA, against which the performance of the model during the validation exercise can be judged. For wave modelling Pye *et al*. (2017) suggest that the magnitude of discrepancies between modelled and measured datasets should meet the following criteria.:

- Modelled predictions of significant wave height should be within 10% of the measured data; and,
- Modelled predictions of the parameters of wave period (i.e. T_p T_z) should be within 20% of the measured data.

For hydrodynamic modelling Pye *et al*. (2017) further suggest that:

- Modelled predictions of flow speeds should be within 0.2 m\sec;
- Water level predictions should be within 0.2 m; and,
- the phase difference observed between the modelled data and the validation data should be within +/- 20 min.

All of the above criteria have been achieved for the wave and hydrodynamic modelling[3] developed for the purposes of the EIAR assessment.

3 Interrogation of individual time steps showed discrepancies between modelled predictions and observations which, on occasion, exceeded the criteria specified in the guidance. However interrogation of the absolute error and mean percentage error indicates that these criteria were met both within the high-resolution nested grid implemented across the development area and the coarser resolution grid implemented across the wider region.

5 Model Simulations

5.1. Post Construction Impact

The model simulations performed focused on the assessment of the representative scenarios in regard to the impact upon the prevailing hydrodynamic, wave and sediment regime and coastal processes due to the installation of WTG turbines, foundations, and scour protection measures.

5.1.1. Simulations Performed

To assess the effects on the prevailing regimes, WTG option A was implemented in the model domain (shown in Figure 35[4]). To account for the footprint of scour protection measures, the bed roughness coefficients were enhanced to reflect the presence of rock protection around the base of the foundations. The p50, p90 and p100 wave and hydrodynamic condition derived from the hindcast data record (pre-construction of WTG turbines) were re-run including for the constructed windfarm. The hydrodynamic (current speed, direction, and water level) and wave (wave height [H_s], direction, mean zero crossing period [T_z] and peak wave period [T_p]) data were extracted for each turbine location and two inshore locations. The pre-and post-construction data were then cross compared to quantify the impact of the construction of the windfarm on the prevailing regimes.

4 The planning application boundary in the figure is shown in red for application consistency, however it is presented in black hereafter for ease of visual representation.

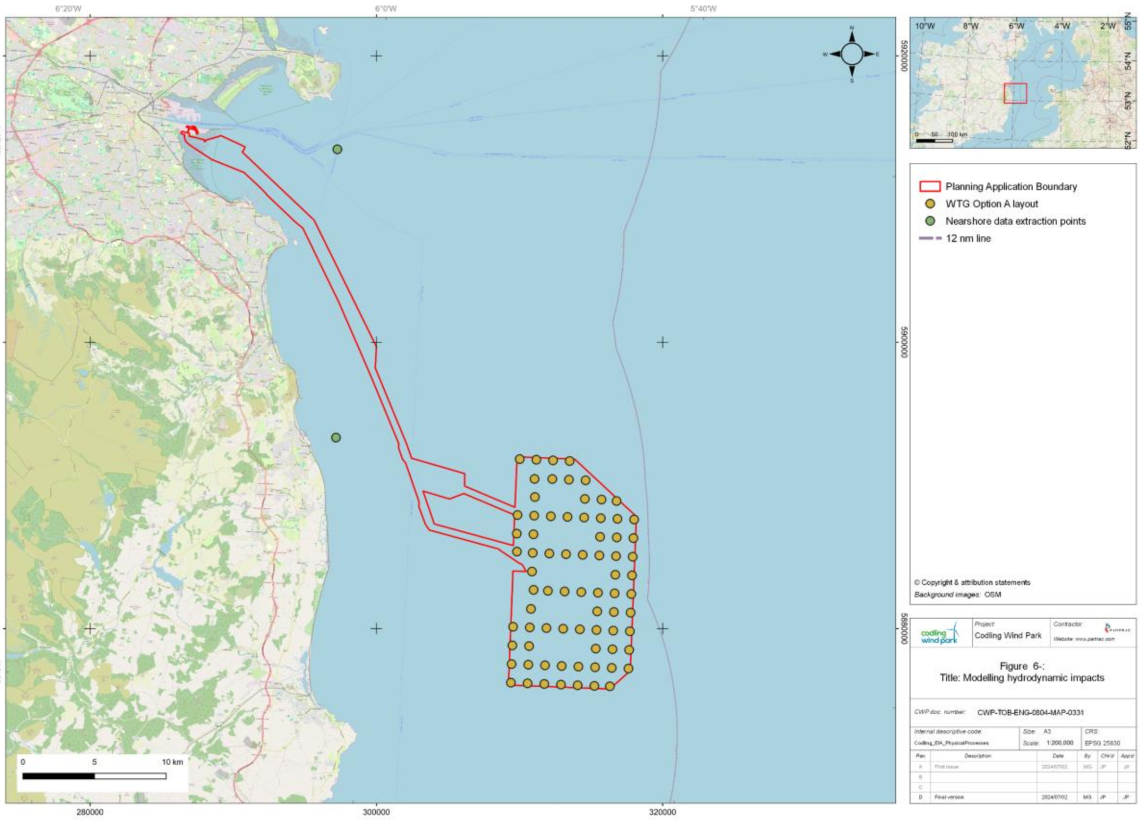

Figure 35. Pre and post construction data comparison points being locations proximal to the WTG locations and two inshore locations

5.1.2. Results

Across a range of typical (p50) and high energy (p90 and p100) events, the impact of the construction of the windfarm is predicted to have only a small effect on the prevailing hydrodynamic and wave regimes, both at locations proximal to the individual turbines and at locations nearer to shore. During the p50, p90 and p100 wave conditions, the construction of the windfarm was predicted to have a negligible impact on the wave parameters assessed (i.e. wave height, period, and direction) with < 0.1 % difference between pre and post construction conditions predicted. During the p50, p90 and p100 hydrodynamic conditions, the construction of the windfarm was predicted to have a slightly greater effect with up to ~3% difference in current speed and up to ~5% difference in current direction predicted at locations proximal to the individual turbines due to the construction of the windfarm. These effects have negligible difference on the tidal regime away from the MAC application boundary, with < 0.3% difference between pre and post construction estimates of current speed and direction predicted at the inshore points. The effect of construction on water level across the array site and at the inshore locations nearer to the coastline is predicted to be < 0.4% difference between pre and post construction scenarios.

5.2. Sediment Transport Simulations

The model simulations performed focused on the assessment of the *representative scenario* in regard to the liberation and spatiotemporal distribution of sediments during proposed construction activities.

5.2.1. Sediment Plume Dispersion

Plume dispersion simulations were performed to quantify the SSC's, depositional footprint (thickness of the deposit on the seabed) and transport trajectory of sediment plumes that may be generated as a result of the following construction related activities:

1. ***Bedform clearance activities***: At various locations along the IAC and OECC routes, dredging using a Trailer Suction Hopper Dredger (TSHD) may be required for the purposes of bedform clearance/lowering. It is intended that sediment arising from dredging operations will be disposed of within the MAC application boundary by direct release from the hopper to the seabed or fluidising the sediment and discharging it at an appropriate disposal location, ideally in close proximity (if possible) to the dredging works.

2. ***Cable trenching activities***: Sediment plumes are also likely to be generated during cable trenching activities. Depending on the prevailing soil conditions, a combination of cable burial methods may be used including jetting, cutting, and ploughing. These simulations included for areas of necessary deeper cable burial (up to 3m) where the OECC crosses the approaches to Dun Laoghaire harbour and the RWE cable.

5.2.2. Disposal of Dredge Arisings: Environmental and Engineering Constraints

Prior to undertaking the plume dispersion modelling exercise, both engineering and environmental constraints related to the disposal of dredge material and trenching activities must be considered to assess a representative scenario. Such constraints may restrict disposal of dredge material within the cable corridor and in turn, define areas which may be considered more suitable for disposal. This exercise identified several constraints, being:

- Disposal will not occur outside the MAC application boundary;
- Disposal will not occur in areas of existing large ripples or sandwaves to ensure that the deposited material does not unintentionally back-fill the dredged area;
- Disposal will not occur at locations where water depth is too shallow for the dredger to operate;
- Disposal will not occur in areas of existing in-service cable routes / crossings;

- Post disposal, the deposited thickness of sediment on the seabed, arising as a result of the dredge and disposal operations is such that it will not significantly impact upon the navigable depth (i.e. the navigable depth will not be reduced by > 5 %).

The environmental constraints included:

- In order to avoid sensitive and / or designated habitats, for example, deposition will not occur proximal to:
    - *Sabellaria spinulosa* reef habitat.
    - Identified potential wrecks or targets of archaeological interest.

The results of this exercise allowed for the designation of representative areas that could be deemed suitable for consideration for offshore disposal for sediments dredged during bedform clearance activities within the array site and along the OECC. These areas, and the simulated disposal locations, are delimited in Figure 36.

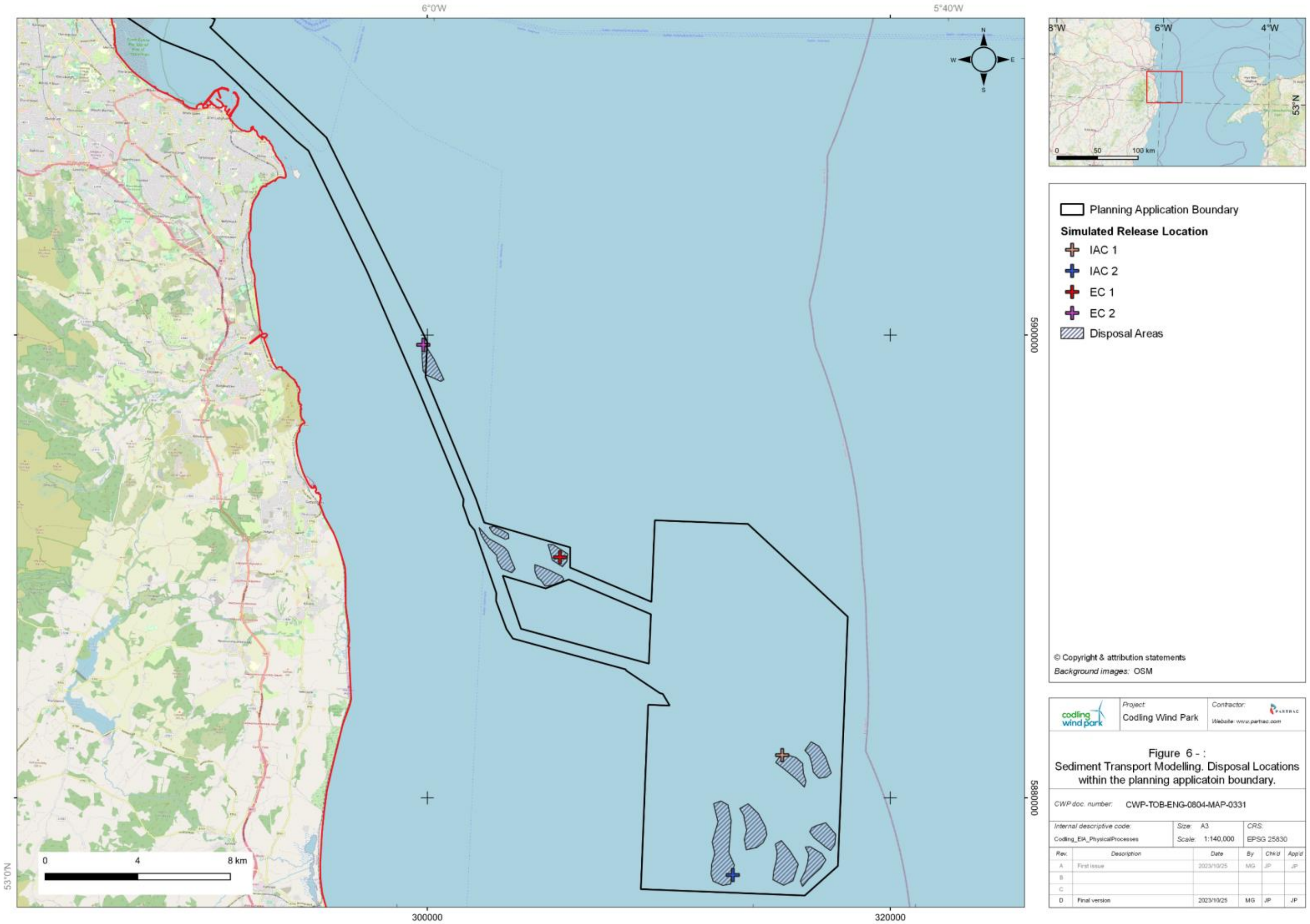

Figure 36. Potential areas which may be suitable for disposal of dredge arisings within the MAC application boundary. The release locations simulated are marked.

5.2.3. Simulations Performed

In total, 9 scenarios were simulated, 4 representative[5] scenarios focused on the disposal of dredge arisings within the MAC application boundary, 5 representative scenarios focused on the trenching activities along the IAC, OECC and along the export cable transition zone.

Disposal of Dredge Arisings

To assess the disposal of dredge arisings, the scenarios simulated were as follows:

Scenario 1: Release of all material dredged from within the IAC array, disposal at a representative location close to the centre of the Array Site (Figure 36). Material released as a continuous discharge, reflecting 12-hour operations.

Scenario 2: Release of all material dredged from within the IAC array, disposal at a representative location close to the southern boundary of the array site (Figure 36). Material released as a continuous discharge, reflecting 12-hour operations.

Scenario 3: Release of all material dredged from within the OECC, disposal to the east of the possible dredge disposal sites along the OECC (Figure 36). Material released as a continuous discharge, reflecting 12-hour operations.

Scenario 4: Release of all material dredged from within the OECC, disposal to the west of the possible dredge disposal sites along the OECC (Figure 36). Material released as a continuous discharge, reflecting 12-hour operations.

Trenching Activities

To assess the disposal of dredge arisings, the scenarios simulated were as follows:

Scenario 1: Release of liberated sediments during jet trenching activities along a representative southern cable string within the IAC array (Figure 37). Plumes of liberated sediments released reflect

5 As it is likely that bedform clearance and trenching activities will be intermittent in nature, rather than continuous, (e.g. installation of sections of the IAC and OECC routes will be performed independently of one another during the period of construction), representative scenarios were simulated independently.

12-hour trenching operations and typical trenching rates based on a 1.5 m maximum trench depth and a 15 m maximum trenching width along the entire length of the simulated IAC route.

Scenario 2: Release of liberated sediments during jet trenching activities along a representative central cable string within the IAC array (Figure 37). Plumes of liberated sediments released reflect 12-hour trenching operations and typical trenching rates based on a 1.5 m maximum trench depth and a 15 m maximum trenching width along the entire length of the simulated IAC route.

Scenario 3: Release of liberated sediments during jet trenching activities along a representative northern cable string within the IAC array (Figure 37). Plumes of liberated sediments released reflect 12-hour trenching operations and typical trenching rates based on a 1.5 m maximum trench depth and a 15 m maximum trenching width along the entire length of the simulated IAC route.

Scenario 4: Release of liberated sediments during jet trenching activities along the OECC. Plumes of liberated sediments released reflect 12-hour trenching operations and typical trenching rates based on a 2 m maximum trench depth increasing to 3 m where the OECC crosses the approaches to Dun Laoghaire harbour and the RWE cable (shown in Figure 38), and a 15 m maximum trenching width along the entire length of the simulated OECC.

Scenario 5: Release of liberated sediments during jet trenching activities along the OECC within the transition zone (Figure 39). Plumes of liberated sediments released hourly, reflecting 12-hour trenching operations and typical trenching rates based on a 2 m maximum trench depth and a 20 m maximum trenching width along the entire length of the simulated OECC route within the transition zone.

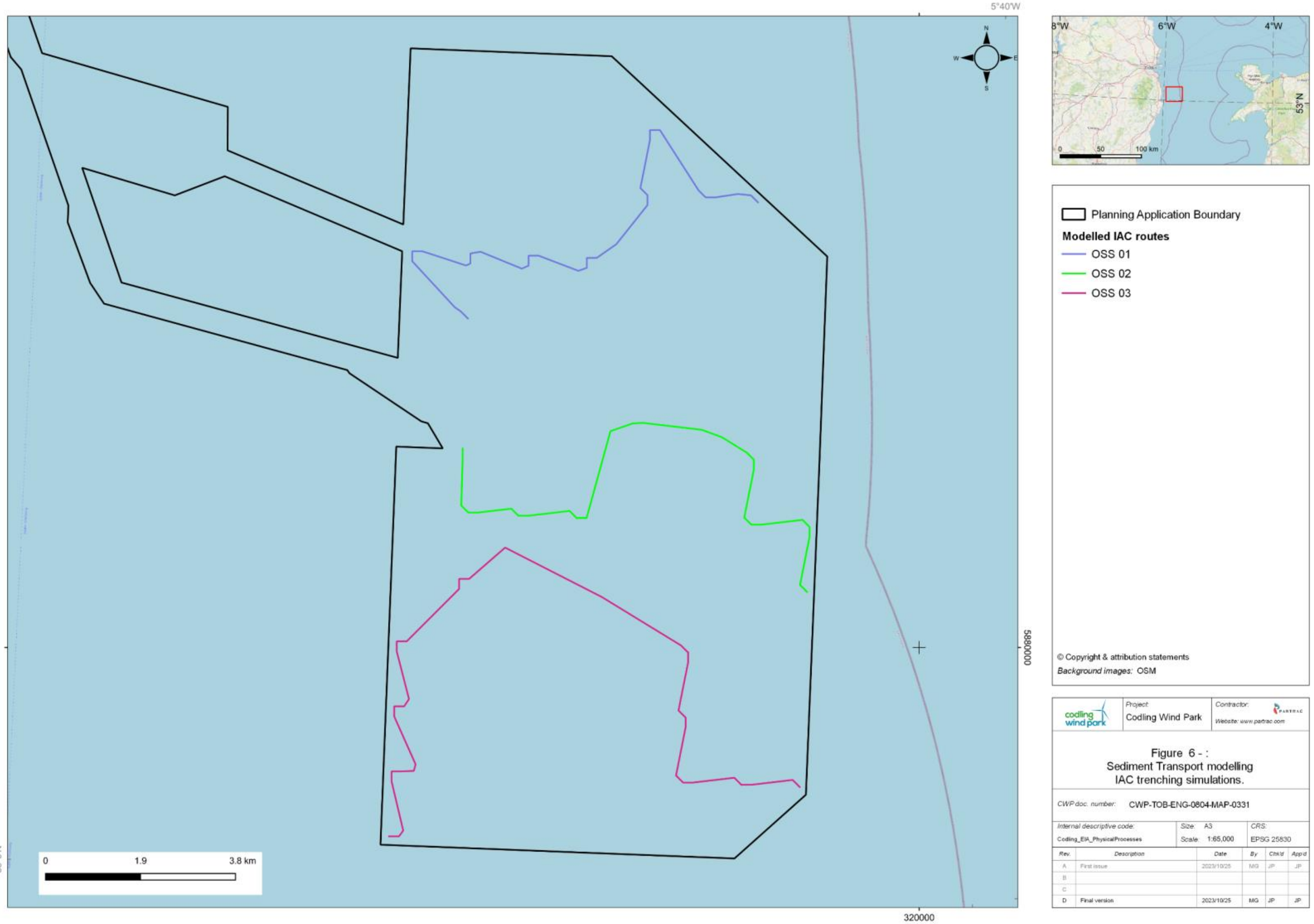

Figure 37. The southern, central, and northern string within the IAC array area simulated as part of the assessment of trenching activities.

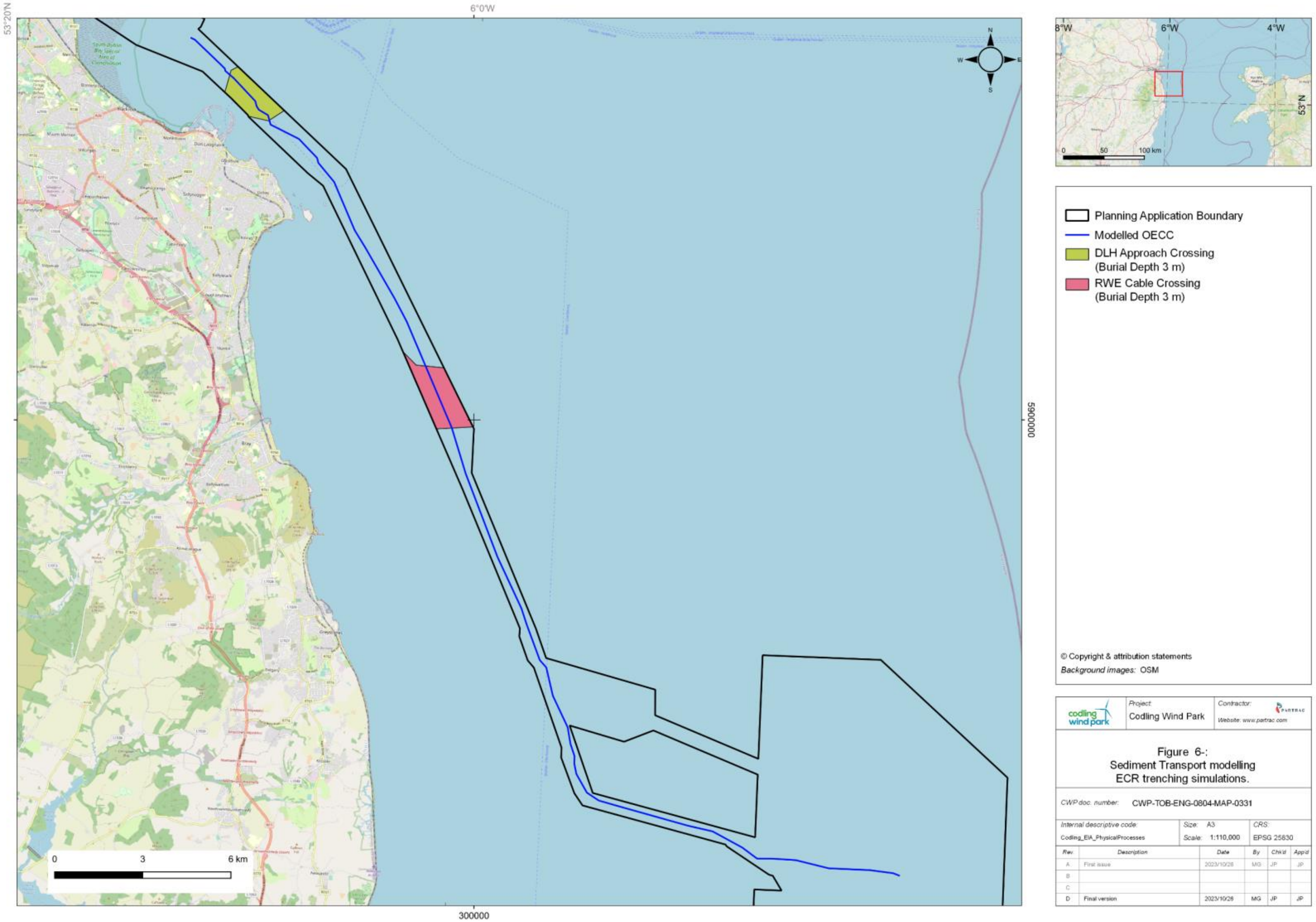

Figure 38. The OECC route simulated as part of the assessment of trenching activities.

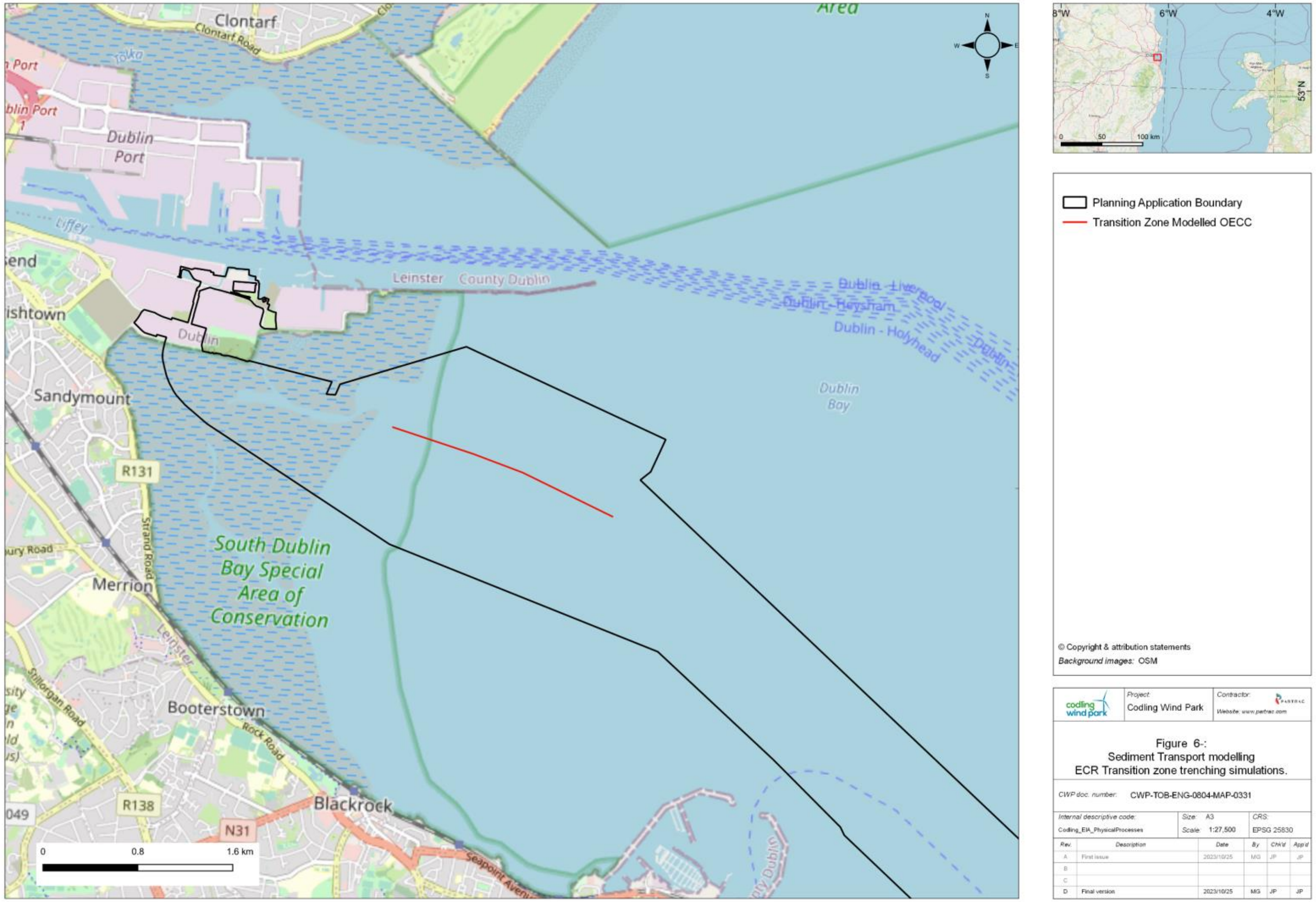

Figure 39. The OECC route within the transition zone area simulated as part of the assessment of trenching activities.

5.2.4. Model Setup

The Particle Tracking module of the MIKE 21 Flow Model was utilised for undertaking sediment transport modelling to assess the fate of the plumes of suspended sediment generated during construction activities. Using driving conditions extracted from the high resolution, coupled 2D Hydrodynamic and Wave model, the particle tracking simulations described in Section 5.3 were performed to estimate the transport trajectory (in a Lagrangian manner) of suspended particles within the model domain. The driving hydrodynamic input for the plume dispersion scenarios were derived from a hydrodynamic hindcast conducted for a representative period (excluding for periods of higher energy events where vessel operability will be limited), encompassing a typical lunar cycle including the Spring, and Neap, tidal phase.

5.2.5. Model Parameterisation

Suitably parameterised particles can be used as a proxy to assess the dispersion, concentration, and depositional footprint (thickness), of sediments liberated during the proposed works. Within the model, the sediment (i.e. each individual particle class) is considered as particles, with inherent hydraulic characteristics (e.g. settling, moving sources and horizontal and vertical dispersion), being advected within the surrounding water body and dispersed as a result of random (turbulent) processes in two dimensions. The model calculates the path of each particle and outputs the instantaneous concentrations of individual classes. A corresponding mass is assigned to each particle released within the model. The mass of material assigned to each particle is a function of the volume of water within the model cell, the volume of sediment to be released into the water column and the target mass to be resolved (in this instance 1 mg l^{-1}). The model was not configured to provide information regarding the erosion, entrainment, resuspension, and subsequent transport of sediments once deposited upon the seabed.

When dredge vessels discharge material, The release mechanisms influence the near and far field impact of the plume created. Sediment released close to the seabed will settle quickly, reducing the impact on the wider environment. Comparatively, sediment released at the surface will take longer to descend through the water column and will therefore subsequently be dispersed across a greater spatial extent. Each mechanism will also be associated with a different rate of release. To simulate this, a distinction is made between near-field and far-field plume motions, based on the differences in the physical processes governing the spreading/dispersion mechanisms. A dynamic plume descends rapidly to the seabed because of its high density relative to the surrounding seawater. A passive plume forms as the dynamic plume descends through the water column and mixes due to turbulent processes and interaction with the ambient seawater. To account for these processes within the model an empirical coefficient which limits the volume of fine sediment released into the water column is utilised. In this scenario a conservative 10% rate of loss (to the passive plume) of fine sediment (sand, silt, and clay) was applied. This rate is based upon findings reported by Becker *et al.* (2015). Coarser gravel sized materials are assumed to be deposited almost instantaneously on the seabed in the immediate vicinity of the disposal location, and therefore materials of this size are not available for transport (in the modelling) as part of the passive plume. For trenching activities, sediments that are liberated into the water column are released within the model domain, at 3 m above the seabed, as a semi-continuous, moving (at the pace of the trencher) passive plume. For all trenching simulations, 100% disaggregation is assumed during jetting.

The particles released as part of the simulations were parameterised using site specific sedimentological data derived from grain size data collected during the benthic ecology field campaign and sediment transport coefficients detailed by Soulsby (1997). These data were derived from samples proximal to the activity of interest (i.e. either from sediment samples coincident with bedform fields, or sediment samples proximal to cable routes). Three grain size classes were defined for input to the model (Table 10). The mean value of each grain size class was utilised, and the volume of sediment apportioned according to the mean value from relevant samples.

Table 10. The three grain size classes simulated.

Grain size class	Size range (mm)	Median grain size (mm)	Settling velocity (m s^{-1})
Coarse Sand and Gravel	0.6 – 64.0	32.30	N/A*
Fine to Medium Sand	0.064 – 0.590	0.33	0.042
Clay and Silt	0.001 – 0.063	0.001	0.001

* Note an arbitrary high value was chosen to ensure that this material is immediately deposited on the seabed.

Representative case maximum dredge volumes for bedform clearance were calculated and reported by the CWP Marine Engineering Team, being 832,500 m^3 and 595,650 m^3 for the IAC array and OECC, respectively. The volume of material to be dredged was determined from the geophysical survey data, identifying areas of potentially mobile bedforms that could constrain cable installation operations. Model scenarios simulated a single Trailing Suction Hopper Dredger ('TSHD'), working 12-hour operations. Jet trenching activities were simulated based on maximum hourly progress rates.

5.2.6. Model Outputs

Model outputs included geospatial plots showing the SSC and any increases in sediment thickness on the seabed through time, in the form of time-sliced snapshots and time series plots derived from each disposal location, local conservation zones and protected areas. The model outputs were interrogated to establish the maximum and instantaneous SSC (mg l^{-1}) and maximum and instantaneous deposited sediment thickness (mm) arising from the disposal operations. These metrics are considered key output parameters required for the assessment of potential environmental impacts.

6. Results

6.1. Disposal of Dredge Arisings following Bedform Clearance

During the modelled representative scenarios suspended sediment plumes created during dredge disposal operations were predicted to enhance SSC, local to dredge operations, and across the wider environment, transiently. Table 11 presents a summary of the main findings obtained from each simulation.

Table 11. Findings obtained from the four simulations of the disposal of dredge arisings following bedform clearance.

Scenario	Location	Transport Direction	Transport Distance (Km)	Predicted transient increases in SSC (mg\l)	Time required to return to baseline SSCs	cumulative sediment deposition thickness near the disposal location (cm)
Scenario 1	IAC	Eastward	3 - 4 km	~ 150 mg/l	~ 10 days	~ 6 cm
Scenario 2	IAC	Eastward	5 - 6 km	~ 100 mg/l	~ 15 days	~ 3 cm
Scenario 3	EC	Westward	3 - 4 km	~ 80 mg\l	~ 10 days	~ 2 cm
Scenario 4	EC	South eastward	4 - 5 km	~ 50 mg\l	~ 10 days	~ 4 cm

The results indicate that dredging activities within the array site and along the OECC are not expected to impact the SSC's over the long-term, with SSC levels returning to baseline conditions within a maximum of 15 days of completion of disposal activities. It is also noted that the effects are localised to the point of disposal with sediment plumes predicted to disperse < 7 km away from the disposal location, across which sediments transported as part of the passive plume would be depositing on the seabed. The thickness of the deposit on the seabed at the disposal location is anticipated to be on the order of a few metres as a result of the immediately deposited portion of the dredged material, these sediments are anticipated to be rapidly integrated into the sediment regime[6].

The results for disposal scenario 1 are presented in Figure 40 to Figure 49. Figure 50 to Figure 59 presents the results for disposal scenario 2, and Figure 60 to Figure 69 presents the results for disposal scenario 3. Figure 70 to Figure 79 presents the results for disposal scenario 4. These results, for each of the four simulations performed, are presented as:

- A spatial plot showing the maximum observed values at any time during the model run (representing the maximum footprint of SSC resulting from the dredging operations); and timeseries of SSC and the deposited thickness at the release locations.
- A spatial plot representing the trajectory of the suspended particles; and
- A series of time-sliced snapshots showing the location (and predicted concentration) of the suspended sediment plume during the simulation.

6 At the location of disposal of each hopper load, the estimated thickness of the deposit on the seabed is a function of the area across which the material was deposited. To estimate the thickness of the deposit, approximations are made based on vessel specification, operational objectives etc. However, caution is urged when considering the cumulative thickness of deposits as this calculation does not account for the erosion, entrainment, mobilisation, and transport of these sediments once deposited on the seabed. Consequently, where several hopper loads are deposited within the same spatial area significant variability in the thickness of the observed deposit is likely.

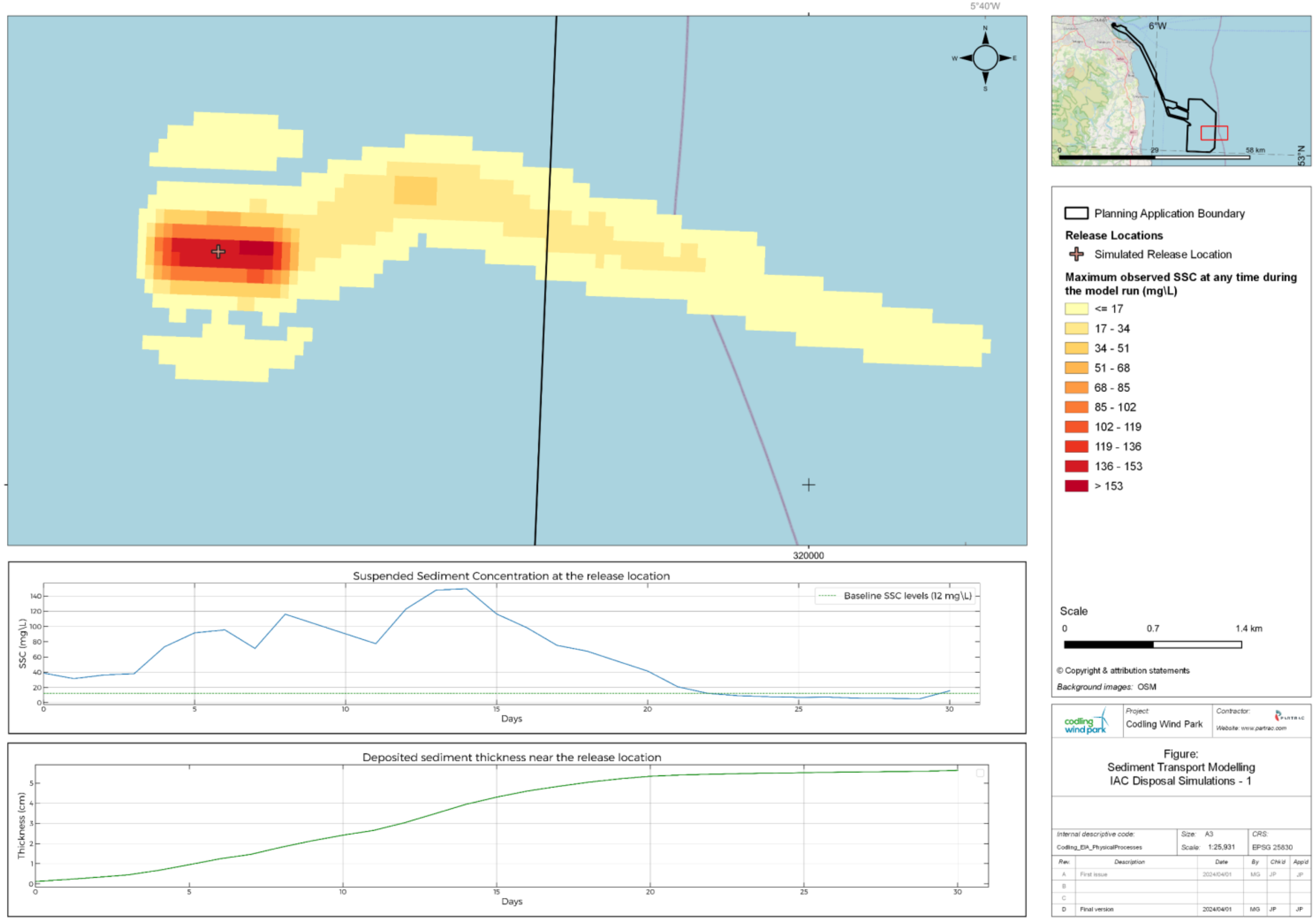

Figure 40. Maximum observed SSC levels at any time during scenario 1 run are presented in the spatial plot, the timeseries show 1) suspended sediment concentrations at the release location, and 2) the deposited sediment thickness at the release location.

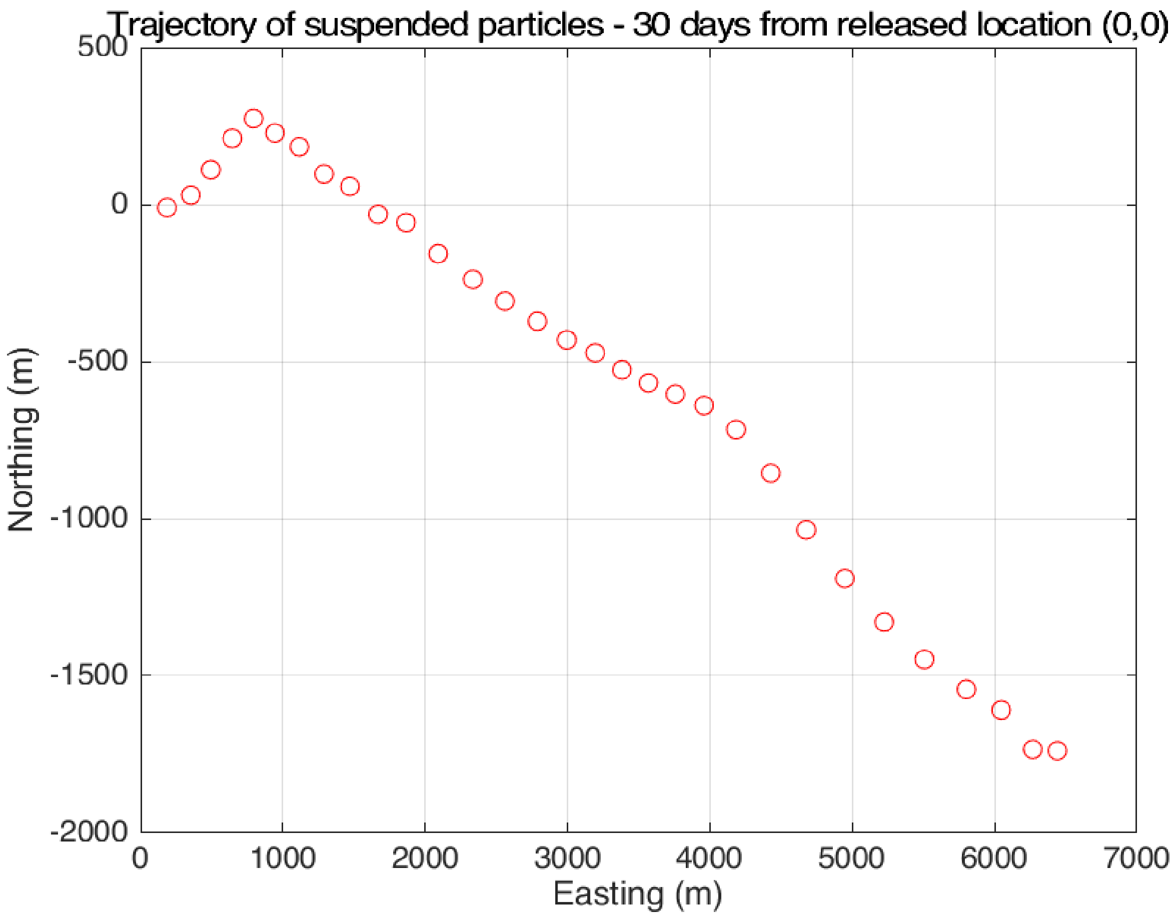

Figure 41. Trajectory of suspended sediments – Scenario 1.

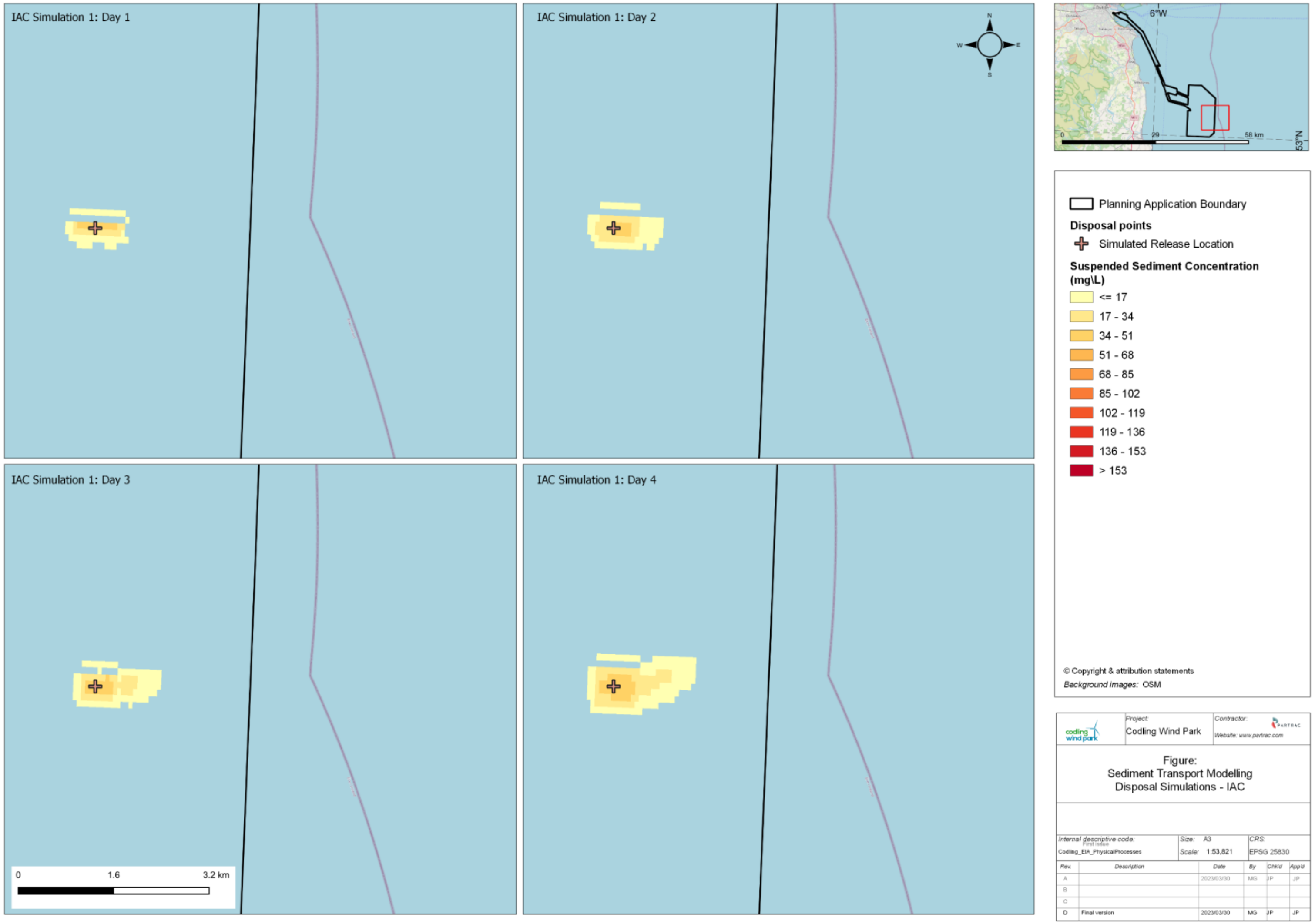

Figure 42 : SSC levels observed @ days 1 to 4 - Scenario 1.

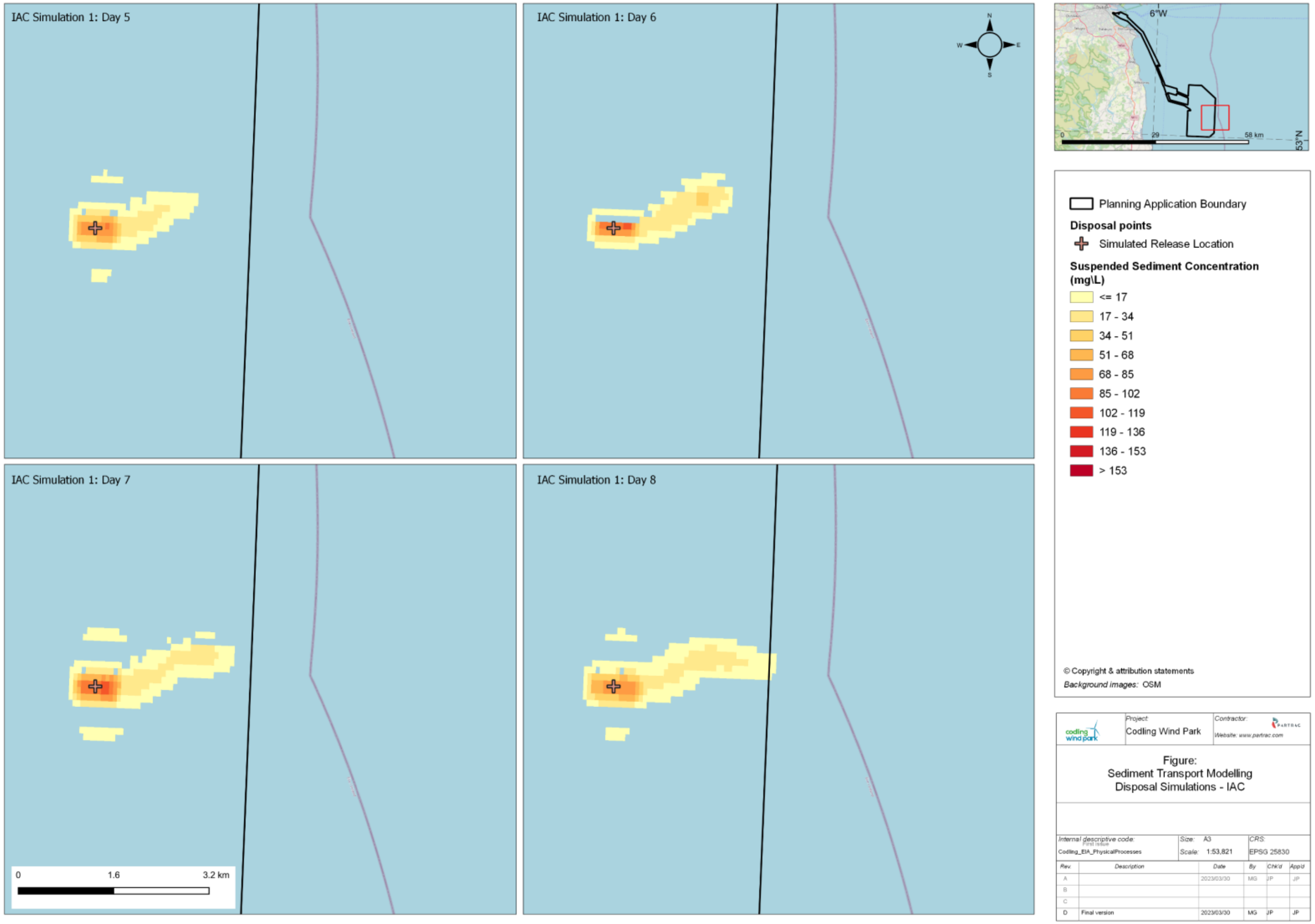

Figure 43 : SSC levels observed @ days 5 to 8 - Scenario 1.

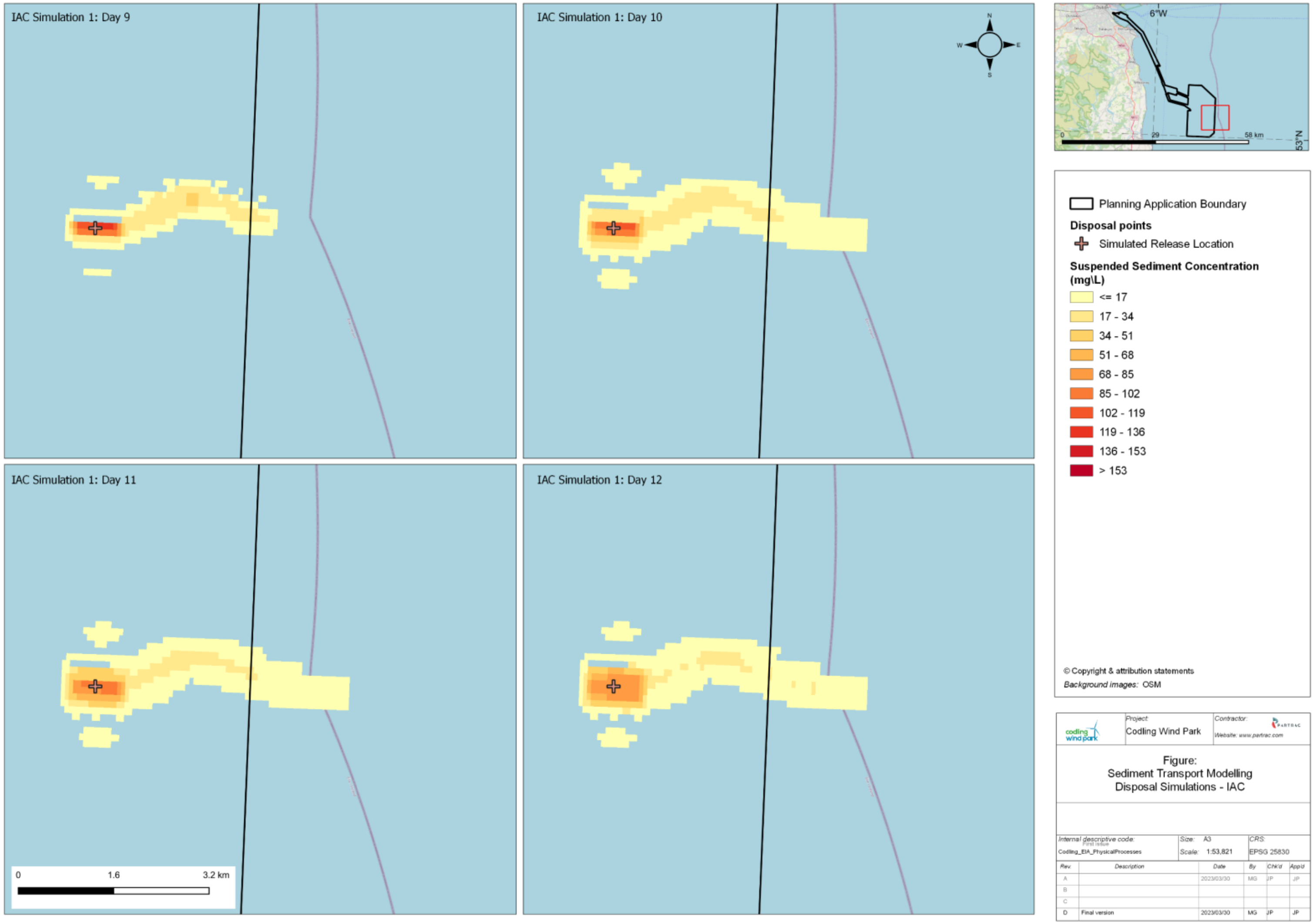

Figure 44 : SSC levels observed @ days 9 to 12 - Scenario 1.

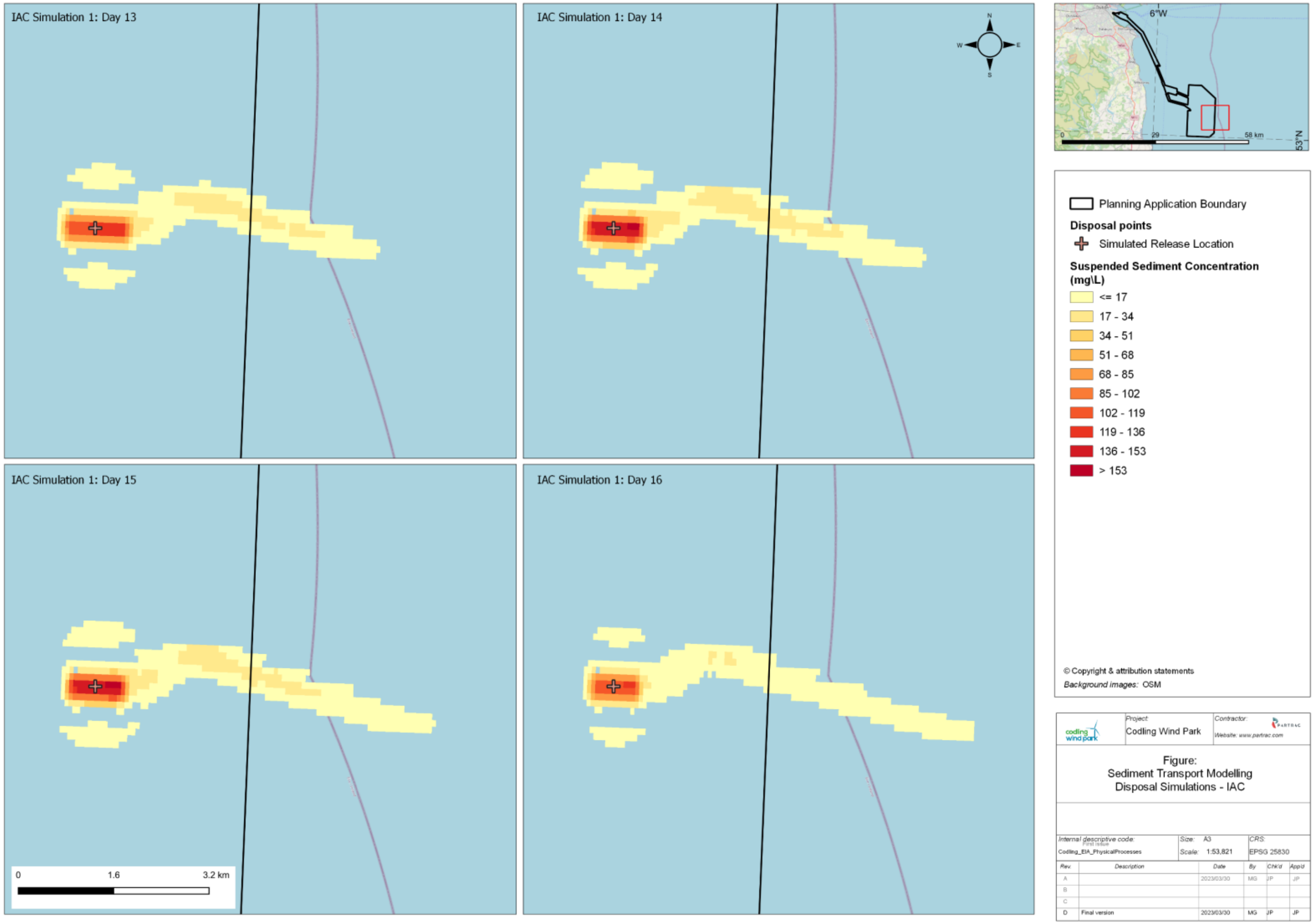

Figure 45 : SSC levels observed @ days 13 to 16 - Scenario 1.

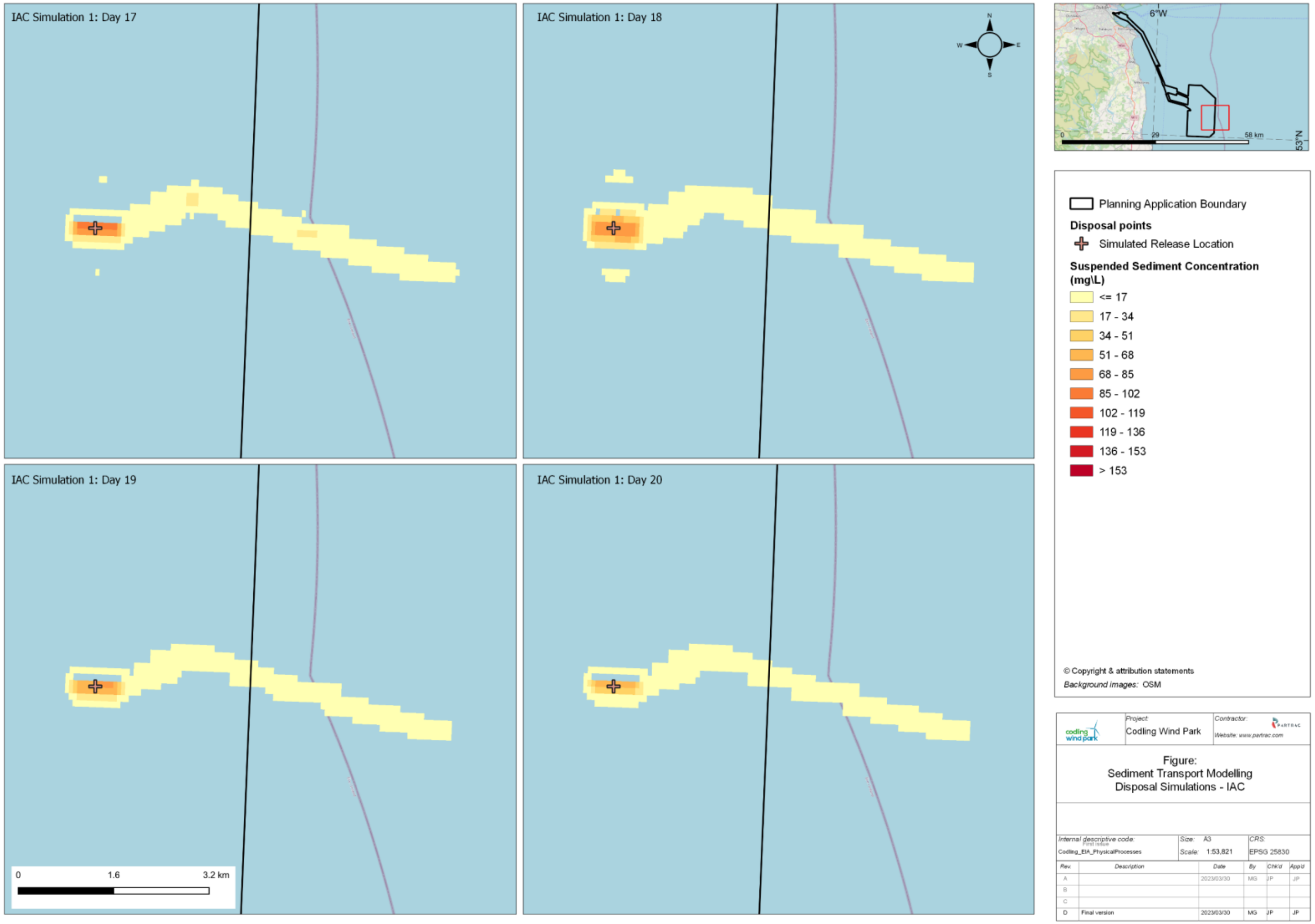

Figure 46 : SSC levels observed @ days 17 to 20 - Scenario 1.

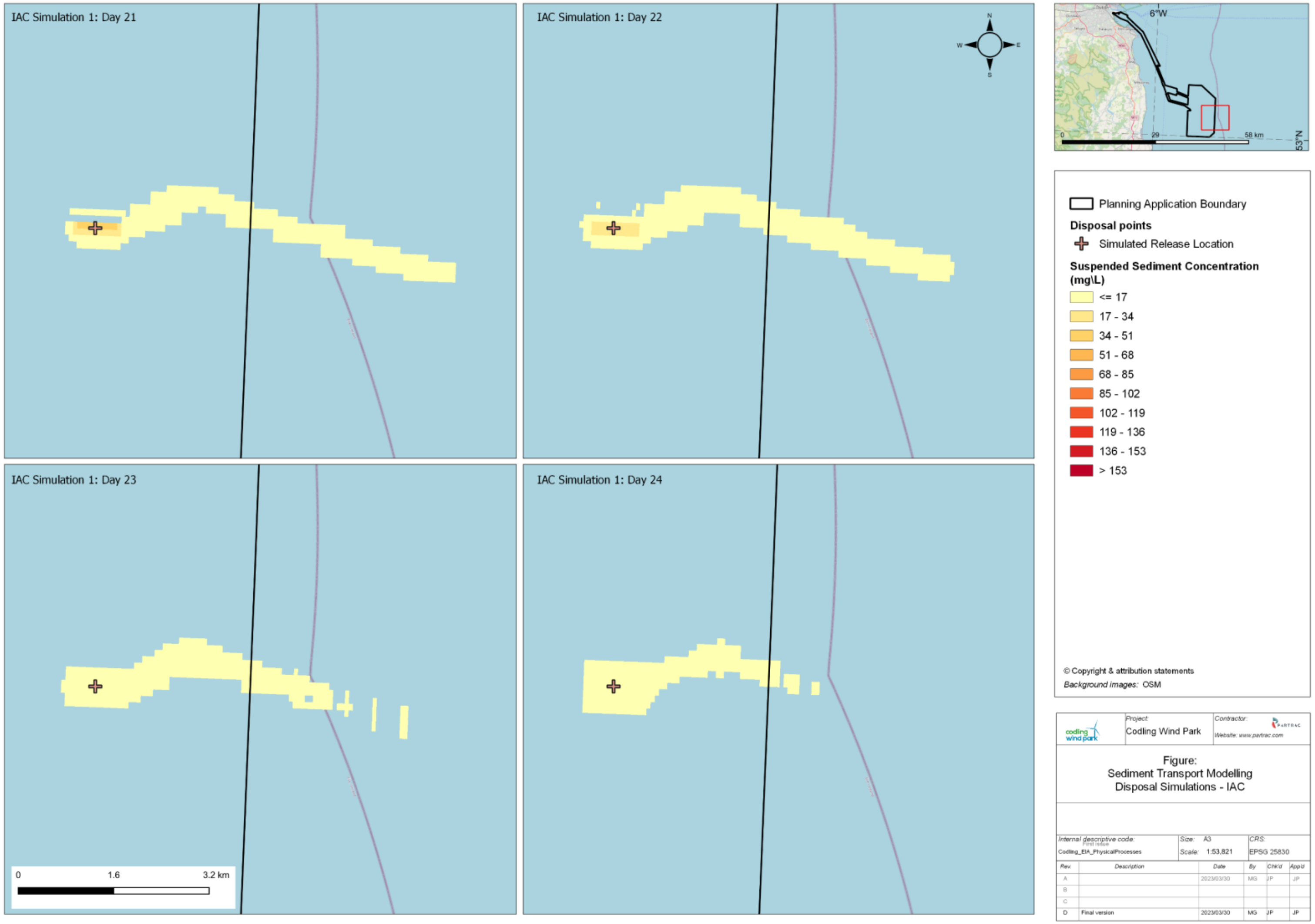

Figure 47 : SSC levels observed @ days 21 to 24 - Scenario 1.

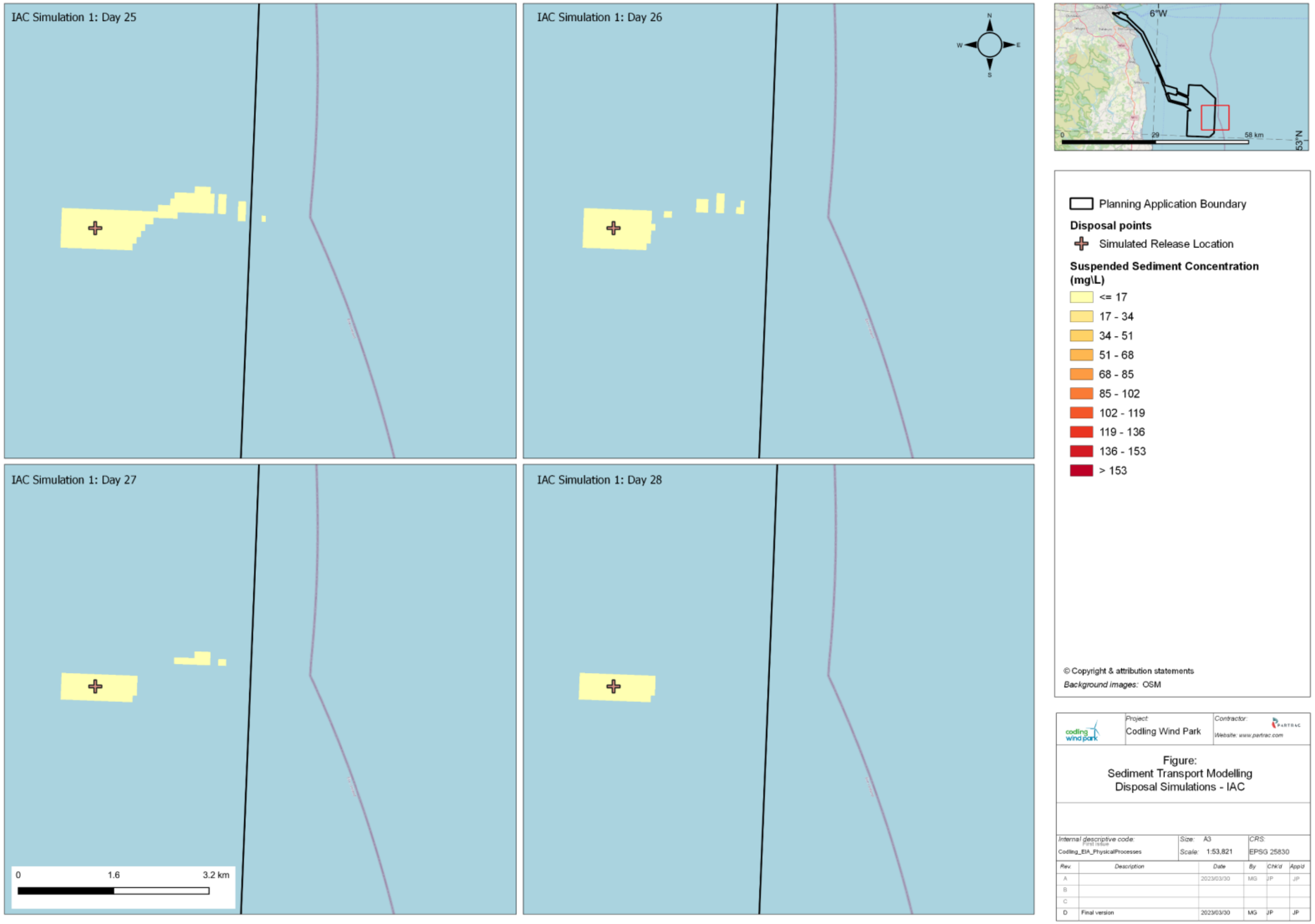

Figure 48 : SSC levels observed @ days 25 to 28 - Scenario 1.

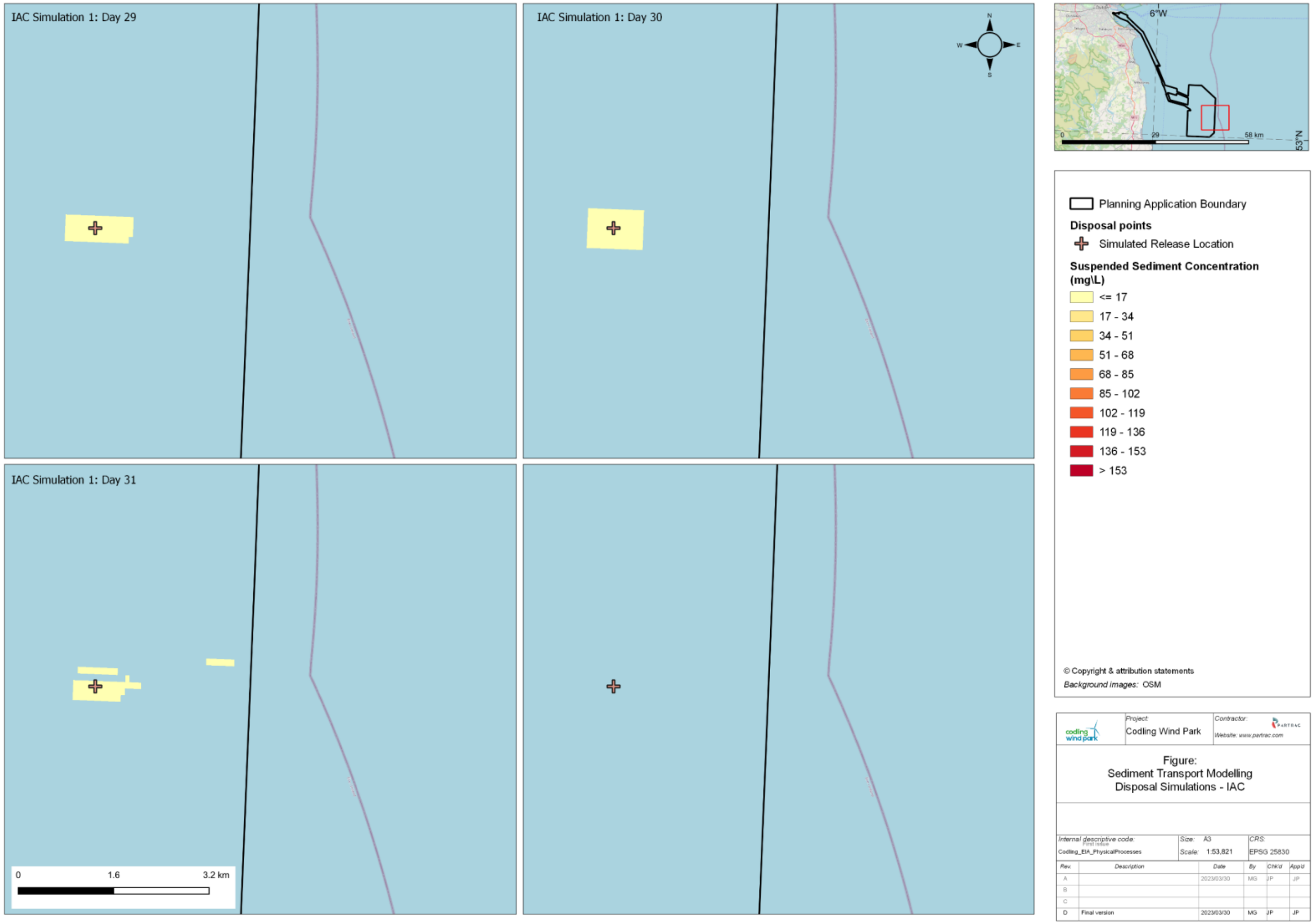

Figure 49 : SSC levels observed @ days 29 to 31 - Scenario 1.

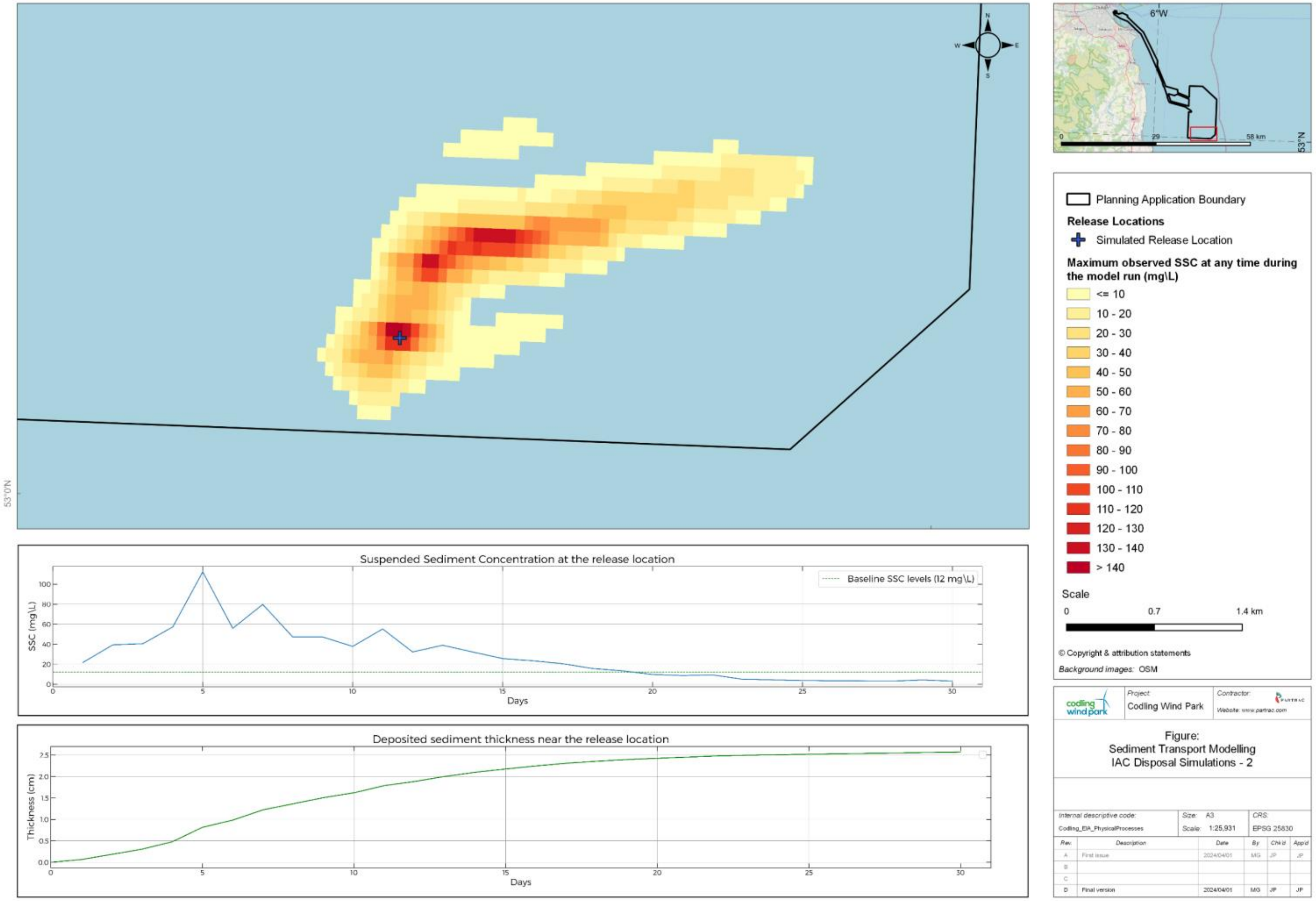

Figure 50: Maximum observed SSC levels at any time during scenario 2 run are presented in the spatial plot, the timeseries show 1) suspended sediment concentrations at the release location, and 2) the deposited sediment thickness at the release location.

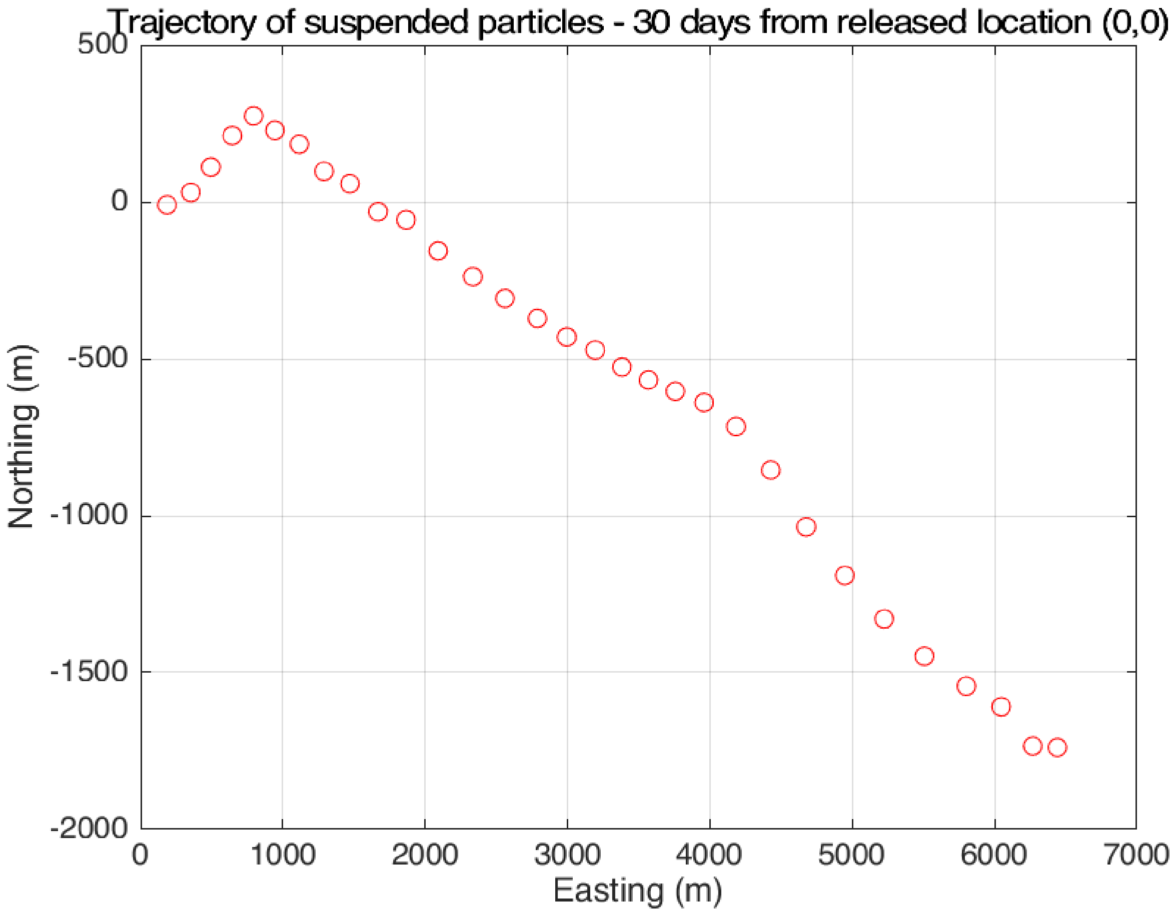

Figure 51: Trajectory of suspended sediments – Scenario 2.

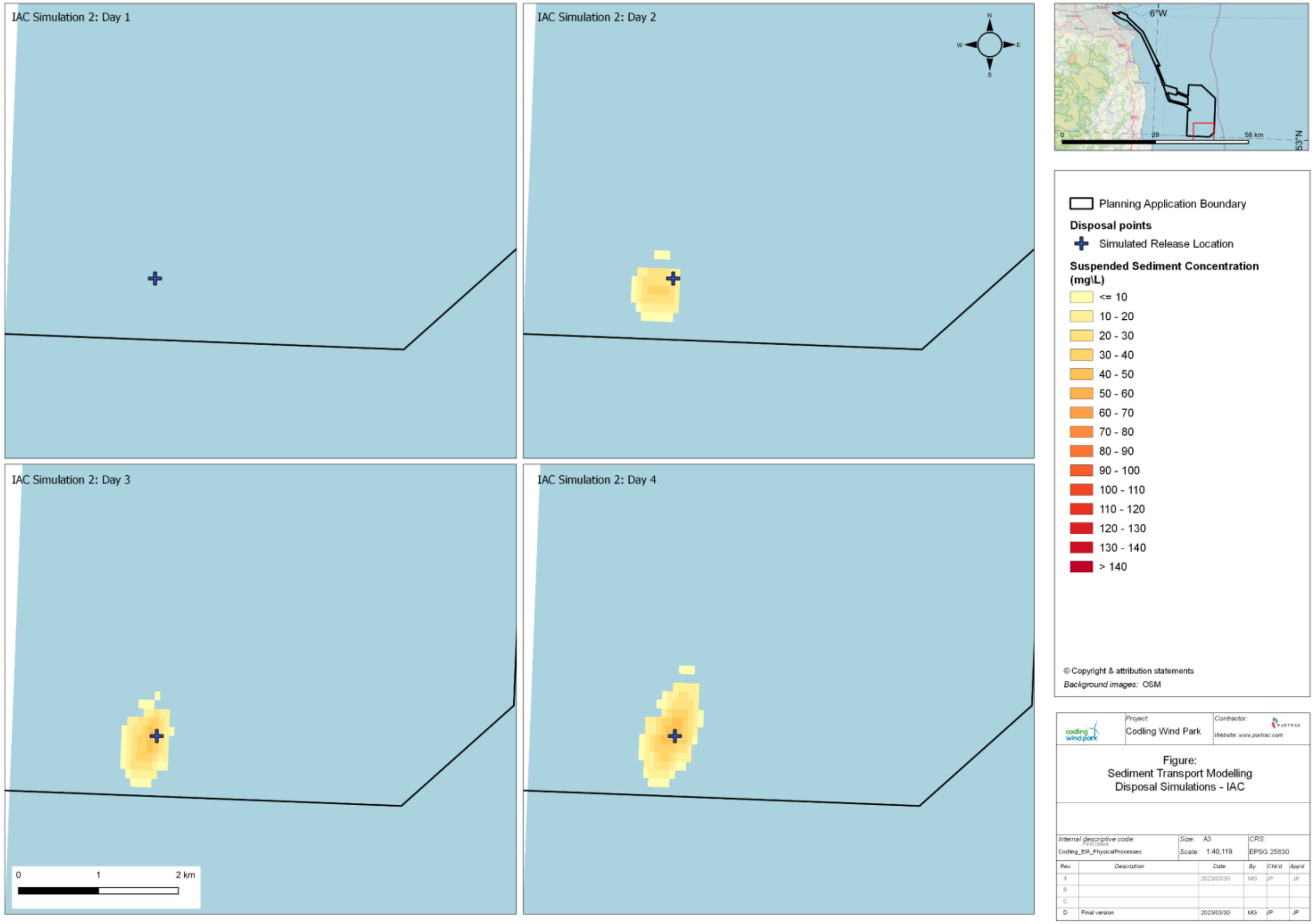

Figure 52 : SSC levels observed @ days 1 to 4 - Scenario 2.

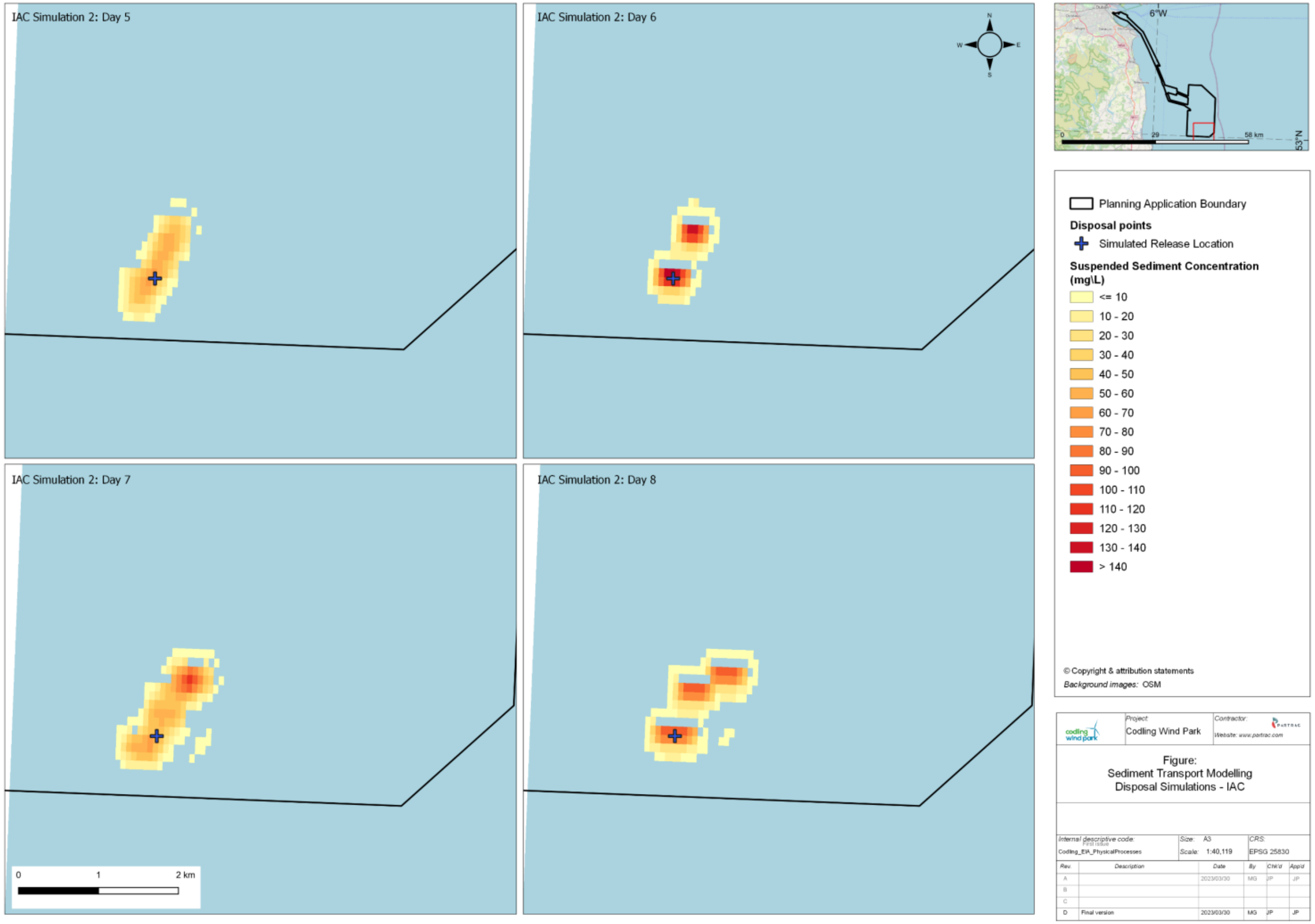

Figure 53 : SSC levels observed @ days 5 to 8 - Scenario 2.

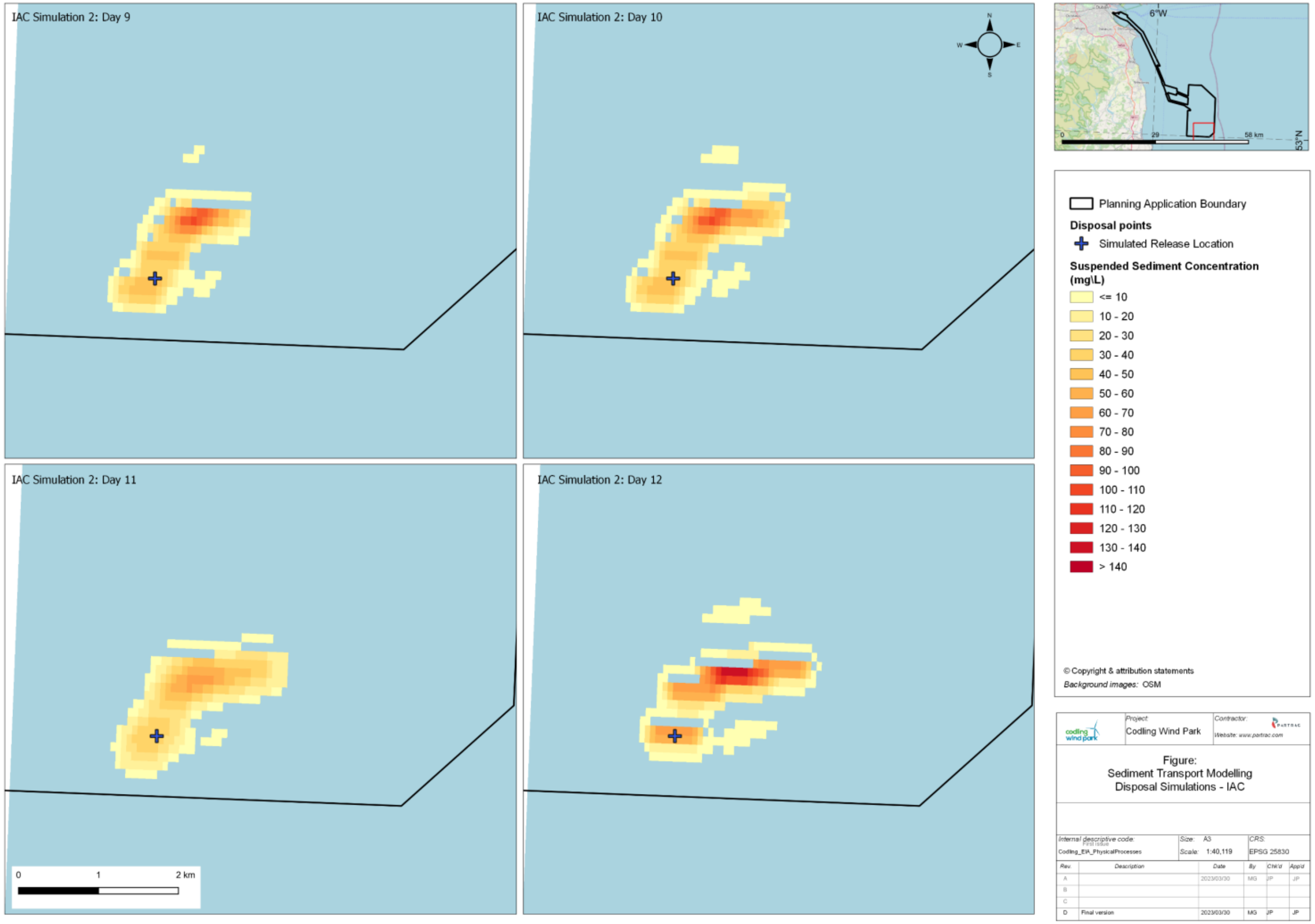

Figure 54 : SSC levels observed @ days 9 to 12 - Scenario 2.

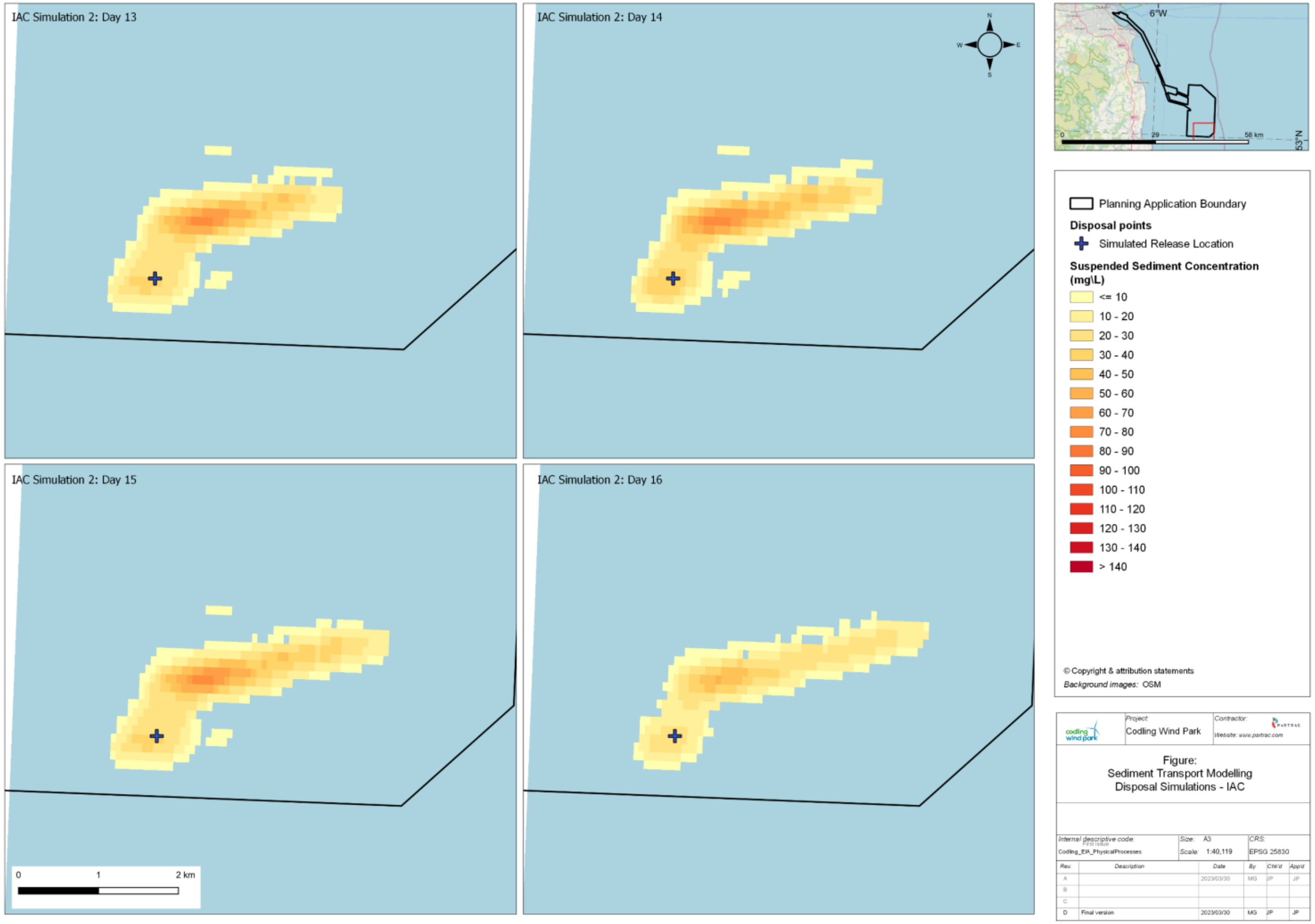

Figure 55 : SSC levels observed @ days 13 to 16 - Scenario 2.

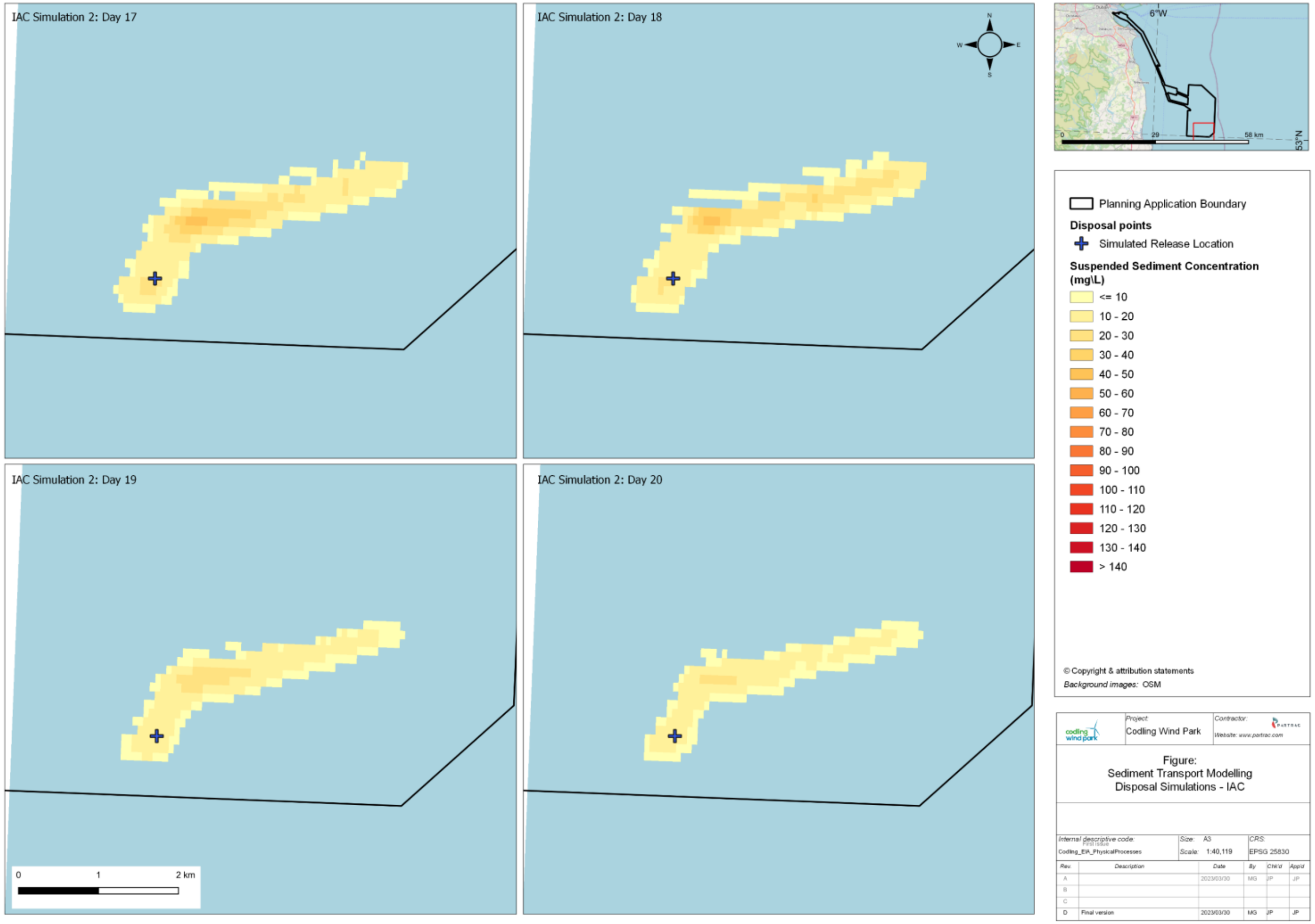

Figure 56 : SSC levels observed @ days 17 to 20 - Scenario 2.

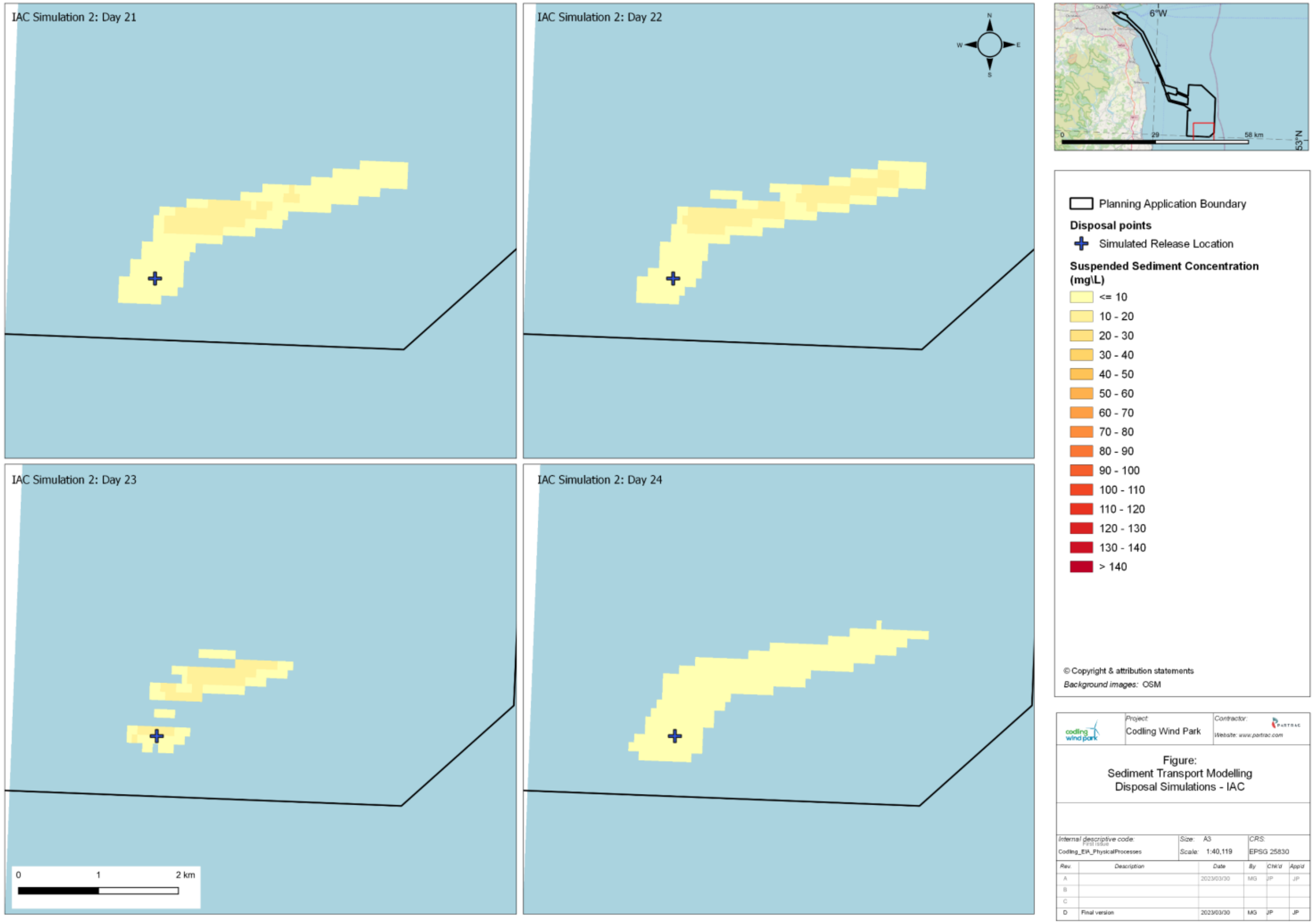

Figure 57 : SSC levels observed @ days 21 to 24 - Scenario 2.

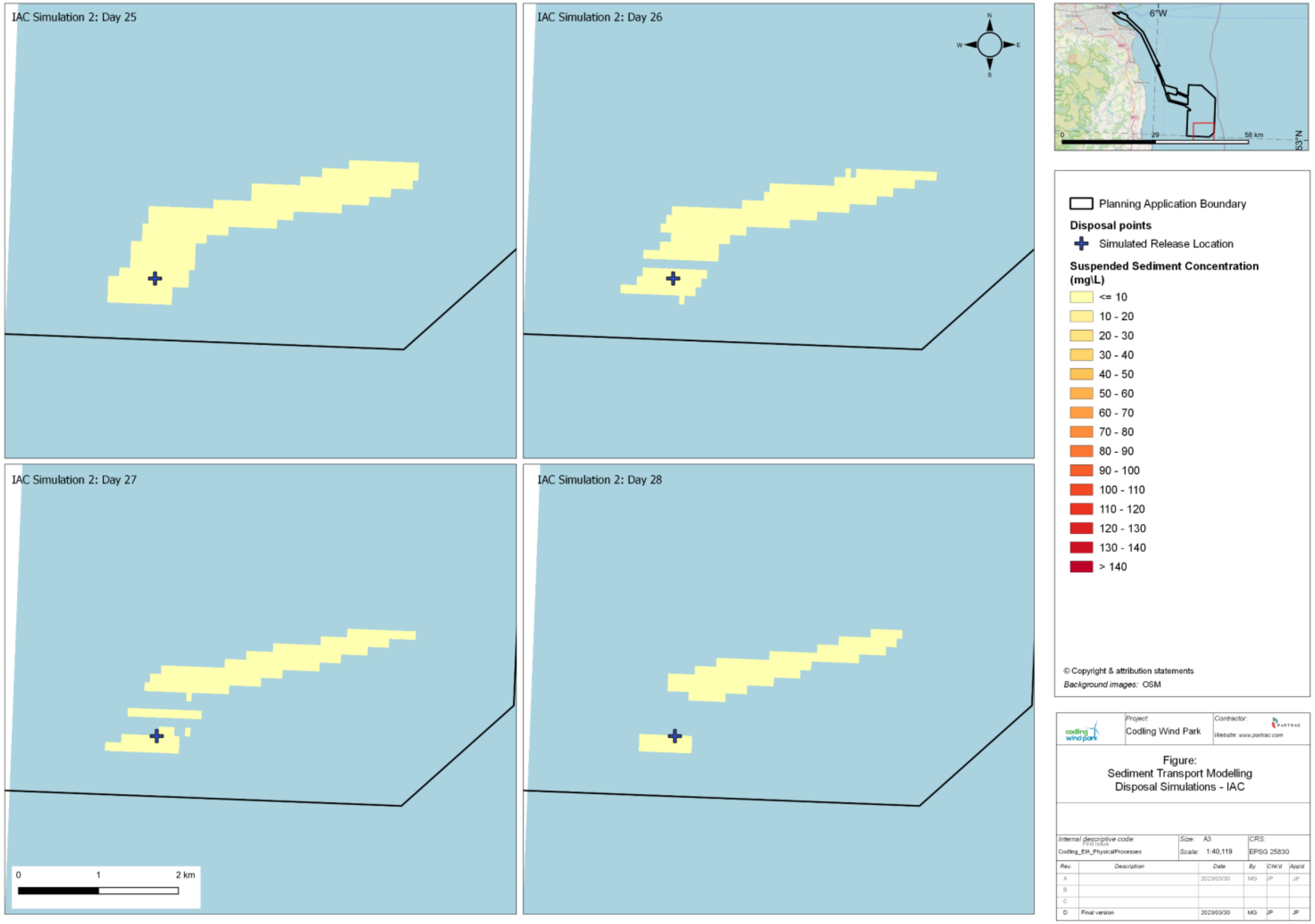

Figure 58 : SSC levels observed @ days 25 to 28 - Scenario 2.

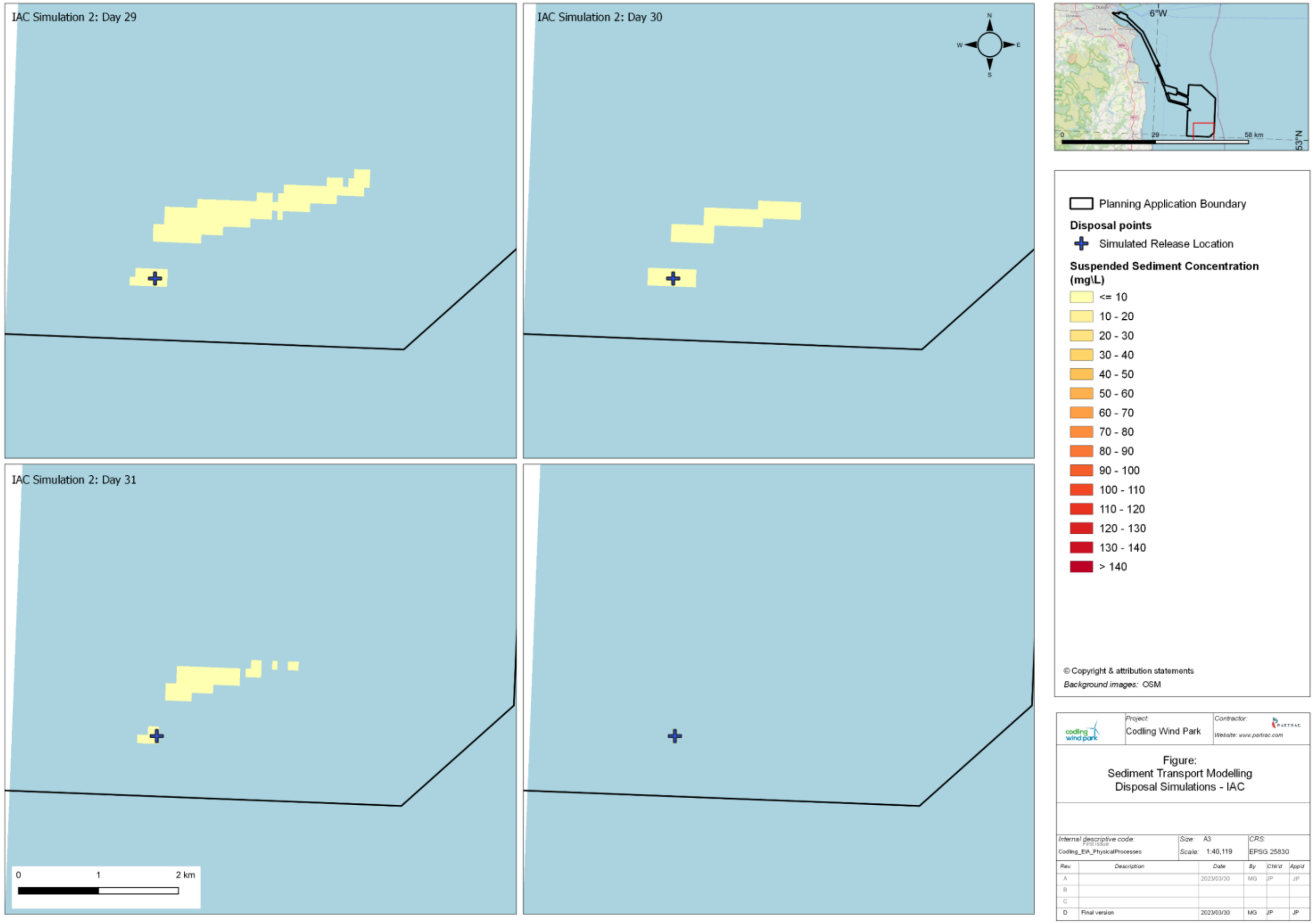

Figure 59 : SSC levels observed @ days 29 to 31 - Scenario 2.

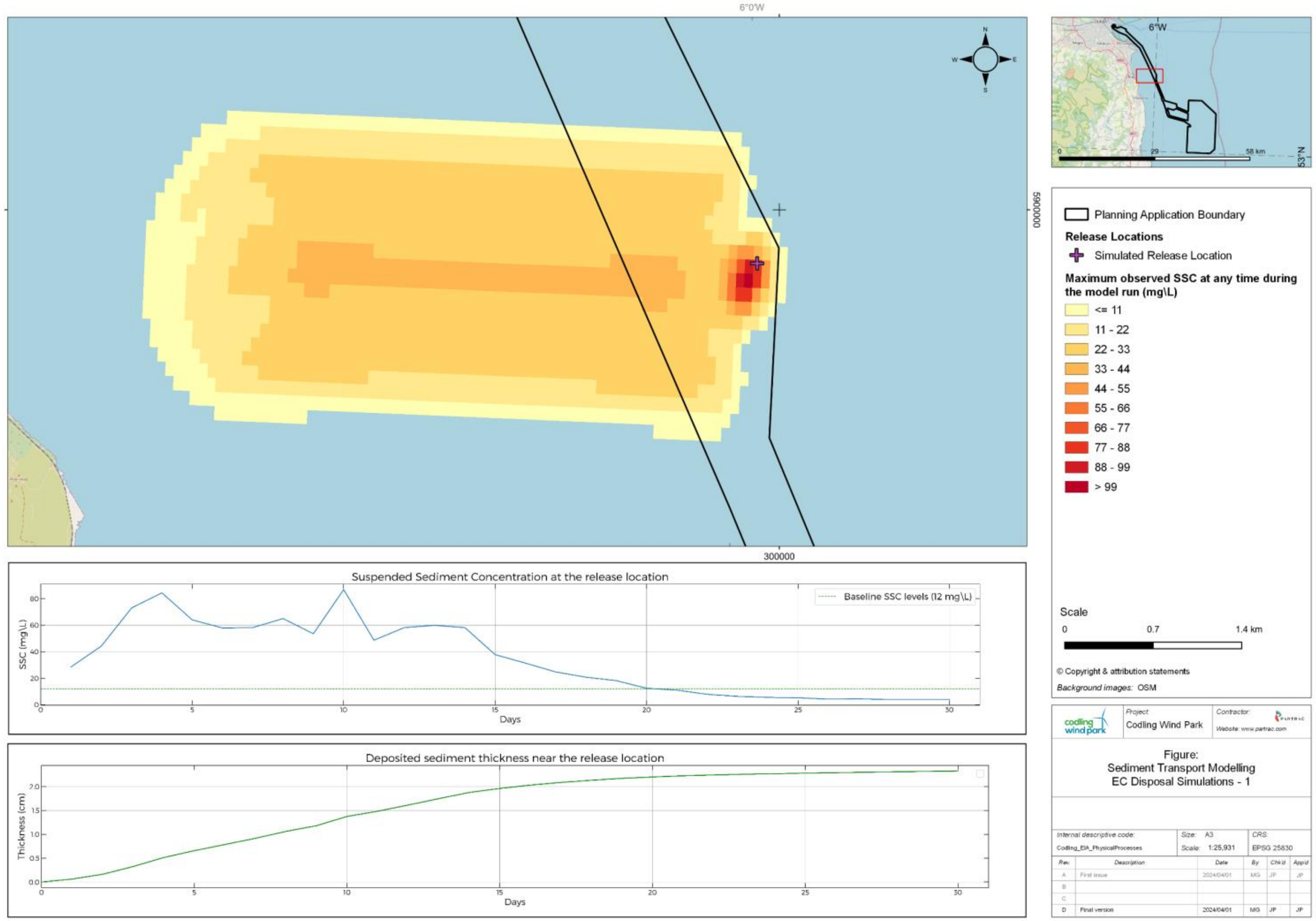

Figure 60: Maximum observed SSC levels at any time during Scenario 3 run are presented in the spatial plot, the timeseries show 1) suspended sediment concentrations at the release location, and 2) the deposited sediment thickness at the release location.

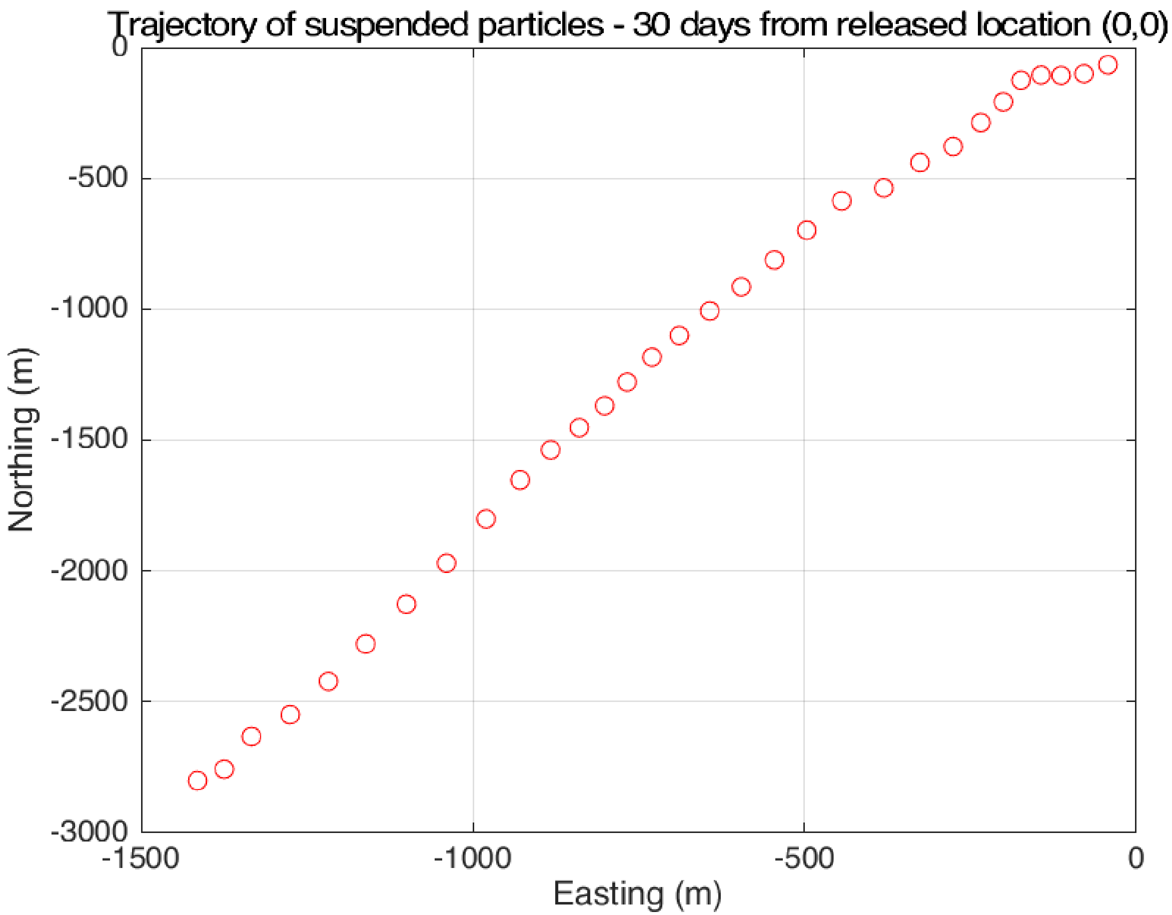

Figure 61: Trajectory of suspended sediments – Scenario 3.

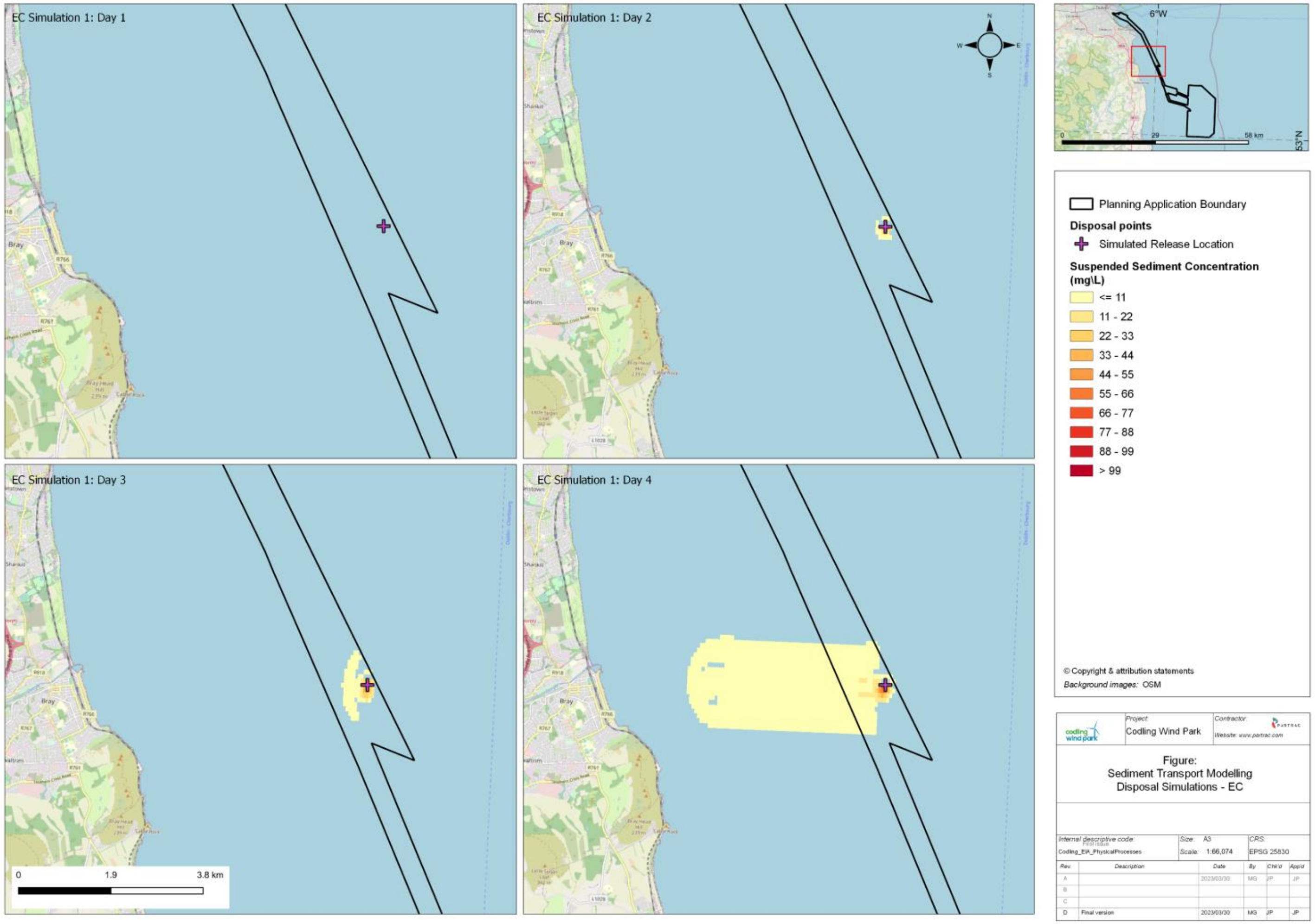

Figure 62 : SSC levels observed @ days 1 to 4 - Scenario 3.

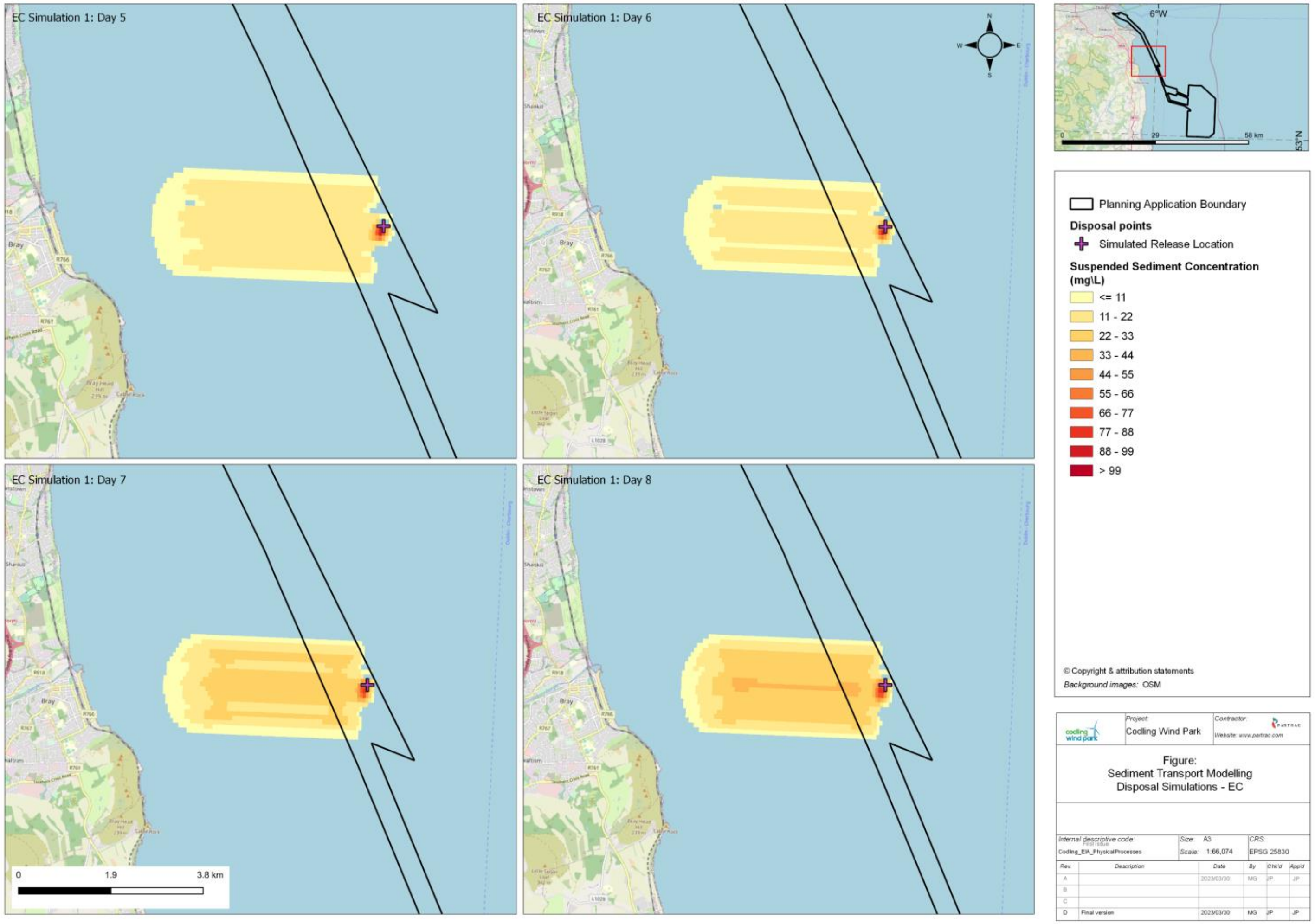

Figure 63 : SSC levels observed @ days 5 to 8 - Scenario 3.

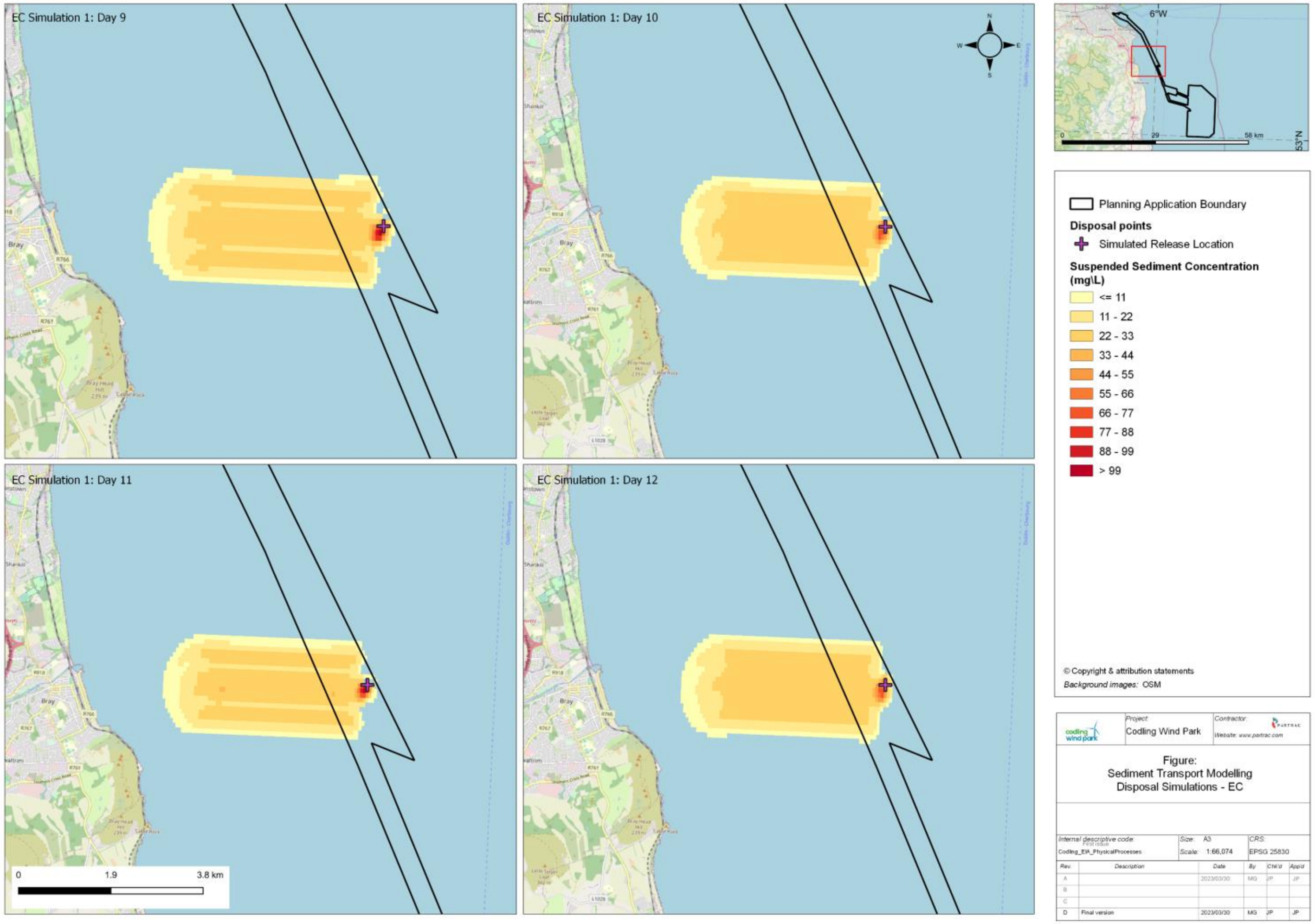

Figure 64 : SSC levels observed @ days 9 to 12 - Scenario 3.

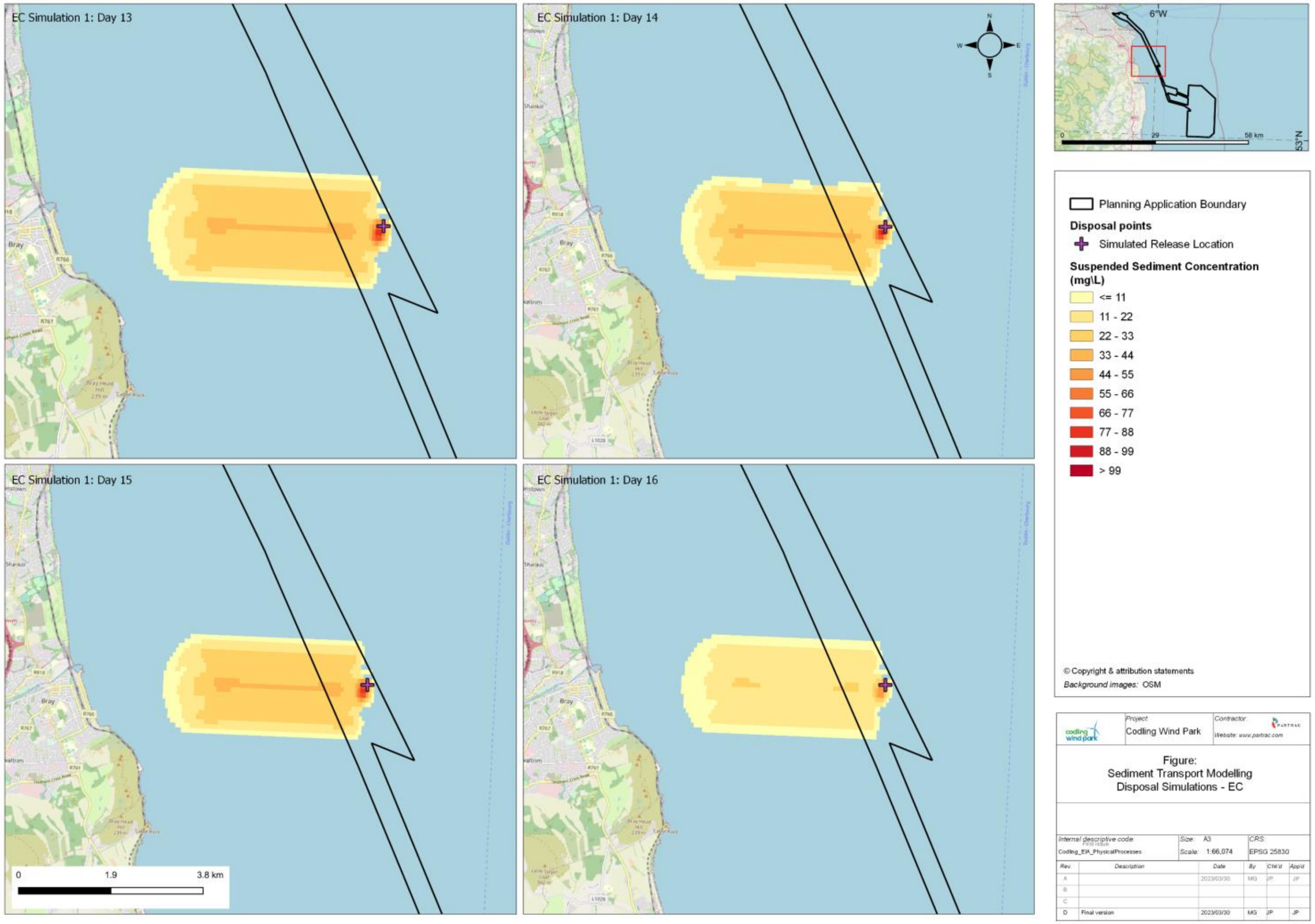

Figure 65 : SSC levels observed @ days 13 to 16 - Scenario 3.

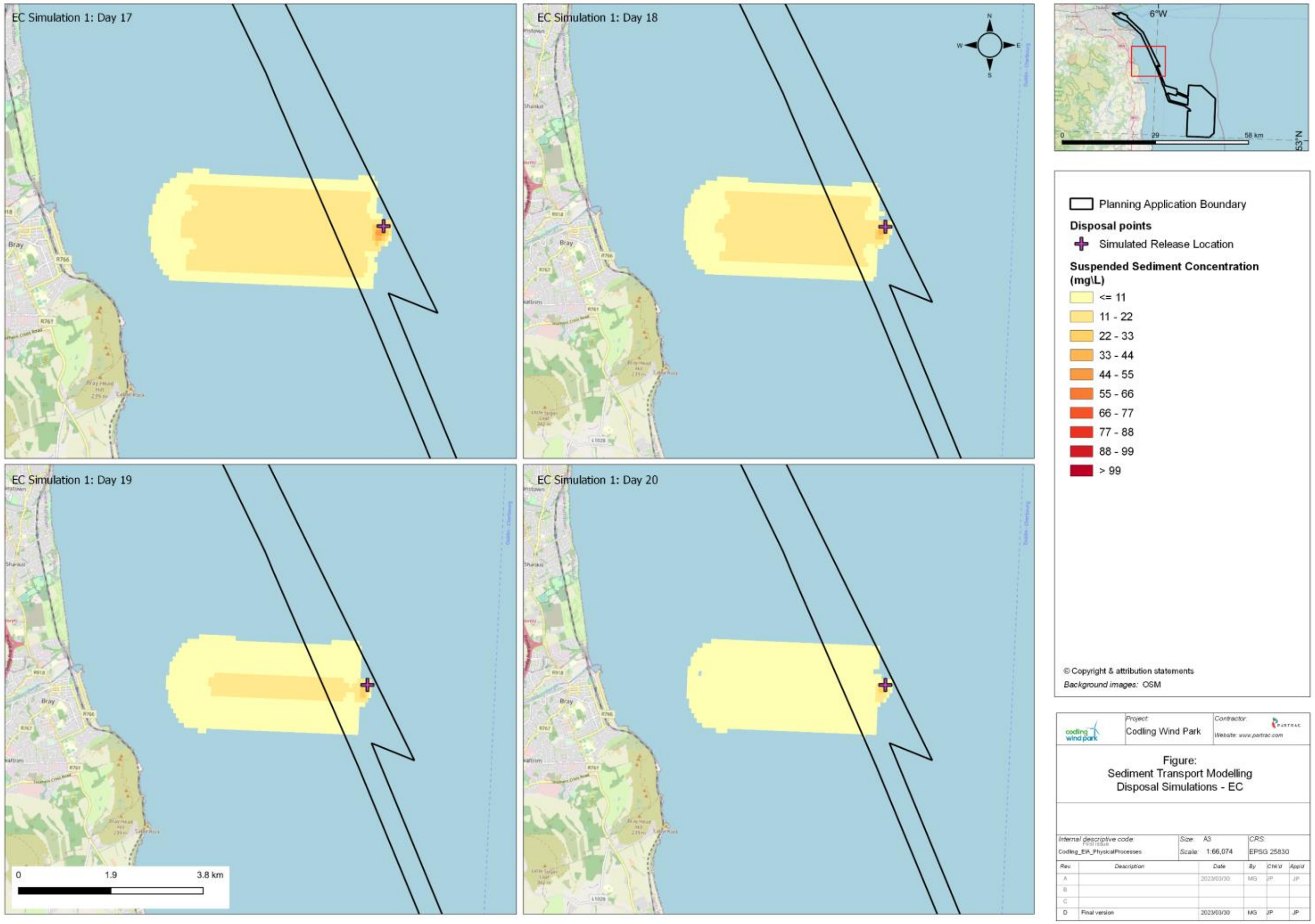

Figure 66 : SSC levels observed @ days 17 to 20 - Scenario 3.

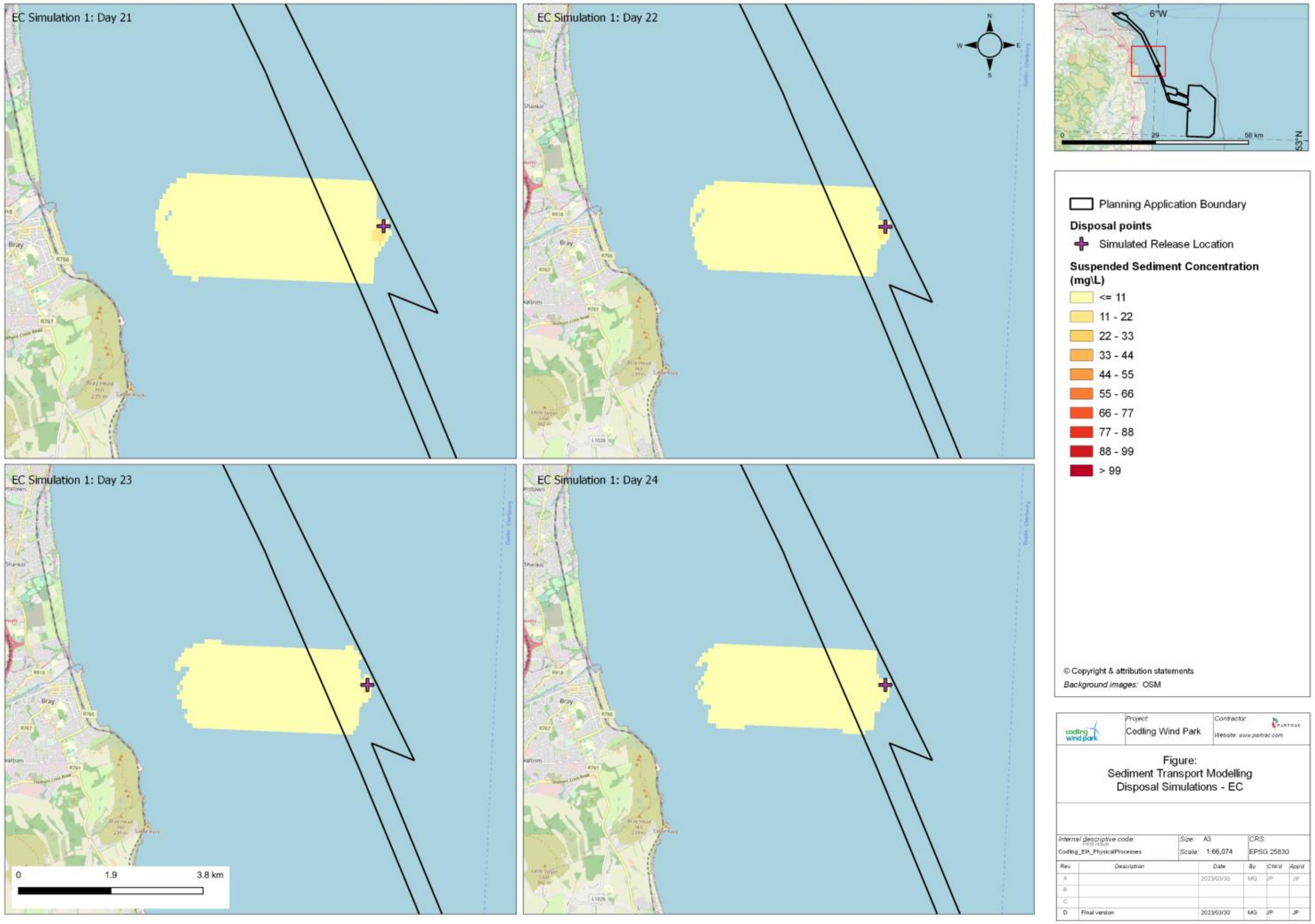

Figure 67 : SSC levels observed @ days 21 to 24 - Scenario 3.

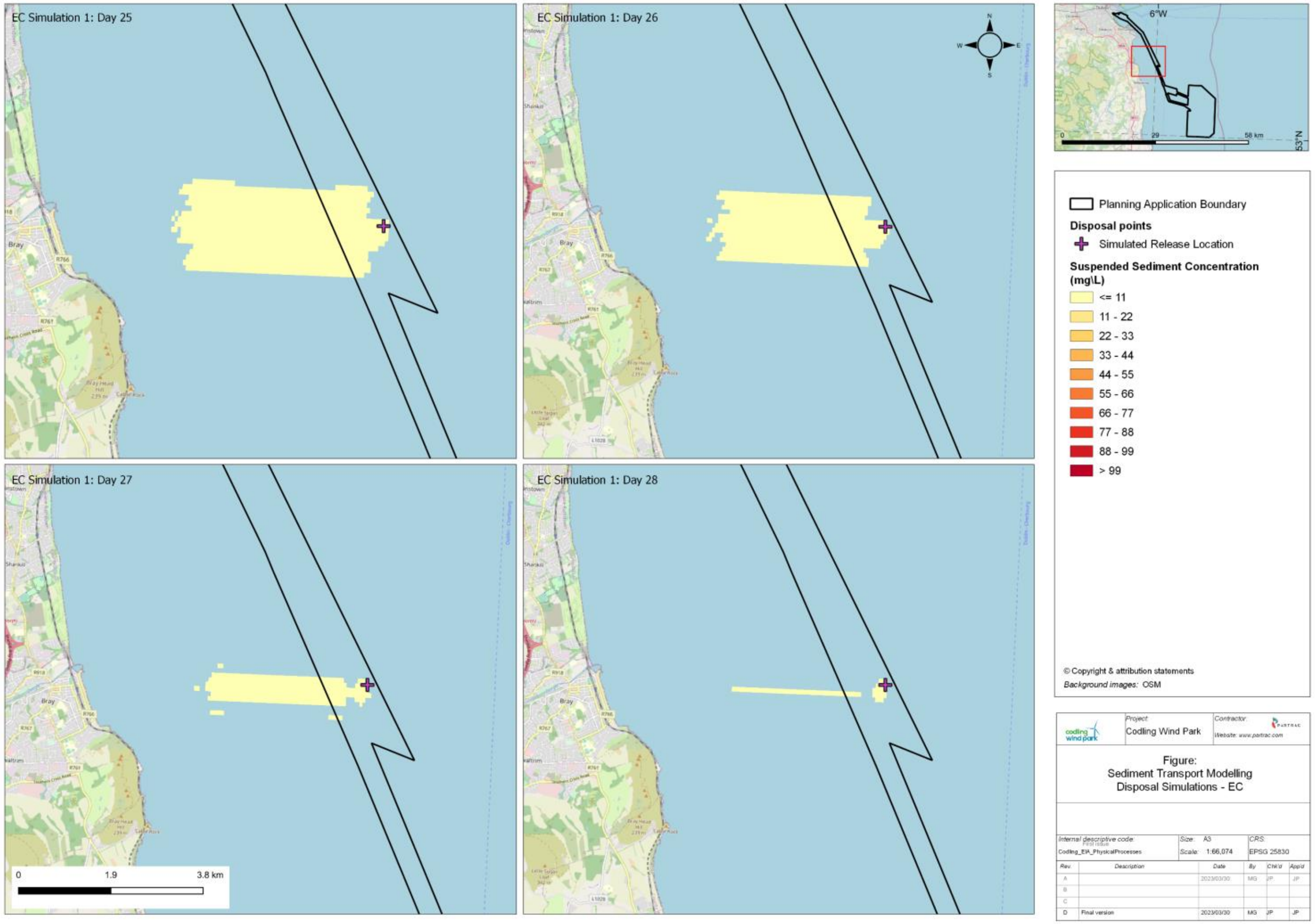

Figure 68 : SSC levels observed @ days 25 to 28 - Scenario 3.

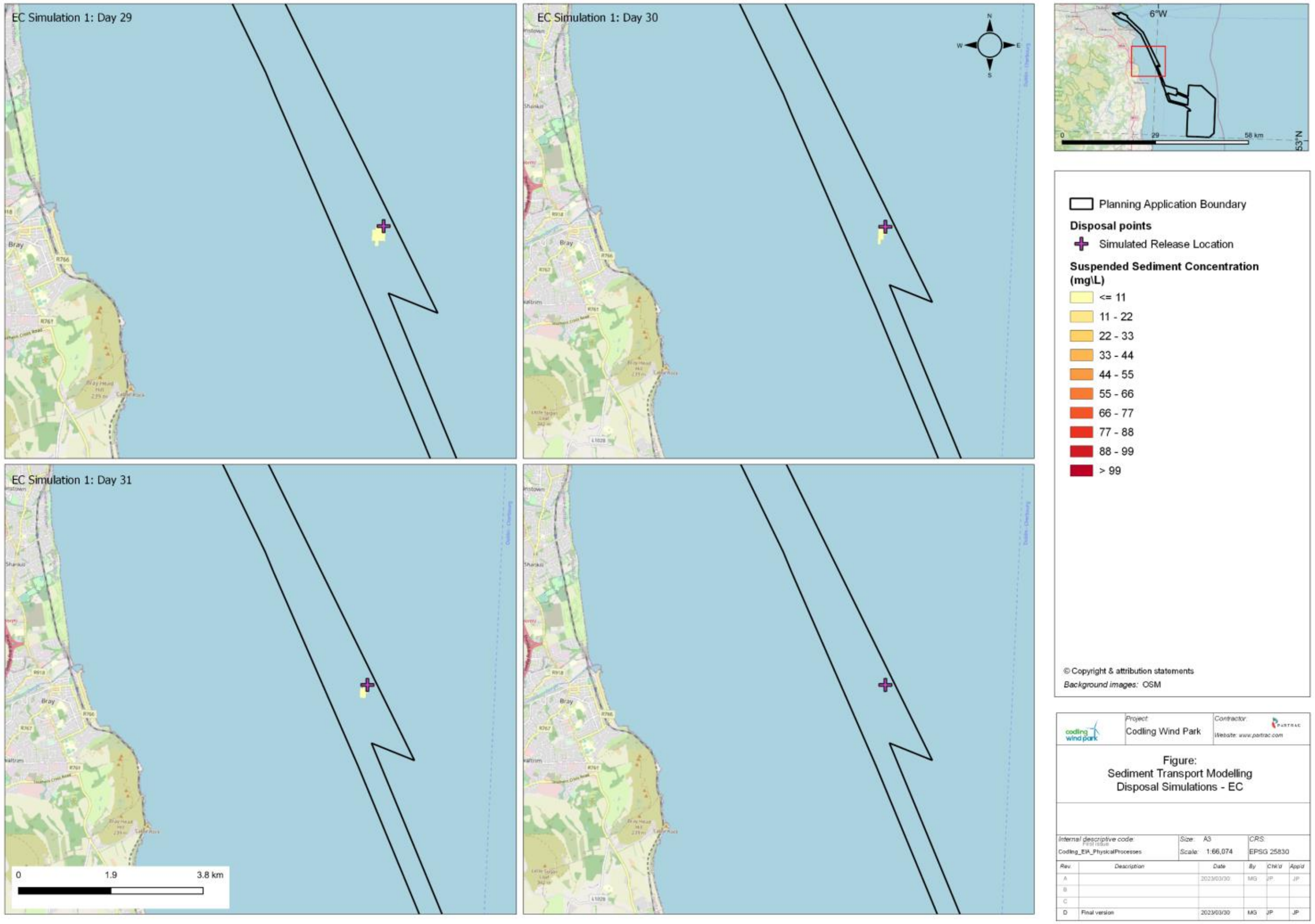

Figure 69 : SSC levels observed @ days 29 to 31 - Scenario 3.

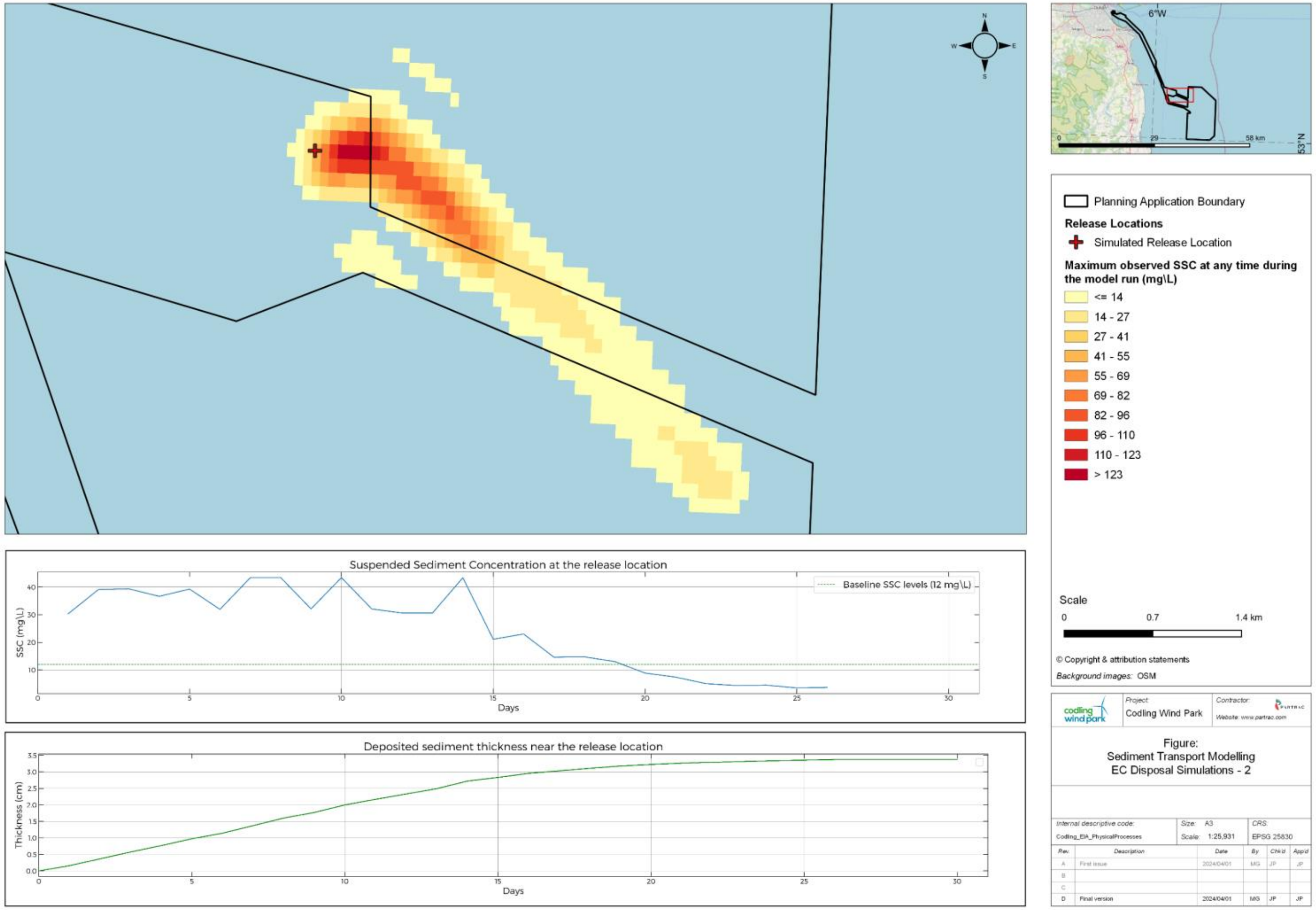

Figure 70: Maximum observed SSC levels at any time during scenario 4 run are presented in the spatial plot, the timeseries show 1) suspended sediment concentrations at the release location, and 2) the deposited sediment thickness at the release location.

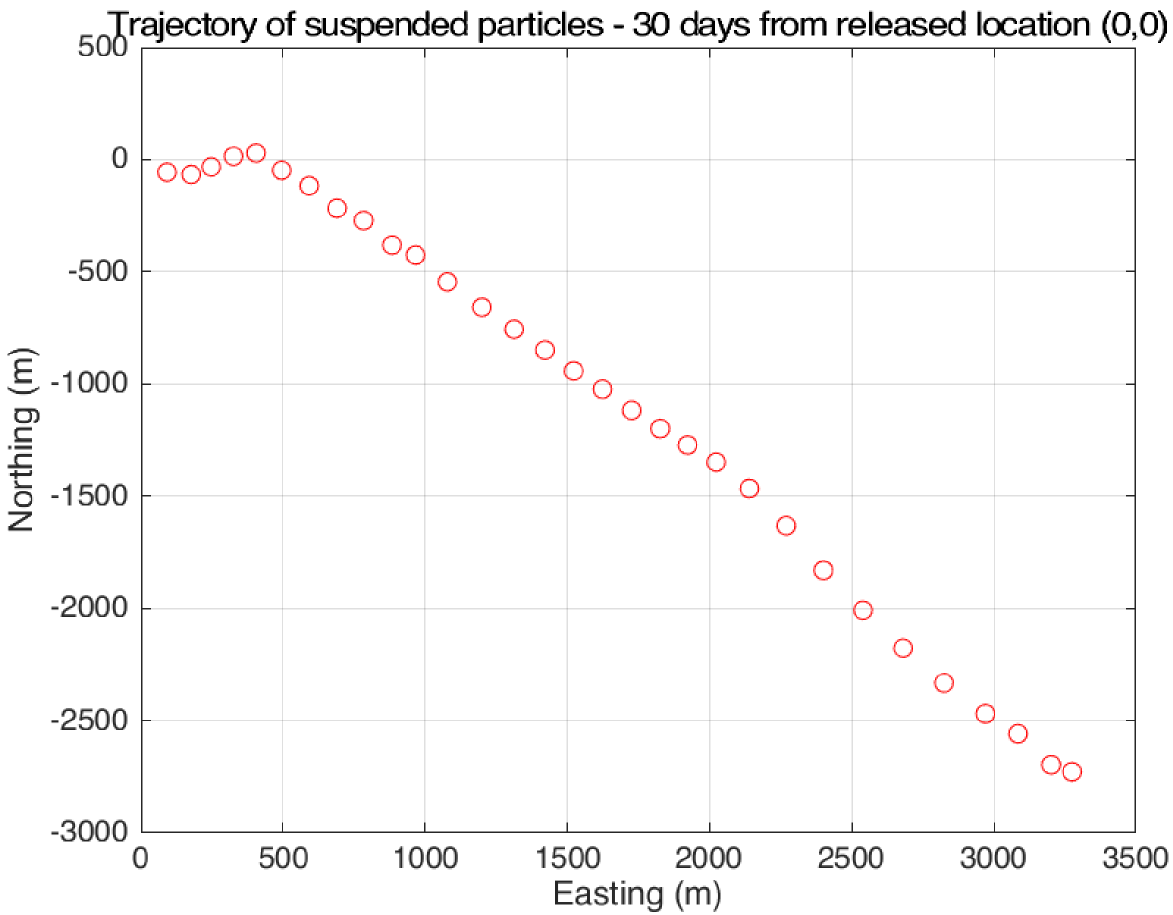

Figure 71: Trajectory of suspended sediments – Scenario 4.

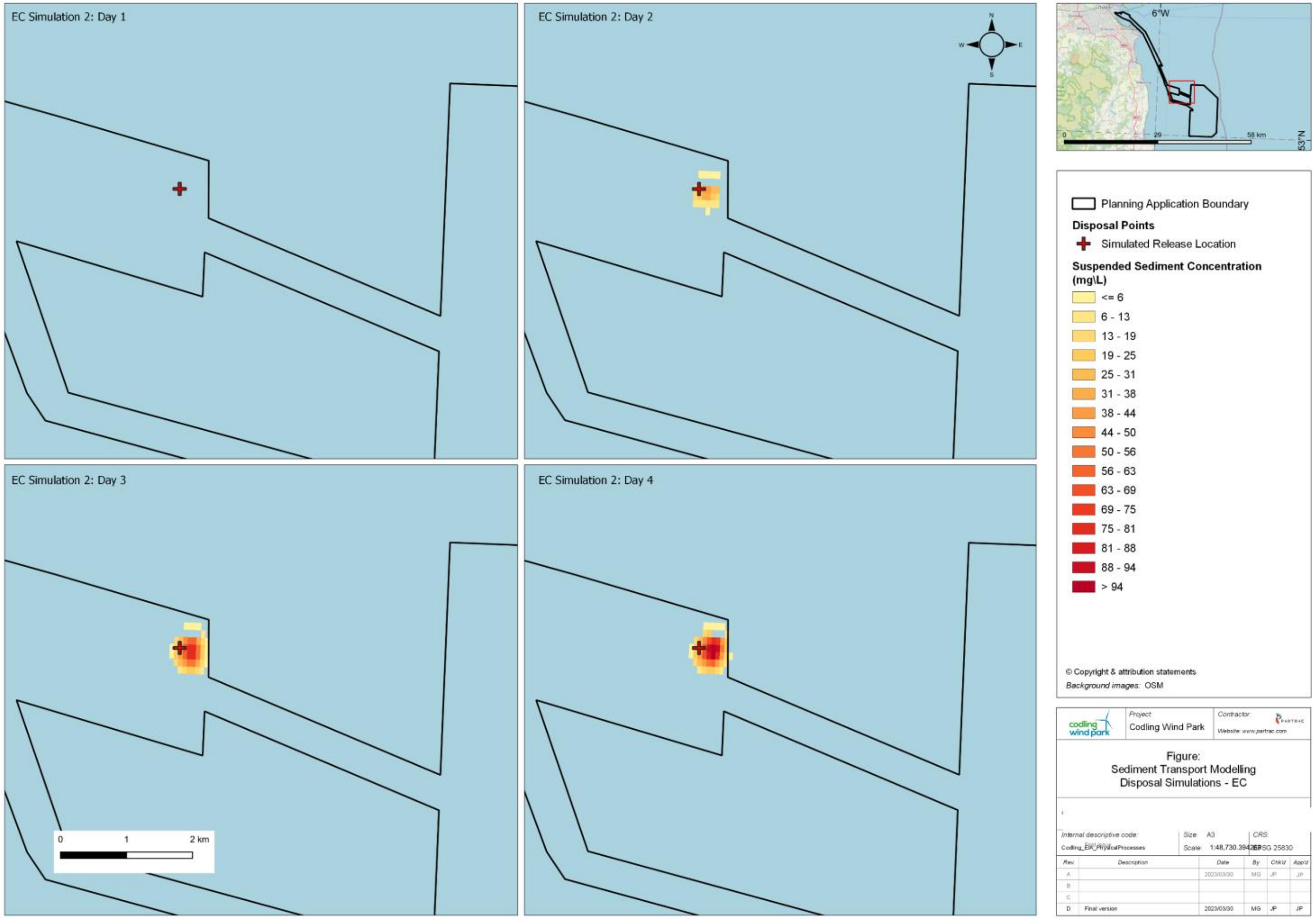

Figure 72 : SSC levels observed @ days 1 to 4 - Scenario 4.

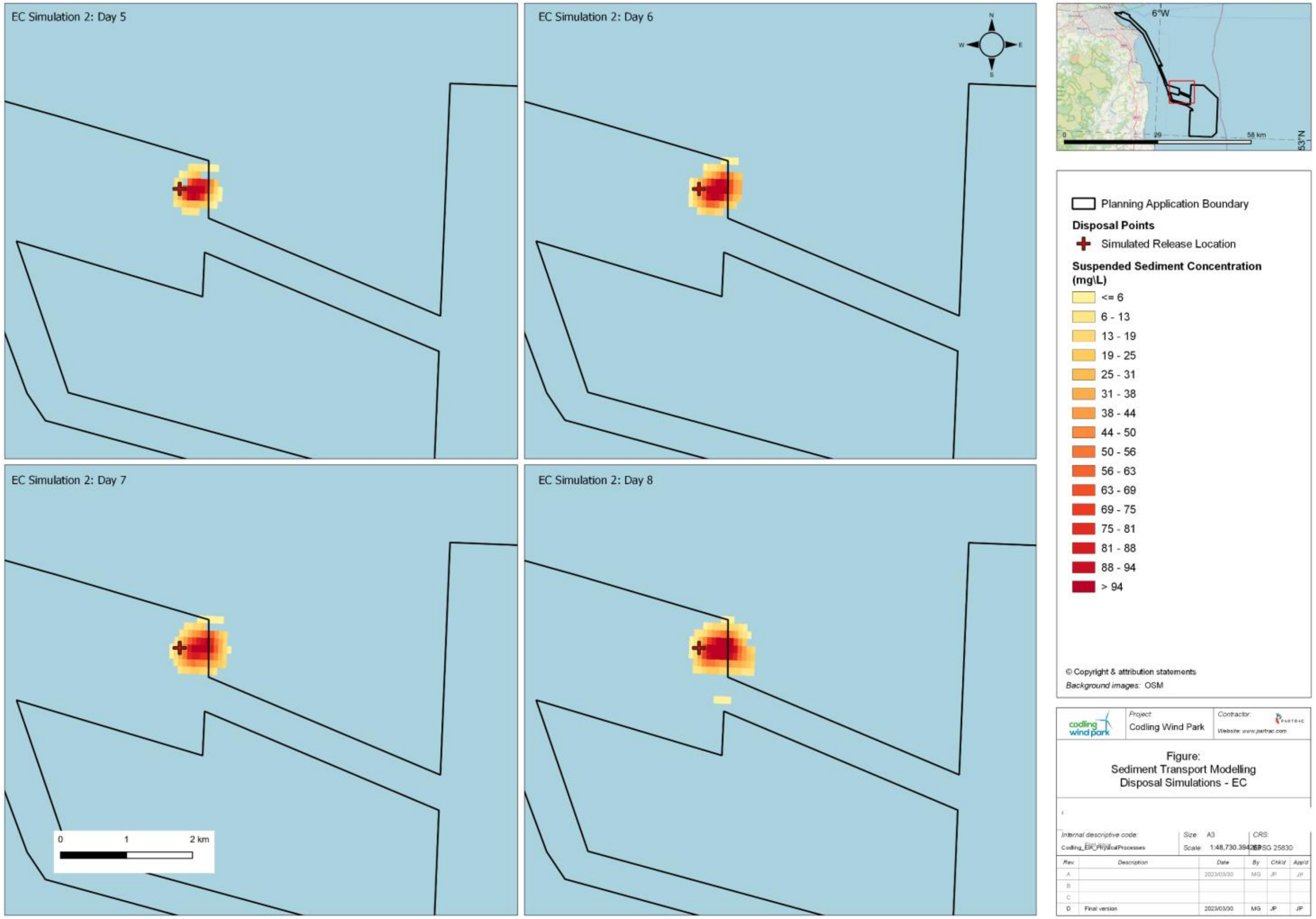

Figure 73 : SSC levels observed @ days 5 to 8 - Scenario 4.

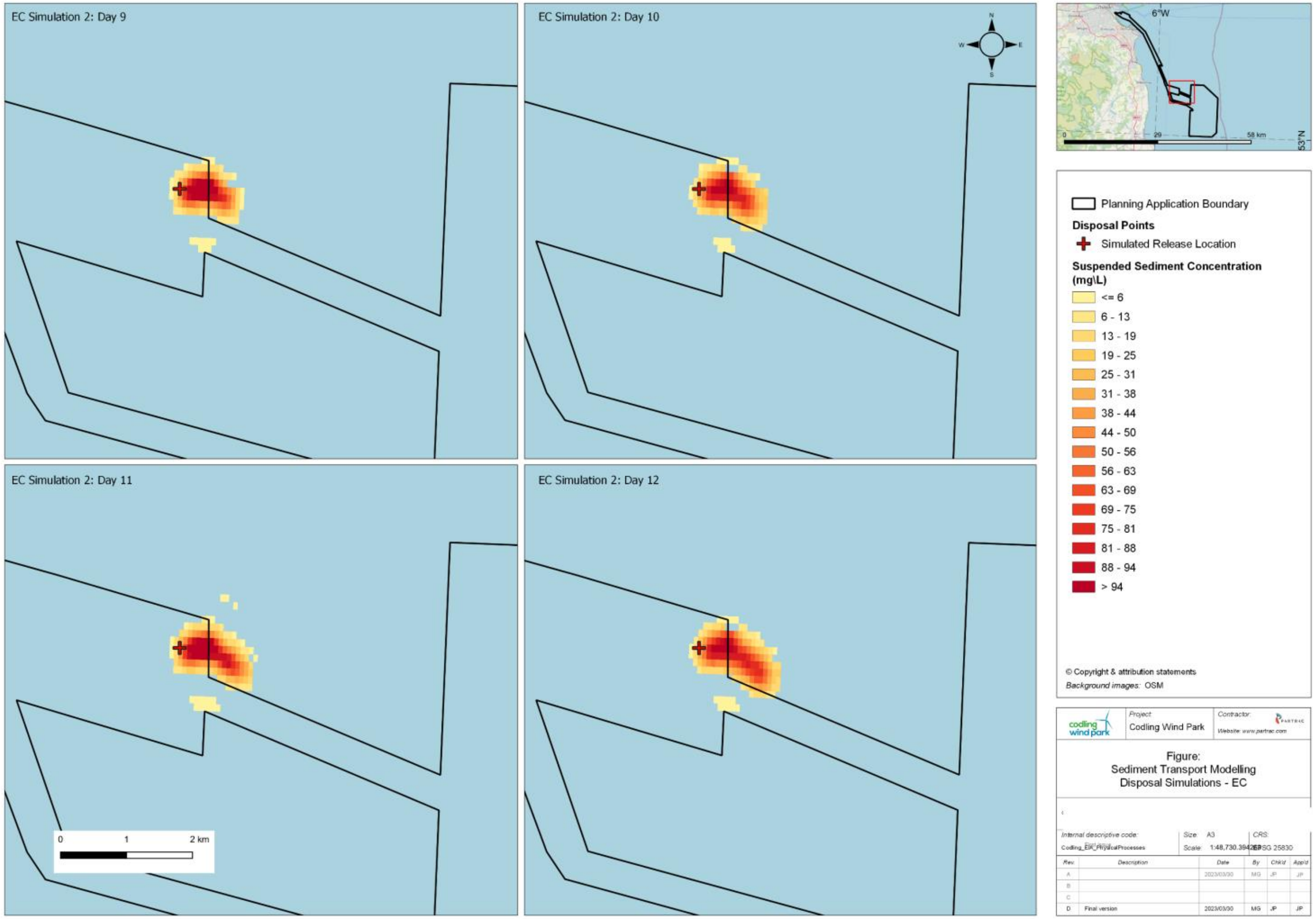

Figure 74 : SSC levels observed @ days 9 to 12 - Scenario 4.

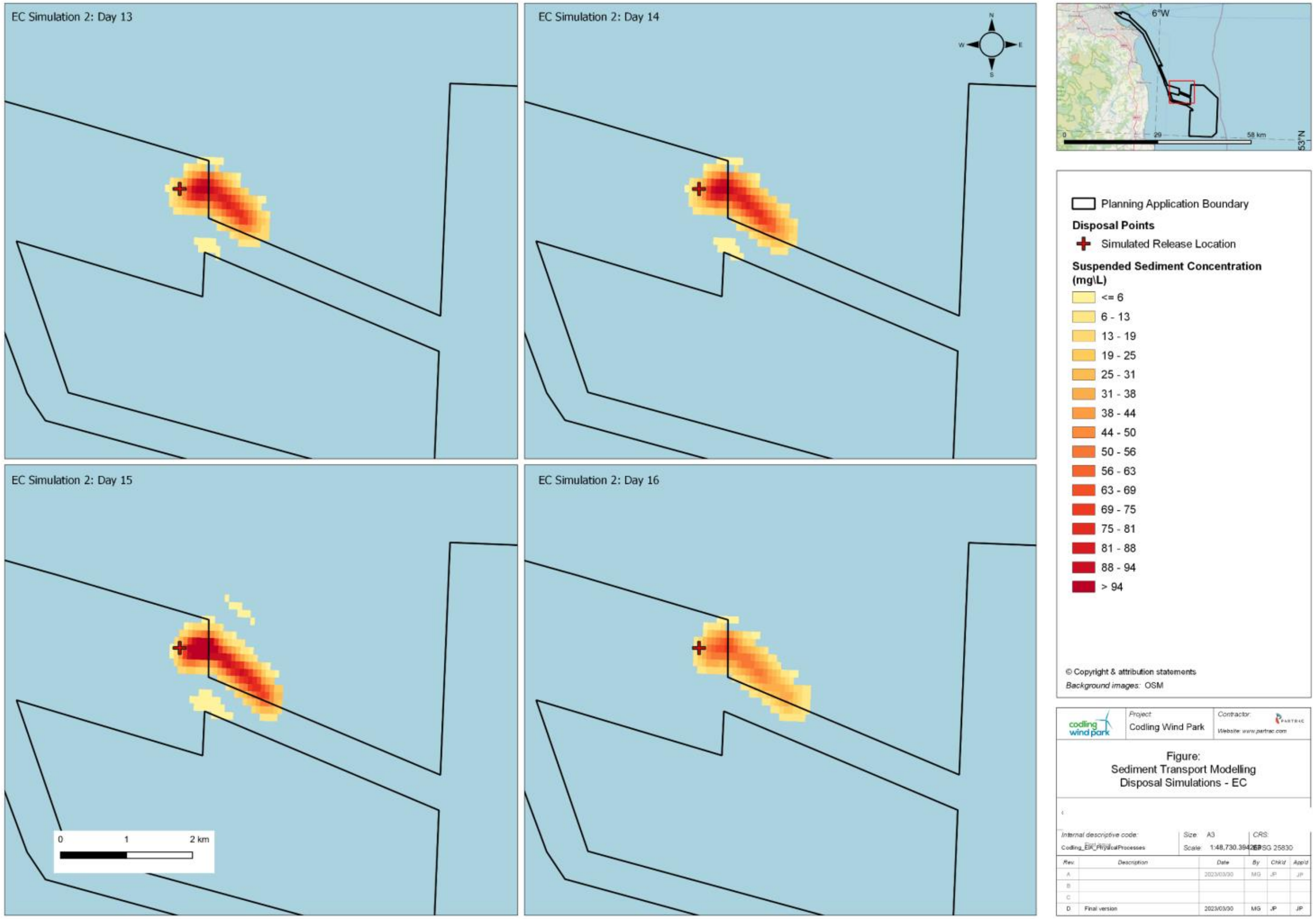

Figure 75 : SSC levels observed @ days 13 to 16 - Scenario 4.

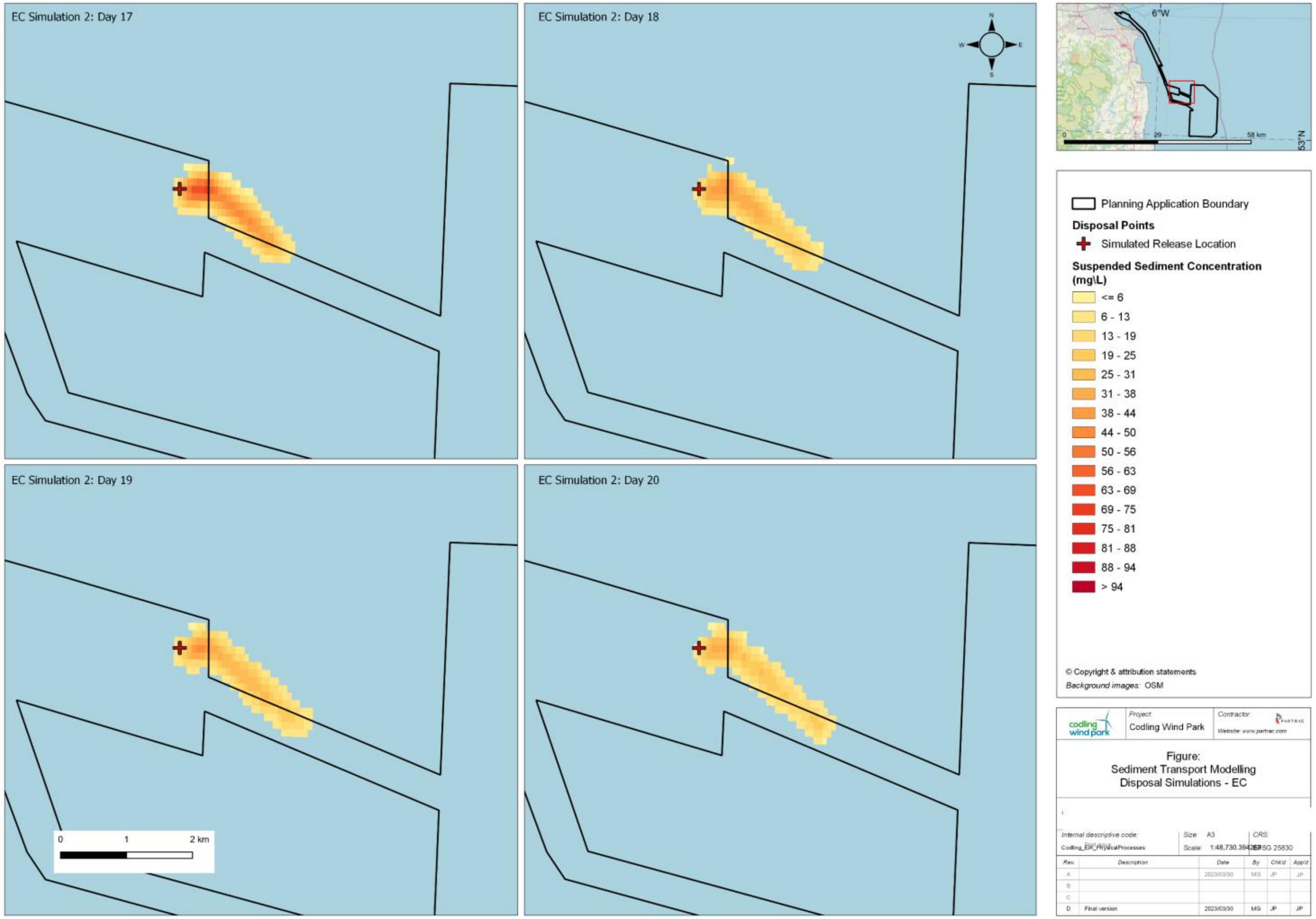

Figure 76 : SSC levels observed @ days 17 to 20 - Scenario 4.

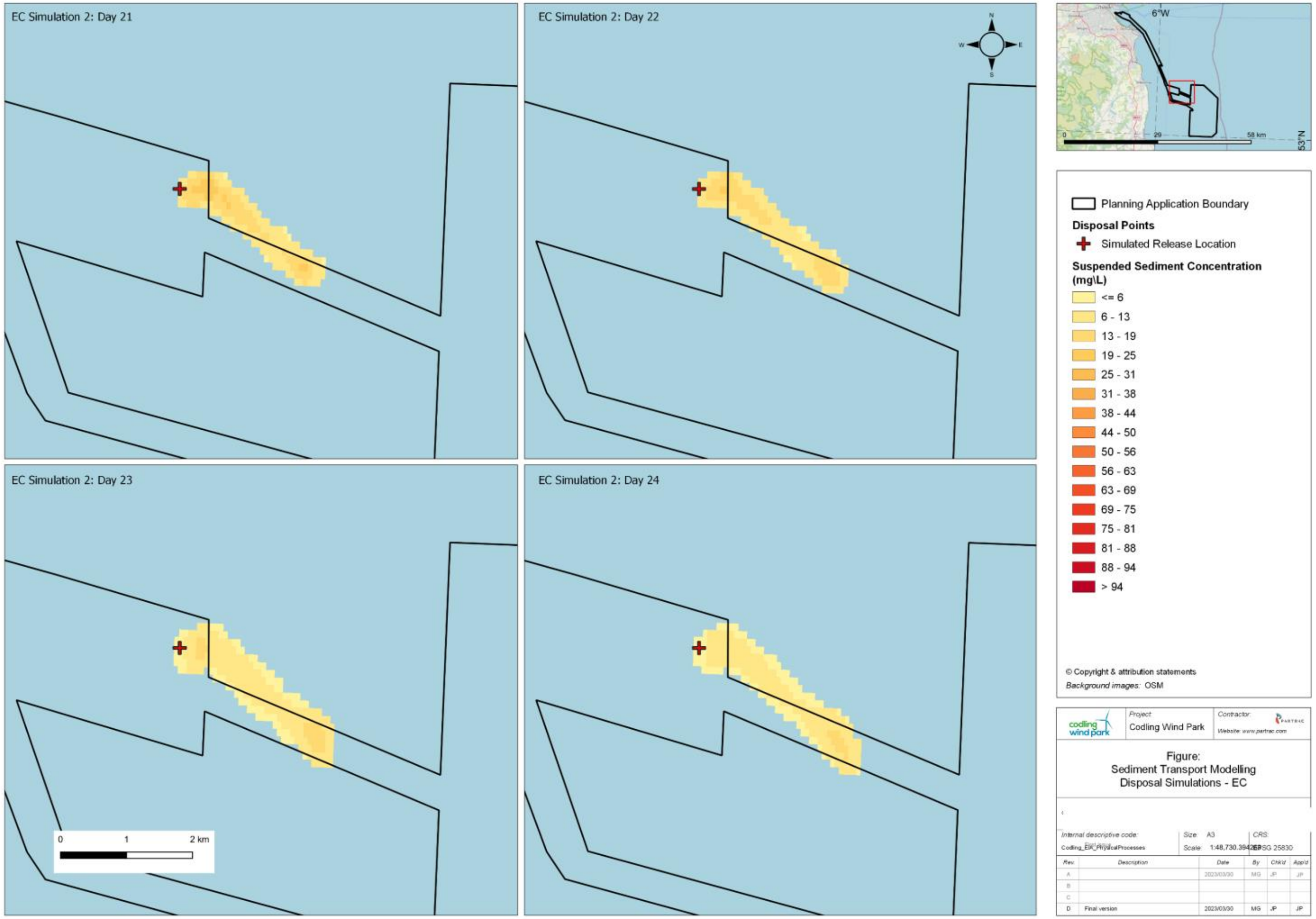

Figure 77 : SSC levels observed @ days 21 to 24 - Scenario 4.

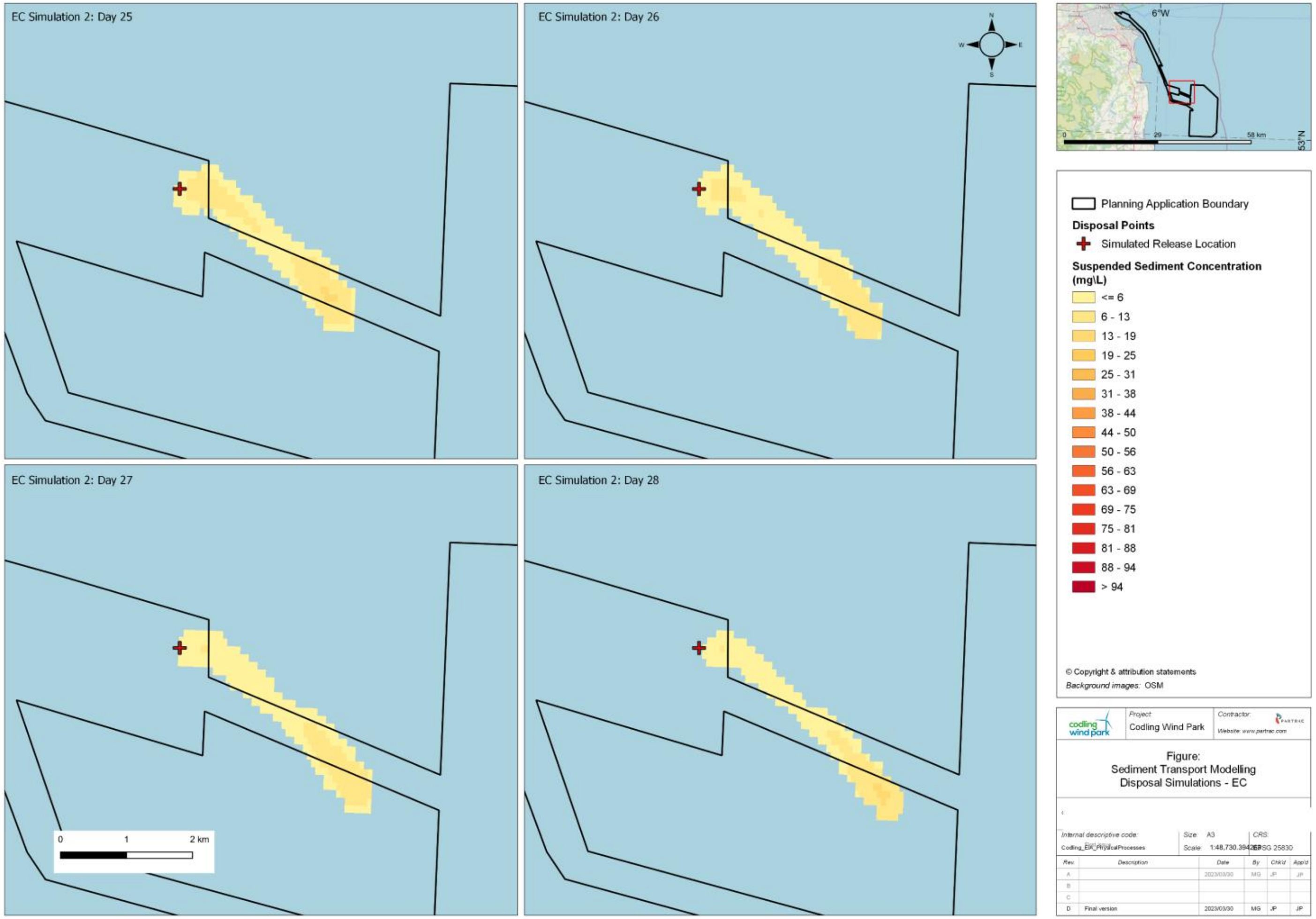

Figure 78 : SSC levels observed @ days 25 to 28 - Scenario 4.

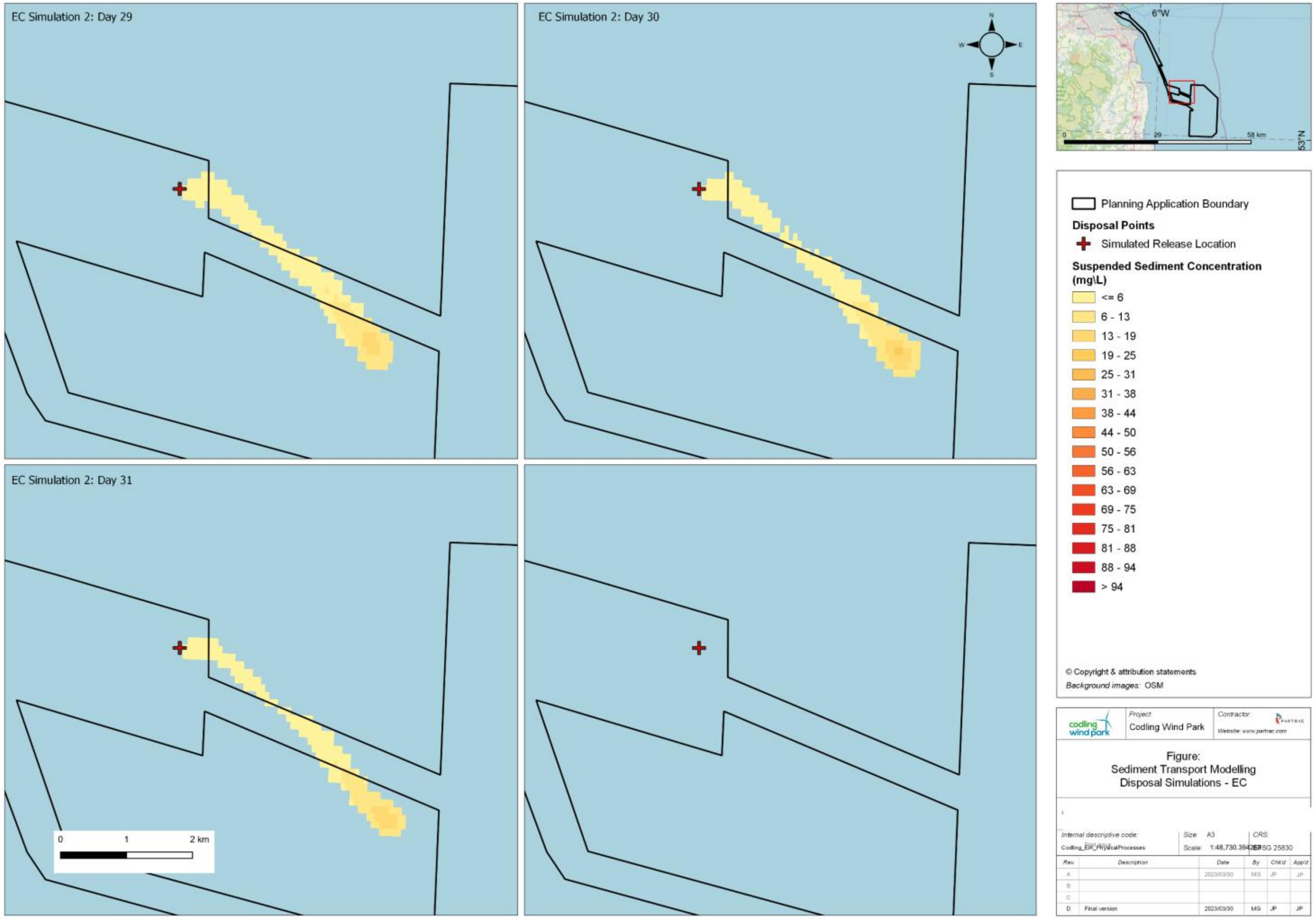

Figure 79 : SSC levels observed @ days 29 to 31 - Scenario 4.

6.2. Trenching Activities

Similar to the dredge disposal activities, trenching activities to be performed as part of the construction phase of the CWP project are predicted to have a spatially limited, and transient, impact on SSCs local to the activity. A total of five representative scenarios were simulated to assess these impacts. Table 12 summarises the results of these simulations.

Table 12: Findings obtained from the five installation simulations.

Scenario	Location	Transport Direction	Transport Distance (Km)	Predicted transient increases in SSC (mg\l)	Time required to return to baseline SSCs	cumulative sediment deposition thickness near the release location (cm)
Scenario 1	IAC	Eastward	3 - 4 km	~ 40 mg\l	~ 15 days	~ 1 cm
Scenario 2	IAC	Eastward	9 - 10 km	~ 20 mg\l	~ 15 days	~ 0.5 cm
Scenario 3	IAC	South eastward	3 - 4 km	~ 20 mg\l	~ 15 days	~ 0.5 cm
Scenario 4	OECC	Eastward \ Southward	6 - 7 km	~ 50 mg\l	~ 15 days	~ 2.0 cm
Scenario 5	OECC transition	Eastward	< 1 km	~ 80 mg\l	~ 15 days	~ 0.4 cm

The results indicate that trenching activities within the array site and along the OECC are not expected to have a significant impact on local and regional SSCs over the long-term, with SSC levels returning to baseline conditions within a maximum of 15 days of trenching completion. The effects are largely limited to those areas local to the trenching routes, as the sediment plumes generated deposit rapidly or are dispersed to baseline levels within circa 10 km of the trenched cable route. The thickness of the deposit on the seabed at the release location is anticipated to be on the order of a few metres as a result of the immediately deposited part of the released material, these sediments are anticipated to be rapidly integrated into the sediment regime.

The results for the IAC installation scenario 1 are presented in Figure 80 to Figure 89. Figure 90 to Figure 99 presents the results for the IAC installation scenario 2, and Figure 100 to Figure 109 presents the results for the IAC installation scenario 3. Figure 110 to Figure 119 presents the results for the OECC installation scenario 4, and results for the OECC transition installation scenario 5 are presented in Figure 120 to Figure 129.

The results for each of the five simulations are presented as follows

- A spatial plot showing the maximum observed values at any time during the model run (representing the maximum footprint of SSC resulting from the dredging operations); and timeseries of SSC and the deposited thickness near to the release locations. The figure also shows the potential sediment plume extent when the IAC LoD is considered, represented by a 100 m buffer (each side) of the maximum plume extent;
- A spatial plot representing the trajectory of the suspended particles; and
- A series of time-sliced snapshots showing the location (and predicted concentration) of the suspended sediment plume during the simulation.

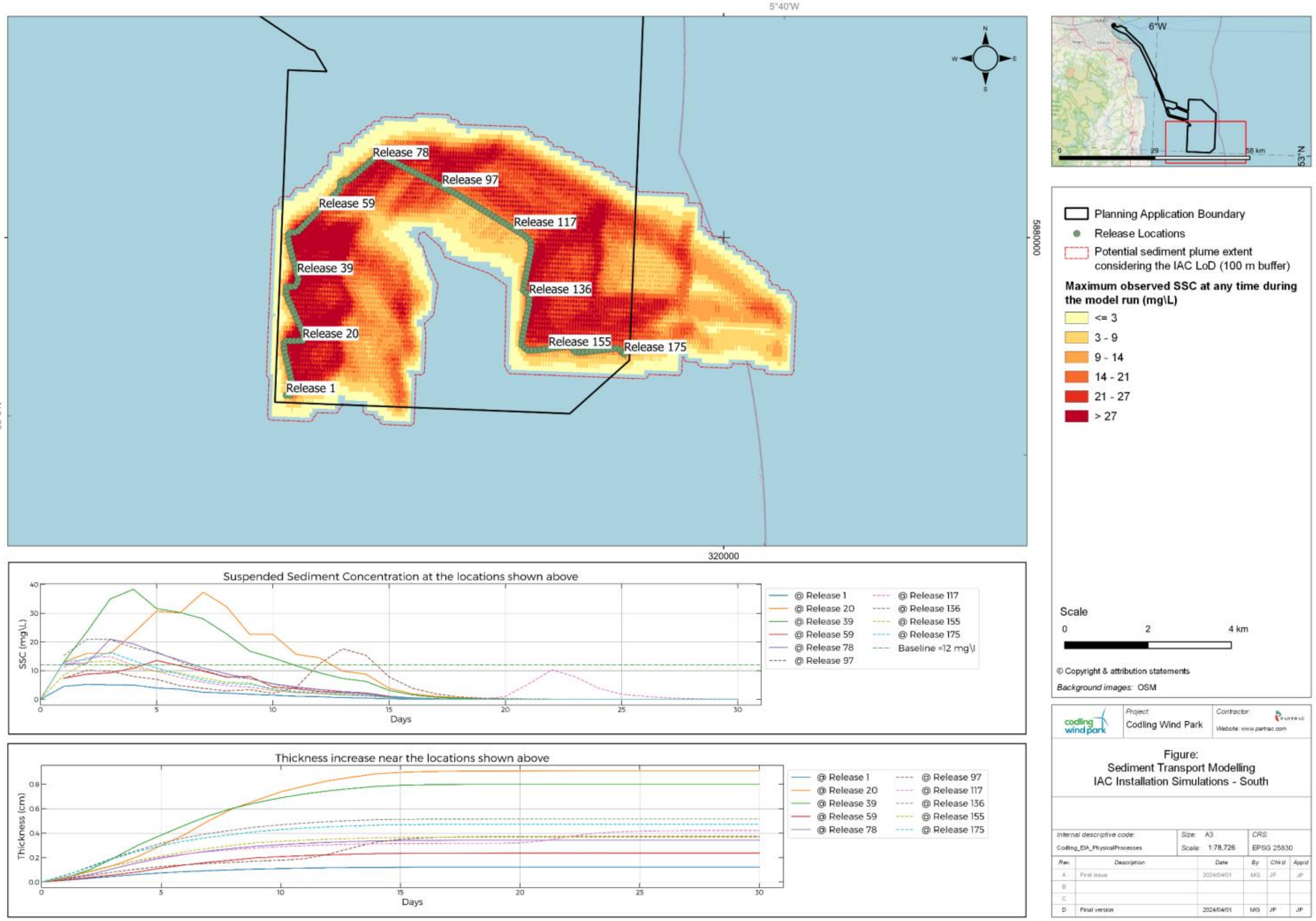

Figure 80: Maximum observed SSC levels at any time during Scenario 1 are presented in the spatial plot, the timeseries show 1) suspended sediment concentrations at the shown release locations, and 2) the deposited sediment thickness at the release locations.

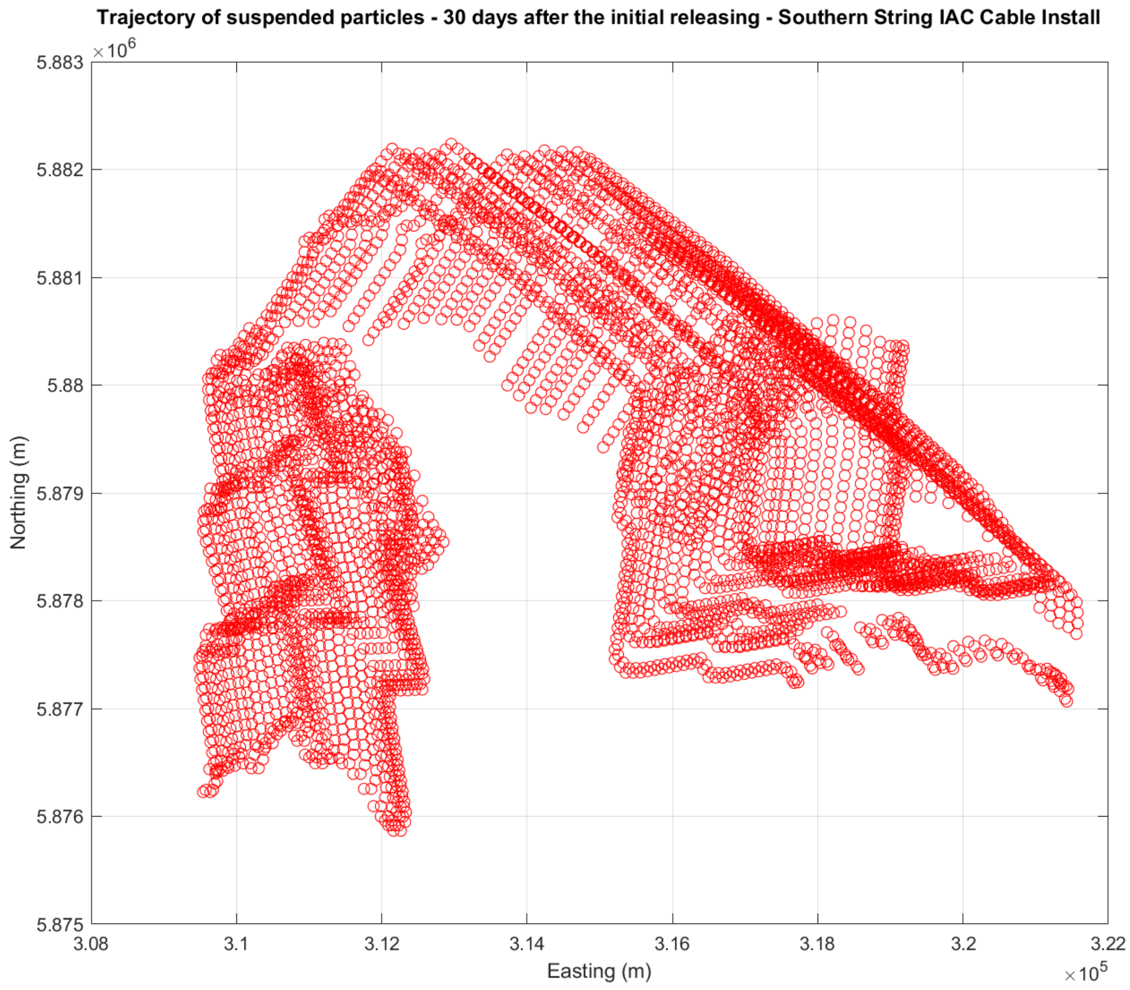

Figure 81: Trajectory of suspended sediments – Scenario 1.

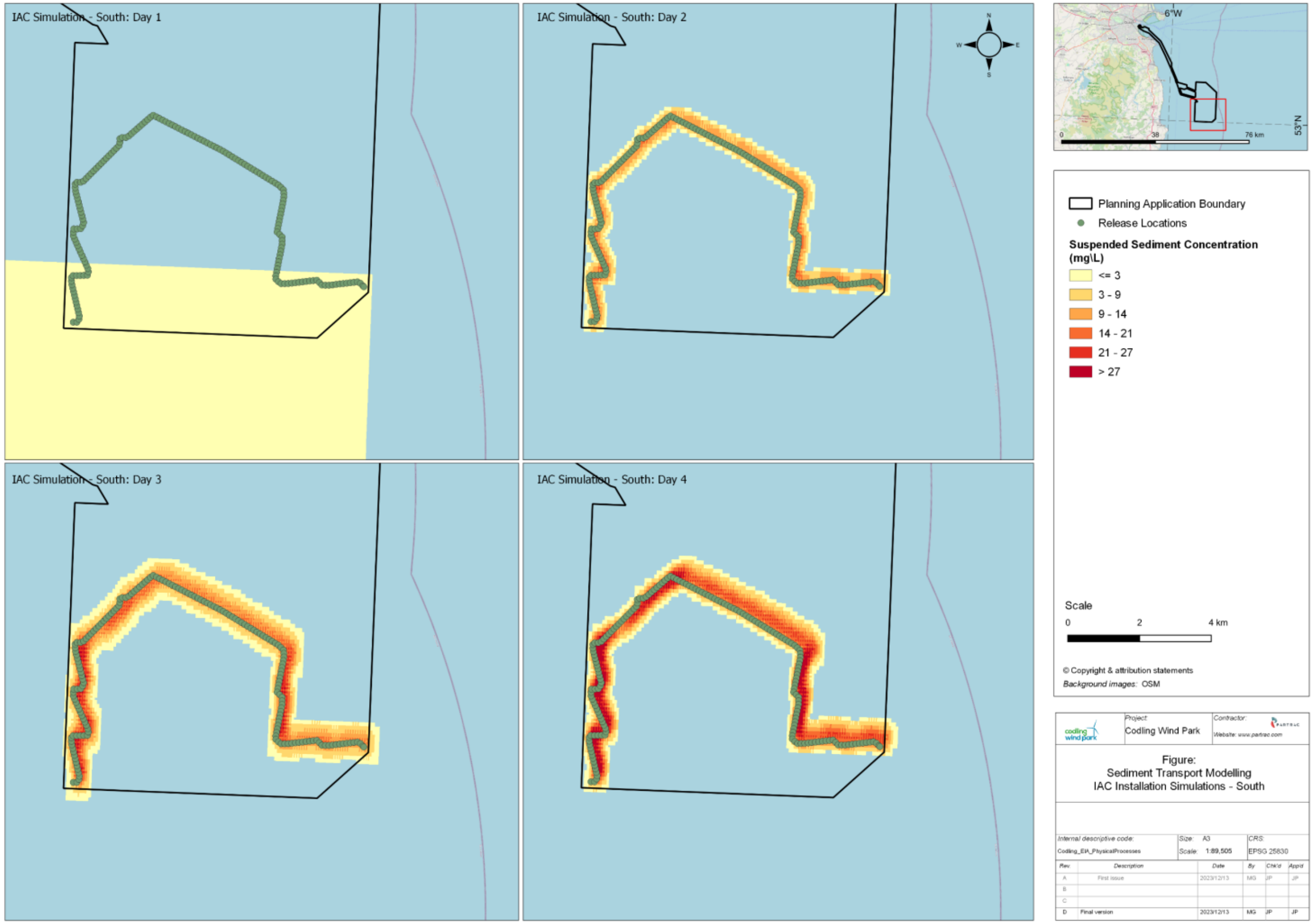

Figure 82 : SSC levels observed @ days 1 to 4 - Scenario 1.

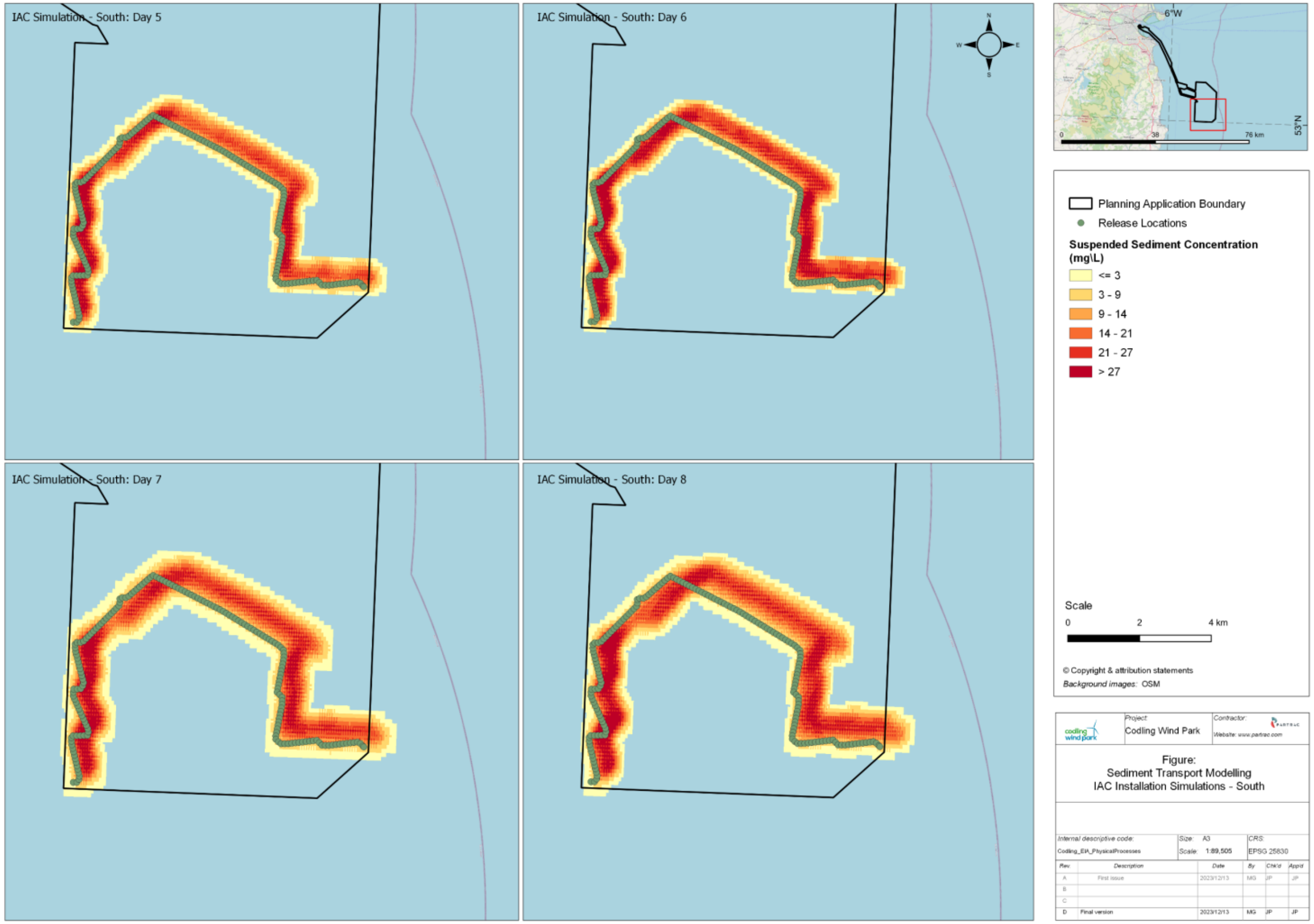

Figure 83 : SSC levels observed @ days 5 to 8 - Scenario 1.

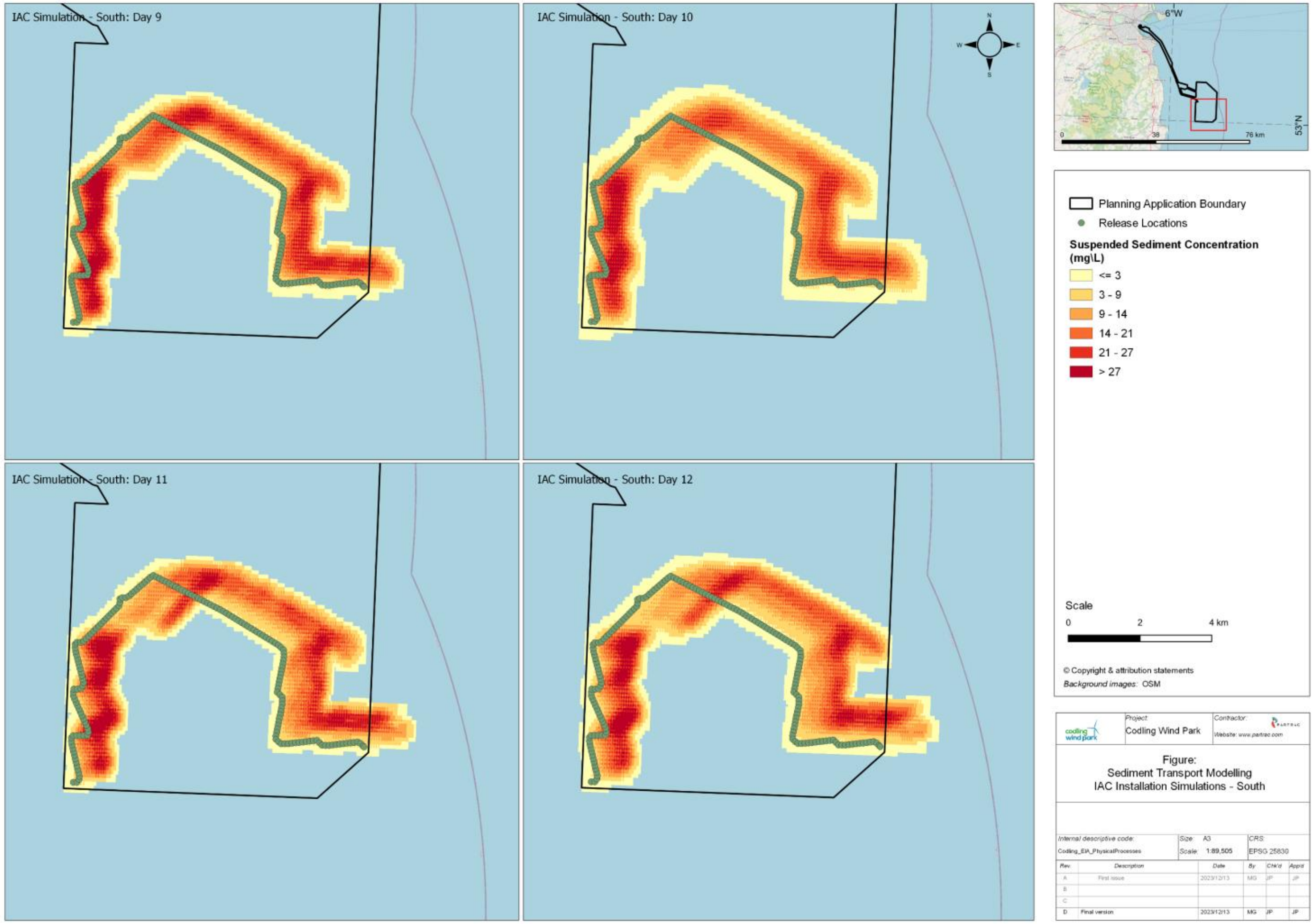

Figure 84 : SSC levels observed @ days 9 to 12 - Scenario 1.

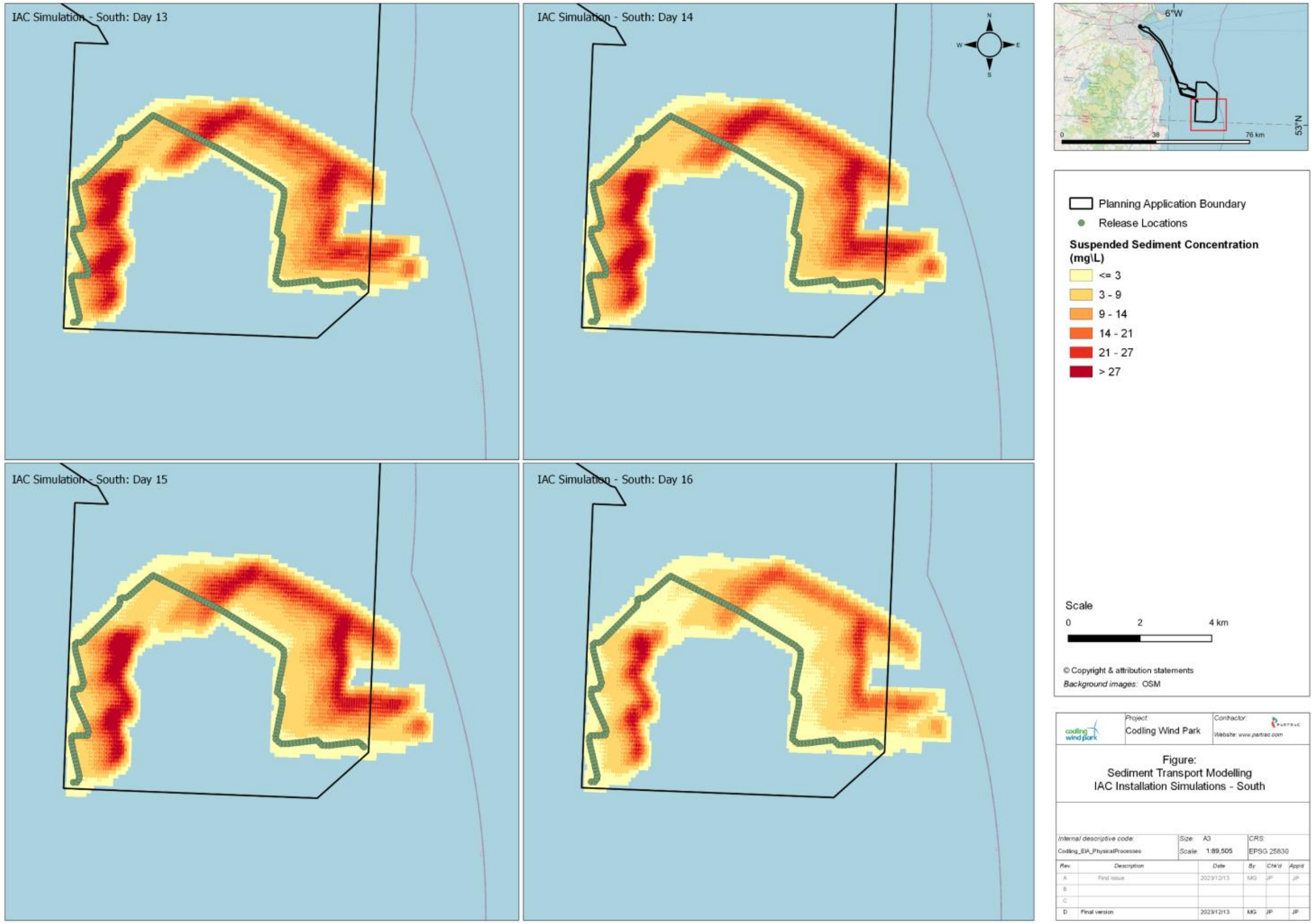

Figure 85 : SSC levels observed @ days 13 to 16 - Scenario 1.

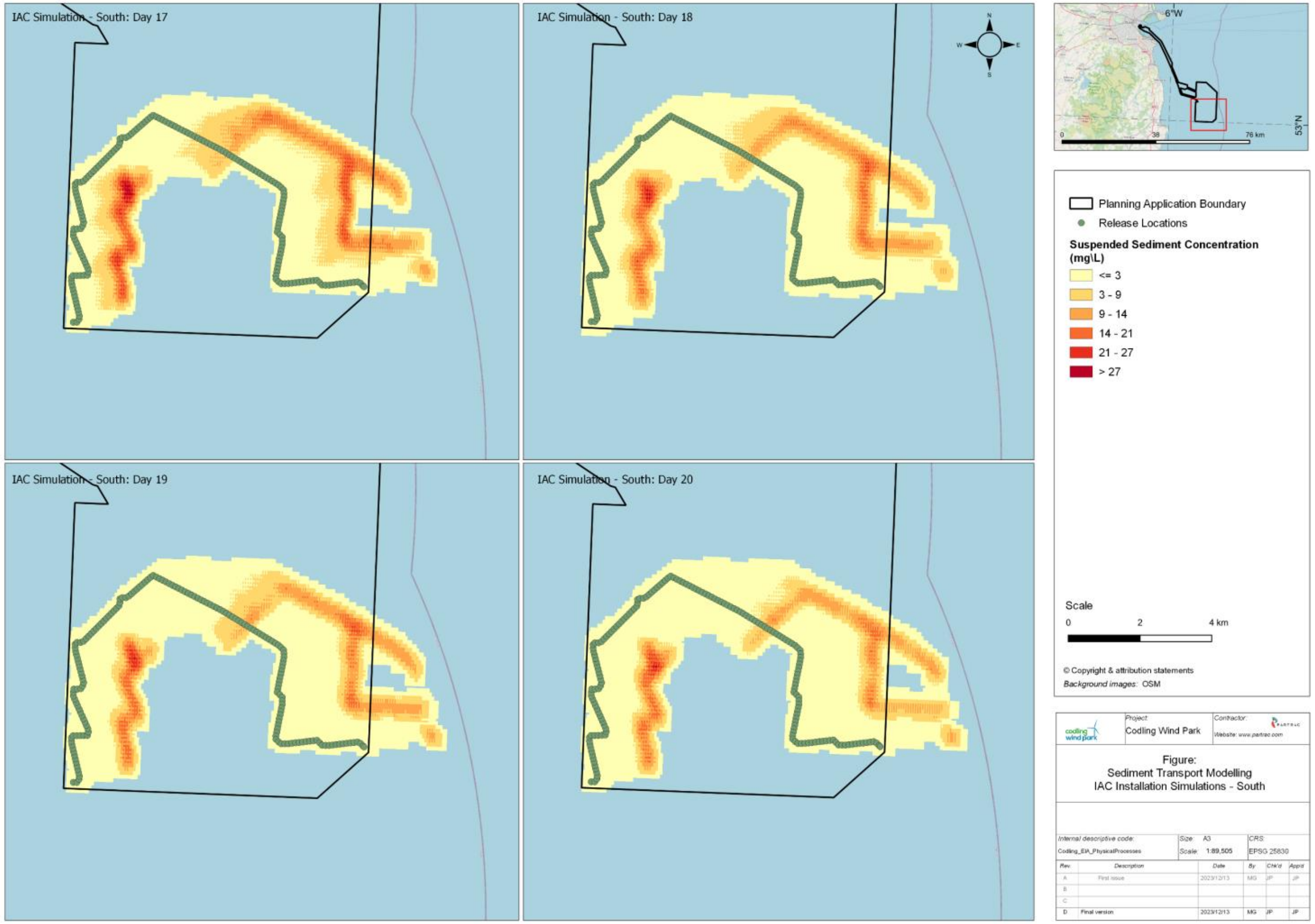

Figure 86 : SSC levels observed @ days 17 to 20 - Scenario 1.

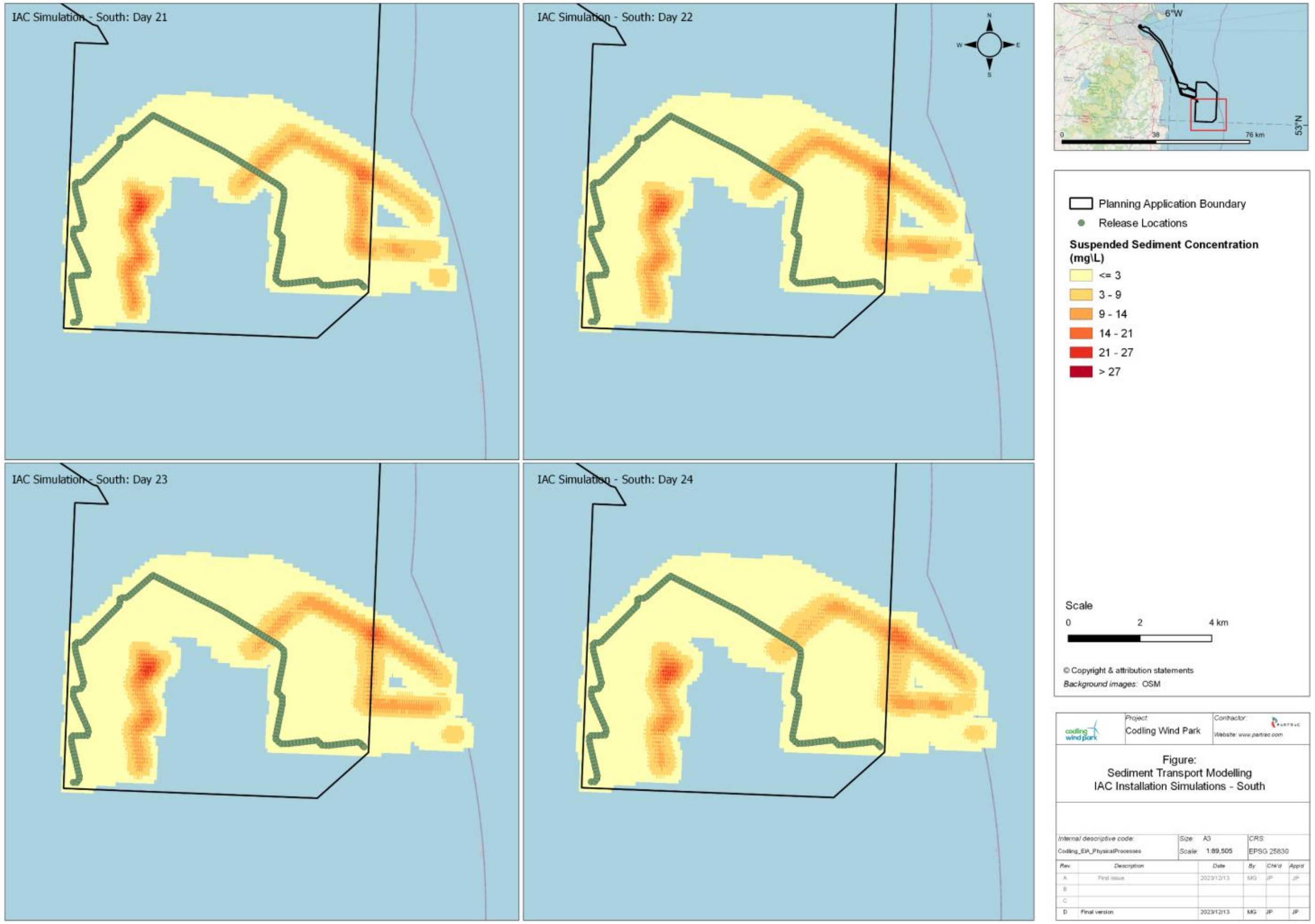

Figure 87 : SSC levels observed @ days 21 to 24 - Scenario 1.

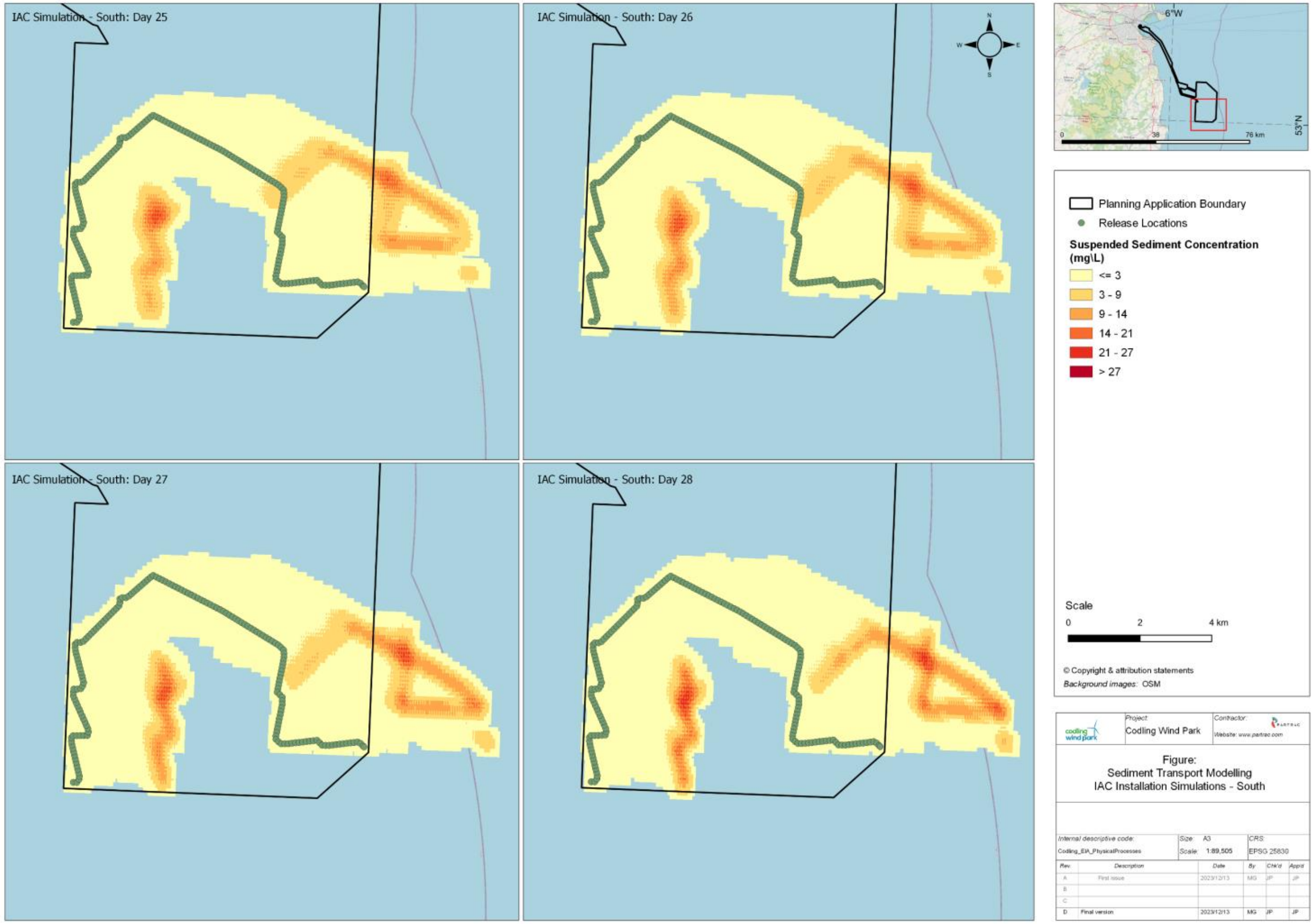

Figure 88 : SSC levels observed @ days 25 to 28 - Scenario 1.

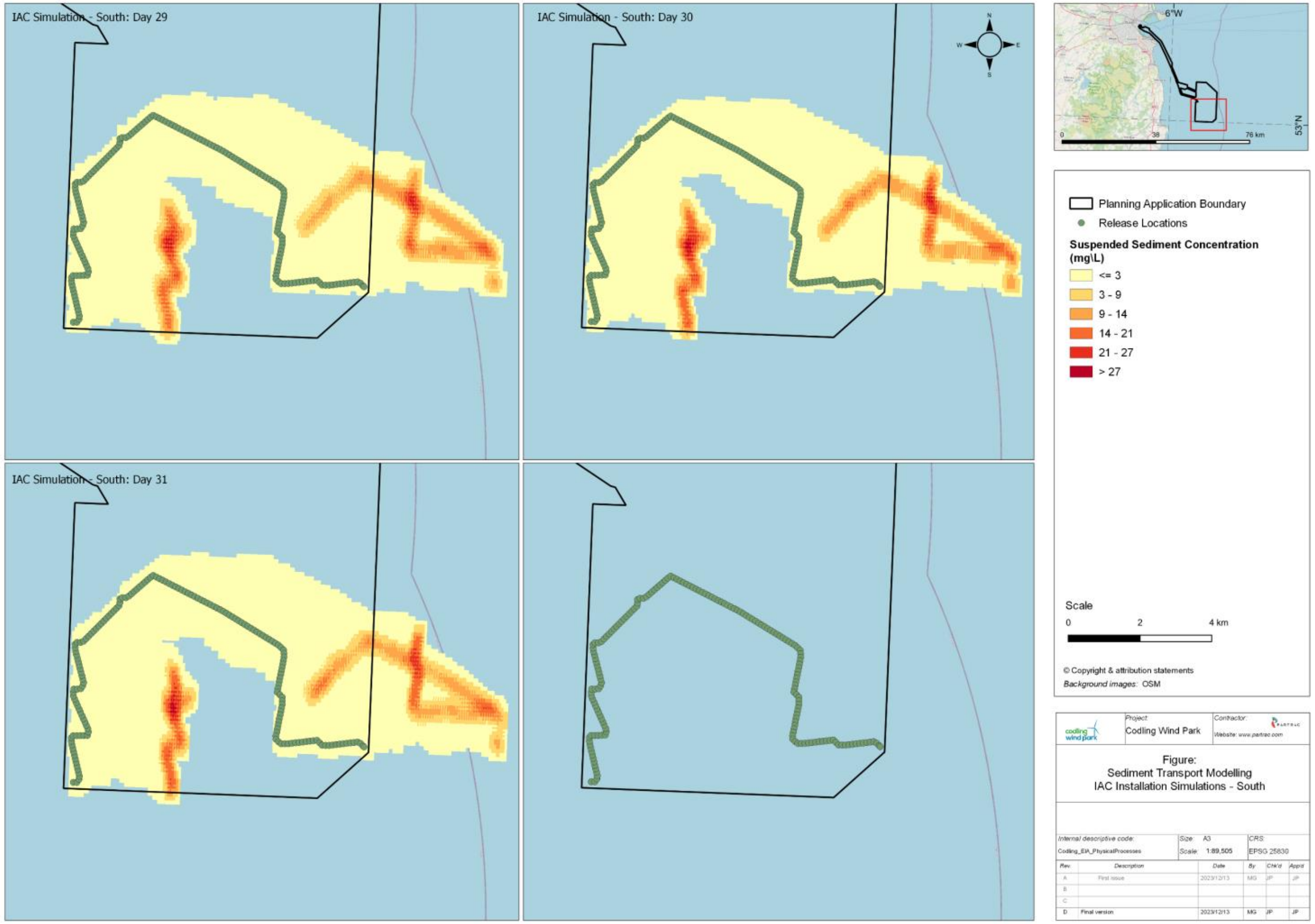

Figure 89 : SSC levels observed @ days 29 - 31 - Scenario 1.

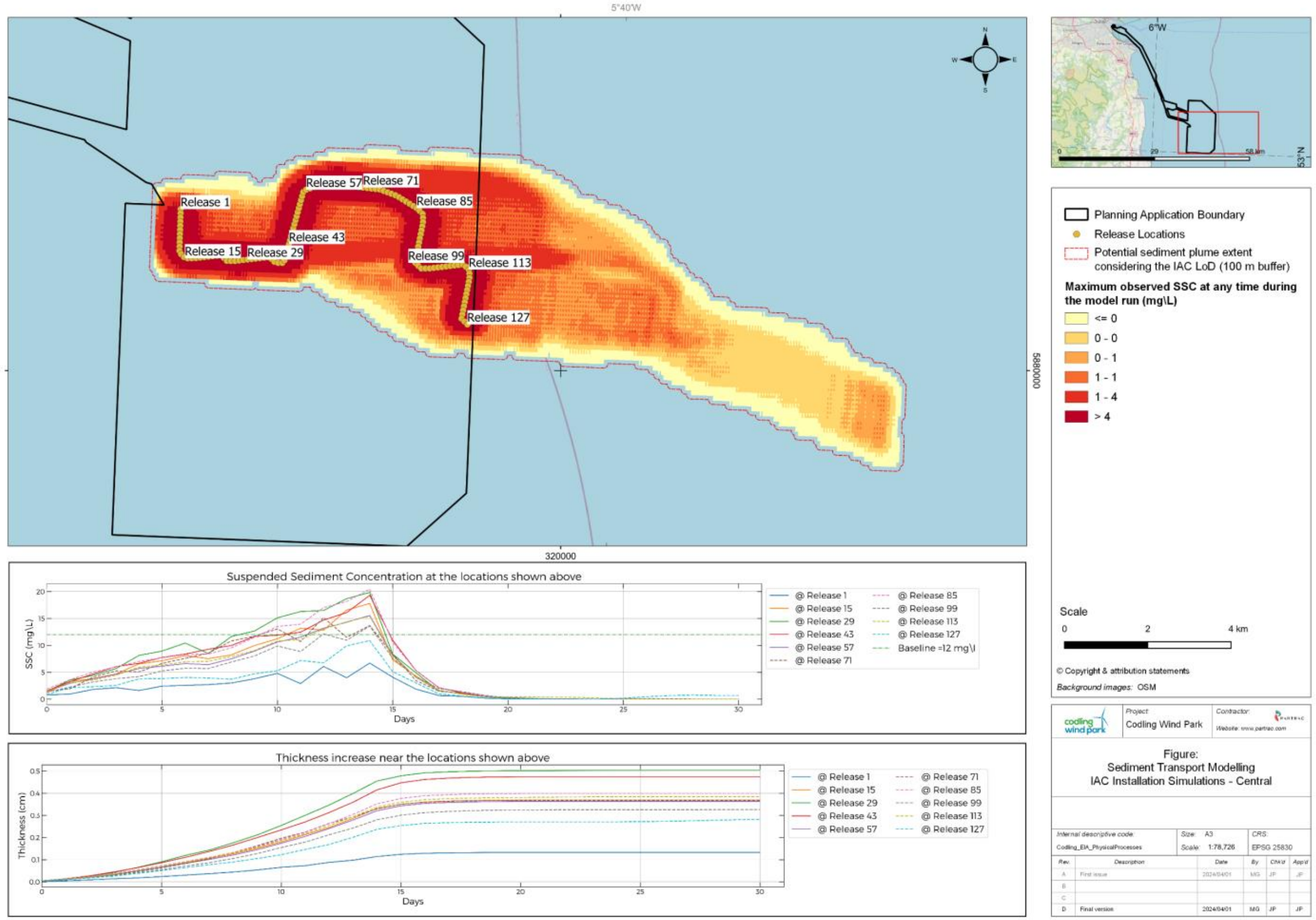

Figure 90: Maximum observed SSC levels at any time during Scenario 2 are presented in the spatial plot, the timeseries show 1) suspended sediment concentrations at the shown release locations, and 2) the deposited sediment thickness at the shown release locations.

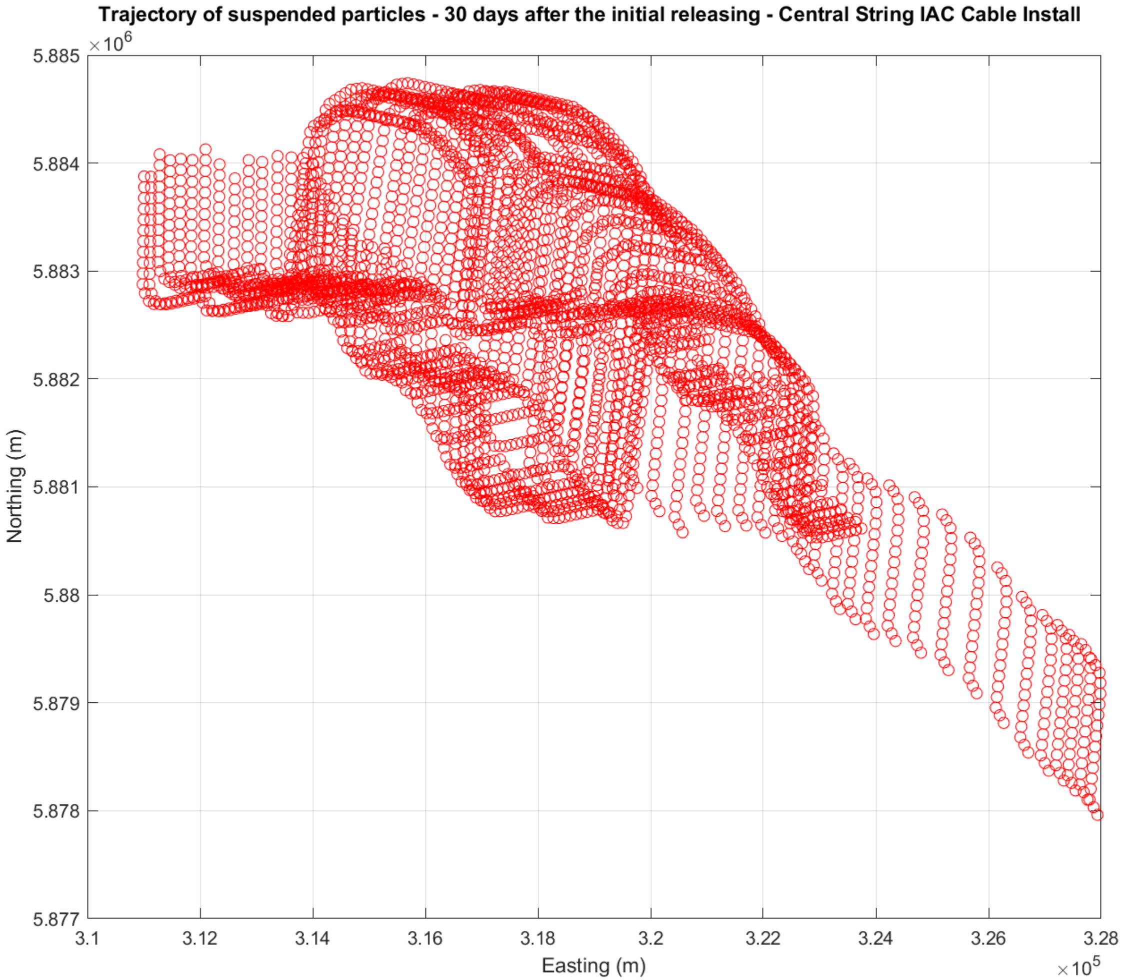

Figure 91: Trajectory of suspended sediments – Scenario 2.

Figure 92 : SSC levels observed @ days 1 to 4 - Scenario 2.

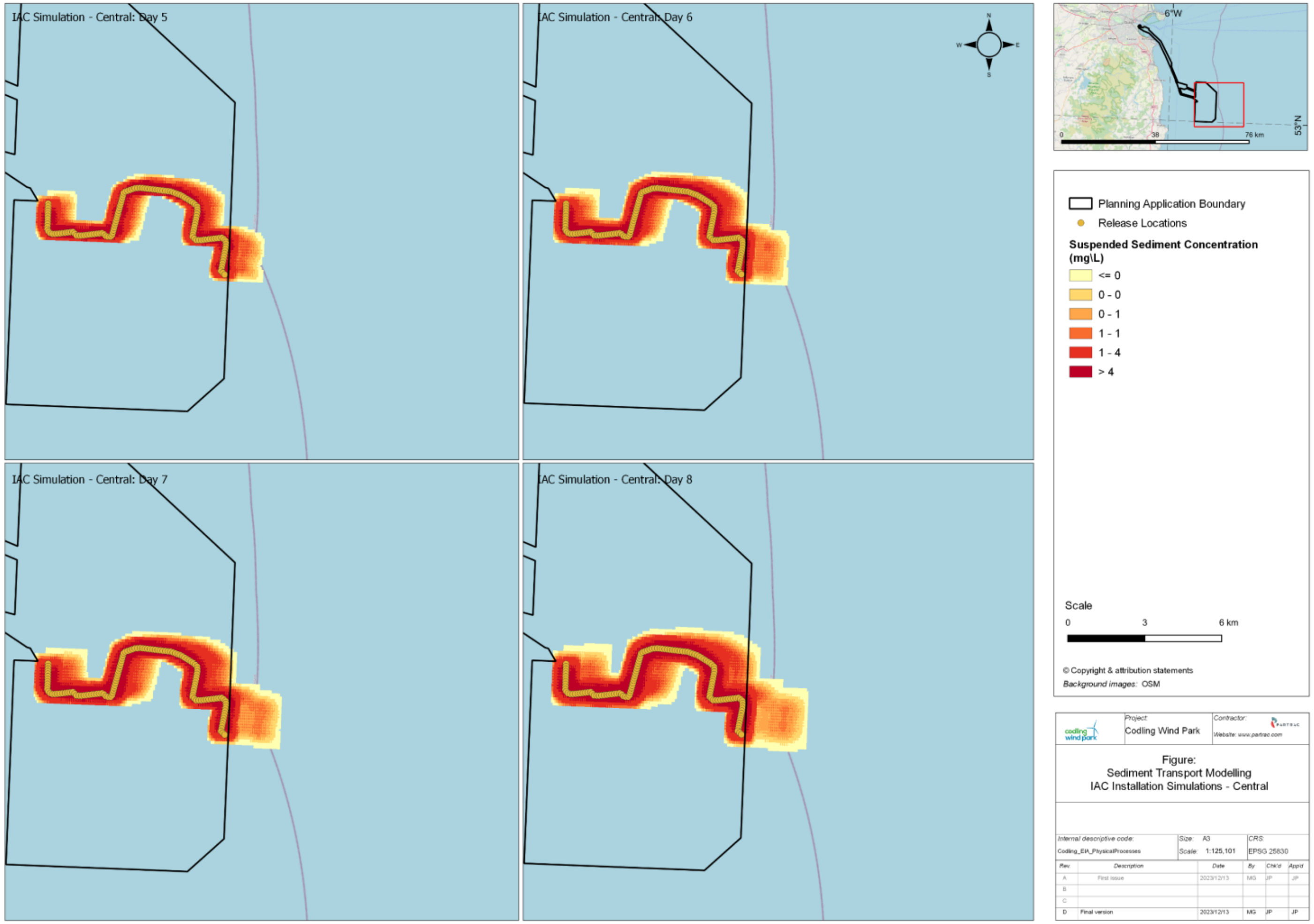

Figure 93 : SSC levels observed @ days 5 to 8 - Scenario 2.

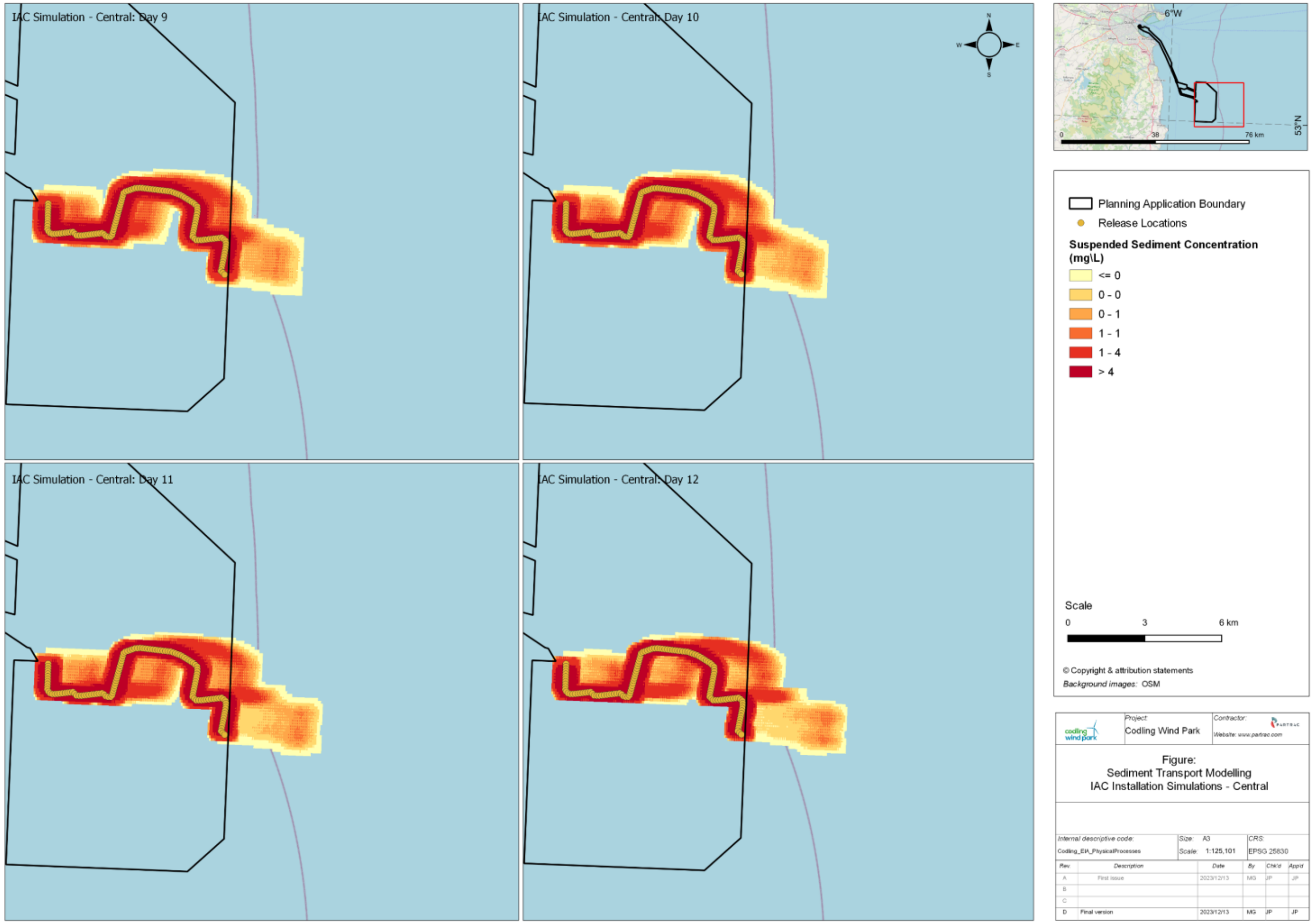

Figure 94 : SSC levels observed @ days 9 to 12 - Scenario 2.

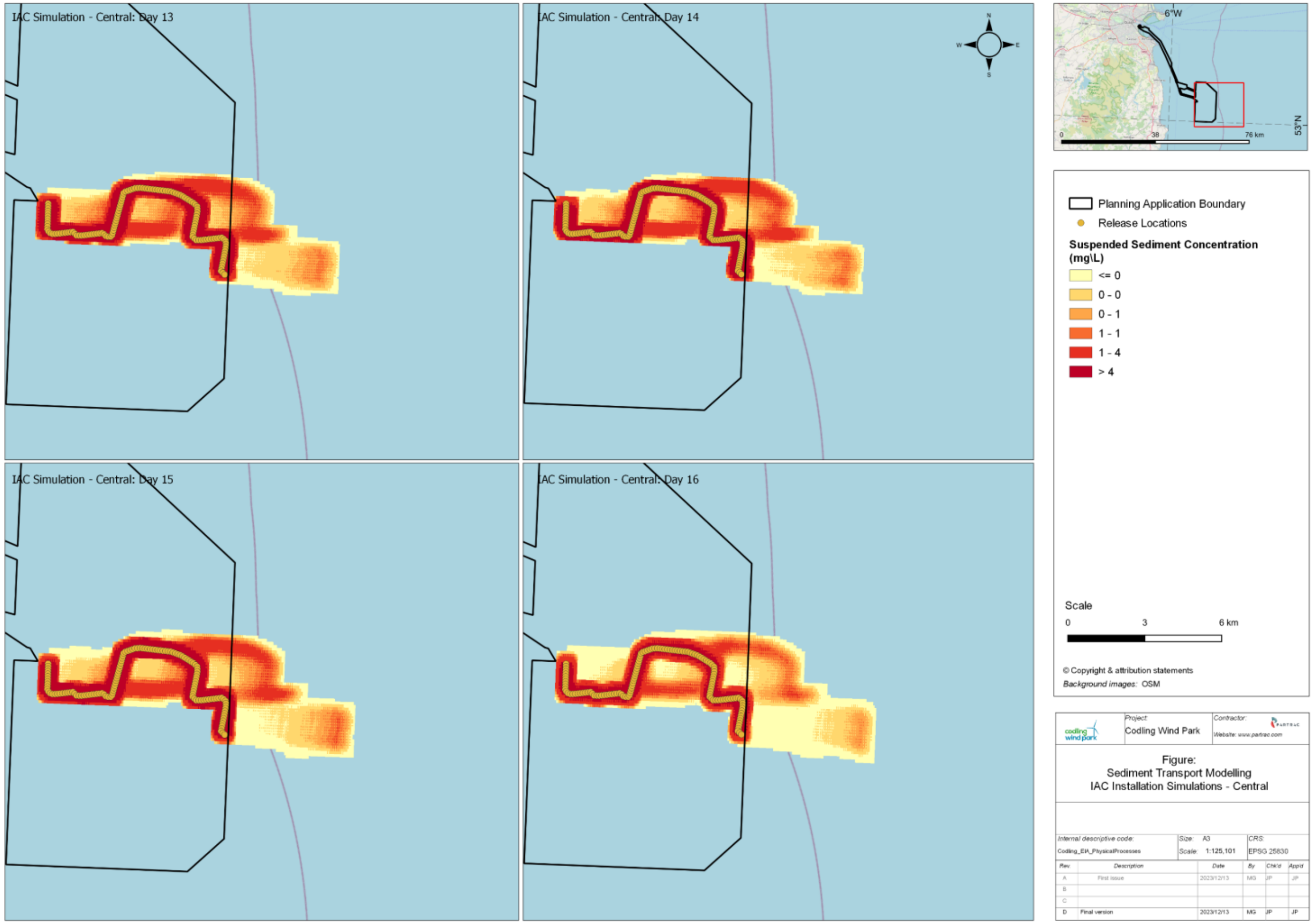

Figure 95 : SSC levels observed @ days 13 to 16 - Scenario 2.

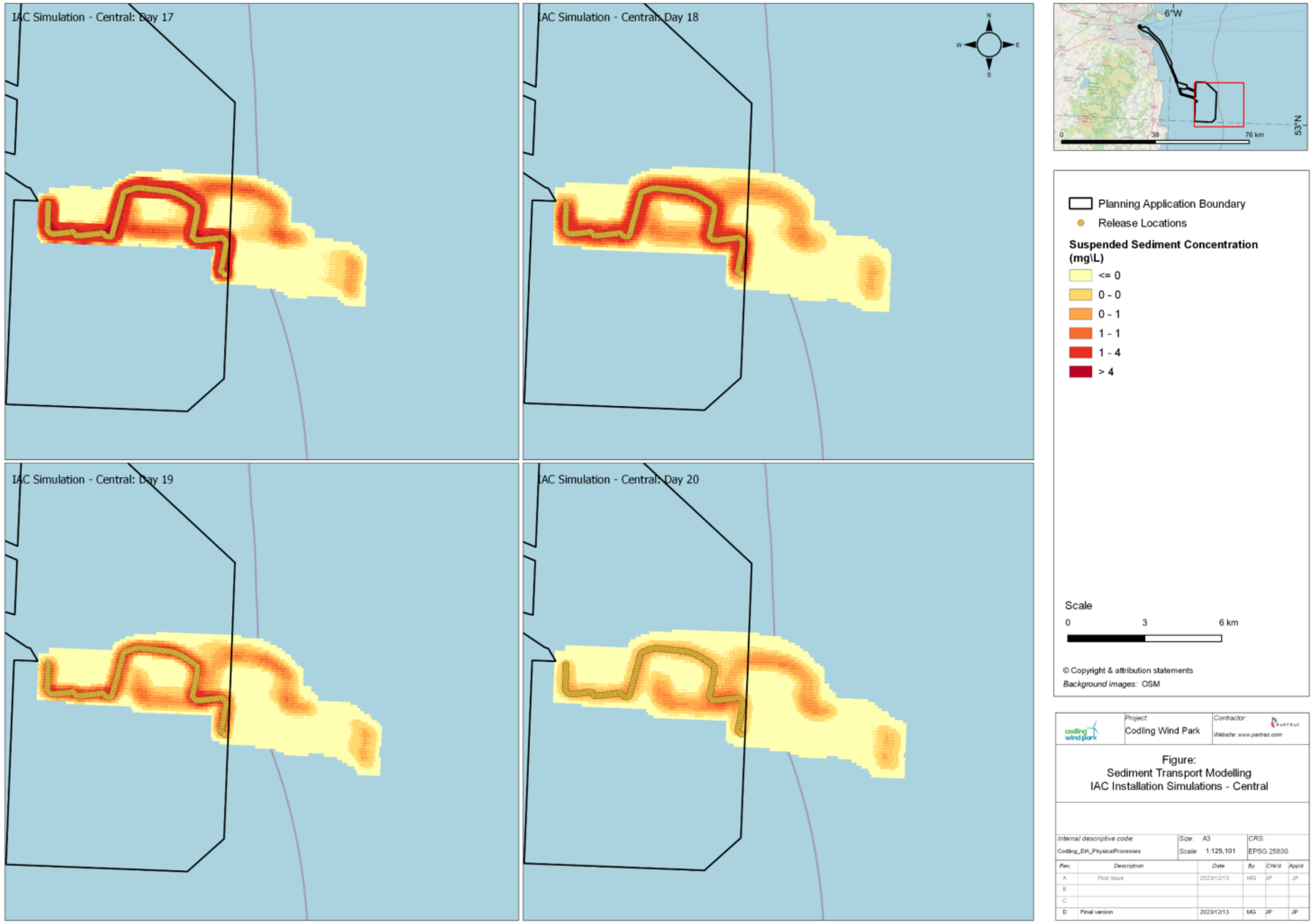

Figure 96 : SSC levels observed @ days 17 to 20 - Scenario 2.

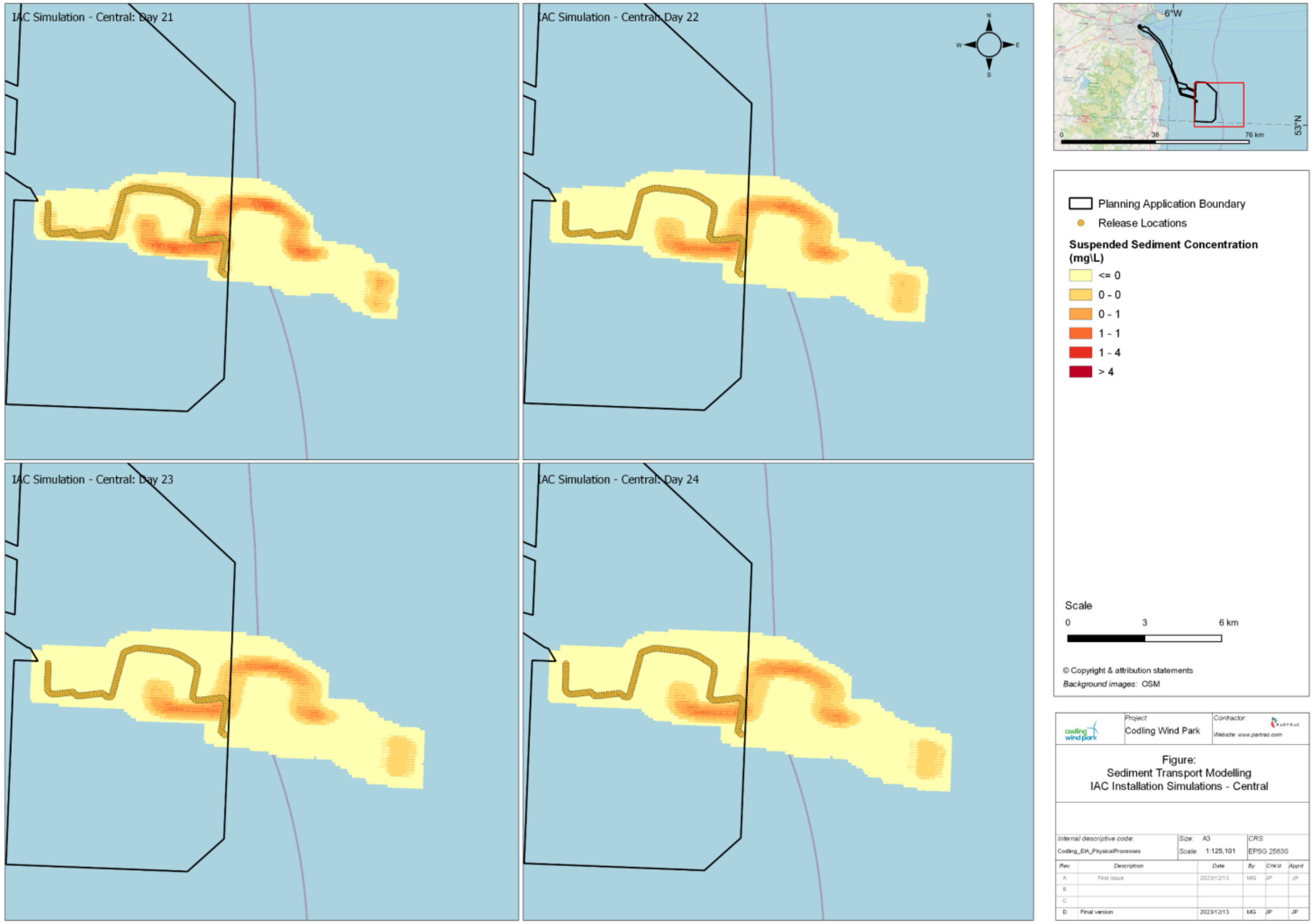

Figure 97 : SSC levels observed @ days 21 to 24 - Scenario 2.

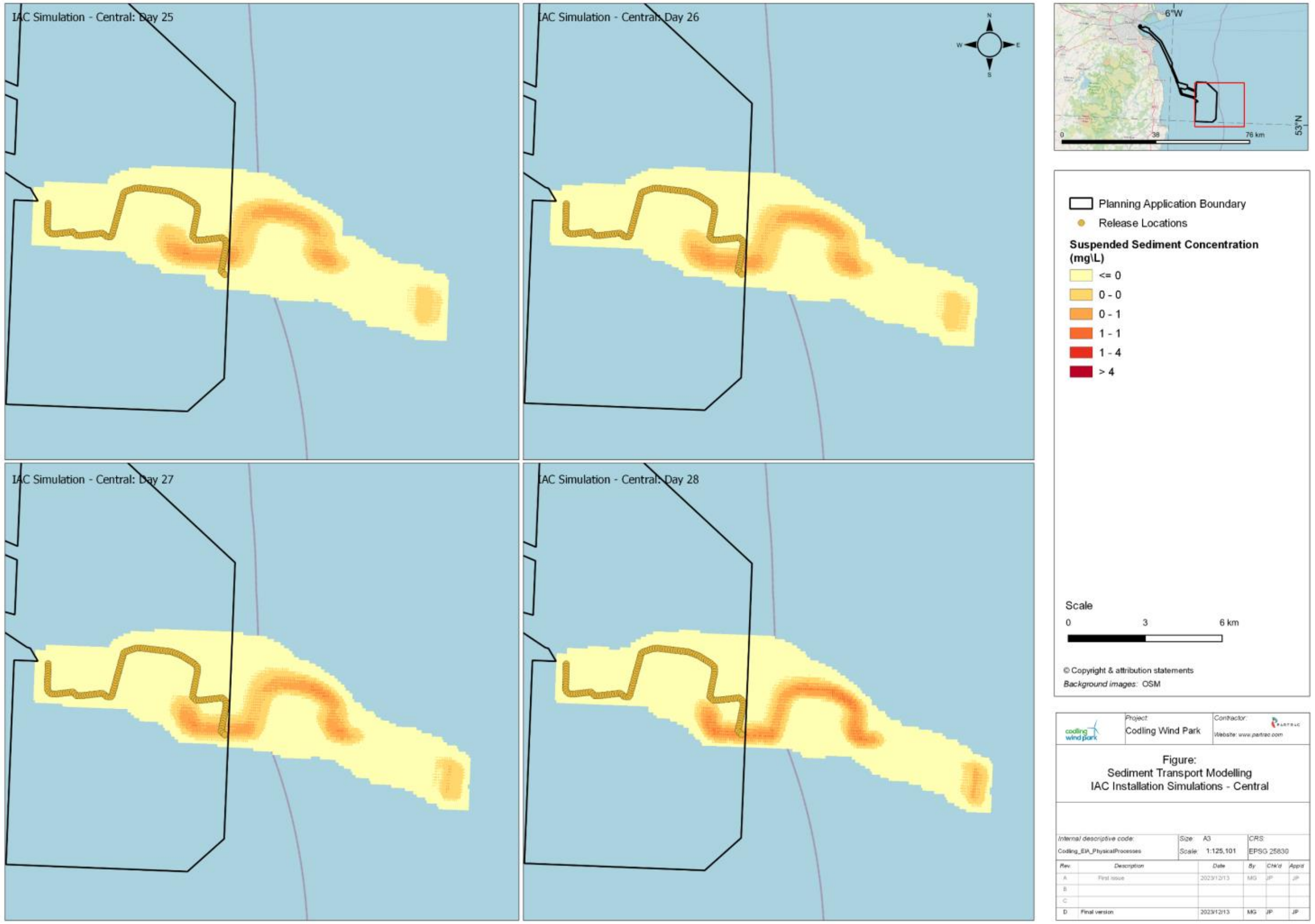

Figure 98 : SSC levels observed @ days 25 to 28 - Scenario 2.

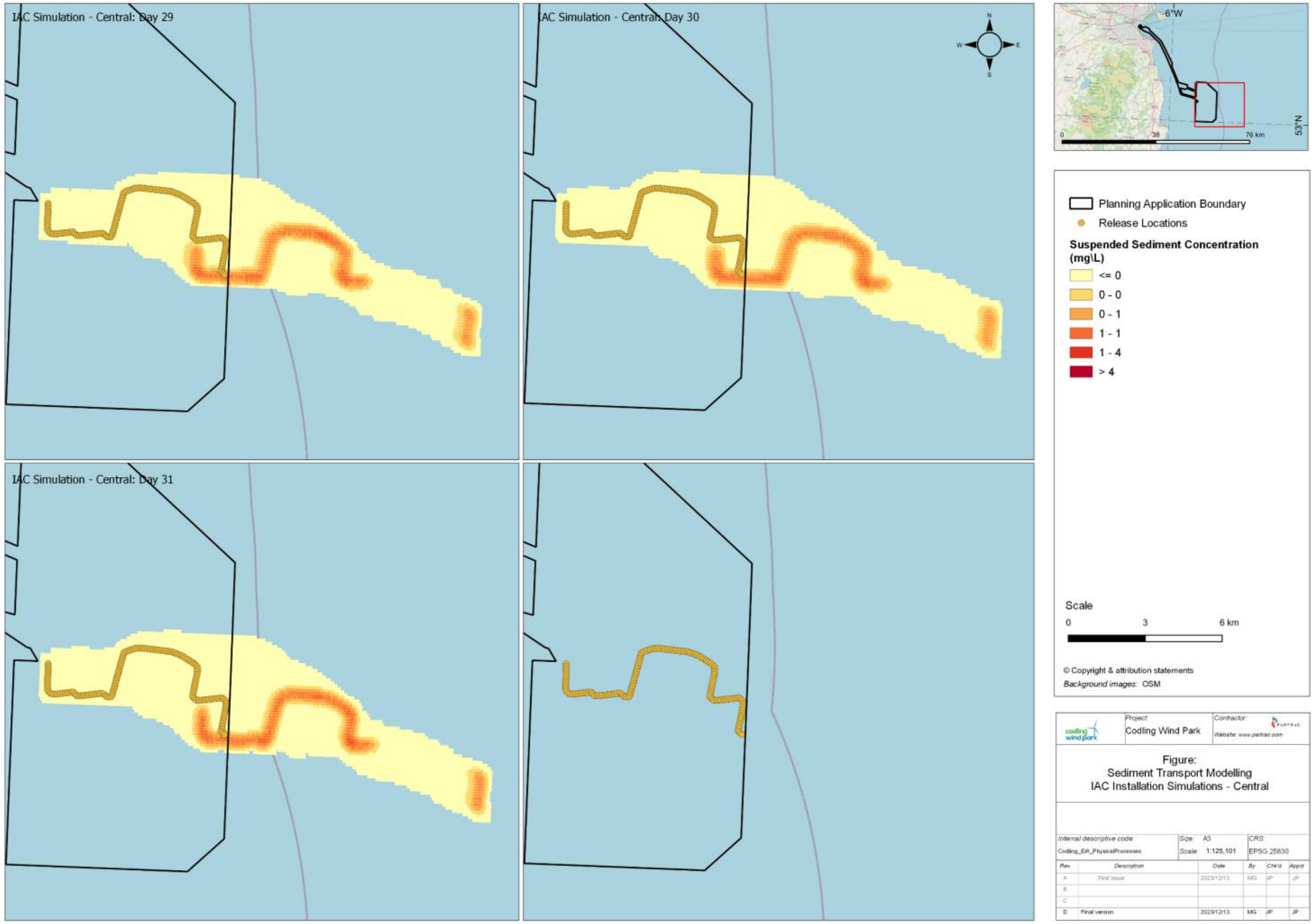

Figure 99 : SSC levels observed @ days 29 to 31 - Scenario 2.

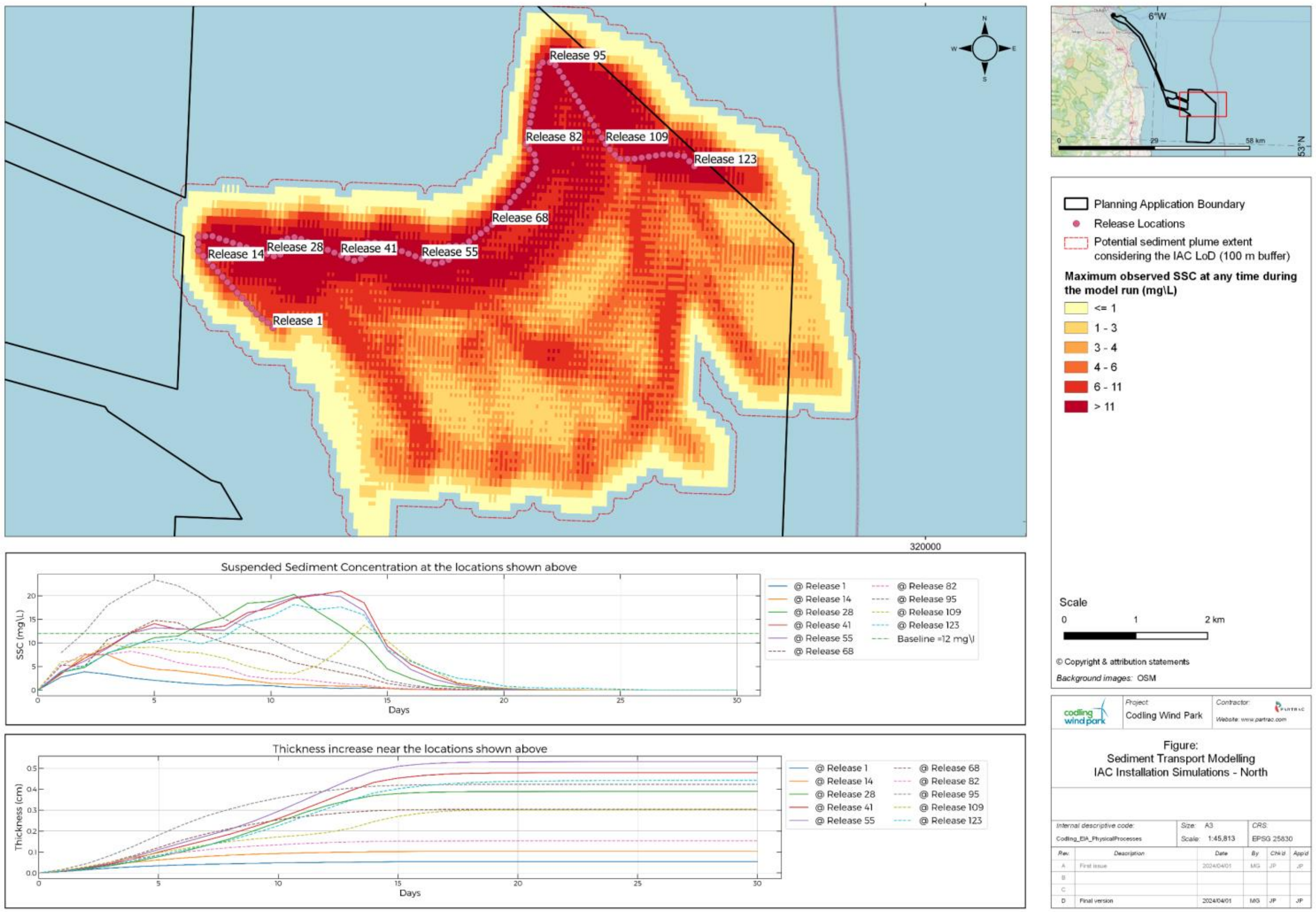

Figure 100: Maximum observed SSC levels at any time during Scenario 3 are presented in the spatial plot, the timeseries show 1) suspended sediment concentrations at the shown release locations, and 2) the deposited sediment thickness at the shown release locations.

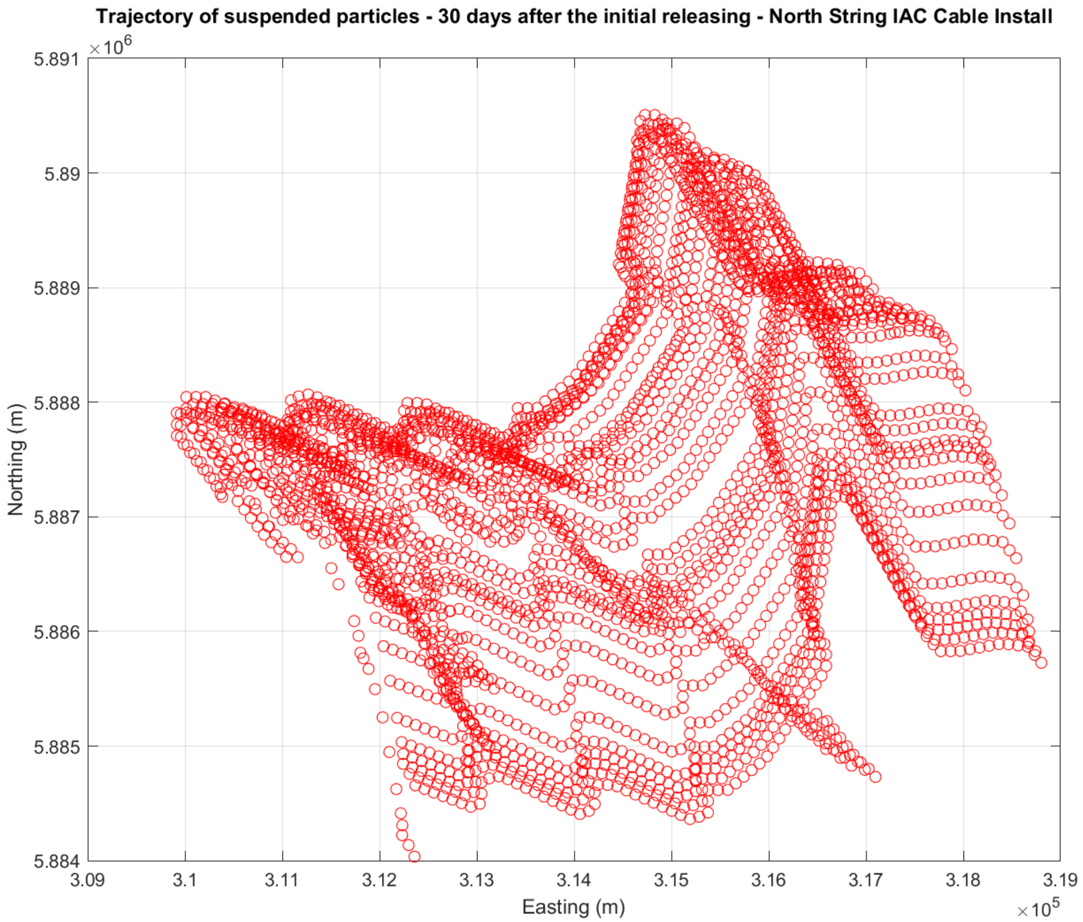

Figure 101: Trajectory of suspended sediments – Scenario 3.

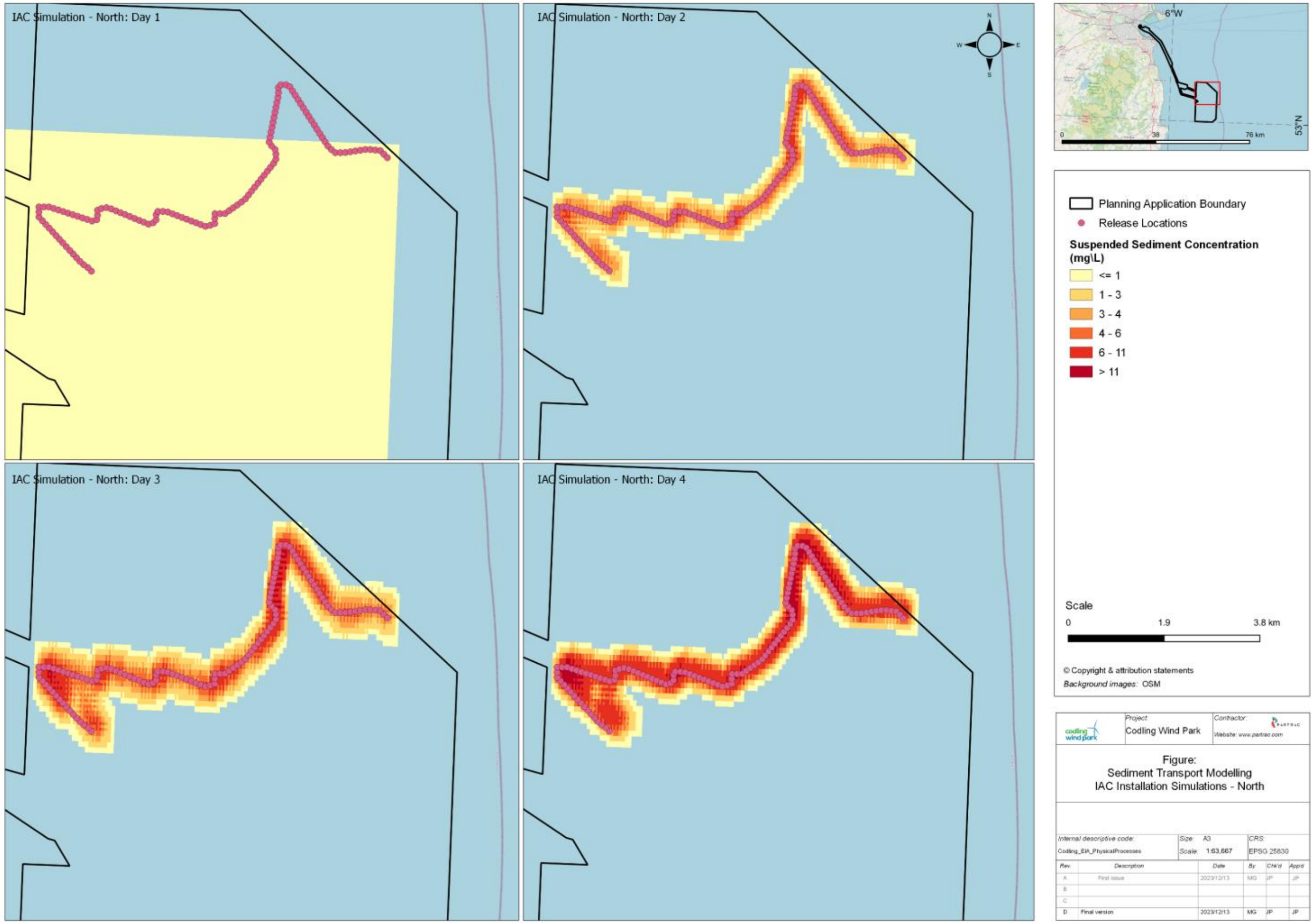

Figure 102 : SSC levels observed @ days 1 to 4 – Scenario 3.

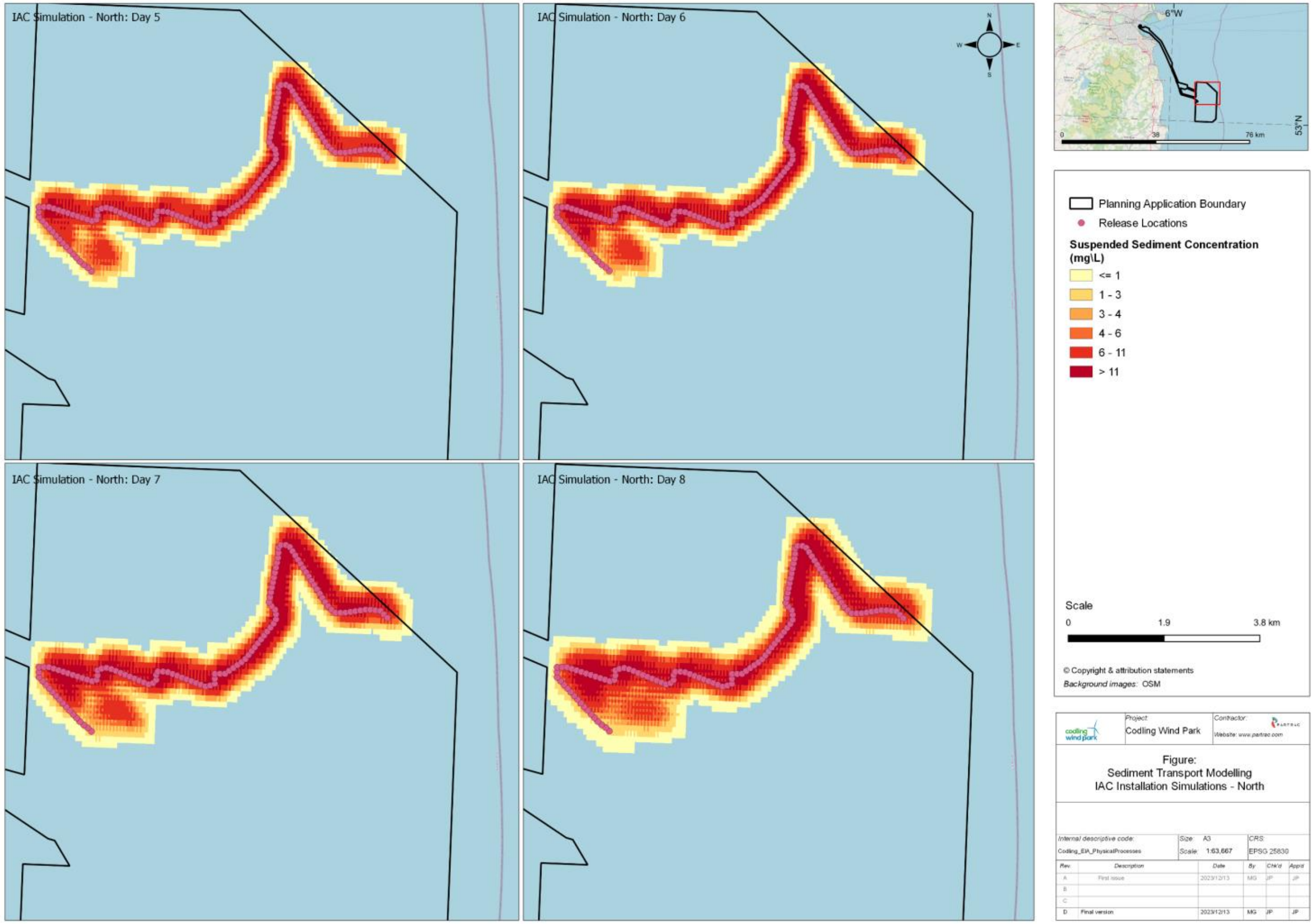

Figure 103 : SSC levels observed @ days 5 to 8 - Scenario 3.

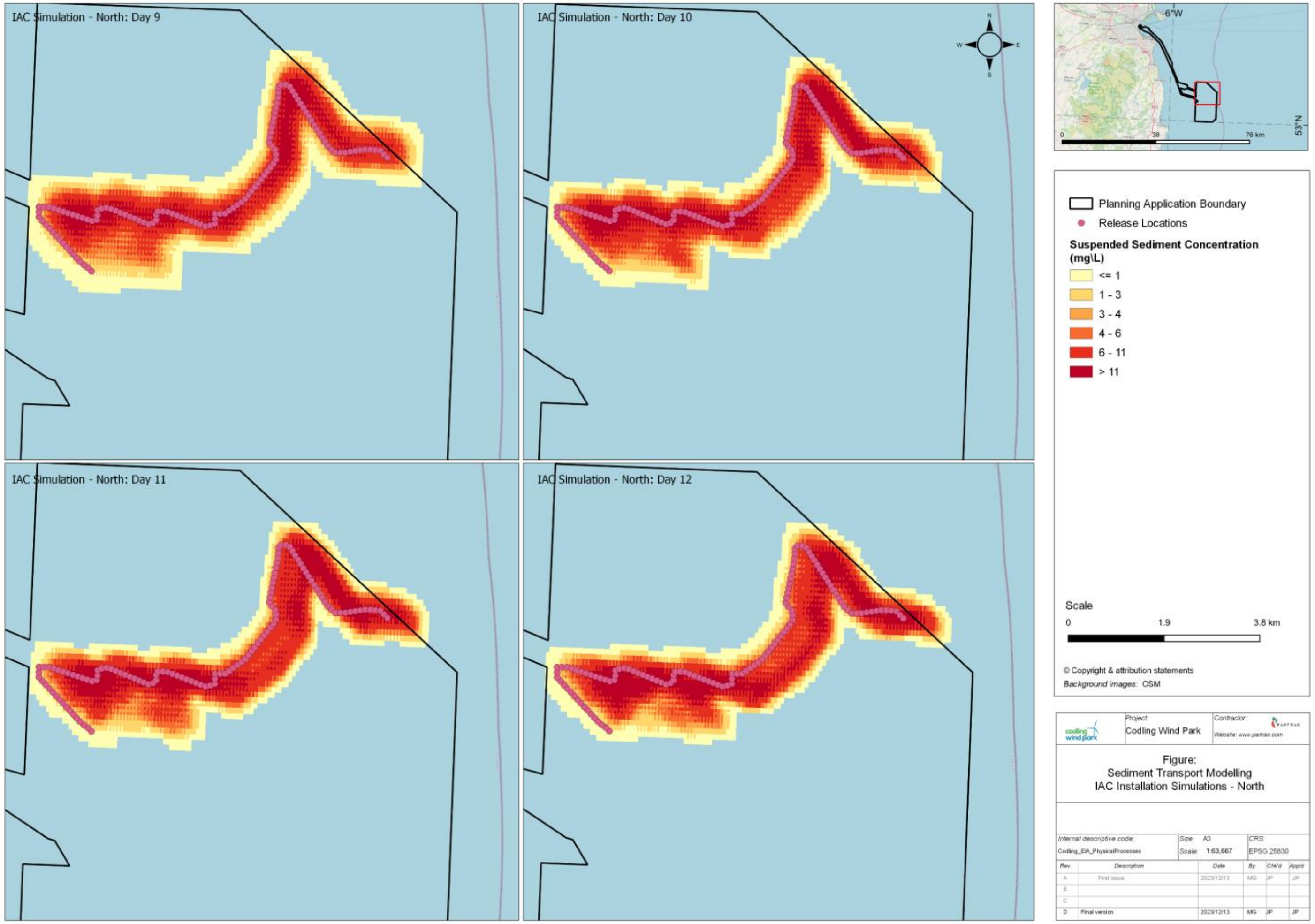

Figure 104 : SSC levels observed @ days 9 to 12 – Scenario 3.

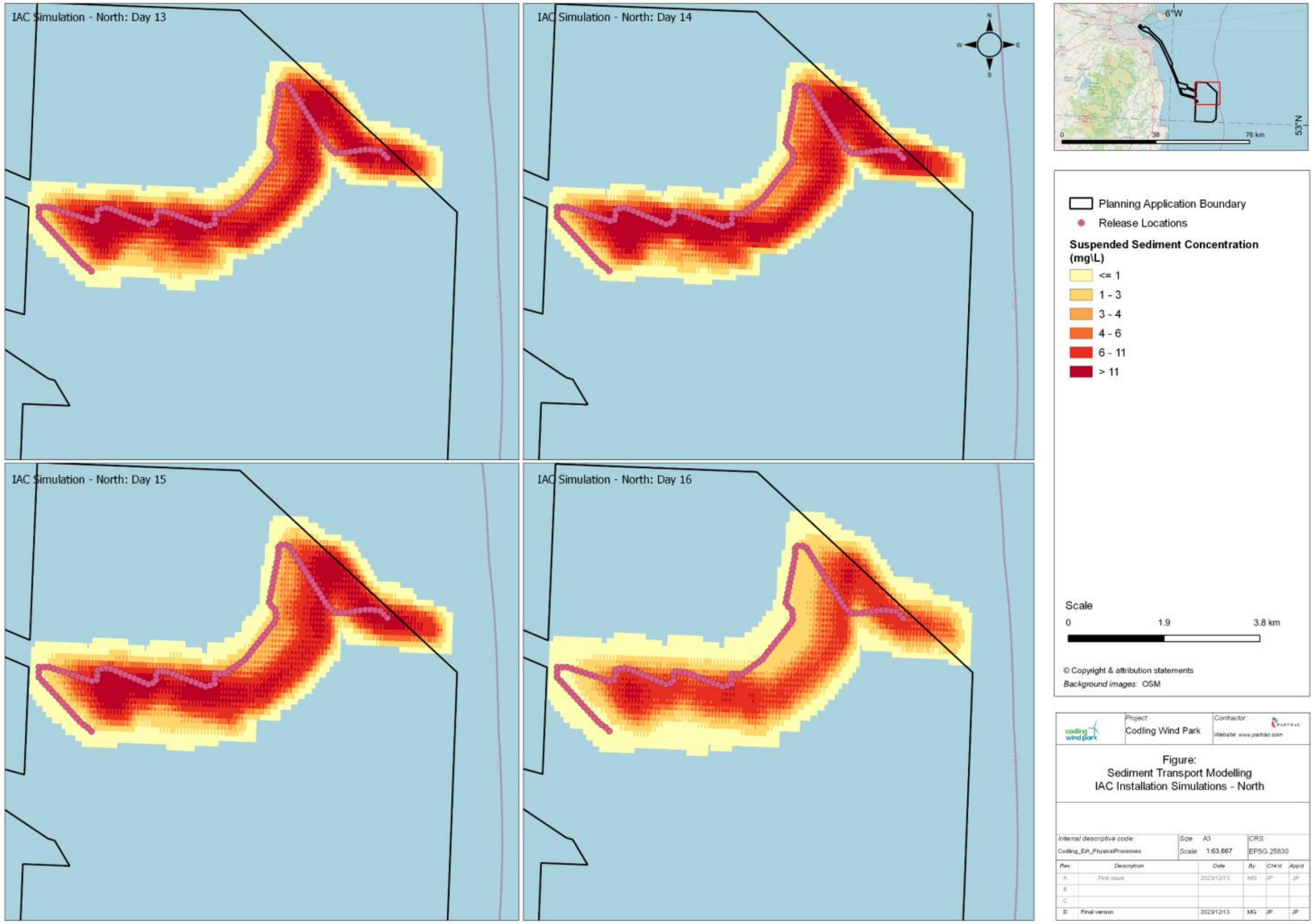

Figure 105 : SSC levels observed @ days 13 to 16 - Scenario 3.

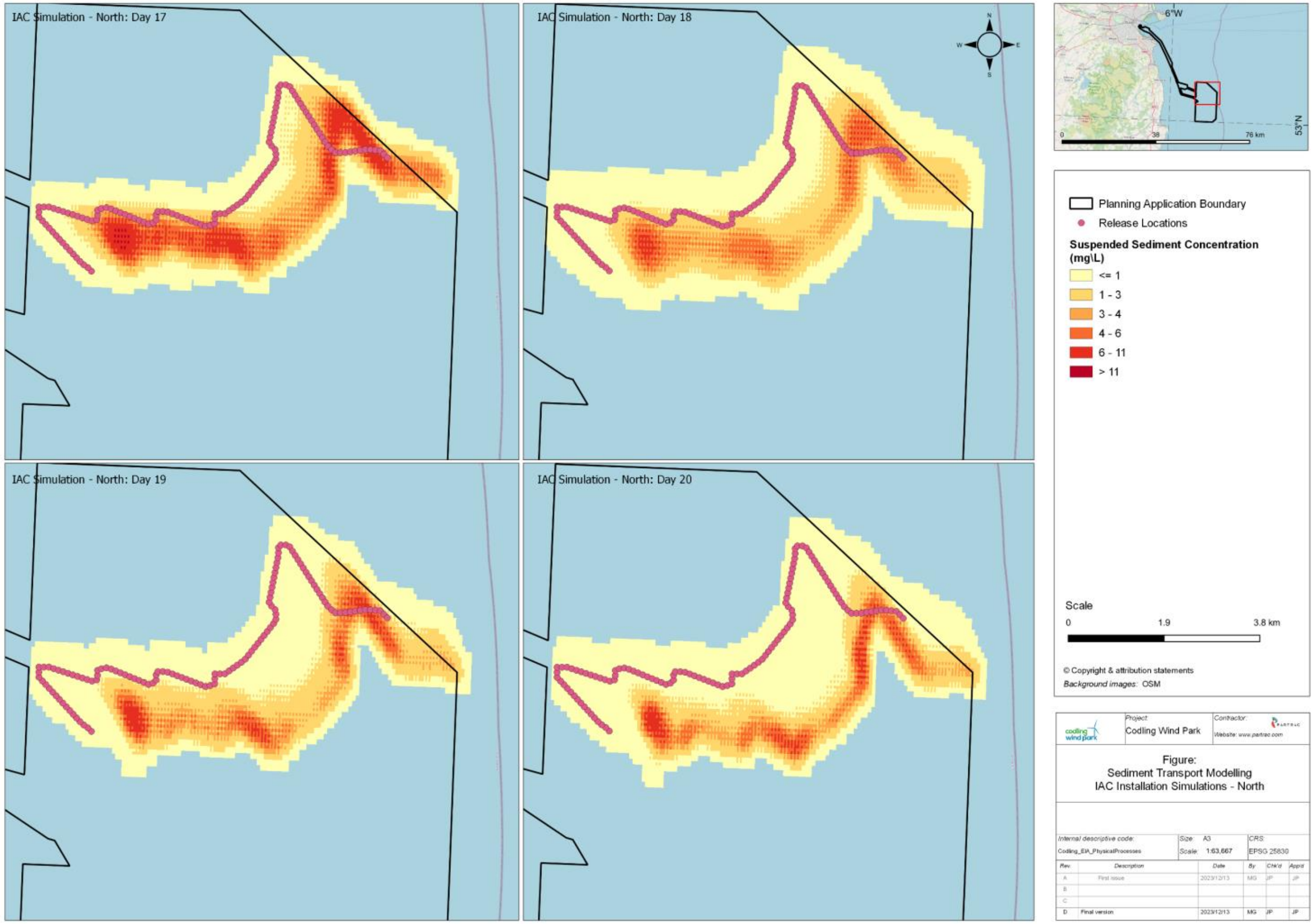

Figure 106 : SSC levels observed @ days 17 to 20 – Scenario 3.

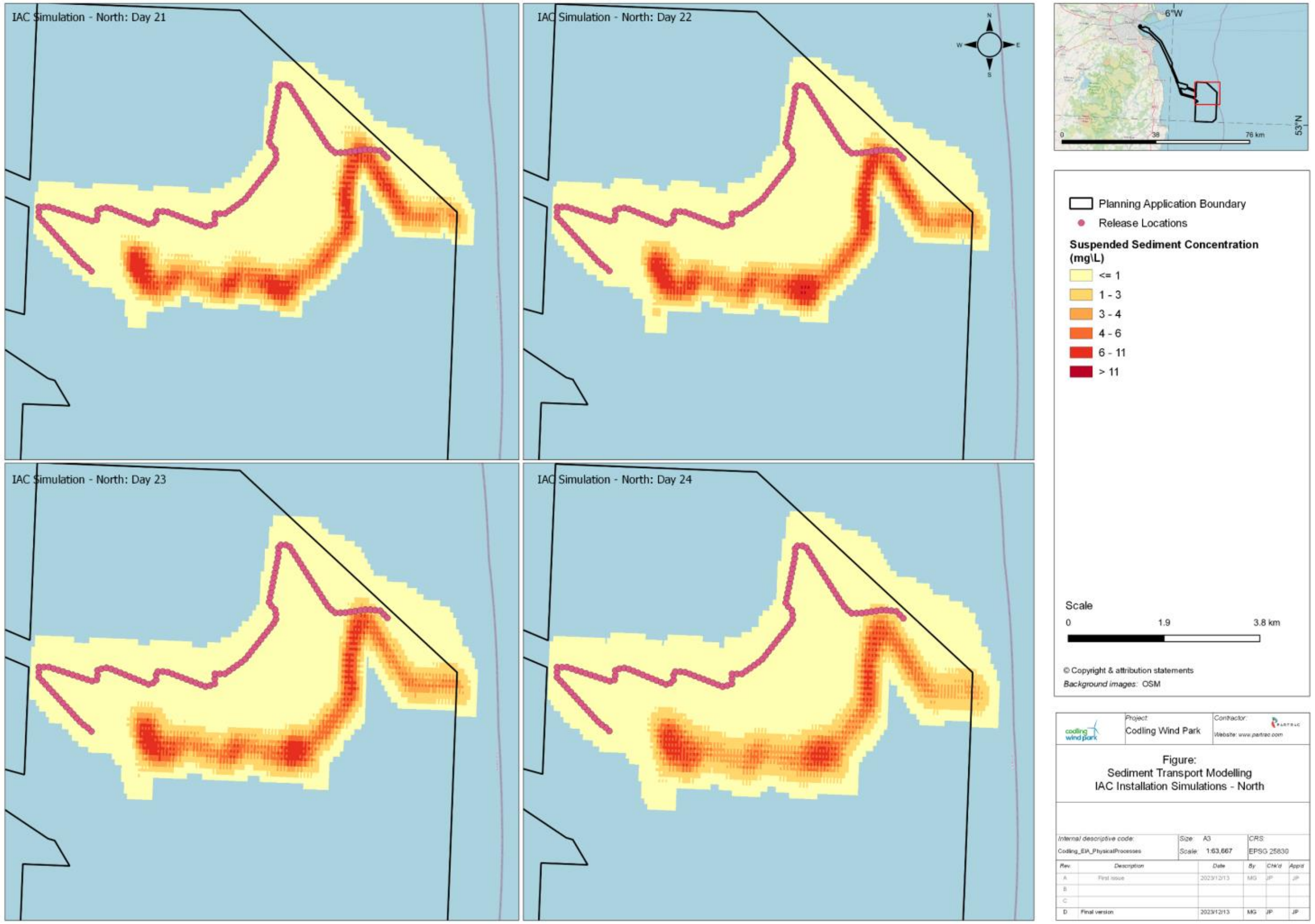

Figure 107 : SSC levels observed @ days 21 to 24 - Scenario 3.

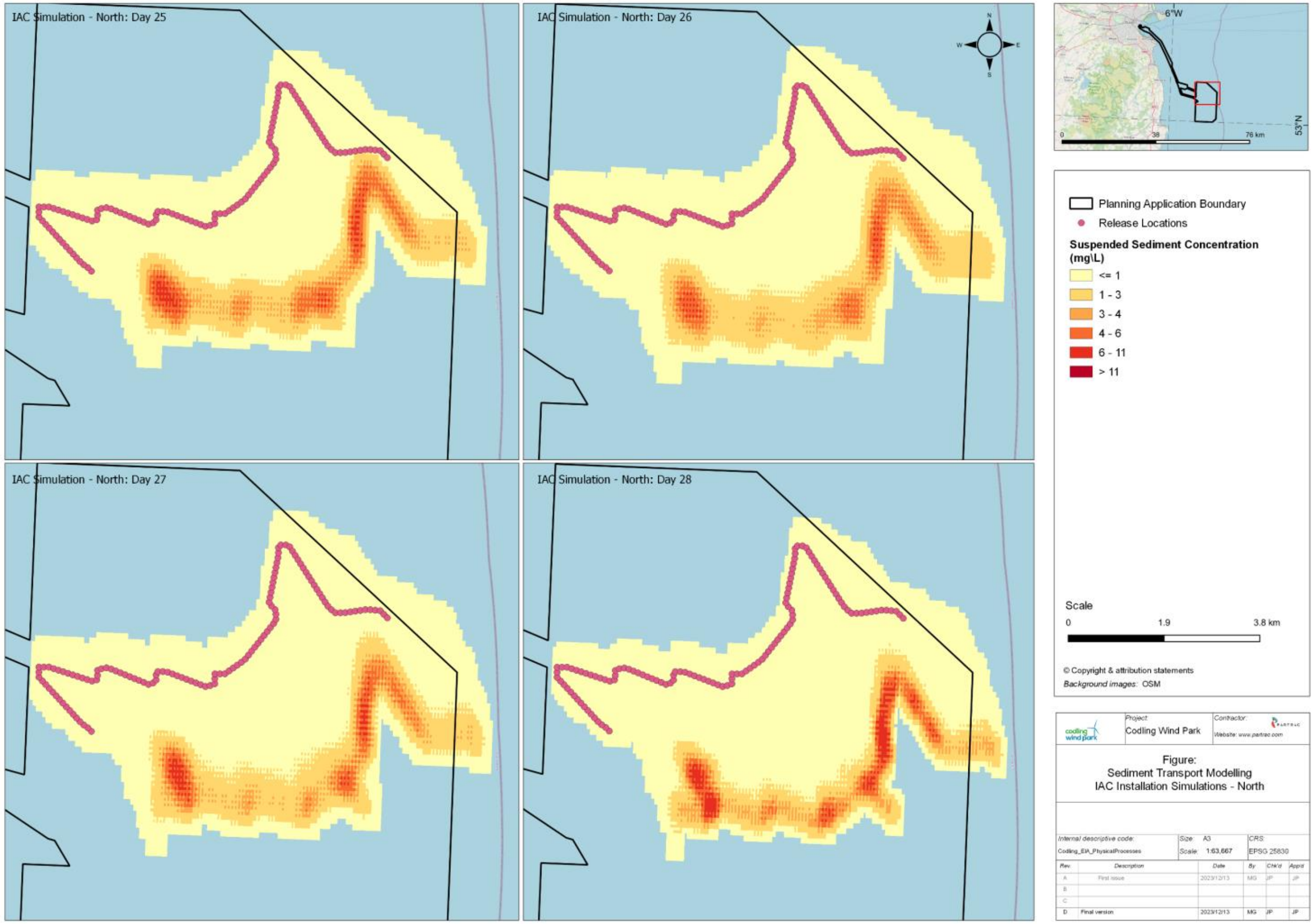

Figure 108 : SSC levels observed @ days 25 to 28 – Scenario 3.

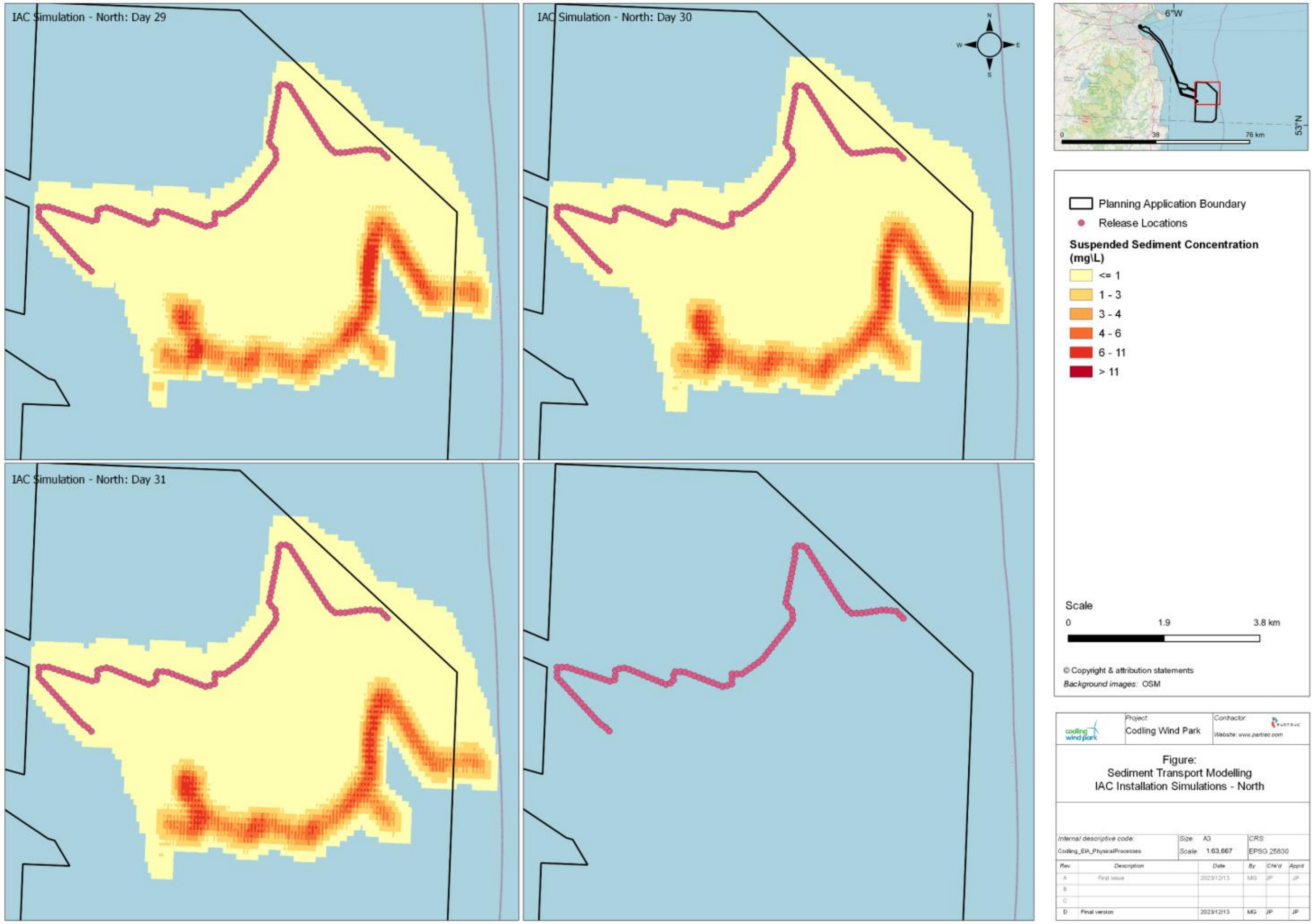

Figure 109 : SSC levels observed @ days 29 - 31 - Scenario 3.

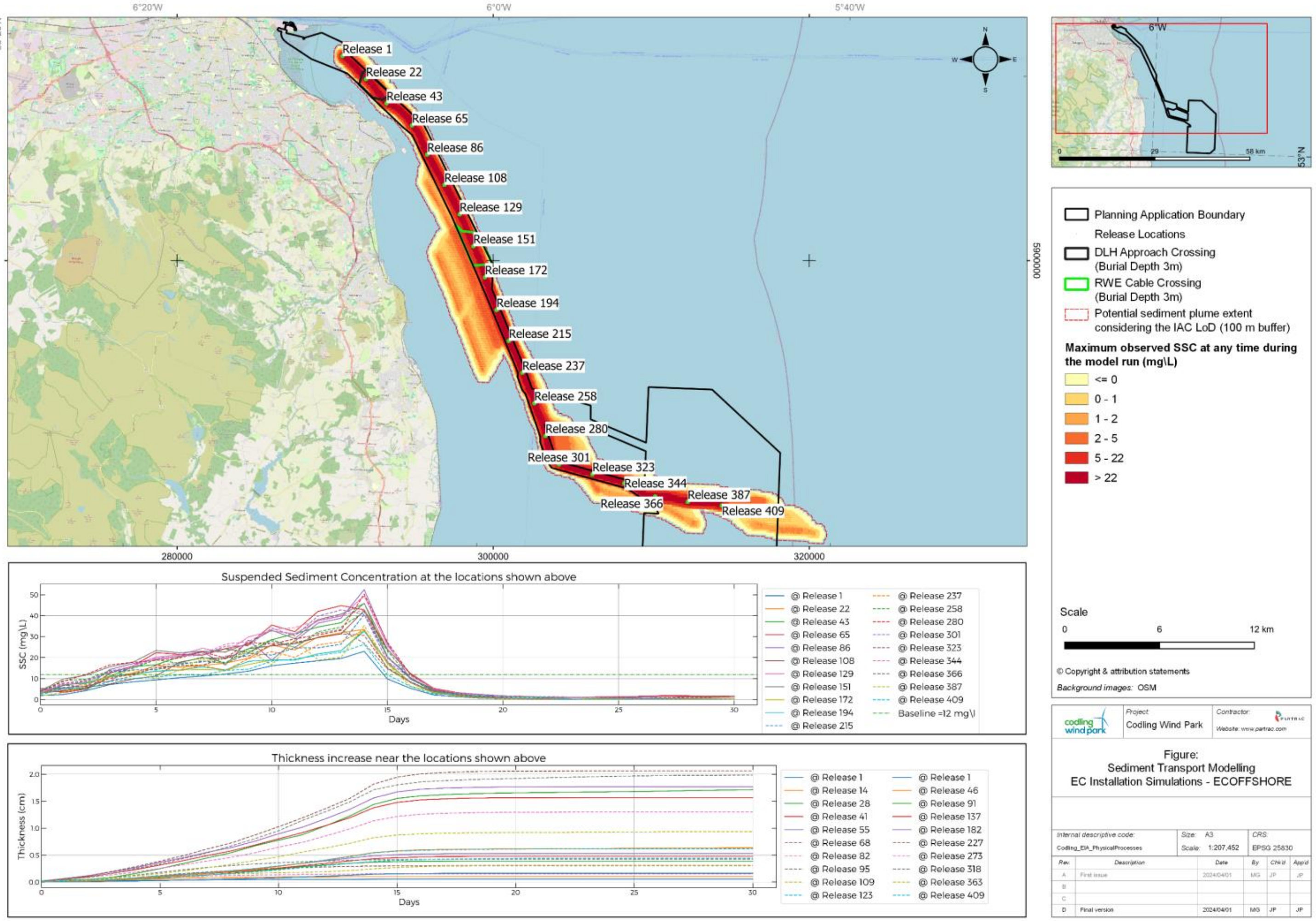

Figure 110: Maximum observed SSC levels at any time during Scenario 4 are presented in the spatial plot, the timeseries show 1) suspended sediment concentrations at the shown release locations, and 2) the deposited sediment thickness at the shown release locations.

Figure 111: Trajectory of suspended sediments – Scenario 4.

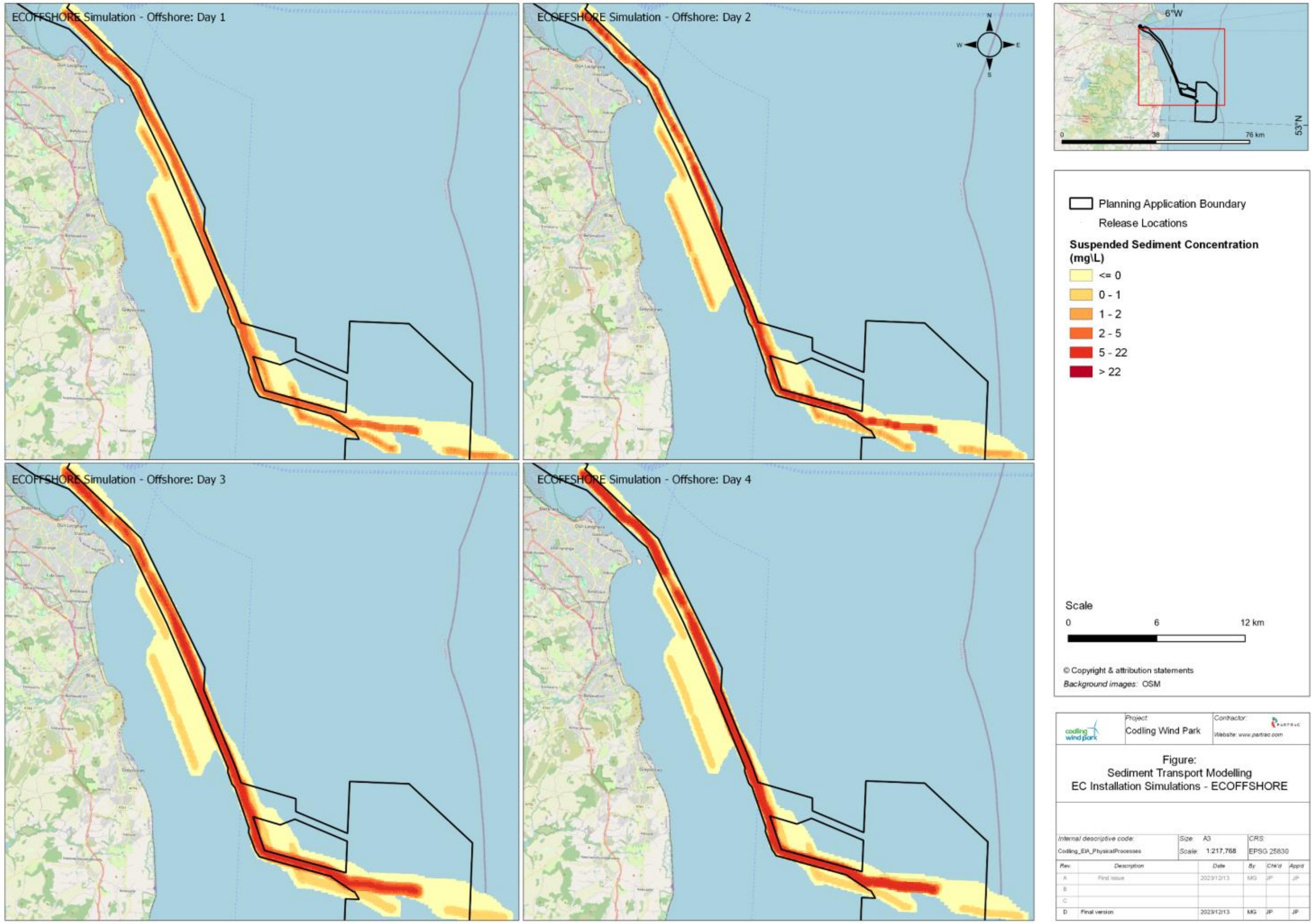

Figure 112 : SSC levels observed @ days 1 to 4 - Scenario 4.

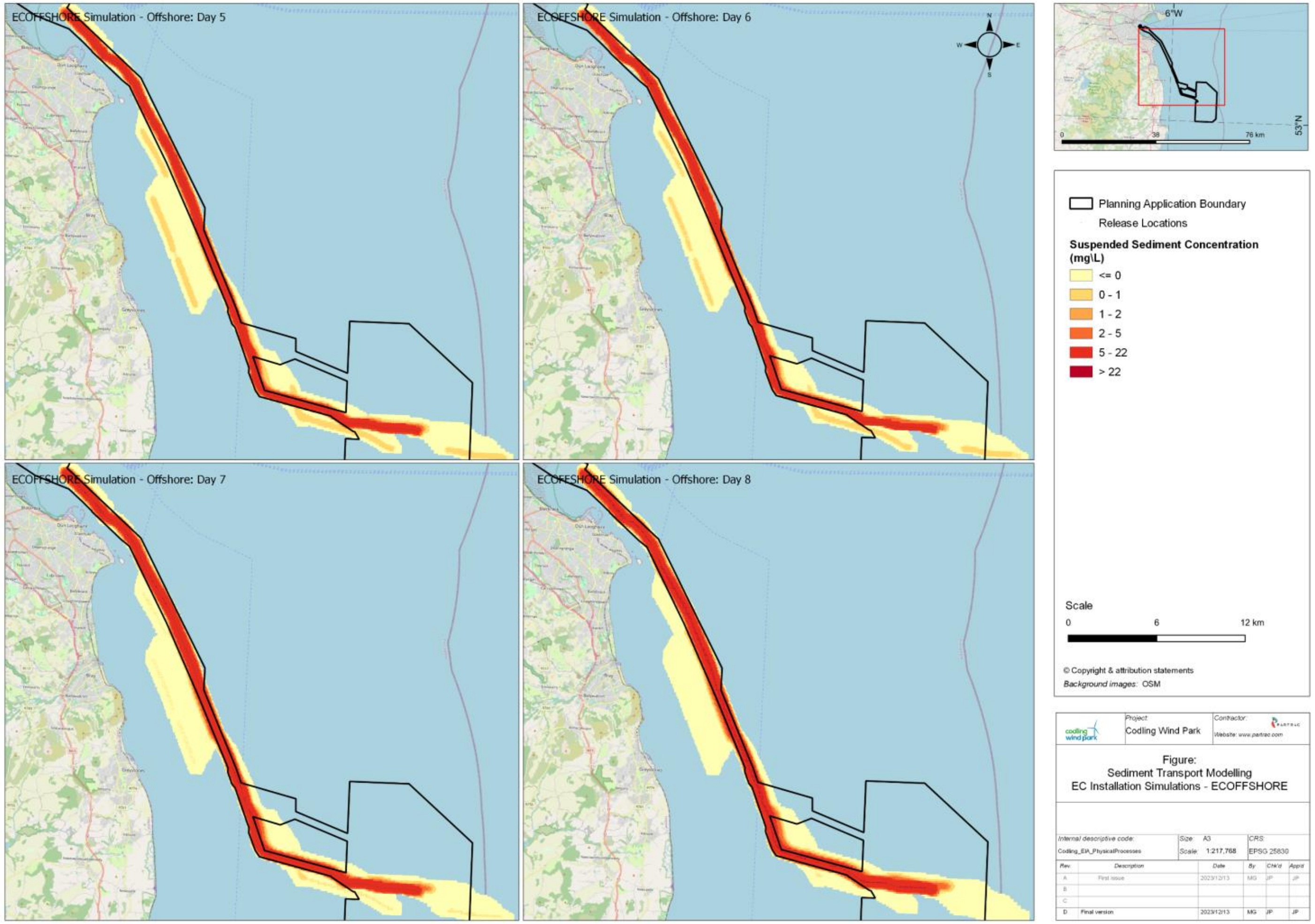

Figure 113 : SSC levels observed @ days 5 to 8 - Scenario 4.

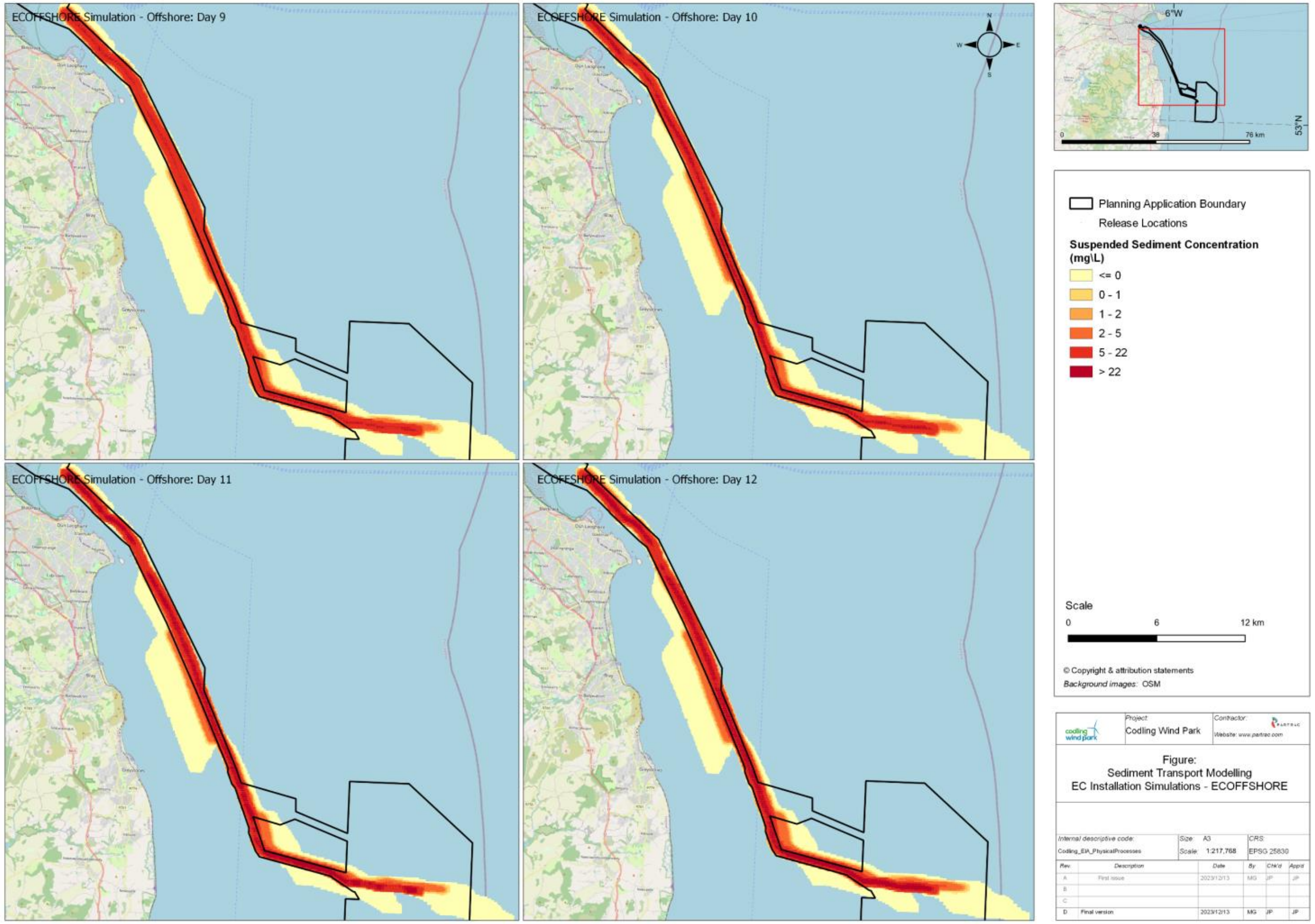

Figure 114 : SSC levels observed @ days 9 to 12 - Scenario 4.

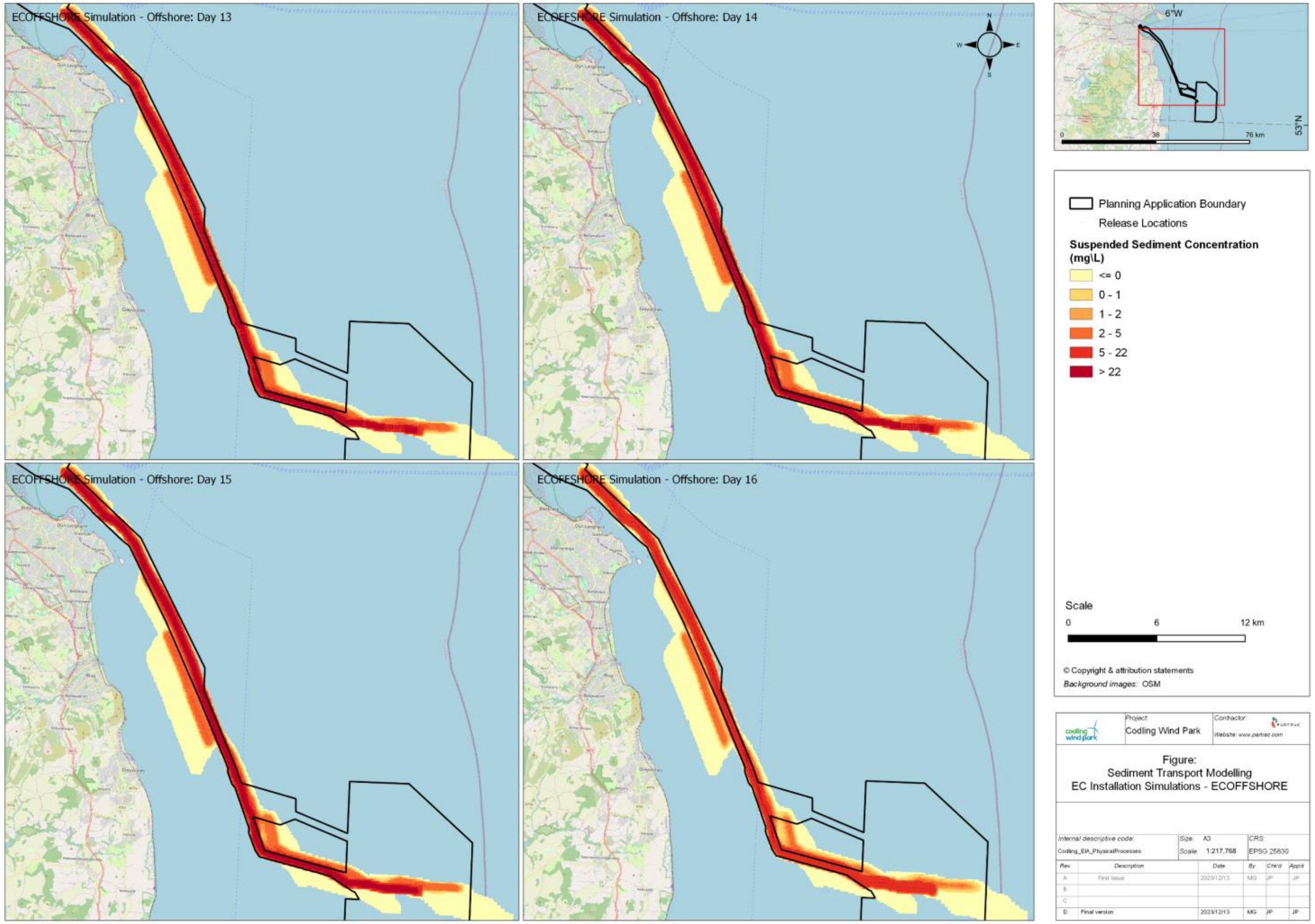

Figure 115 : SSC levels observed @ days 13 to 16 - Scenario 4.

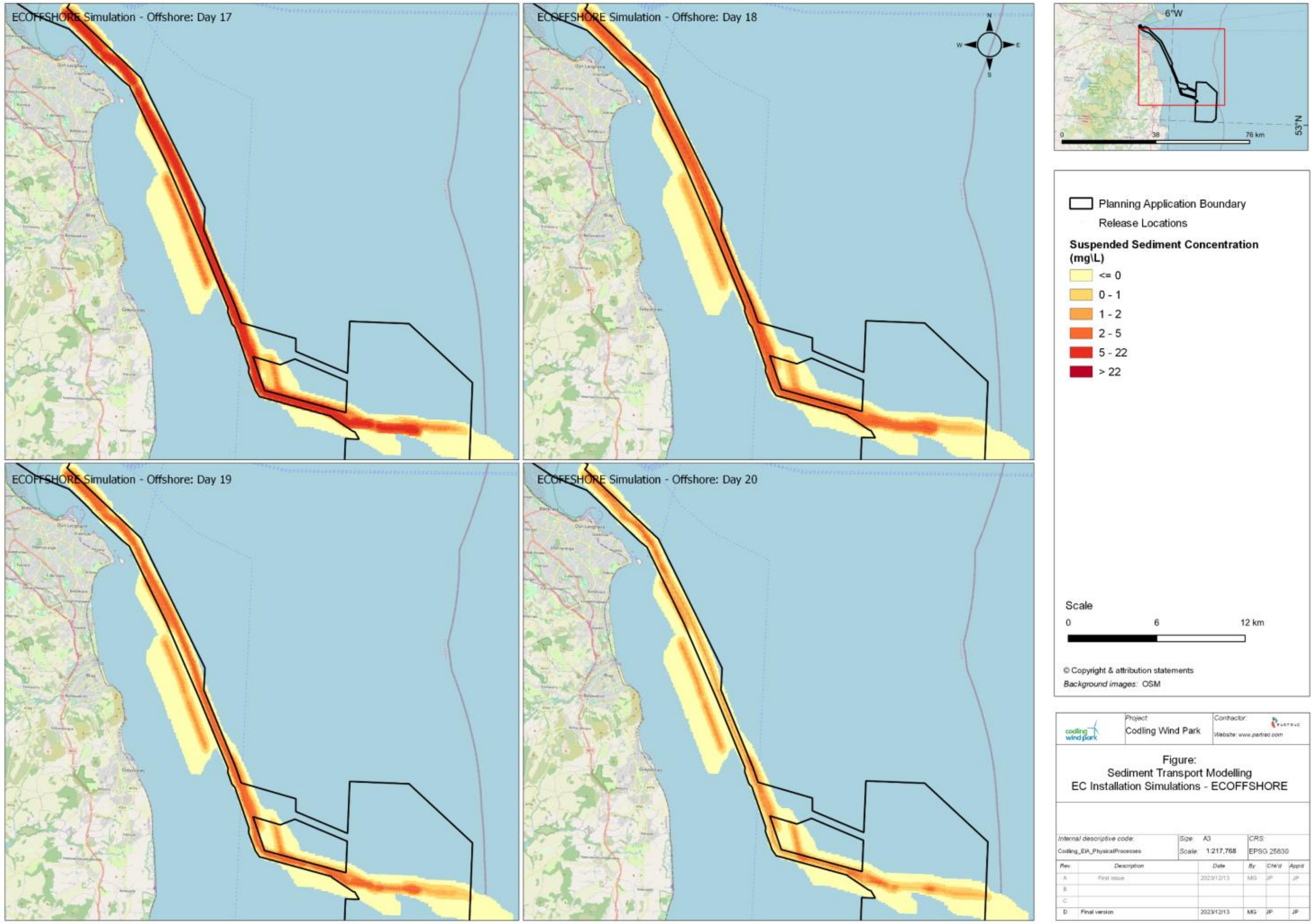

Figure 116 : SSC levels observed @ days 17 to 20 - Scenario 4.

Figure 117 : SSC levels observed @ days 21 to 24 - Scenario 4.

Figure 118 : SSC levels observed @ days 25 to 28 - Scenario 4.

Figure 119 : SSC levels observed @ days 29 to 31 - Scenario 4.

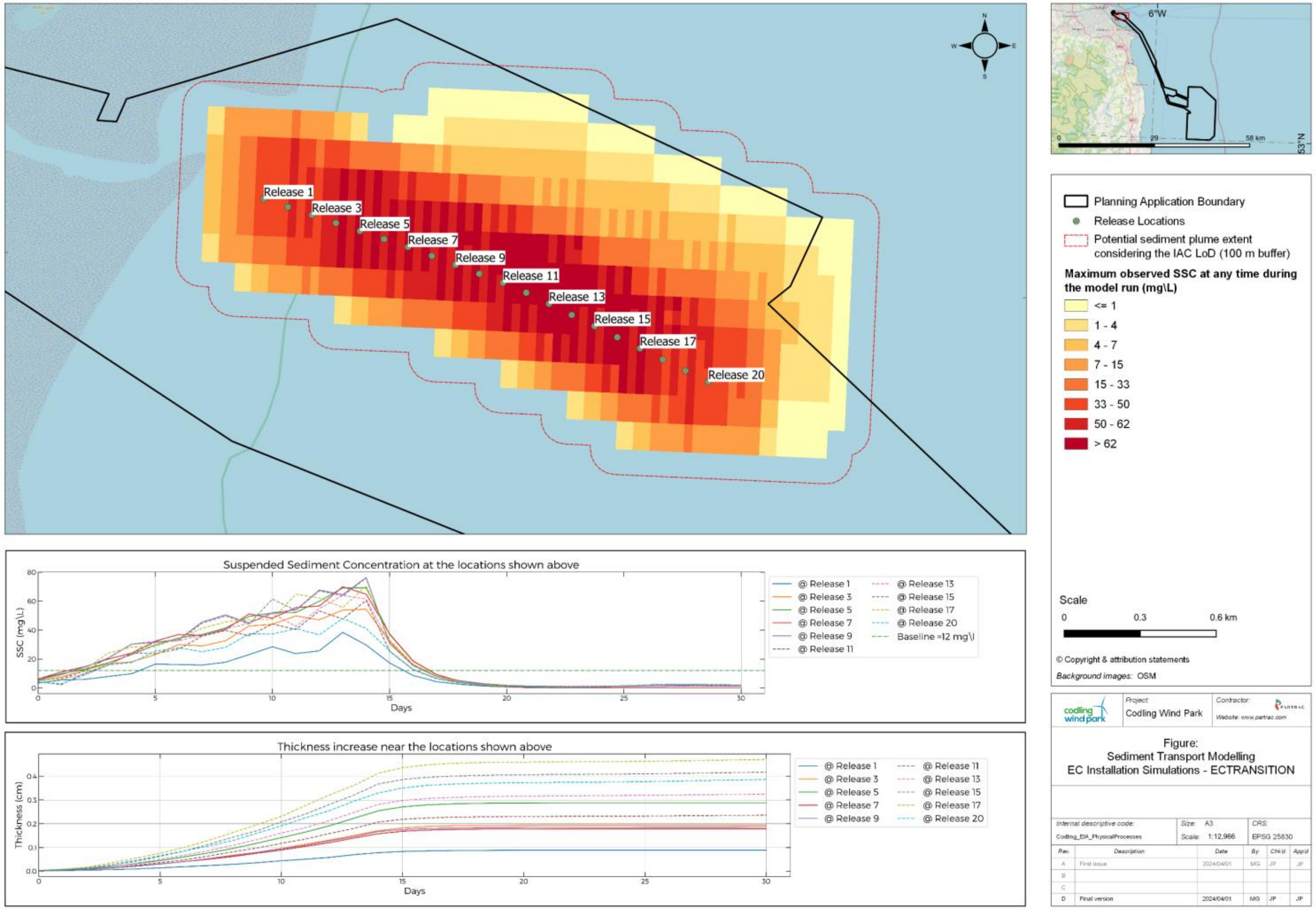

Figure 120: Maximum observed SSC levels at any time during Scenario 5 are presented in the spatial plot, the timeseries show 1) suspended sediment concentrations at the shown release locations, and 2) the deposited sediment thickness at the shown release locations.

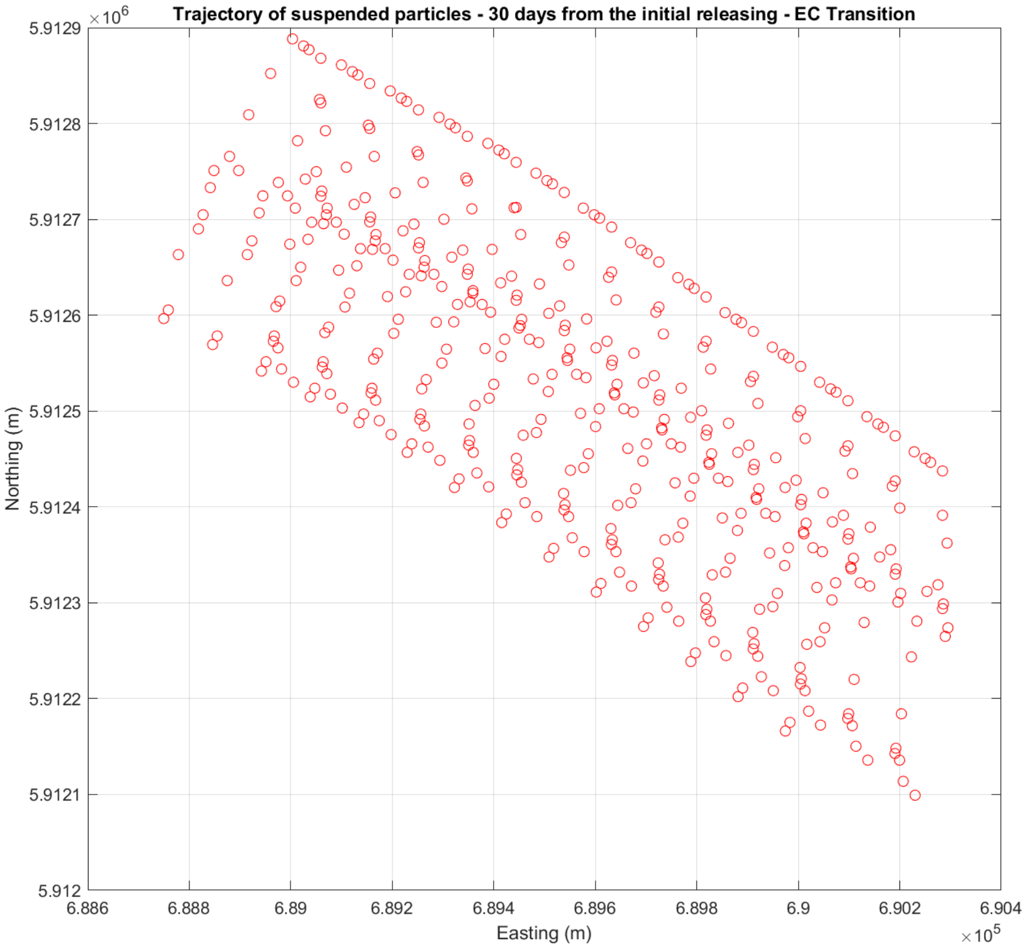

Figure 121: Trajectory of suspended sediments – Scenario 5.

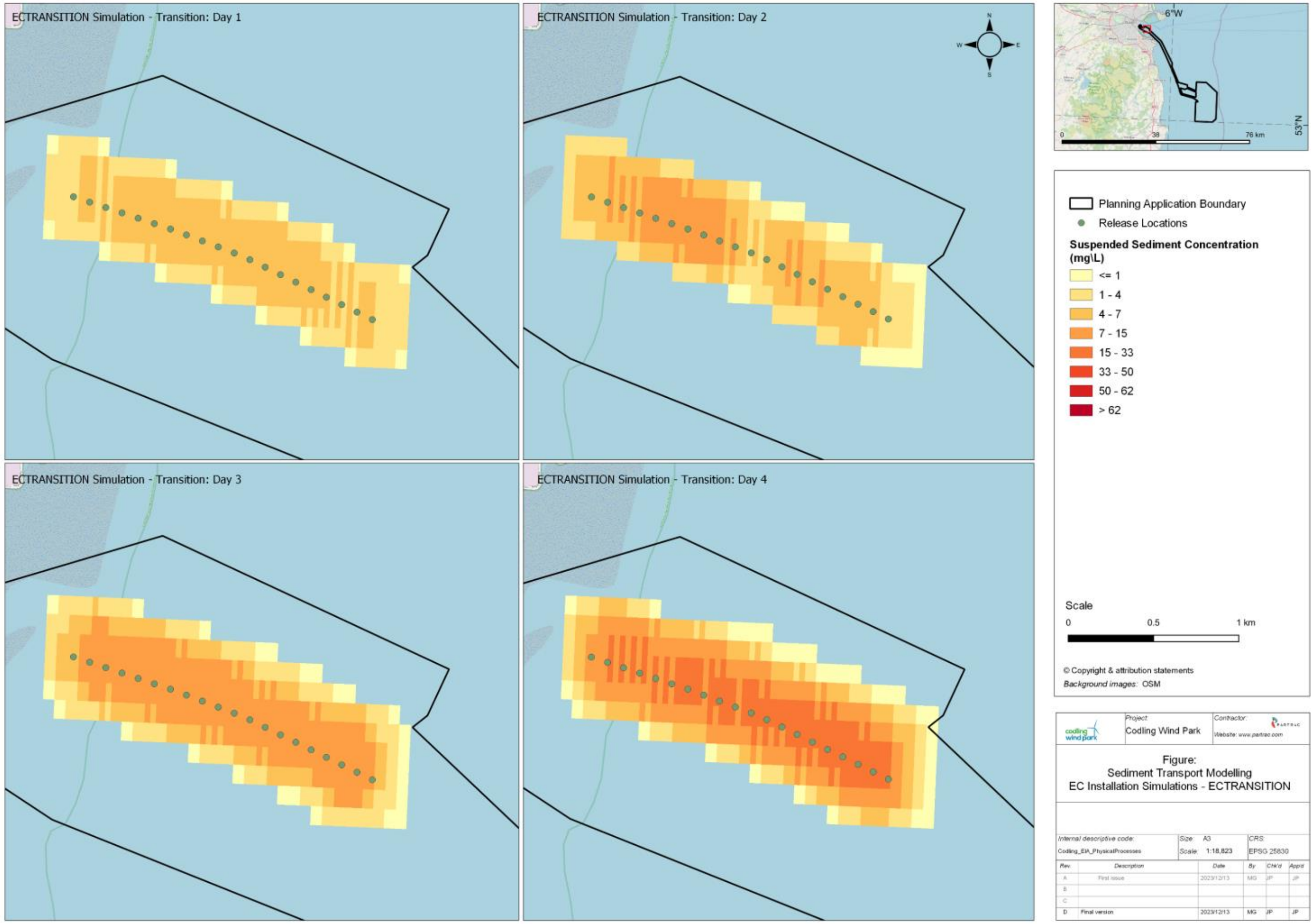

Figure 122 : SSC levels observed @ days 1 to 4 - Scenario 5.

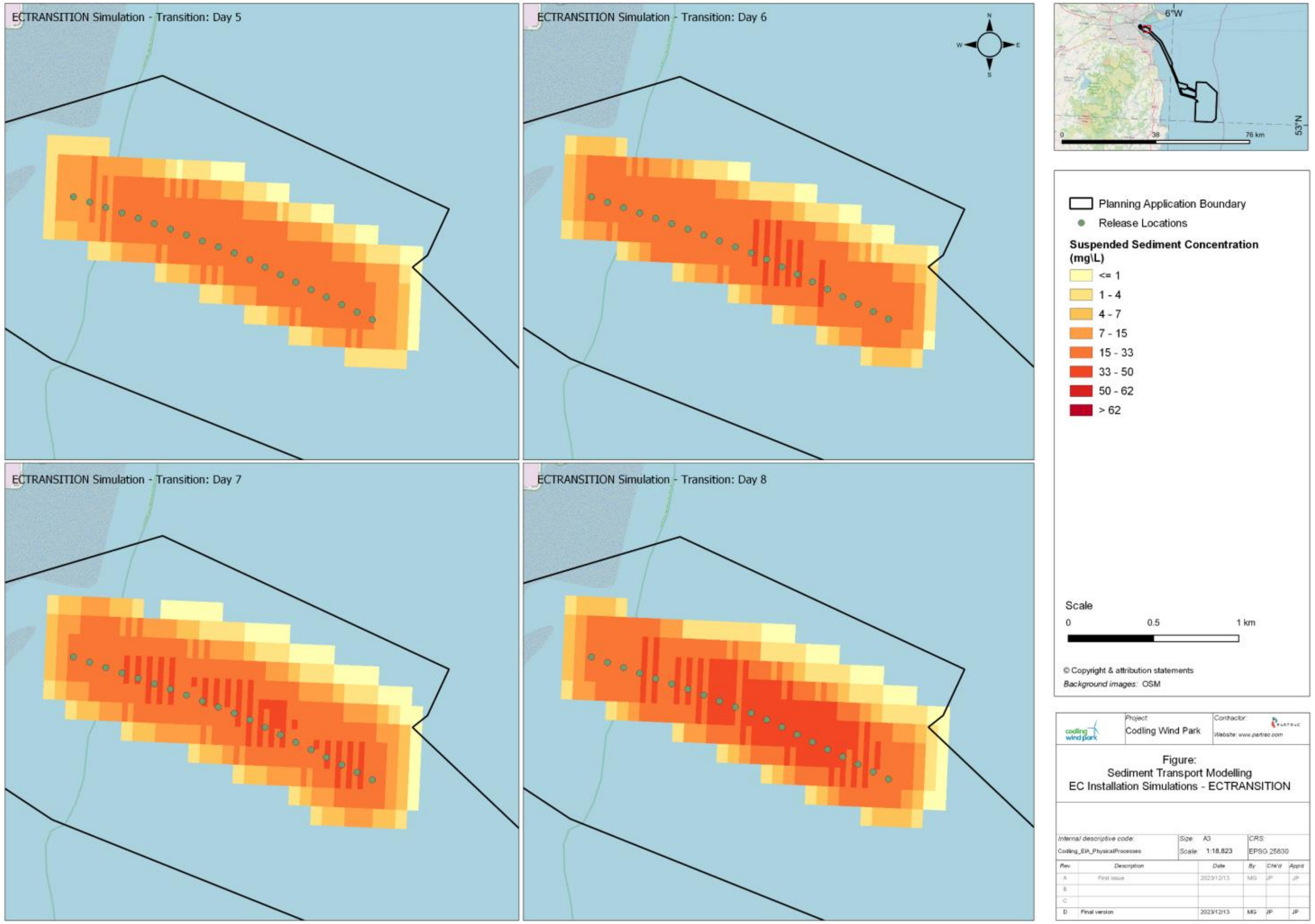

Figure 123 : SSC levels observed @ days 5 to 8 - Scenario 5.

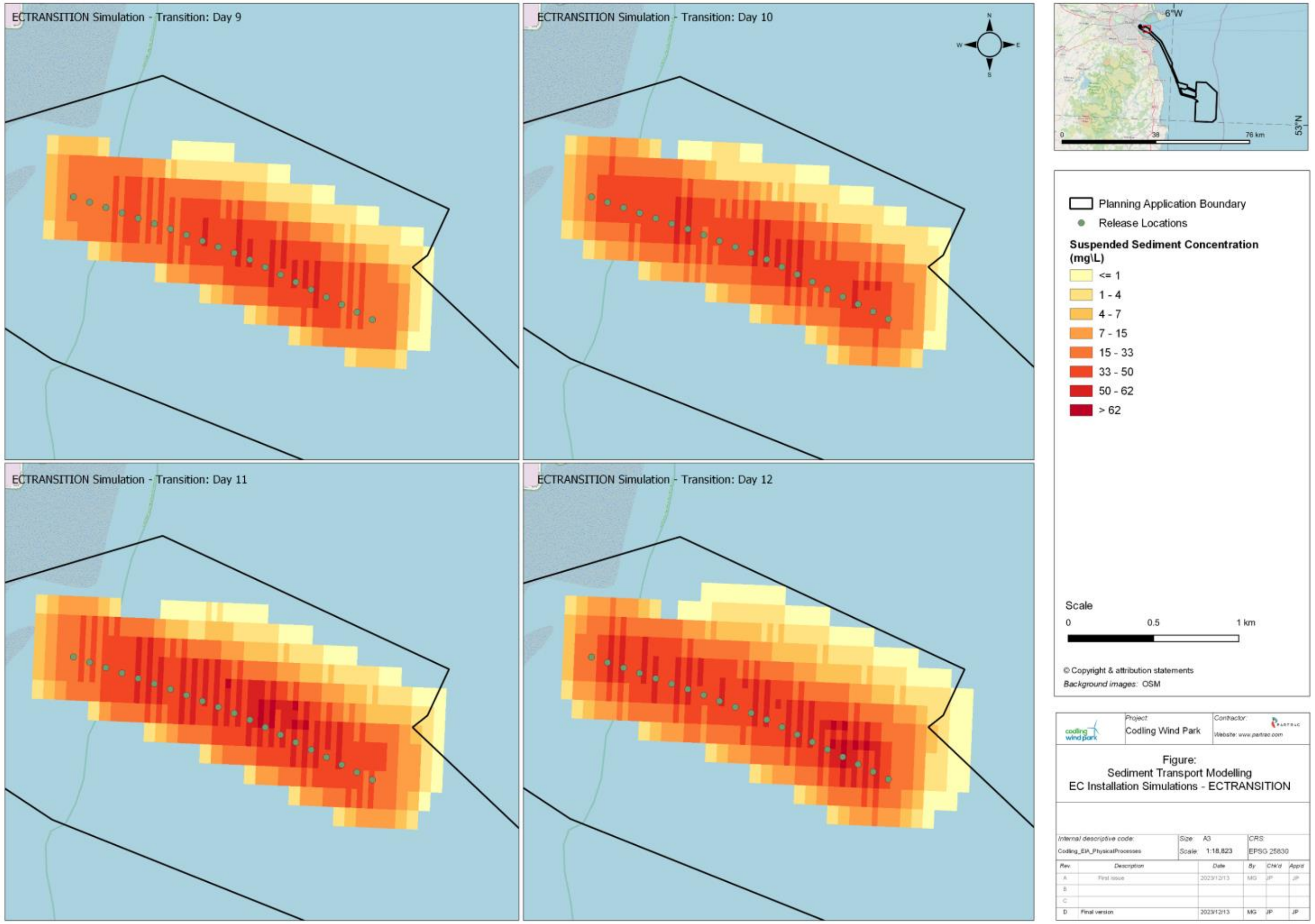

14

Figure 124 : SSC levels observed @ days 9 to 12 - Scenario 5.

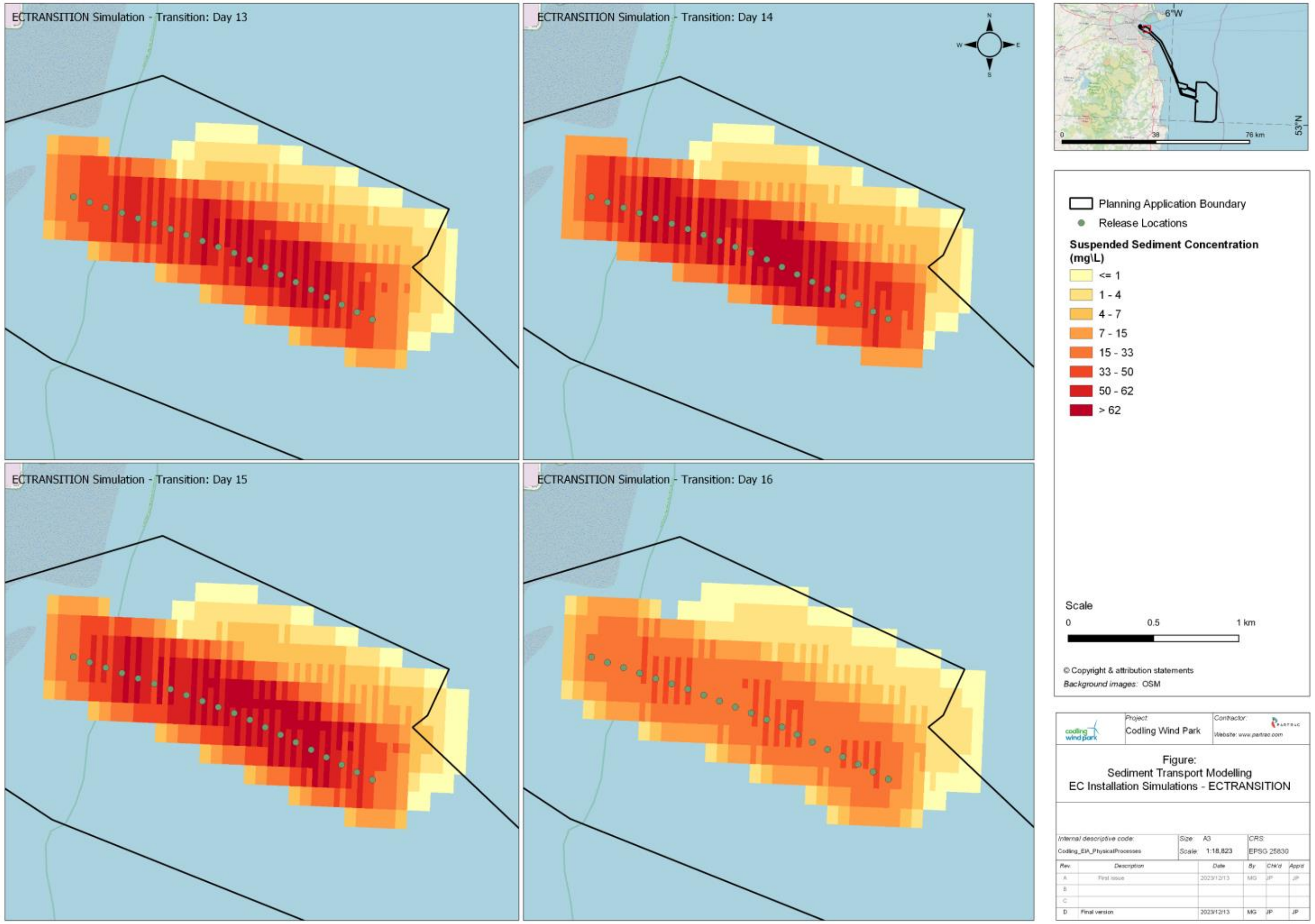

Figure 125 : SSC levels observed @ days 13 to 16 - Scenario 5.

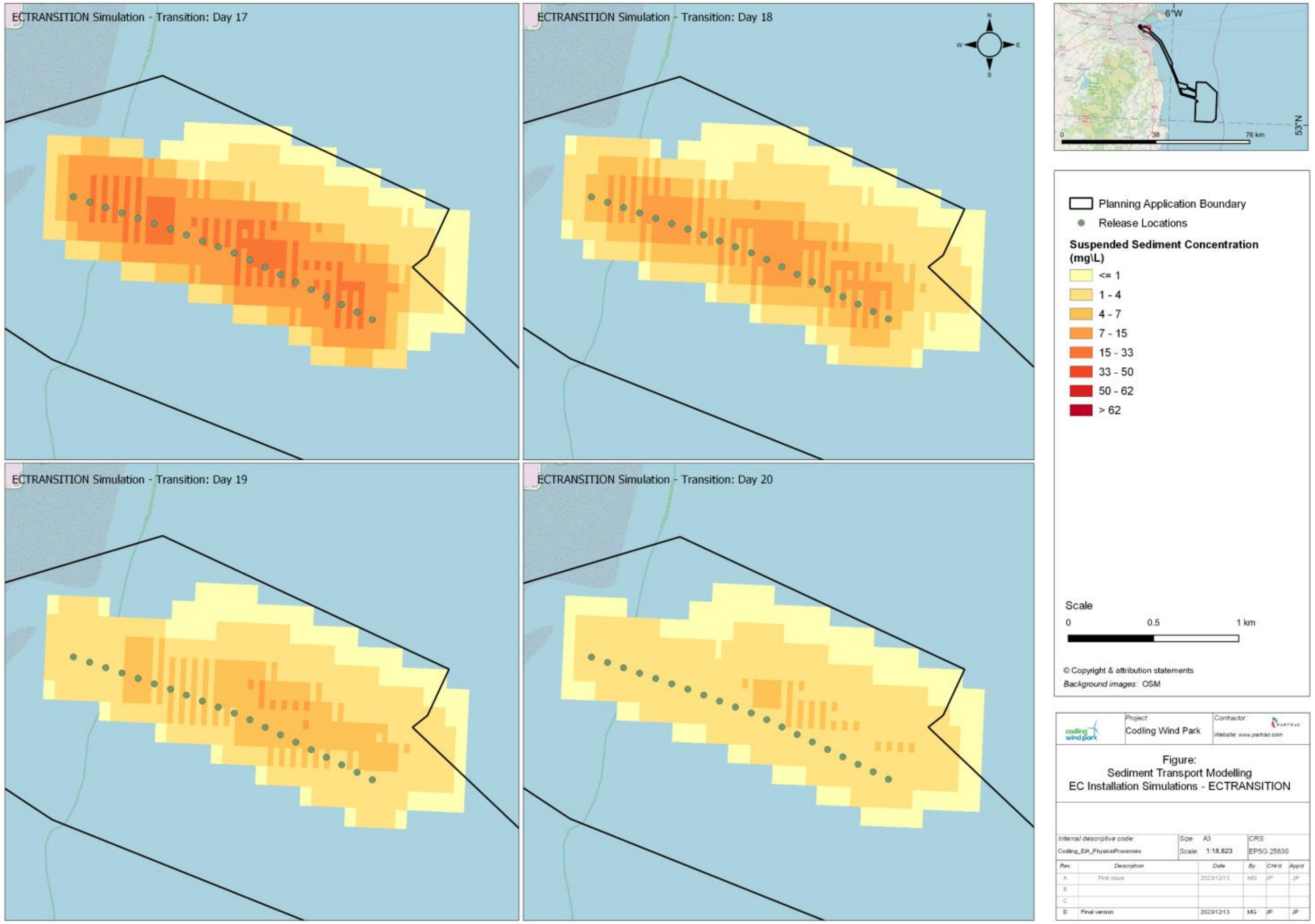

Figure 126 : SSC levels observed @ days 17 to 20 - Scenario 5.

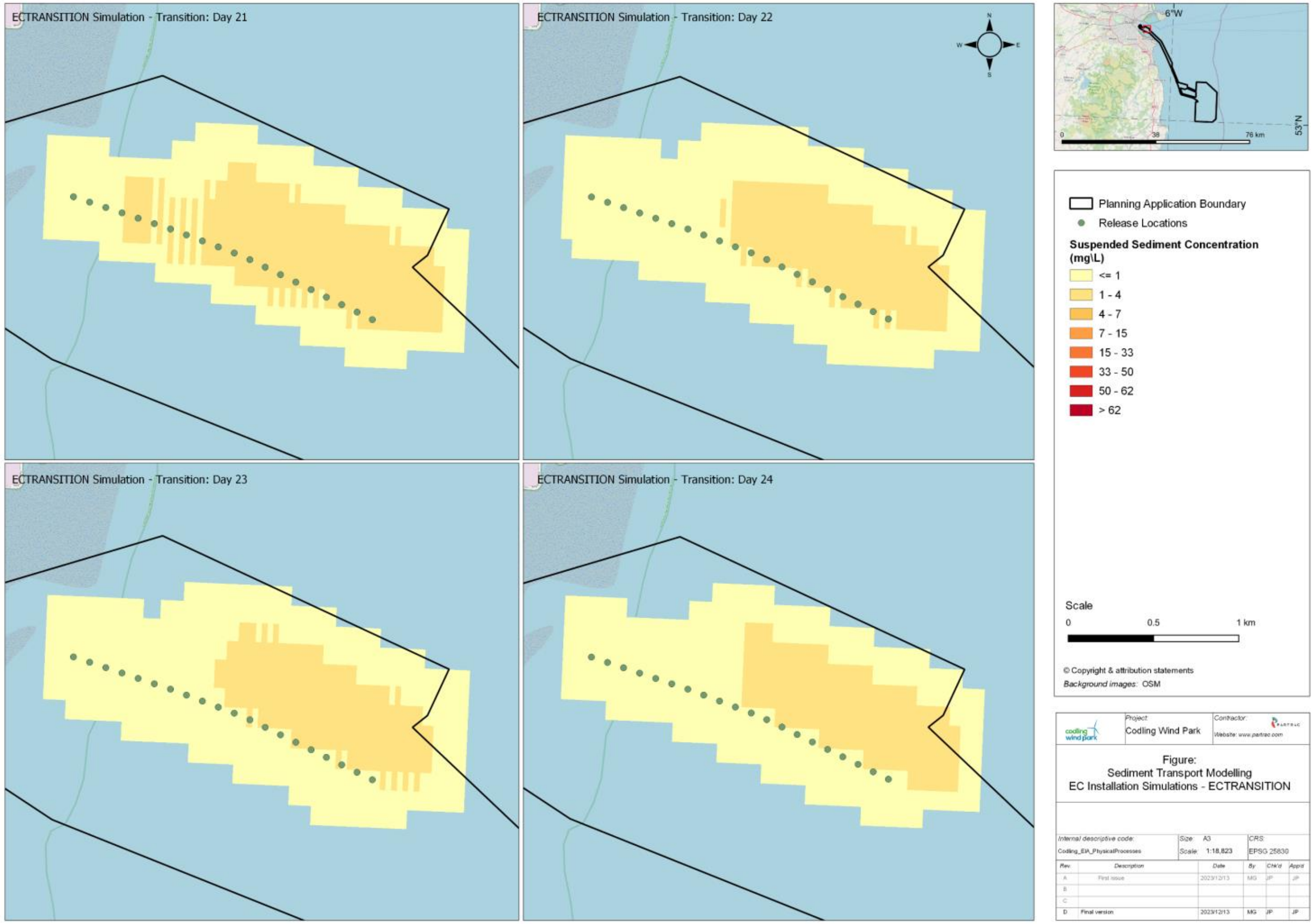

Figure 127 : SSC levels observed @ days 21 to 24 - Scenario 5.

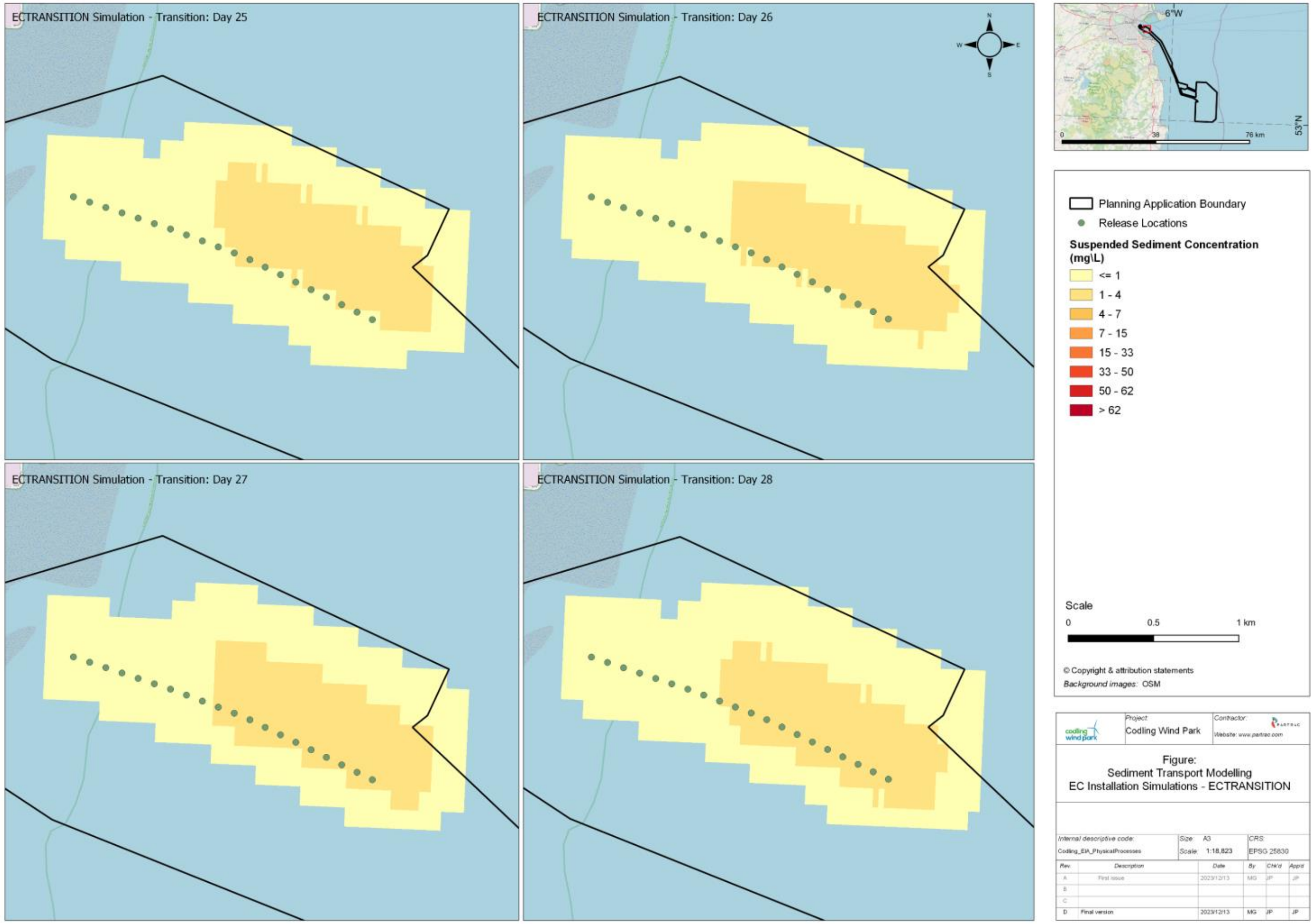

Figure 128 : SSC levels observed @ days 25 to 28 - Scenario 5.

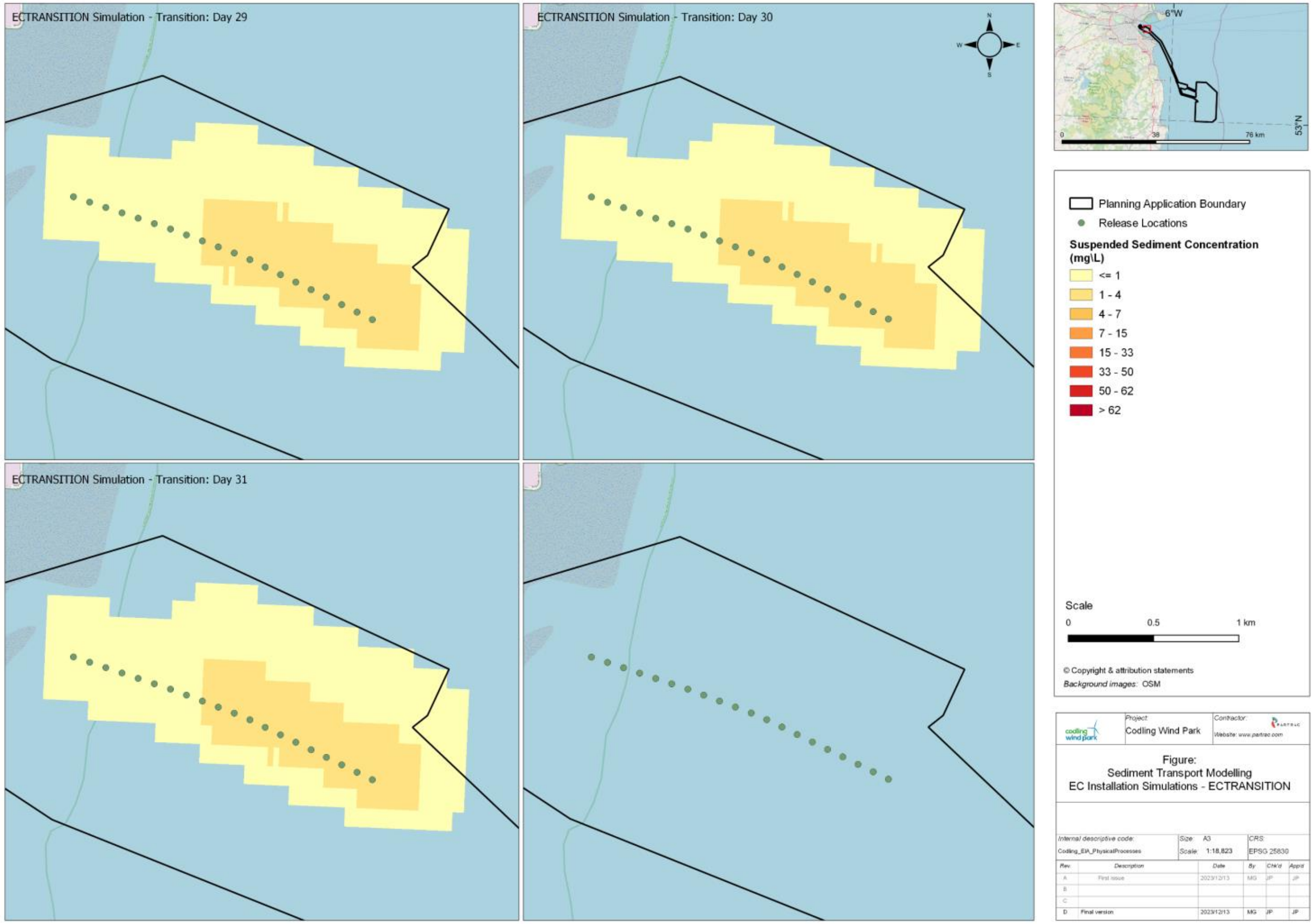

Figure 129 : SSC levels observed @ days 29 - 31 - Scenario 5.

7. Concluding remarks

A marine area coupled hydrodynamic wave model was constructed to support determination of the baseline hydrodynamic and wave regimes prevailing within the MAC application boundary and wider region. These models provided the driving conditions used for post construction and sediment transport simulations performed to support the assessment of potential impacts of the CWP project upon relevant receptors. This appendix describes the approach adopted to set-up, calibrate, and validate the marine area model. The primary purpose of the calibration and validation exercise was to demonstrate robust model skill, to provide quantitative evidence to prove that the developed marine area models are considered to be acceptable for application as part of the EIAR. Comparing model performance against criteria set out in established industry guidance indicates that the model is of suitable skill to be utilised as part of this assessment.

Following model calibration and validation, an exercise was performed to assess the potential impacts of the CWP project upon the Marine Geology, Sediments and Coastal Processes receptors at, and in proximity to, the Proposed Development. These results were also used separately by other EIA topics in relation to other sensitive receptors. These included:

- Chapter 7 Marine Water Quality (Document No. CWP-CWP-CON-08-03-03-REP-0002);
- Chapter 8 Subtidal and Intertidal Ecology (Document No. CWP-CWP-CON-08-03-03-REP-0003) and
- Chapter 14 Marine Archaeology and Cultural Heritage (Document No. CWP-CWP-CON-08-03-03-REP-0009).

Significant points to note from the outputs of the model simulations performed are:

- The construction activities of the CWP project are predicted to have only a small effect on the prevailing hydrodynamic and wave regimes both within the array site and at locations towards the coastline.
- During disposal of dredge arisings following bedform clearance and cable trenching activities, SSC's local to the release locations are predicted to be enhanced to up to circa 150 mg\L.
- Enhanced SSCs are transient, and concentrations are predicted to reduce to baseline levels no more than circa 15 to 25 days after completion of the activity responsible for liberating sediments into suspension.
- The suspended sediment plumes estimated during the simulation testing were predicted to be dispersed mainly towards the East quadrant (i.e. offshore), except for the disposal of dredge arisings during scenario 1 where a dominantly westward (inshore) propagation was observed. The predicted thickness of the sediment deposited away from the release locations during the simulations of dredge disposal following bedform clearance and cable trenching activities were almost negligible (e.g. sediment deposits on the seabed generated during these activities were predicted to be < 6 cm

thick). Though the fate of sediments liberated into suspension during construction activities is a function of:

- o Sediment composition and hydraulic characteristics.
- o Volumes of sediments liberated (released) into suspension.
- o Release location.
- o Height above the seabed of the release.
- o Timing of the release.
- o Residual tidal patterns, wave and wind action.

The simulations performed are sufficient to assess the impacts of these activities upon the relevant receptors.

References

Lambkin, D.O., Harris, J.M., Cooper, W.S. and Coates, T. (2009). Coastal Process Modelling for Offshore Wind Farm Environmental Impact Assessment: Best Practice Guide. COWRIE.

Battjes, J.A. and Janssen, J.P.F.M. (1978). Energy loss and set-up due to breaking random waves. Coastal Engineering.

Becker, J., van Eekelen, E., van Wiechen, J., de Lange, W., Damsma, T., Smolders, T. and van Koningsveld, M. (2015) Estimating source terms for far field dredge plume modelling. Journal of Environmental Management. 14, 282-293.

Brooks, AJ., Whitehead, PA. and Lambkin, DO. (2018). Guidance on Best Practice for Marine and Coastal Physical Processes Baseline Survey and Monitoring Requirements to inform EIA of Major Development Projects. NRW Report No: 243, 119 pp, Natural Resources Wales, Cardiff.

DNV-GL. (2018). Metocean Characterization Recommended Practices for U.S. Offshore Wind Energy. BOEM 2018-057. Document No: 100396...63-HOU-01

IMarEST Offshore Renewables Special Interest Group. (2018). Metocean Procedures Guide for Offshore Renewables. URL: https://www.imarest.org/reports/650-metocean-procedures-guide

Komen, G.J., Hasselmann, S. and Hasselmann, K. (1984): On the Existence of a Fully Developed Wind-Sea Spectrum. J. Phys. Oceanogr., 14, 1271–1285, https://doi.org/10.1175/10485(1984)014<1271:OTEOAF>2.0.CO;2

MetOceanWorks. (2022). Metocean Study Basis. CWP document number CWP-E6-MET-01-REP-0001.

Pye, K., Blott, S. and Brown, J. (2017). Advice to Inform Development of Guidance on Marine, Coastal and Estuarine Physical Processes Numerical Modelling Assessments. NRW Report No: 208, 139 pp, Natural Resources Wales, Cardiff.